UNIVERSITY OF
KWAZULU-NATAL

INYUVESI
YAKWAZULU-NATALI

Global transcriptome analysis of THP-1 cells infected with an *rpfB* gene knockout strain of *Mycobacterium tuberculosis*

Compiled by

DEEPIKA MOTI

BSc, BMedSci (Hons) (UKZN)

Submitted as the dissertation component in fulfilment for the degree of Masters in Medical Science (Medical Microbiology)

In the School of Laboratory Medicine and Medical Sciences

University of KwaZulu-Natal

South Africa

DATE SUBMITTED: February 2021

DECLARATION

I, Miss Deepika Moti, declare as follows:

1. The work described in this dissertation has not been submitted to UKZN or other tertiary institution for purposes of obtaining an academic qualification, whether by myself or any other party.

2. That the work performed by others or obtained from various sources have been indicated and appropriately acknowledged in this dissertation.

3. My contribution towards the project was as follows:

I. Performance of all experimental work, data analysis and interpretation

II. Writing up of dissertation and individual manuscripts

D. Moti

Student Signature
(Deepika Moti)

4th February 2021
Date

[redacted]

4th February 2021

Supervisor signature
(Prof. Manormoney Pillay)

Date

[redacted]

4 February 2021

Co-supervisor Signature
(Dr. Nontobeko Mvubu)

Date

DEDICATION

For my parents, Deepak and Sharla Moti.

You have made this possible for me as a result of your unwavering support, encouragement, faith and most of all, the love you both have shown me. Herein lies the outcome of all the sacrifices you have made for me. I am eternally grateful and proud to have achieved this under your name.

This is for you.

To my father in heaven

02 February 60 – 14 July 2020

Throughout your lifetime you have etched in the walls of my heart the importance of education, with love, compassion and understanding. In your name, then, now and always,

Your little girl.

ACKNOWLEDGEMENTS

I would like to sincerely thank:

My supervisor, Professor Manormoney Pillay. I started off this journey with you as one of your top 5 students from the previous degree and finished off this one as your worst. Despite my circumstances, you've showed unwavering support and motivation, not only on a professional level but as one human being to another. Your remarkable knowledge in this field and your command of impeccable writing skills has greatly contributed to this research project and dissertation. It was an absolute honour being your student and you will always be remembered, not only for your skill but the empathy you bestowed upon me.

My co-supervisor, Dr. Nontobeko Mvubu, thank you for providing me with your expertise in bioinformatics analysis and the software tools to complete the analysis, for your knowledge in areas I lack and for assistance and guidance in formulating this manuscript. I am grateful for your understanding and belief in me as a professional and person.

Dr. Charissa Camille Naidoo, to you I would like to extend my humble gratitude for providing the *rpfB* gene deficient strain of *M. tuberculosis*, excellent BSL2+ and BSL3 facility training, and for assisting with the study design.

Professor Balakrishna Pillay, for providing the Ingenuity Pathway Analysis bioinformatics tool used for downstream RNA sequencing analysis. The approach taken to complete this work would not be possible without your assistance.

Hollis Shen and Pamela Ramkalawon from the Africa Health Research Institute, for allowing me to use your Bio-Plex 200 instrument for cytokine analysis, also for their time and patience during work after hours.

Dr. Ravesh Singh, my utmost appreciation and heartfelt thanks goes to you for providing training in completing cytokine multiplex assays, for providing the QuantStudio™ 5 Real-Time PCR System, and for assisting me through the process overtime.

Dr. Suventha Moodley, a sincere thank you for the extensive tissue culture facility training, and most of all for your constant support, guidance and research expertise in times of need. All the knowledge I have gained in this aspect is through your magnificent teaching skills and ever willingness to assist.

Dr. Saiyur Ramsugit, for his steadfast encouragement, support, and his willingness to assist and provide resources when need be but mostly for your strong belief in the person that I am.

Ms. Sanisha Muniram, for the guidance in generating the *rpfB* complemented strain, your expertise and training skill in molecular biology is astonishing and highly appreciated.

To all friends and colleagues at the Medical Microbiology department, DDMRI, Nelson R. Mandela School of Medicine, UKZN, thank you for assisting me without reservation whenever it was needed.

National Research Foundation (NRF) for providing financial support throughout the duration of this research project.

My siblings, Deepesh & Sarisha Moti. I am ever so grateful for your words of wisdom, love, understanding, and your constant ability to cheer me up. Love and gratitude, always.

To my best friend, Selina Gopaul, blood couldn't make us any closer. No amount of thank you will ever be enough to express my gratitude for the role you've played in our lives, especially over the past few years. Thank you for the constant reassurance, encouragement and endless faith you have in me.

I smile and tear as I complete this because I know without the strength of GOD and my father, this would be undone.

LIST OF TABLES

Appendix

LIST OF FIGURES

Chapter 2

Appendix

LIST OF ABBREVIATIONS

Mtb/ M. tuberculosis	*Mycobacterium tuberculosis*
AEC	Airway epithelial cells
AES	Allelic exchange substrate
AG	Aminoguanidine
AM	Alveolar macrophage
ATP	Adenosine triphosphate
BCG	Bacille Calmette-Guerin
BP	Biological processes
CC	Cellular components
cDNA	Complementary DNA
CFU	Colony forming units
CR	Complement receptor
DC	Dendritic cell
DS-TB	Drug susceptible tuberculosis
ELISA	Enzyme-linked immunosorbent assay
EMB	Ethambutol
FBS	Fetal bovine serum
FDA	Food and drug administration
FDR	False rate discovery
HIV	Human Immunodeficiency virus
Hyg	Hygromycin
IFN	Interferon
IL	Interleukin
INH	Isoniazid
IPA	Ingenuity pathway analysis
ISG	Interferon stimulating genes
ISRE	Interferon stimulating
Kan	Kanamycin
KZN	Kwa-Zulu Natal
LPA	Line probe assay
LTBI	Latent TB infection
MDR	Multi-drug resistant
MF	Molecular functions
MHC	Major histocompatibility complex

MOI	Multiplicity of infection
mRNA	Messenger RNA
NGS	Next generation sequencing
NK	Natural Killer
OADC	Oleic acid dextrose
PAMP	Pathogen associated molecular patterns
PBS	Phosphate buffered saline
PCR	Polymerase chain reaction
PG	Peptidoglycan
PMA	Phorbol myristate acetate
PZA	Pyrazinamide
qRT-PCR	Quantitative real time PCR
RIF	Rifampicin
RIN	RNA integrity number
RNA	Ribonucleic acid
RNI	Reactive nitrogen intermediate
ROI	Reactive oxygen intermediate
Rpf	Resuscitation promoting factor
RR-TB	Rifampicin resistant TB
SA	South Africa
sac	Saccharide
SDEG	Significantly differentially expressed genes
TB	Tuberculosis
TDR-TB	Totally drug resistant TB
TGF	Transforming growth factor
Th	T helper
TLR	Toll-like receptor
TNF	Tumour necrosis factor
Treg	Regulatory T cells
TYK	Tyrosine kinase
UKZN	University of Kwa-Zulu Natal
UV	Ultraviolet
XDR-TB	Extensively drug resistant TB

DISSERTATION OUTLINE

This dissertation is presented in manuscript format. Chapter 1 provides a review on relevant literature and Chapter 2 is the original research manuscript titled: The *rpfB* gene contributes to the regulation of the host innate immune response in THP-1 macrophages infected with *Mycobacterium tuberculosis* V9124.

This will be formatted according to the authors instructions for submission to the Journal of Molecular Medicine.

TABLE OF CONTENTS

ABSTRACT

Background: Since the initial isolation of *Mycobacterium tuberculosis* (*Mtb*), tuberculosis (TB) remains among the top 10 causes of death. In 2019, 10 million people globally were burdened with TB, of which 25 %were from Africa. A fundamental process in determining the outcome of *Mtb* infection is host-pathogen interactions. These interactions may lead to eradication of bacteria via the innate immune response or latent TB infection (LTBI) in which the bacilli reside in a non-replicating, low metabolic state (dormancy) within alveolar macrophages (AM). Ten percent of the global population develops LTBI leaving them at greater risk of developing active TB. Initiation of an immune response requires effective antigenic stimulation that induces multiple signalling cascades and the production of pro-inflammatory and anti-inflammatory cytokines, effective against or beneficial to *Mtb*. The pathogen has a family of 5 resuscitation promoting factors (*rfps A-E*) that have been previously characterized in *Mtb* growth, persistence and reactivation, *in vitro* and *in vivo*, using single and multiple *rpf* gene knockouts. Among the other Rpf proteins, RpfB was shown to be highly antigenic and immunogenic, with the ability to induce a Th1 phenotype immune response in dendritic cells (DC) through binding of toll-like receptor 4 (TLR4). Since macrophages are the target cell of *Mtb* and the reservoir of dormant bacilli, this study investigated the effect of *rpfB* in THP-1 macrophages at a late phase of replication (72 hours post-infection) using an *Mtb rpfB* gene knockout strain, through global transcriptomic analysis.

Material and Methods: THP-1 macrophages seeded at 7.5 x 105 cells/ mL, were infected at a MOI of 1 with wildtype (WT), Δ*rpfB* mutant and *rpfB*-complemented strains. To elucidate host transcriptomic changes attributed to *rpfB*, mammalian RNA was isolated 72 hours post-infection (P.I) and sequenced using the Illumina High Seq platform. Bioinformatics analysis was performed using the tuxedo suite and Ingenuity Pathway Analysis (IPA). THP-1 cytokine production was analysed at 24-, 48-, and 72 hours P.I using the human *GM-CSF* and *IL-1β* multiplex panel (Bio-Rad Laboratories) in a Bio-Plex 200 System (Bio-Rad Laboratories). RNA sequencing data was validated using quantitative real-time PCR (qRT-PCR).

Results: Global transcriptomic analysis revealed that *rpfB* induced differential transcriptional regulation in THP-1 macrophages. The total number of significantly enriched genes (SDEGs) induced by the WT strain was 5 times more than the mutant. Furthermore, the WT also induced a greater number of networks and upstream regulators. In addition this study showed *rpfB* stimulates, but is not essential to, IFN signalling, Role of JAK family kinases in IL-6 type cytokine signalling and Activation of IRF by Cytosolic PRRs, enhances IL-10 signalling and DC maturation, and enriches Acute phase response signalling, Phagosome formation, LXR/RXR activation, CAMP-mediated signalling, Gαi signalling and GADD45 signalling. In summary, the findings suggest *rpfB* contributes to the host protective immune response against *Mtb* infection. Upstream regulators induced by both infection models were

all cytokines, however, they regulated genes that were exclusive to each pathway and mostly interferon stimulated genes (ISGs) in WT infected macrophages.

Discussion and conclusion: Transcriptomic analysis showed *rpfB* induced recognition of host immunity and enhanced the THP-1 macrophage host immune response during late stages of *Mtb* infection. These findings provide basic evidence, which requires further interrogation, that *rpfB* regulates the immune response through interferon signalling and possibly plays a role in IL-10 signalling and DC maturation. Collectively, these findings indicate *rpfB* contributes to protective immunity of THP-1 macrophages against *Mtb* and may be used as a recombinant in vaccines against active TB, and in combination with LTBI antigens, against LTBI. However, since these observations are reported for the first time, further investigation to validate these findings would be valuable.

1.1 INTRODUCTION

Since the initial isolation and characterization of *Mycobacterium tuberculosis* bacilli in 1882 (Cambau and Drancourt, 2014) the airborne causative agent of tuberculosis has become and remains a major global health concern. Ranking above the Human Immunodeficiency Virus (HIV), TB remains among the top 10 causes of death, and is the leading cause of death due to a single infectious agent (WHO, 2020). In 2019, 10 million people across the globe developed the disease, of which 8.2% were HIV positive. South Africa, one of the top 30 high TB burden countries, was the second country with the highest TB burden (25 %) in 2019. South Africa accounted for 3.6 % of the 10 million incidence cases in 2019 (WHO 2020).

Despite the development and availability of treatment regimens, TB claimed 1.2 million and 208 000 lives among HIV negative and positive people in 2019, respectively (WHO, 2020). Over time, the pathogen has evolved into more complex strains resulting in multi, extensively and totally drug-resistant TB (MDR-, XDR-, TDR-TB) (Gillespie, 2002; Meacci et al., 2005; Naidoo et al., 2017). Approximately 500 000 people worldwide were burdened with Rifampicin resistant TB (RR-TB) in 2019, of which 78% were MDR-TB cases (WHO, 2020) These strains are resistant to multiple anti-TB drugs and are therefore, more successful in manipulating host immune responses. Drug resistance has led to prolonged treatment regimens leading to lower rates of treatment completion as well as increased toxicity (Meacci et al., 2005; Munoz et al., 2015) and mortality, globally (WHO, 2020). Furthermore, 23% of the global population have latent TB infection (LTBI) (WHO, 2020) for which there are no available treatment options. These individuals contain a reservoir of dormant bacilli (Commandeur et al., 2011) and are therefore at risk of developing active disease (WHO, 2020).

The poor level of efficacy of the only existing TB vaccine, *Mycobacterium bovis* Bacillus-Calmette Guerin (BCG), is highlighted by its failure to provide protection against active TB in adolescence and adults (Davenne and McShane, 2016; Kim et al., 2013; Murray et al., 2015)**.** The lack of vaccines or therapeutic alternatives targeting the prevention of active TB from latently infected individuals adds to the many challenges faced in the goal to combat TB. Collectively, these challenges magnify the necessity for extensive research in unravelling novel approaches to elucidate therapeutic targets and to improve the existing vaccine (Ottenhoff and Kaufmann, 2012).

A fundamental process in *Mtb* pathogenesis is its interactions with host (AMs) and (DCs) (Davenne and McShane, 2016; Sohn et al., 2011). Alveolar macrophages are the preferred target cell for uptake and the primary defence cell against the tubercle bacilli since they express multiple pathogen recognition receptors (PRRs) through which *Mtb* pathogen associated molecular patterns (PAMPs) can bind and invade the host cell (Davenne and McShane, 2016; Sohn et al., 2011). Recognition of mycobacterial PAMPs by macrophage PRRs induces a network of signalling pathways that lead to

distinct gene expression profiles at different stages of macrophage infection (Davenne and McShane, 2016; Espitia et al., 2012; Hossain and Norazmi, 2013)**.**

Early innate immune interactions between the host and *Mtb* determines the eventual outcome of infection (Agrawal et al., 2018). The spectrum of clinical outcome includes 4 possibilities - eradication of bacteria via the innate immune response, failure of the innate immune response to do so leads to bacilli growth and multiplication resulting in active disease, LTBI in which the bacilli reside in a non-replicating, low metabolic state (dormancy) within AMs, and resuscitation of dormant bacilli leading to reactivated disease (Downing et al., 2004; (Davenne and McShane, 2016; Marino et al., 2007; Sasindran and Torrelles, 2011)**.**

Beyond our complete understanding, *Mtb* has developed strategies that prevent formation of the phago-lysosome, inhibition of autophagy (Davenne and McShane, 2016; Liu et al., 2017; Saleh and Longhi, 2016) and intracellular trafficking, acquisition of cytosol access, and neutralization of reactive oxygen and nitrogen intermediates (ROI, RNI) (Davenne and McShane, 2016; Liu et al., 2017; Marino et al., 2007). Among other survival mechanisms, these enable *Mtb* to evade host defence responses and influence host cytokine and chemokine profiles (Davenne and McShane, 2016; Liu et al., 2017; Saleh and Longhi, 2016), thus facilitating its survival and persistence within AMs (Davenne and McShane, 2016; Liu et al., 2017).

Over time, many novel *Mtb* antigens have been identified and proposed as vaccine candidates and TB biomarkers, however, only a few are utilised in diagnostics and/or as vaccine antigens in clinical trials for active TB (Ahsan et al., 2016; Ottenhoff and Kaufmann, 2012). This highlights the urgency of developing more efficient strategies in controlling TB and elucidating novel antigens expressed during *Mtb* infection and capable of eliciting an immune response against LTBI (Davenne and McShane, 2016; Ottenhoff and Kaufmann, 2012).

The 16-17 kDa resuscitation promoting factor (*rpf*) was first discovered in *Micrococcus luteus* (Mukamolova et al., 1998), with 5 homologues (*rpfA-E*), which was later identified in *Mtb* (Mukamolova et al., 2002). With the ability to exert biological function in picomolar concentrations, these peptidoglycan (PG) remodelling enzymes (Kana et al., 2008) are largely associated with latent TB and its transition into active disease. Both *in vitro* and *in vivo* studies have revealed that Rpf proteins resuscitate quiescent *Mtb* bacilli (Demina et al., 2009).

Resuscitation promoting factor B (*rpfB*) (*Rv1009*) is both secreted, (Yeremeev et al., 2003) and the only membrane associated protein of its family, with unique structural similarity to lysozymes and soluble lytic transglycosylase (PG cleaving enzymes) in its Rpf domain (Gupta and Srivastava, 2012; Kana and Mizrahi, 2010; Tufariello et al., 2004; Tufariello et al., 2006). These properties permit host recognition

of the protein and exertion of its hydrolysis effects on the PG layer, respectively (Chaves et al., 2015; Demina et al., 2009; Tufariello et al., 2006)**.**

More importantly, analysis of host immune recognition revealed RpfB protein is highly antigenic and immunogenic and is therefore a potential target of the host immune response (Romano et al., 2012; Yeremeev et al., 2003). Some cellular and *in vivo* studies have demonstrated that exposure to the RpfB protein leads to the development of T cell immunity, specifically the Th1 phenotype (Kim et al., 2013). In addition, cytokine profiles of murine bone marrow derived macrophages (Russell-Goldman et al., 2008) and dendritic cells (Kim et al., 2013) show increased levels of pro-inflammatory cytokines when infected with mycobacterial *rpfB* deficient strains compared to wild type strains and uninfected controls. As an antigen, RpfB has potential to generate protective immunity, supported by the induction of expanding memory $CD4^{+}/CD8^{+}$ $CD44^{high}$ $CD62^{low}$ T cells in the spleen of *Mtb* infected mice (Russell-Goldman et al., 2008). RpfB was shown to interact with DCs expressing Toll-like receptor (TLR) 4 to regulate innate immunity and activates adaptive immunity, assessed specifically through binding of RpfB to TLR4 of DCs. The immune response to *Mtb* is multifaceted and incompletely characterized, which further impedes attempts to develop and/or improve new tests, vaccines and therapeutic treatments (O'Garra, 2013). Narrowing down the analysis of the immune response to specific pathogenic determinants may elucidate integral biomarkers and therapeutic targets that could be interrogated in vaccine and treatment regimens associated with the biological function of that determinant (Agarwal et al., 2009; Gupta and Srivastava, 2012; Kana et al., 2008).

The transcriptome of a host or pathogen is defined as the repertoire of transcripts and their quantity has been used to decipher molecular mechanisms that are involved during the pathogenesis process (Lowe et al., 2017). Analyzing the transcriptome by simultaneous identification and quantification of known and novel transcripts, as well as gene expression patterns has revolutionized biomedical research by facilitating interpretation of functional components of the genome, thus in revealing molecular constituents of cells (O'Garra, 2013; Wang et al., 2009)**.** With the rapid development and evolution of next generation sequencing and maturation of bioinformatics tools, RNA sequencing is at the forefront of high throughput transcriptome analysis (Wolf, 2013)**.** Microarray analysis has long been the preferred method of analysis due to its popularity among researchers, ease of analysis and cost effectiveness. However, recent studies have shown RNA sequencing overcomes limitations of microarrays and is superior in detecting low abundance transcripts and differentiating biological transcript isoforms (Ignatov et al., 2013; Zhao et al., 2015).. Traditionally, qRT-PCR is a method that is often used to validate gene expression levels quantified by high throughput technologies (Costa et al., 2013). While RNA sequencing and qRT-PCR can be used for cytokine quantification, the most recent Luminex and Bioplex technology platforms permit direct analysis of multiple analytes within a single sample in a robust, rapid, accurate manner, without the need for bioinformatics tools (Cohen et al., 2015). This

approach is appealing for experimental studies interrogating the production of multiple cytokines from a single sample under multiple conditions.

As a result of its importance in resuscitation, several studies (Downing et al., 2005; Russell-Goldman et al., 2008; Tufariello et al., 2004; Tufariello et al., 2006) to date have focused on elucidating and interrogating the role and impact of *rpfB* on *Mtb* growth kinetics, resuscitation of dormant bacilli and persistence during chronic *Mtb* infection both *in vitro* and *in vivo* using single and multiple *rpf* deletions that include the loss of *rpfB*. There are less studies that focus on the impact of *rpfB* alone on the host immune response during active *Mtb* infection. A significant study conducted by (Kim et al., 2013) showed *rpfB* has the ability to induce a pro-inflammatory, Th1 immune response via DCs. While DCs are important mediators of the adaptive immune response, macrophages are the target for therapeutic intervention since it's the first to interact with *Mtb* and serves as a reservoir for dormant bacilli (Downing et al., 2005; Russell-Goldman et al., 2008; Tufariello et al., 2004; Tufariello et al., 2006). To date, no study has been performed to determine the regulatory effect of *rpfB* on the THP-1 macrophage host immune response using a global transcriptome approach.

The current study revealed *rpfB* stimulates, but is not essential to, IFN signalling, Role of JAK family kinases in IL-6 type cytokine signalling and Activation of IRF by Cytosolic PRRs, enhances IL-10 signalling and DC maturation, and enriches Acute phase response signalling, Phagosome formation, LXR/RXR activation, CAMP-mediated signalling, Gαi signalling and GADD45 signalling. In summary, the findings suggest *rpfB* contributes to the host protective immune response against *Mtb* infection.

1.2 CHAPTER 1: LITERATURE REVIEW

1.2.1 Ongoing TB epidemic

Despite the progressive reduction of TB burden in most countries and all World Health Organization (WHO) regions, (WHO End TB strategy, 2020), 10 million people were burdened with the disease in 2019, globally. The largest number of incident cases occurred in South East Asia (44 %), Africa (25 %) and Western Pacific (18%) (WHO, 2020). Eight countries of the top 30 high TB countries, India (26 %), Indonesia (8.5 %), China (8.4 %), Philippines (6 %), Pakistan (5.7 %), Nigeria (4.4 %), Bangladesh (3.7 %) and South Africa (3.7 %) ,accounted for two thirds of the global total number of incident cases (WHO, 2020) (Figure 1.2.1.).

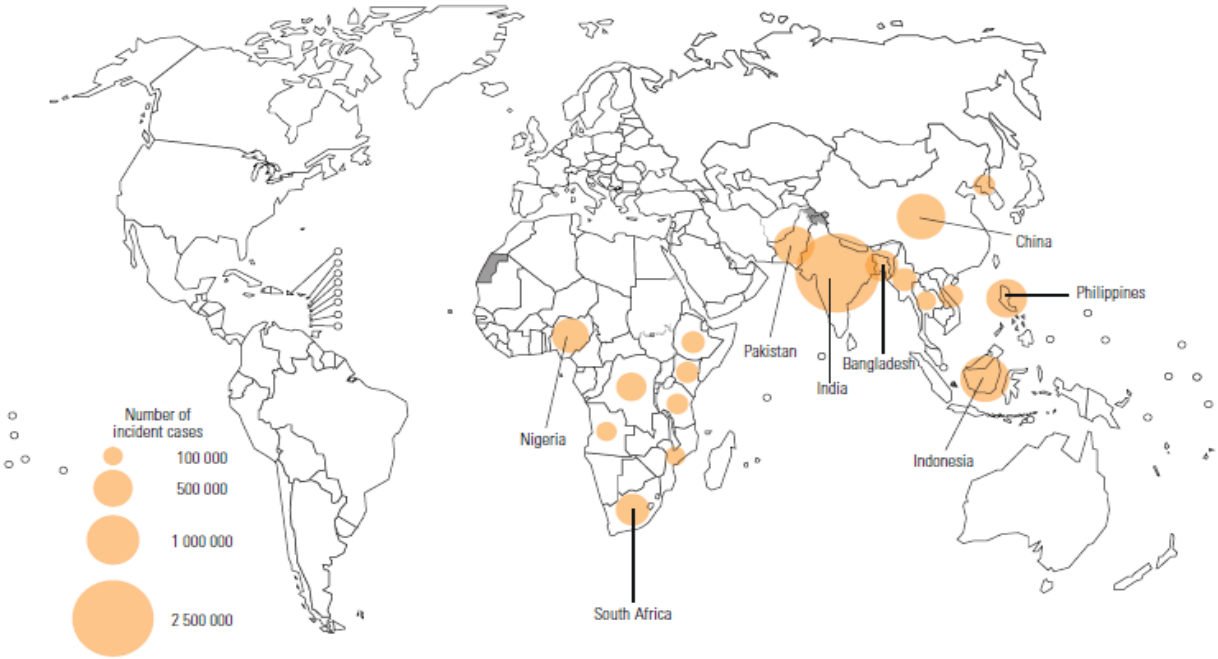

Figure 1.2.1: Geographical distribution of annual TB incidence in 2019 for countries with at least 100 000 incident cases. India, Indonesia, China and the Philippines displayed the highest burden (WHO, 2020).

In 2019, 8.2 % of global TB incidence was among people co-infected with HIV (WHO, 2020). The African region accounted for the majority of these cases with certain parts of Southern Africa exceeding 50 % (WHO, 2020) (Figure 1.2.2). HIV-TB co-infection resulted in 208 000 deaths in 2019 (WHO, 2020). HIV compromises a patients' immune system which increases the patients' susceptibility to TB. According to WHO, 2020, those living with HIV (38 million) are at 18 times higher risk for developing TB than HIV negative people.

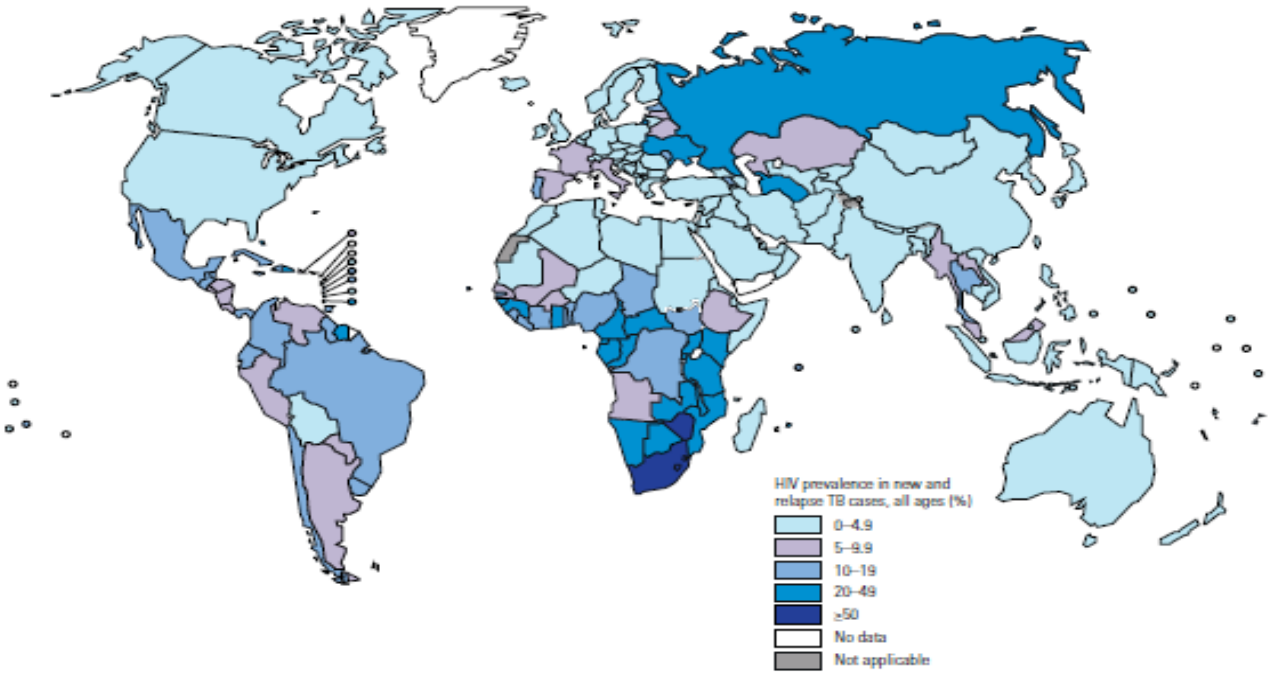

Figure 1.2.2: Geographical distribution of HIV prevalence in new and relapse TB cases, in 2019, displaying increased prevalence in the African region (WHO, 2020).

Among HIV negative people, 1.2 million succumbed to TB. The African region, alongside South East Asia, produced the highest percentage of TB deaths among HIV negative people (Figure 1.2.3). Collectively, these regions account for 85% of the total number of TB deaths in HIV negative and positive people in 2019. According to WHO, 2020 reports, many of the deaths were preventable if patients were diagnosed early and provided appropriate treatment since statistical evidence illustrates a treatment success rate of 82% in 2016 among those whose TB was diagnosed early and treated.

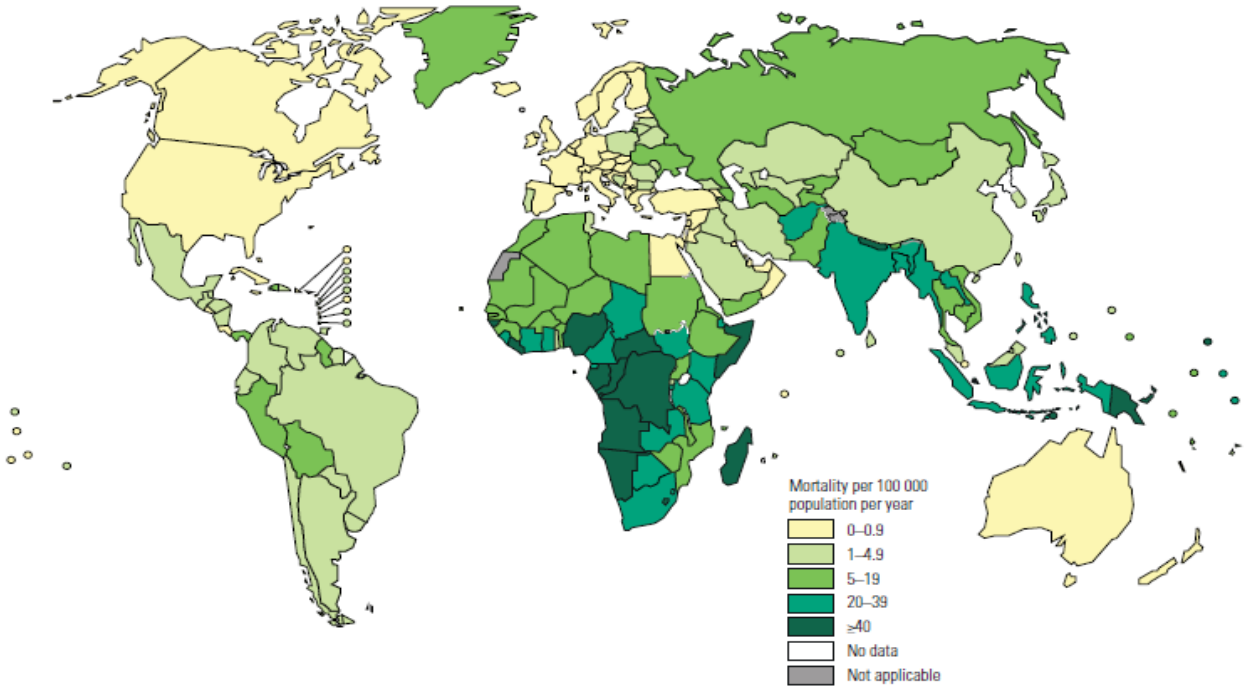

Figure 1.2.3: Geographical distribution of TB mortality rates among HIV negative people in 2019. The African region and South East Asia display the highest TB mortality rates (WHO, 2020)

1.2.2 Drug resistant *Mtb* strains

The global crisis of TB disease is further compounded by the emergence of drug resistant strains that cannot be eradicated by standard TB treatment regimens. The failure of 2 effective first line drugs, rifampicin (RIF) and isoniazid (INH), to kill *Mtb* bacilli resulted in the emergence of a multi-drug resistant strain (MDR-TB) (WHO, 2020). In some cases, MDR-TB evolved into a more lethal form of drug resistance known as extensively drug resistant *Mtb* (XDR-MTB) in which case the bacilli are resistant to first line drugs, at least one drug each from the injectable second line anti-TB drugs and fluoroquinolones (Zager and McNerney, 2008). In other cases, isolates may become totally drug resistant (TDR-TB) for which there are no effective treatments available. In 2019, 3.3% of global TB incidence cases (Figure 1.2.4A) and 18% of previously treated cases were MDR/RR-TB. China reported the highest incidence rate followed by India and the Russian Federation (Figure 1.2.4B).

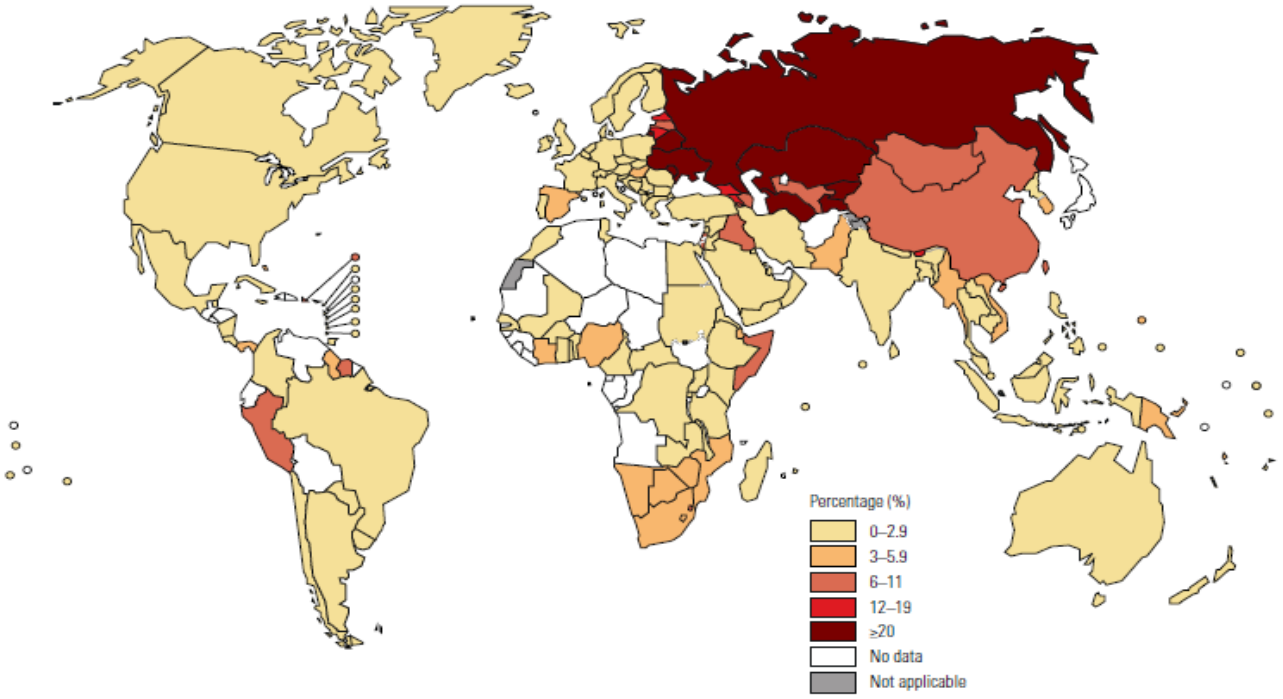

Figure 1.2.4A: Geographical distribution of new MDR/RR-TB incidence cases in 2019. Several countries of the former Soviet Union show the highest proportion of incidence (WHO, 2020)

Figure 1.2.4B: Geographical distribution of estimated incidence of MDR/RR-TB in 2020, for countries with at least 1000 incident cases. India, China and the Russian Federation accounted for nearly 50 % of the total TB incidence cases (WHO, 2020).

1.2.3 *M. tuberculosis* strain diversity and predominant genotypes in KZN

M. tuberculosis strain diversity varies in different countries and regions within a country (Maguga-Phasha et al., 2017). Previous geographical-genotyping studies identified the W/Beijing and/or Latin-American-Mediterranean (LAM) strains as two of the most widespread predominant sources of drug susceptible (DS-TB) and/or MDR and/or XDR-TB in many TB burdened provinces – Free-State, Gauteng, KwaZulu-Natal (KZN), Limpopo, North West and Western Cape (Hove et al., 2015; Van der Spoel van Dijk et al., 2016), countries – Brazil and Mozambique (Koivula et al., 2010) and cities – Pretoria (Nchabeleng et al., 2012) and Cape Town (Wilkinson et al., 2005). In 2005, KZN experienced the largest global outbreak of XDR-TB in Tugela Ferry, South Africa (SA) (Gandhi et al., 2014; Gandhi et al., 2006). The causative agent was later identified as the highly virulent F15/LAM4/KZN strain, evolved from and initially discovered as an MDR-TB strain in South Africa in 1994 (Cohen et al., 2015; Pillay and Sturm, 2007).

When assigned to spoligotype lineages to determine the geospatial distribution of *Mtb* genotypes in Africa, thousands of clinical isolates from 25 African countries accounted for T (24.8%), LAM (19.3%), Cameroon (11.4%), H (9.0%), Beijing (7.4%), and CAS (6.4%). These lineages accounted for 78.3% of all isolates from the Africa region (Figure 1.2.5) (Chihota et al., 2018).

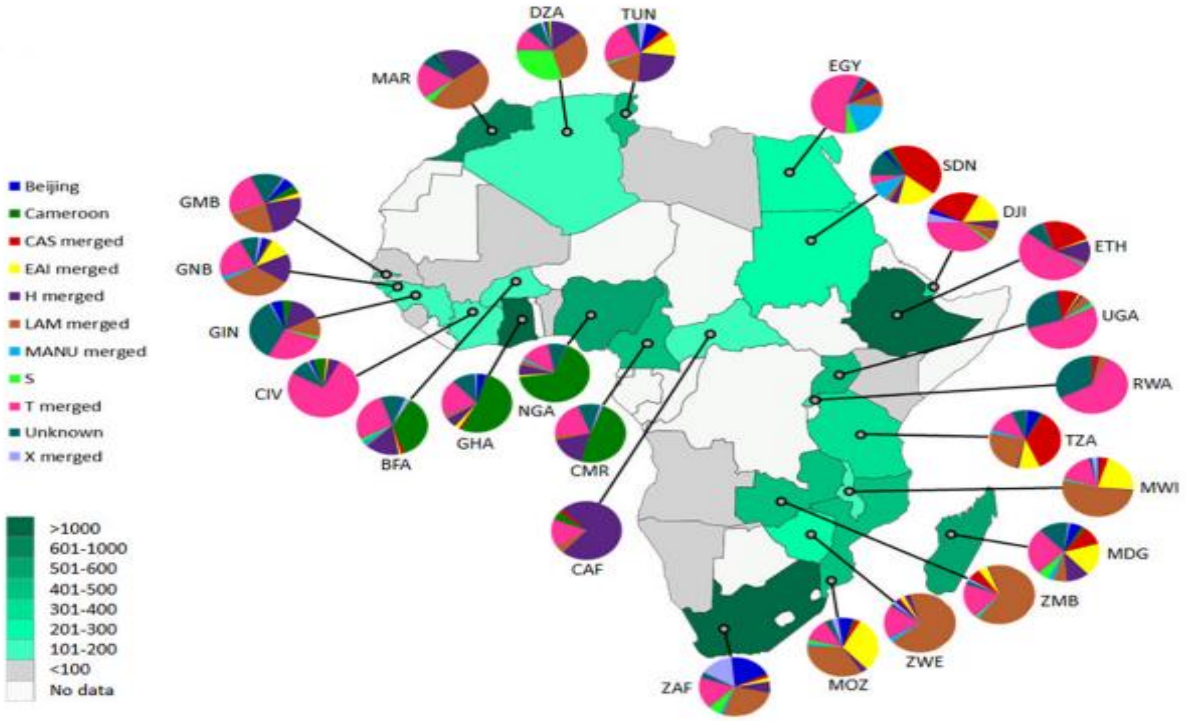

Figure 1.2.5: Geographical distribution of *Mtb* lineages in Africa. Each pie chart segment reflects the relative proportion of *Mtb* isolates belonging to respective major lineages for each country. Each country has been shaded according to the number of isolates contributed to the analysis (Chihota et al., 2018).

1.2.4 Impact of COVID-19 on Tuberculosis

In January 2020, a newly emerged global pandemic, COVID-19, caused by a novel pathogen, Severe Acute Respiratory Syndrome Coronavirus-2 (SARS-CoV-2) has burdened millions of people across the globe. By the first week of April 2020, there were a million incident cases of which 50 000 resulted in death (Togun et al., 2020).The symptoms of the disease vary ranging from flu-like symptoms in mild cases to severe acute respiratory distress in its worst form (Togun et al., 2020). Severe pneumonia and potential long-term pulmonary damage were noticed in elderly people and those with comorbidities (Togun et al., 2020).

Despite the urgency to treat, manage and find a cure for COVID-19, TB remains a global threat, claiming thousands of lives each year with millions of incident cases. Since the emergence of the pandemic, resources have been diverted to COVID-19 management, testing and diagnostic capacity. It is anticipated that the divergence may cause hindrance to important milestones in TB treatment, management (Togun et al., 2020), and the WHO's End TB Strategy proposal of ending the TB epidemic in 15 years (WHO, 2020). The extent to which health services were diverted has resulted in 25-50% decrease in the number of people diagnosed and treated for TB (WHO, 2020) (Figure 1.2.6).

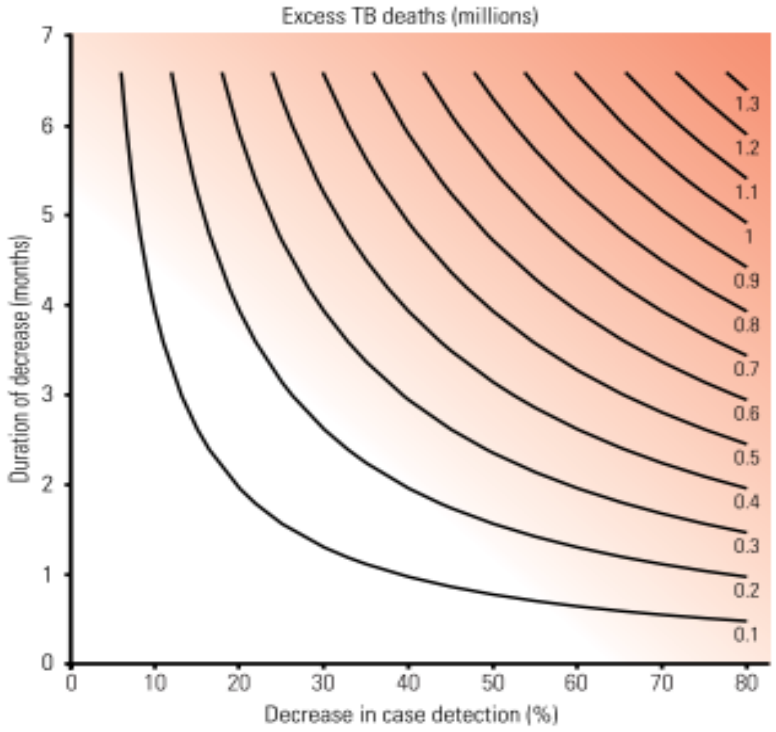

Figure 1.2.6: **Estimated impact of the COVID-19 pandemic on global TB mortality in 2020. The graph includes different combinations of decreases in case detection and the duration of these decreases (WHO, 2020).**

It is predicted that the economic impact of the pandemic will worsen GDP per capita and undernutrition, two key determinants of TB incidence. The impact on livelihoods of those faced with loss of income or unemployment may also increase the percentage of people with TB and burden their households with increased costs. Forty-three countries including 13 high TB burden countries, have reported the use of GeneXpert instruments for detection of SARS-CoV-2 instead of TB diagnostics. Eighty-five countries including 20 high TB burden countries, have had staff reassigned from TB programmes to COIVD-19 response duties. Fifty-two countries including 14 high TB burden countries, reallocated budgets to treat, control and manage COVID-19 (WHO, 2020).

Of the million incident cases including 50 000 resulting deaths observed by April 2020, Africa accounted for 3766 of these cases and 96 deaths (Togun et al., 2020). Many studies indicate the quality of TB care in Africa is sup-optimal even prior to the emergence of COVID-19. Given the impact of the disease at the macroeconomic level, it is expected that COVID-19 will worsen patient care and efforts to control and manage TB in Africa. As an example, Nigeria, the highest TB burdened country in Africa and one of the 30 high TB burden countries globally, has announced 300 of their GeneXpert instruments will be diverted to improve COVID-19 diagnosis. This will ultimately impact the control of TB, including routine diagnosis, treatment monitoring and provision of preventative therapy. The same various socioeconomic and behavioural factors that enhance transmission of *Mtb* are the same factors

that could potentially enhance SARS-CoV-2 in Africa. Interventions such as physical distancing, constant hand washing, and community lockdowns to reduce COVID-19 transmission is more challenging for the impoverished who likely reside in crowds, some with limited or no water access, and with minimal earnings. In addition, adolescent TB is commonly acquired within their household therefore with implementing social distancing, households will be crowded for longer periods, potentially exposing more children to infectious TB. Collectively, these findings indicate the impact of COVID-19 in Africa will be devastatingly worse in poor communities that already have pre-existing challenges of accessing basic healthcare and facilitating TB and HIV management (Togun et al., 2020).

To alleviate some of the consequences resulting from resource and health services divergence on essential TB services globally, the WHO has recommended expanded use of digital technologies for remote advice and support, implemented in 108 countries including 21 high TB burden countries thus far. Preference to those on home-based treatment to reduce the need for visits to health care facilities by providing a month's supply of TB drugs, so far implemented in a 100 countries including 25 high TB burden countries (WHO, 2020).

1.2.5 TB Diagnostics

Despite the intensified effort of multiple countries to improve TB diagnosis, there was still a large gap between newly diagnosed people (2.9 million) and those estimated to have developed TB (10 million) in 2019 (WHO, 2020). This large gap was attributed to underreporting of diagnosed individuals and/or underdiagnoses due to the inability to access healthcare or if accessible, are incorrectly diagnosed (WHO, 2020). The perfect TB diagnostic tool would produce immediate and accurate results for all strains of TB in HIV negative and positive populations, low cost, patient and user friendly, and be easily accessible and sustainable in developing countries (Mulder et al., 2017).

The gold standard of TB diagnosis is sputum smear microscopy. However, in HIV-coinfected patients, this method has limited sensitivity and cannot differentiate between susceptible and drug resistant *Mtb* (Vassall et al., 2017). Standardized drug susceptible testing (DST) permits identification of drug susceptible or resistant *Mtb* strains but at a long turnaround time of 8-12 weeks on solid media (Caminero et al., 2017; Migliori et al., 2008). This renders this method undesirable, especially in MDR and XDR infected patients that require immediate treatment (Caminero et al., 2017; Migliori et al., 2008). Automated liquid culture systems were developed to reduce turnaround time and increase sensitivity. The BACTEC 460 TB radiometric system was introduced as a major advancement but was shortly replaced by the Mycobacteria Growth Indicator Tube system (MGIT) for its efficiency in rapidly detecting resistance to first- and second-line TB drugs in a shorter turnaround time of just days, rather than weeks. However, the system is still uneconomical in low resource countries (Migliori et al., 2008). The microcolony method permits rapid detection of drug resistance directly from sputum samples in

one week and is relatively economical. Other phenotypic methods include TK Medium, Microscopic Observation Drug Susceptibility Assay (MODS) and FASTPlaque-Response bacteriophage assay, all of which are more cost effective but not user friendly and requires increased standards of quality control and biosafety (Migliori et al., 2008).

Since rifampicin resistance is used as a predictor of MDR-TB in patients who have previously received treatment, the need to identify specific mutations responsible for drug resistance has played a vital role in the development of many rapid molecular diagnostic tools. Some of these methods include nucleic acid amplification and sequencing or hybridization. These techniques specialize in detection of TB complex isolates, drug resistance and alleles associated with drug resistance in clinical isolates like sputum in 24-48 hours without having to grow cultures (Caminero et al., 2017; Migliori et al., 2008). The sequencing and polymerase chain reaction (PCR) methods can also be used to detect mutations through wild type primer sequences or specific probes, but is expensive and in the case of sequencing, time consuming. Line probe assays (LPA), also known as reverse hybridization-based assays are more useful for its cost effectiveness. Detection of mutations in genes associated with rifampicin (*rpoB*) and isoniazid (*katG* and *inhA*) drug resistance can be detected by hybridization of wild type and specific mutation sequences in the clinical isolate being tested (Caminero et al., 2017; Migliori et al., 2008). It exhibits high specificity and moderate sensitivity but is accurate in detecting drug resistance directly from patient samples within 5-7 hours (Caminero et al., 2017; Migliori et al., 2008). The disadvantage is that only a limited number of genes can be analysed at once and it fails to distinguish insertion mutations. Despite it being far more economical than sequencing, rapid and user friendly, it's still expensive and requires sophisticated laboratory infrastructure which is a limitation in low income countries (Caminero et al., 2017; Migliori et al., 2008). In 2010, Xpert MTB/RIF was introduced as a WHO recommendation for use as a primary diagnostic tool of TB. Detection of rifampicin resistance is performed by amplification of a fragment of the *rpoB* gene including its hot spot which is then hybridized to multiple molecular beacon probes that is labelled with fluorescent dyes within 2 hours. The disadvantage lies in its inability to detect isoniazid resistance which is failure to detect MDR-TB in its earliest form since isoniazid resistance was observed in whole genome sequencing studies to occur before rifampicin resistance in all lineages, geographical regions and time periods. Overall, Xpert MTB/RIF combats many of the previous concerns by providing superior specificity, sensitivity, including in HIV positive populations. It is user friendly and minimises cross contamination between samples (Caminero et al., 2017; Nguyen et al., 2019; Vassall et al., 2017). To interrogate the genotype of any organism, sequencing is the best technology which can be targeted or next generation sequencing (whole genome). Along with identifying species, detecting drug resistance and predicting organism evolution, this method is advantageous for identifying both known and unknown mutations. Commercial NGS-based kits for targeted sequencing are available and used to analyse the whole genome of *Mtb* in 2 days, to identify first and second line drug resistance using the torrent personal

genome machine (PGM). The limitations of using sequencing, especially in low income countries, is the requirement of robust bioinformatics software and database tools, skilled personnel in data analysis, high cost, high quality input DNA (Nguyen et al., 2019).

1.2.6 TB therapy

Anti-TB drugs are grouped according to efficacy, and their ability to successfully treat TB patients relies on their bactericidal and sterilising capacity (Migliori et al., 2008). The standard treatment regimen for DS-TB is a combination of rifampicin (RIF), isoniazid (INH), ethambutol (EMB) and pyrazinamide (PZA) over 6 months (2 months intensive, 4 months continuation phase) (Meyer-Rath et al., 2012). While the standard treatment is effective when taken as prescribed, multiple challenges of the treatment regimen often lead to patient non-compliance. As a consequence of non-compliance, intolerance and sub-optimal drug levels, susceptible and MDR-TB strains develop resistance to individual and/or multiple anti-TB drugs through random point mutations and/or sequential accumulation of mutations in various drug resistance genes (Almeida Da Silva and Palomino, 2011; Bryson et al., 2019; Kwon et al., 2017; Nguyen et al., 2019; Zhang et al., 2009). Treatment of MDR-TB include at least 5 drugs (including one injectable) in the intensive phase (8 months) followed by at least 4 oral drugs in the continuation phase (up to 12 months). Due to the extent of drug resistance in XDR-TB strains, treatment options are limited. The most promising outcome for management of XDR-TB was observed when patients were treated with at least 6 drugs in intensive phase (up to 9 months) and 4 in continuation phase (total of 25 months), in addition to incorporating fluoroquinolones (Falzon et al., 2013).

Over the past few years, researchers have developed new, and repurposed existing, anti-TB drugs associated with all types of TB. The current drug pipeline includes 8 candidates (old and new) under preclinical and phase II – III trials for MDR and XDR-TB (D'Ambrosio et al., 2015; Tiberi et al., 2018). Approved by the US Food and Drug administration (FDA) and European Medicines Agency, Bedaquiline and Delamanid were released in 2012-2013 as the first two new anti-TB drugs (D'Ambrosio et al., 2015; Sloan and Lewis, 2016; Tiberi et al., 2018). Bedaquiline exerts bactericidal and sterilizing activity by acting as an inhibitor of the mycobacterial ATP synthase proton pump. Previous clinical trials have shown that MDR-TB treatment regimens that contain bedaquiline, in combination with linezolid, resulted in higher favourable outcomes than those without bedaquiline (Zhang et al, 2018). However, there were multiple concerns regarding patient safety and drug efficacy.these include potential risk of prolonged QT interval (disorder of the hearts electrical system), cross resistance between clofazimine and bedaquiline increases the risk of primary resistance to bedaquiline, and the drug has a long half-life which could result in monotherapy exposure.Despite these concerns and challenges, the use of bedaquiline offers an opportunity for successful treatment against MDR- and XDR-TB (Zhang et al, 2018). Delamanid is a mycolic acid biosynthesis inhibitor, tested against MDR-

TB (Zhang et al, 2018; Schnirring, 2019). With more research underway, a phase 3 clinical trial showed no significant reduction in time to sputum culture conversion but did reveal it was safe to use and well tolerated. Like bedaquiline, one of the concerns using delamanid is increased QT interval. Despite its safety and tolerance, the WHO has classified it as group C drug and requires stronger evidence as priority drug (Schnirring, 2019).

1.2.7 Vaccines

The only licensed vaccine administered globally, Bacille Calmette-Guerin (BCG), is used for immunization of infants for its protective efficacy against severe meningeal and disseminated TB mainly in children (Ottenhoff and Kaufmann, 2012; Ritz et al., 2012). The vaccine fails to provide consistent protective efficacy in adolescents and adults (Ottenhoff and Kaufmann, 2012; Ritz et al., 2012). Failure to provide adequate protection could be a result of the immunological memory induced at a stage when the immune system is not fully developed (infancy) which later proves to be inadequate in adolescence, a stage during which there is high chances of developing active disease. Other possibilities include comorbidities such as HIV and helminth infections (Ottenhoff and Kaufmann, 2012). It is evident a stronger vaccine is needed for the control of TB, one that can improve priming and protective effects of BCG or one that is superior (Ottenhoff and Kaufmann, 2012). However, the challenge in developing new vaccines against *Mtb* is that its control depends on the cellular immune response, like many other pathogens. Better preventive methods need to be developed to inhibit *Mtb* transmission through vaccines that prevent establishment of *Mtb* infection progression towards active disease (Ritz et al., 2012).

An investigational candidate vaccine, M72/AS01$_E$ (GlaxoSmithKline) that was tested in Kenya, South Africa and Zambia was found to provide significant protective efficacy (point estimate of vaccine efficacy was 54 %) in a Phase IIb trial in people with latent TB infection. The vaccine composition included the M72 recombinant fusion protein, derived from immunogenic antigens (Mtb32A and Mtb 39A), AS01 adjuvant, component of the RTS,S/AS01 malaria vaccine, and recombinant zoster vaccine (Shingrix). The vaccine was efficient in eliciting specific lymphoproliferation and interferon gamma production in both latent and actively infected individuals. It also displayed safety and induced humoral and cell mediated immunity in healthy and HIV infected individuals, *Mtb* infected adults and infants and BCG vaccinated infants. In a total sample population of 3283, a similar percentage of people (1.6 % in the vaccine group and 1.8 % in the placebo group) reported at least one serious adverse event within 6 months after the final dose of either injection. Both groups reported pyrexia and hypertensive encephalopathy thought to be related to the trial regimen. Overall, the vaccine group reported 2 cases of potential immune mediated diseases, 7 deaths of which 6 were trauma related and none related to the trial regimen, and the placebo group reported 5 cases of potential immune mediated diseases and 17 deaths of which 8 were trauma related. The findings also revealed 28 of 33 pregnant woman who

received either vaccine were able to deliver healthy infants. The M72/AS01$_E$ vaccine significantly reduced incidence of pulmonary TB compared to the placebo group in *Mtb* infected, BCG vaccinated, HIV negative adults. This vaccine provides the opportunity to elucidate mechanisms through which it offers protection against *Mtb*. (Brazier and McShane, 2020; Hatherill et al., 2019; Van Der Meeren et al., 2018; Vekemans et al., 2019).

1.2.8 Characteristics and lipid profile of *Mtb* bacilli

M. tuberculosis is structurally a Gram-Positive organism but also displays properties of Gram-Negative bacteria. The ability to retain the crystal violet dye is weak or in some cases, like Gram Negative bacteria, displays complete inability to retain the dye (Hett and Rubin, 2008). The slow growing tubercle bacilli are rod shaped cells that stain acid fast due to its high lipid content (Figure 1.2.7) (Springer et al., 1996; Meena and Rajni, 2011).

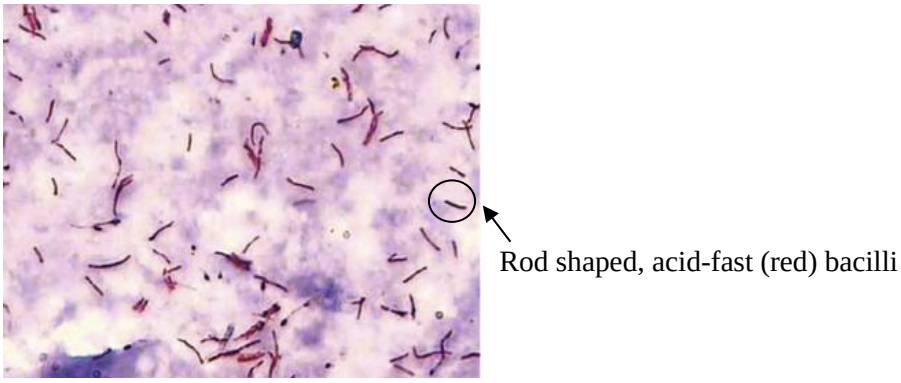

Figure 1.2.7: Microscopic image of tubercle bacilli after Ziehl-Nielsen staining.

M. tuberculosis can be distinguished from other bacteria by its lipid rich cell wall and a cell envelope abundant in mycolic acids (Ghazaei, 2018; Hett and Rubin, 2008). The cell wall outer layer contains lipids such as lipoarabinomannan (LAM), lipomannan (LM), phthiocerol dimycocerosate (PDIM), cord factor, phosphatidyl inositol mannosides (PIM) and sulfolipids (Figure 1.2.8) (Ghazaei, 2018; Hett and Rubin, 2008). The mycolic acids are an essential component of *Mtb* virulence and is the primary determinant of cell wall permeability due to its hydrophobic nature and its formation of a capsule around the cell (Figure 1.2.8) (Ghazaei, 2018; Hett and Rubin, 2008). This unique feature proves advantageous under stressful conditions such as desiccation, antimicrobial attack, osmotic shock, and host defence responses. They can protect the cell from external forces such as lysozyme, cationic proteins and even oxygen radicals found in phagosomes. This complex is the essential core of the pathogens cell wall and is therefore the target of many antimicrobial drugs (Hett and Rubin, 2008).

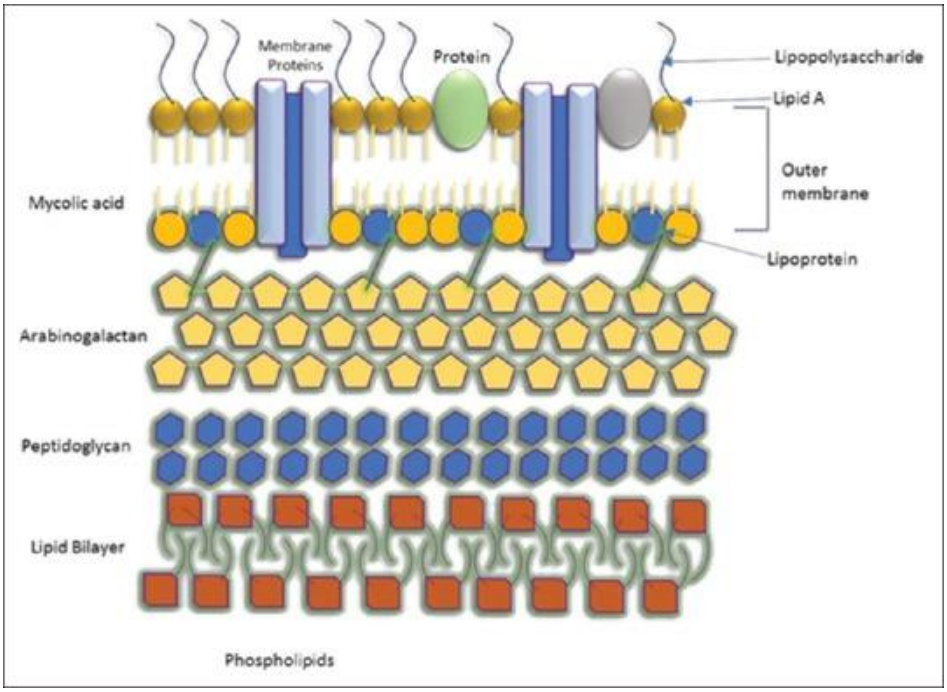

Figure 1.2.8: Lipid rich cell wall layers of *Mtb* (Ghazaei, 2018).

1.2.9 Pathogenesis of *Mtb*

1.2.9.1 Transmission

M. tuberculosis is transmitted through internalization of infectious aerosol droplets. The aerosol droplets measure 0.5-7 µm and contain at least 1 – 400 bacilli. When infected people generate droplets, by sneezing or coughing, a susceptible individual that inhales the droplets is at risk of developing TB (Churchyard et al., 2017; Sakamoto, 2012). The smaller particles traverse the nasal passages, upper respiratory tract and can avoid defences of the bronchi and settle in the alveoli of the lungs where phagocytosis or disease progression occurs (Ahmad, 2011). In an airborne state, the droplets become evaporated, but the desiccated bacilli remain in airborne circulation for prolonged periods (Churchyard et al., 2017). Exposure to infectious droplets containing tubercle bacilli results in either asymptomatic latent infection, in which the bacilli reside in a dormant state within the host alveolar macrophages, or active disease characterized by excessive coughing - with blood, fever and weight loss. The outcome is dependent on host and bacterial factors and the determining interaction between the two (Sakamoto, 2012) (Figure 1.2.9).

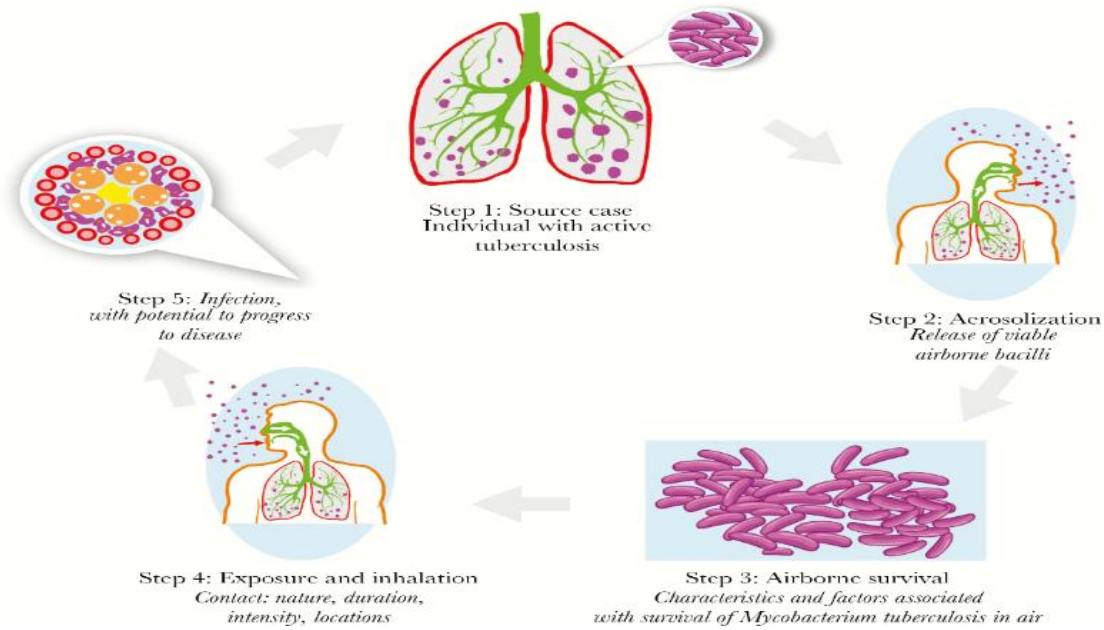

Figure 1.2.9: Outline of *Mtb* transmission and pathogenesis (Churchyard et al., 2017)

1.2.9.2 Early innate immune response

A subset of individuals exposed to *Mtb* are capable of inducing sterilising immunity often referred to as early clearance, before adaptive immunity develops (Brazier and McShane, 2020). Once the bacilli from inhaled droplets reach the alveoli of the lungs, *Mtb* first encounters phagocytic cells such as alveolar macrophages (AM) (Philips and Ernst, 2012). The forefront of host-*Mtb* interactions is focused on AMs since it serves as the reservoir for dormant bacilli and is the primary target cell of early infection (Verrall et al., 2014). The recognition of *Mtb* by AMs through phagocytosis leads to the production of pro-inflammatory cytokines, chemokines and antimicrobial peptides, which activates other immune target cells. The subsequent inflammatory response leads to intracellular mycobacterial killing (Verrall et al., 2014). However, the same factors that influence eradication of intracellular *Mtb* like pathogen recognition, cytokine production, intracellular killing and mode of macrophage death, also influence mycobacterial growth and manipulation of AMs by *Mtb* that favour its survival. Hence, the outcome of infection largely depends on the interaction between the AMs and *Mtb* at the early stage of infection (Verrall et al., 2014).

1.2.9.3 Airway epithelial cells

Even though AMs are the primary target, epithelial cells are the first to initiate defence against inhaled *Mtb* and they play a significant role in initiating airway defence responses in the lung (Brazier and McShane, 2020; Li et al., 2012; Ryndak and Laal, 2019). Airway epithelial cells (AEC) express multiple PRRs and surfactant proteins that bind to mycobacterial cell wall components. Resulting in the activation of various signalling pathways and production of *TNF-α, IFN-γ, IL-6* and *IL-8* cytokines (Brazier and McShane, 2020; Harriff et al., 2014; Li et al., 2012). AECs are potent enablers of crosstalk based on their efficient response to *IL-1β* and type I interferons that are released by infected macrophages. They also stimulate *IFN-γ* production by directly presenting intracellular antigens to resident CD8+ T cells via MHC class I molecules (Brazier and McShane, 2020; Harriff et al., 2014; Li et al., 2012).

1.2.9.4 Alveolar macrophages

Once *Mtb* pathogen associated molecular patterns (PAMPs) are recognised by specific AM pattern recognition receptors (PRRs), the process of phagocytosis is activated and mediated by complement receptor (*CR4*) (Brazier and McShane, 2020). In the absence of the complement, phagocytosis is initiated by ligation of mannose receptors (*MR*) that are highly expressed on AMs with mannose capped lipoarabinomannan of non-opsonized *Mtb* (Verrall et al., 2014). The binding of specific PRRs to *Mtb* PAMPs induces specific events of immune related responses. When *Mtb* PAMPs are recognised by AM Toll-like receptors (*TLRs*), nucleotide-binding oligomerization domain (*NOD*) – like receptors and c-type lectins mediates cytokine signals that influence mycobacterial eradication (Verrall et al., 2014). For example, the consequential binding of *TLR2* and *TLR2* as a dimer with *TLR6* with *Mtb* lipoarabinomannan and a lipoprotein, respectively, induces signals through *MyD88* and nuclear transcription factor–$_{K}$B (*NF-* $_{K}$*B*) to promote production of tumour necrosis factor-α (*TNF-α*), an inflammatory cytokine. However, when *MyD88* and *NF-* $_{K}$*B* are activated via binding of *TLR4* to a heat labile cell associated factor, it is interleukin-1β (*IL-1β*) production that is induced. Endosomally located *TLR8* and *TLR9* binds nucleic acids of intraphagosomal *Mtb* to activate *NF-* $_{K}$*B* – dependent cytokines and type I interferons. Binding of *NOD2* induces upregulation of autophagy and cathelicidin production which reduces intracellular growth of *Mtb*. Ligation of *NOD*-like receptor or *IFN*-inducible protein 2 receptor promotes activation of the inflammasome, a multiprotein complex that contains caspase-1 that leads to *IL-1β* activation. Apart from *MR*, two other C-type lectins that are capable of recognizing *Mtb* are dendritic cell-specific intracellular adhesion molecule-3-grabbing non-integrin (*DC-SIGN*) and macrophage C-type lectin. *Mtb* induces expression of *DC-SIGN* on alveolar macrophages and its binding to the pathogens mannose-capped lipoarabinomannan activates an anti-inflammatory signal (Verrall et al., 2014).

1.2.9.5 Intracellular eradication of *Mtb*

Once recognition and engulfment of the pathogen is complete, the phagosome containing intracellular *Mtb* matures through the endocytic pathway. The phagosome undergoes acidification through H^+-ATPase and cathepsin D, a hydrolytic enzyme. Further oxidative stress is induced through upregulation of nitric oxide synthase and nicotinamide adenine dinucleotide phosphate oxidase to produce reactive oxygen and nitrogen intermediates (Mahamed et al., 2017; Sharma et al., 2012; Verrall et al., 2014). This process is influenced by the synergistic action of *IFN-γ* and *TNF-α*. When bound by *MR*, mannose-capped lipoarabinomannan has the ability to inhibit phagolysomal fusion and downregulates transcription of *NF-* $_K$*B*, activating protein-1, signal inducer and activator of transcription, all via peroxisome proliferator-activated receptor. This favours an anti-inflammatory cytokine response and a less efficient oxidative response (Mahamed et al., 2017; Sharma et al., 2012; Verrall et al., 2014). Macrophages may overcome this inhibition by forcing lysosomal fusion by deploying autophagosomes that engulf the *Mtb* containing phagosomes. This process of autophagy is influenced by *IFN-γ*, *TLR4* via toll-IL-1 receptor domain containing adaptor-inducing *IFN-β* signalling, and vitamin D. Infected macrophages release hepcidin and cathelicidin that have direct activity against *Mtb* (Mahamed et al., 2017; Sharma et al., 2012; Verrall et al., 2014).

1.2.9.6 Survival of *Mtb*

Granulomas don't always succeed in eliminating and containing *Mtb*. Processes like macrophage necrosis, apoptosis, cavity formation, and breach into airways can result in outbreak and dissemination of *Mtb* (Mahamed et al., 2017; Verrall et al., 2014). Infected macrophages die through necrosis or apoptosis. Apoptotic macrophages express ATP and phosphatidyl serine to influence its efferocytosis by other phagocytes. This inhibits the growth of *Mtb*. However, virulent strains of *Mtb* are capable of evading apoptosis and inducing necrosis. Necrosis is induced by producing lipoxin 4 that blocks prostaglandin E_2 synthesis and prevents repair of the plasma membrane. Necrotic death then favours disruption of the membrane causing outgrowth of *Mtb* (Mahamed et al., 2017; Verrall et al., 2014).

1.2.9.7 Adaptive immune response

1.2.9.7.1 Dendritic cells

Dendritic cells (DC) are professional antigen presenting cells (APC) that mediate the crosstalk between innate and adaptive immunity. They play a fundamental role in immune defence by antigen presentation, co-stimulation, its capacity to produce cytokines on a large scale and its activity on the lymphocytes cluster of differentiation (*CD4*) (de Martino et al., 2019; Sia et al., 2015; Sia and Rengarajan, 2019). Upon infection, mature DCs and macrophages migrate to present *Mtb* antigens to T cells in lung draining lymph nodes thus initiating the adaptive immune response. This process is largely dependent on chemokine receptor (*CCR7*) and its corresponding *CCL19* and *CCL21* chemokines

(Brazier and McShane, 2020; de Martino et al., 2019; Sia and Rengarajan, 2019). Further, migration of DCs during *Mtb* infection and induction of *IFN-ɣ* responses is powered by *IL-12*, a cytokine secreted by myeloid cells. The soluble, unprocessed *Mtb* antigens presented by DCs are thought to be phagocytosed by uninfected resident lymph node DCs (Sia and Rengarajan, 2019).

However, DCs can also become a niche for *Mtb* cells. Secretion of the *Mtb* antigens can also benefit the survival of the pathogen by antigen diversion away from MHC class II (Ndlovu and Marakalala, 2016; Sia and Rengarajan, 2019). Furthermore, *DC-SIGN*, also called *CD209* serves as the entrance of *Mtb* into DC. *CD209* is a receptor for *CD54*, an intracellular adhesion molecule 1 (*ICAM1*) that is expressed on endothelial cells. Binding between the two also influenced DC migration. When *CD209* recognises mannose-capped lipoarabinomannan, *Mtb* penetrates the cell causing disruption of DC activity. This process is leads to the sequential production of interleukin-10 (*IL-10*) and downregulation of interleukin-12 (*IL-12*) which leads to suppression of T lymphocyte activity. On the other hand, DC-SIGN potentially prevents tissue pathology by maintaining a balanced inflammatory state thus influencing host protection (de Martino et al., 2019)**.**

1.2.9.7.2 Granuloma formation

Following the development of adaptive immunity, driven by both bacterial and host factors, a complex of immune cells in the form of a granuloma is formed to contain and prevent outgrowth of *Mtb* (de Martino et al., 2019; Ndlovu and Marakalala, 2016). A granuloma is an immunological structure rich in immune cells such as DCs, macrophages, epithelioid cells, monocytes, foamy macrophages and multinucleated giant cells, all of which seals in *Mtb* cells. The entire structure is surrounded largely by T lymphocytes, and B lymphocytes (de Martino et al., 2019; Ehlers and Schaible, 2012; Ndlovu and Marakalala, 2016). Inside the granuloma, cholesterol is the only carbon source which leads to a lack of carbon and nutrients, hypoxia and an increased concentration of nitric oxide (de Martino et al., 2019). Macrophages within the granuloma represent two types, M1 (pro-inflammatory) and M2 (anti-inflammatory), each of which have a distinct gene expression profile defined by markers associated with stimulation. The presence of both is required to maintain a balance between the pro- and anti-inflammatory responses (Ito et al., 2013). Studies have shown that *Mtb* is also capable of direct recruitment and motility of uninfected macrophages to the site of infection by *ESX-1*/*RD1* (virulence locus) and by *ESAT-6* (mycobacterial virulence protein) that induces epithelial cell secretion of host matrix metalloproteinase-9 (*MMP-9*) that drives recruitment of new macrophages into the granuloma (Ndlovu and Marakalala, 2016). At early infection, *Mtb* favours an inflammatory response that leads to granuloma formation, however, thereafter its survival requires less or no inflammatory traits. This switch is mediated by *ESAT-6*. This virulence factor is responsible for the transformation of M1 macrophages that produce inflammatory cytokines such as *IL-6*, *IL-12* and *TNF-α* to the M2 phenotype that produces the anti-inflammatory cytokine, *IL-10* (Ndlovu and Marakalala, 2016). Another attribute

to its survival is the DosR regulon that is induced by *Mtb* to survive the environmental pressures within the granuloma such as hypoxia (Ndlovu and Marakalala, 2016). Whether the granuloma is purely protective or promotes disease progression is still a controversial topic. While the hostile environment of the granuloma serves as a host protective measure to prevent dissemination of *Mtb*, over time the pathogen has adapted to survive long term in a state of dormancy making it less susceptible to unfavourable environmental stress (de Martino et al., 2019; Ndlovu and Marakalala, 2016).

1.2.9.8 Role of cytokines and chemokines during *Mtb* infection

Cytokines and chemokines are small, soluble proteins produced by immune cells to influence the activity of other cells (Domingo-Gonzalez et al., 2016). These serve as key determinants for the outcome of *Mtb* infection by playing effectors and regulators of mycobacterial immunity between the innate and adaptive immune response (Cooper et al., 2011). The need for inter-cell communication for efficient migration and induction of specific processes during expression of immunity is where the critical role of both cytokines and chemokines in controlling *Mtb* infection lies (Domingo-Gonzalez et al., 2016). Cytokines can be divided into two groups, those that favour a pro-inflammatory, Th1 response (*TNF-β*, *IL-12*, *IFN-γ*, and *IL-2*) and those that favour an anti-inflammatory, Th2 response (*IL-4*, *IL-2*, *IL-4*, *IL-5*, *IL-9*, *IL-10*, *IL-13* and *IL-25*). Chemokines belong to a large family of chemotactic cytokines with a primary function of recruiting leukocytes. Preventing mycobacterial dissemination and containing inflammation are hallmarks of TB control in addition to the development of the granuloma. Establishment of the granuloma is mediated by coordinated expression of chemokines. They promote migration and recruitment of peripheral cells to the site of infection and into the granuloma (Ansari et al., 2013). Chemokines are classified into four groups, C, CC, CXC and CX3C and can further grouped into homeostatic (example *CCL19*, *CCL21*) and inflammatory chemokines (*CCL3*, *CCL5*, *CXCL8*, *CXCL9*, *CXCL10* and *CXCL11*) (Ansari et al., 2013).

1.2.9.8.1 Pro-inflammatory cytokines

1.2.9.8.1.1 *TNF-α*

Upon phagocyte-*Mtb* interaction, *TNF-α* is produced by macrophages, and other cells such as lymphocytes, mast cells, endothelial cells, fibroblasts, CD4 and CD8 T cells (Domingo-Gonzalez et al., 2016). TNF-α is an important mediator of the pro-inflammatory response enforcing action through *NF-κB*, *JNK* and *p38*. The role of *TNF-α* is multifaceted. It is implicated in macrophage activation, proliferation and differentiation of immune cells, and apoptosis (Domingo-Gonzalez et al., 2016). As infection progresses, *TNF-α* also co-ordinates chemokine responses and facilitates development of the granuloma. The importance of *TNF-α* is further highlighted in *TNF* receptor deficient mice or TNF neutralization following BCG vaccination. *TNF-α* deficiency resulted in heightened susceptibility to *Mtb* infection and increased bacterial loads (Cooper et al., 2011; Domingo-Gonzalez et al., 2016). Neutralization resulted in downregulation of important chemokines such as *CCL5*, *CXCL9* and

CXCL10. *CCL5* normally binds to *CCR1* and *CCR5* expressed on macrophages and neutrophils (innate immune cells) and T and B cells (adaptive immune cells), while *CXCL9* and *CXCL10* bind to *CXCR3* expressed on activated T cells. Failure of *CXCR3* to bind *CXCL9* and *CXCL10* ligands results in failure to recruit T cells into the granuloma thus also promoting dissemination of *Mtb* (Cooper et al., 2011; Domingo-Gonzalez et al., 2016). *TNF-α* is also a biomarker used to distinguish between pulmonary disease and latent infection. Evidence shows *TNF-α* is crucial in initiating phagocyte activation, granuloma organization and maintenance, and control of bacterial growth, but its deregulation and over expression promotes transmission and tissue damage (Cooper et al., 2011; Domingo-Gonzalez et al., 2016).

1.2.9.8.1.2 Type 1 and type II Interferons

Interferons (*IFN*) are crucial for host resistance to *Mtb* infection and is an important component of the innate immune response. While type II *IFN* are structurally related to type I *IFN*, they bind to different receptors with different locations, and type I *IFN* confers beneficial activity to the pathogen while type I *IFN* is essential for host survival (Cooper et al., 2011)**.**

IFN-y, the only type II *IFN*, regulated by *IL-12* and *IL-18*, is characteristic of the Th1 immune response. Binding to *IFN* receptor induces signaling through Janus kinases signal transducers and Janus Kinase-Signal Transducer and Activator of Transcription (*JAK-STAT*) activators of transcription. (Cooper et al., 2011). This results in migratory and functional capacity changes in macrophages, NK cells and T cells, all of which produce *IFN-y* (Domingo-Gonzalez et al., 2016). It mediates activation of macrophages to kill *Mtb* and is necessary for the control of TB. In addition, it also plays a role in IgG2a synthesis, activates NK cells, inhibits the Th2 phenotype and augments MHC I and II (Domingo-Gonzalez et al., 2016). If expression of *IFN-y* is disrupted, susceptibility to infection is increased, less efficient macrophage activation is displayed with exacerbated granulocytic inflammation. Its main function is to influence the change of macrophage activity and other immune cells so when *IFN-y* is absent, the intracellular milieu in which *Mtb* resides has little reactive radical activity; the phagosome does not undergo lysosome fusion and remains at neutral pH (Domingo-Gonzalez et al., 2016).

Type I *IFN* are a group comprised of 13 genes including *IFN-α* and *IFN-β* (*IFN- α/β*) which are the most classified. Engagement of *TLR*s results in a cytosolic cascade signal transduction toward *IFN* regulatory factor 3 and 7 (*IRF3, IRF7*) – mediated transcription of *IFN- α/β*. The sequential engagement of *IFN- α/β* with *IFN* subunit receptors 1 and2 (*IFNAR1*/*IFNAR2*) activates dimers of tyrosine kinases *JAK* and tyrosine kinase (*TYK*). This in turn leads to activation of *IFN* stimulated gene factor (*ISG*) that interacts with *IFN* stimulated response elements (*ISRE*) at the promoters of *IFN- α/β* regulated genes (Domingo-Gonzalez et al., 2016). In contrast to *IFN-y*, Type I *IFN* seem to promote *Mtb* infection. In a mouse *Mtb* infection model, endogenous type I IFN promotes bacterial growth. More virulent strains of *Mtb* have shown enhanced type I *IFN* synthesis related to downregulation of pro-inflammatory

cytokines (*TNF-α*, *IL-6* and *IL-12*) activity, thus resulting in impaired Th1 immune response (Cooper et al., 2011; Domingo-Gonzalez et al., 2016). Analysis of whole blood collected from people with latent and active TB revealed those with active TB displayed an expression signature dominated by *IFN* induced genes in neutrophils, which was also seen in 10 % of the latently infected people suggesting they were at higher risk of developing active disease. Collectively, it seems type I *IFN* promotes down regulation of protective immunity and has confers very little host protective characteristics (Cooper et al., 2011).

1.2.9.8.1.3 *IL-1* cytokine family

The *IL-1* family consists of *IL-1α*, *IL-1β*, *IL-18* and *IL-33*, all of which exhibit potent yet diverse immunologic activities in inflammation and regulation of immune response (Cooper et al., 2011; Domingo-Gonzalez et al., 2016). The receptors of the *IL-1* family and most TLR share a common adaptor molecule, MyD88. Both *IL-1β* and *IL-α* are critical in the defense against TB. *IL-1β* directly kills *Mtb* in human and murine macrophages whilst influencing the recruitment of anti-microbial effector molecules. It also promotes expression of *TNF-α* and *TNFR1* and activates caspase-3**.** Deficiencies in both *IL-1α/β* results in increased bacterial loads and decreased host survival. IL-1β is a potent pyrogenic cytokine. Mice deficient in *IL-1β* only was also found to be acutely susceptible to *Mtb* infection suggesting apart from conferring host resistance, it also has a non-redundant function and can't be compensated for by *IL-1α* that signals via the same receptor (Cooper et al., 2011). The transformation of immature *IL-1β* to its mature form is mediated by a multiprotein inflammasome complex, *NOD*-like receptor 3 (*NLRP3*) that triggers caspase-1 activation, the enzyme responsible for its transformation (Cooper et al., 2011; Domingo-Gonzalez et al., 2016). In combination with vitamin D, *IL-1β* controls mycobacterial growth in macrophages. *IL-1α* is involved in expression of *IL-6* in fibroblasts which may be associated with neutrophil mobilization (Domingo-Gonzalez et al., 2016). *IL-18-MyD88* dependent activation amplifies the Th1immune response. With a similar biological function to *IL-12*, it induces *IFN-γ* expression in hepatic lymphocytes, splenocytes and Th1 cell clones (Cooper et al., 2011; Domingo-Gonzalez et al., 2016). It is activated by caspase-1 activity following neutrophil stimulation, bacterial stimulation, or by *IL-4* or *IFN-γ* (Domingo-Gonzalez et al., 2016). *IL-33* is associated with the Th2 immune response therefore playing a limited role in host resistance to *Mtb* (Cooper et al., 2011).

1.2.9.8.1.4 *IL-12* cytokine family

This family of cytokines belongs to the *IL-6* family. *IL-12* is composed of multiple subunits, *p35/p40, IL-23* of *p19/p40, IL-27* of *p28/Ebi3* and *IL-35* of *p35/Ebi3* with each of these subunits being independently regulated. *IL-12p40*, *IL-12*, and *IL-27* are largely produced by macrophages and DCs, playing a major role in inducing and regulating cytokine expression in antigen stimulated T cell populations (Domingo-Gonzalez et al., 2016). *IL-12p40* exerts activity through induction of *JAK* and

STAT signaling leading to activation of *STAT4* homodimers. Stable and long term *IL-12* production is required and crucial for optimal differentiation and stimulation of *IFN-γ* producing antigen specific Th1 cells, and to limit long term mycobacterial growth (Cooper et al., 2011; Domingo-Gonzalez et al., 2016). Binding of *TLR2* and *TLR9* is necessary for optimal production of *IL-12p40* in response to *Mtb* exposure while *Mtb* induces *IRAK-M* to inhibit *TLR*-mediated *IL-12* production. However, mycobacterial *LprA* promotes *IL-12p40* production. This exhibits that *IL-12p40* is not only beneficial to the host but is also manipulated by *Mtb* induction and regulation for its own benefit (Cooper et al., 2011; Domingo-Gonzalez et al., 2016). *IL-23* is a new member of the *IL-12* family. It stimulates Th17 cell proliferation which is characteristic of producing *IL-17, TNF-α* and *IL-6* inflammatory cytokines. *IL-27* serves as an inhibitory cytokine for *Th17* differentiation and limits inflammation, to prevent extensive immunopathology. It can modulate the intensity and duration of many classes of T cell responses (Cooper et al., 2011; Domingo-Gonzalez et al., 2016)**.**

1.2.9.8.2 Modulators of the inflammatory response

1.2.9.8.2.1 *IL-10*

IL-10 is produced by Th0, Th1, Th2 and Treg cells (Averbakh and Ergeshow, 2018; Sasindran and Torrelles, 2011). It modulates the innate and adaptive immune response, inadvertently creating a favorable milieu for the persistence of *Mtb*. When induced abundantly by macrophages stimulated by *TLR*s, it reduces the host protective immune response against *Mtb* to control long term inflammation but also allows for progression of disease (Cooper et al., 2011; Sasindran and Torrelles, 2011). It exhibits activity by inhibiting Th1 by restricting T effector cell responses and augments class II. It also has the ability to prevent phagosome maturation and macrophage activation in *STAT3* dependent manner, thus permitting long term survival of *Mtb* within the phagosome (Averbakh and Ergeshow, 2018; Cooper et al., 2011; Domingo-Gonzalez et al., 2016). In addition, *IL-10* inhibits *IFN-γ* mediated macrophage activation. It inhibits pro-inflammatory cytokines such as *IL-1, IL-6, IL-12, IL-18, CCL3, CCL4* and *CCL5* chemokines involved in cell recruitment, and generation of reactive radicals by interfering with intracellular signaling cascades like suppressor of cytokine signaling-3 (*SOCS3*) and *NF-$_K$β* (Averbakh and Ergeshow, 2018; Sasindran and Torrelles, 2011). In DCs, *Mtb* induced *IL-10* production inhibits antigen presentation through MHC class II downregulation, decreased *IL-12* production, and inhibition of DC trafficking to lymph nodes for T cell priming (Domingo-Gonzalez et al., 2016; Sasindran and Torrelles, 2011). Benefits of *IL-10* is controversial. While limiting inflammation to prevent host tissue damage, it also provides a favorable environment for *Mtb* to persist (Sasindran and Torrelles, 2011).

1.2.9.8.2.2 *TGF-β*

Defined as a pluripotent cytokine, transforming growth factor β (*TGFβ*) secreted by macrophages, DCs, monocytes and CD4+ T cells, modulates the immune response by deactivating macrophages and downregulating adaptive immunity (Sasindran and Torrelles, 2011). It has a synergistic relationship with *IL-10* to influence immune tolerance and reduce inflammation (Sasindran and Torrelles, 2011). Similar to *IL-10*, it also has the ability to suppress reactive radical production, stimulation of APCs, T cell function and proliferation and cytokine production (*IL-1β* and *TNF-α*) (Sasindran and Torrelles, 2011).

1.2.10 Latent TB infection, persistence and reactivation

The hypoxic state of granulomas restricts the growth of aerobic tubercle bacilli to a microaerophilic/anaerobic non-replicating state, allowing the pathogen to enter and persist in a quiescent/ dormant state (Chaves et al., 2015; Gengenbacher and Kaufmann, 2012**).** The dormant state is characterized by low metabolic activity which protects the pathogen from further host immune responses and antimicrobial treatment (Gupta and Srivastava, 2012). The key characteristics identified during persistence that are fundamental to maintenance of bacterial dormancy were the peptidoglycan structure of and a specific cross-link within the *Mtb* cell wall, and utilization of host lipids as an energy source during persistence (Fattorini L et al., 2013). While the physiological state of the bacteria during persistence is referred to as dormancy, the clinical manifestation is referred to as asymptomatic latent TB infection (LTBI) which occurs approximately in one third of the global population (WHO, 2020). Of those latently infected, 5-10 % may experience reactivation of LTBI to active disease through resuscitation of dormant bacilli. Reactivation risk factors include any illness that compromises the immune system, immune suppressive treatment, malnutrition, malfunction of certain organs, tobacco smoke (Chaves et al., 2015).

1.2.11 Resuscitation promoting factors

M. tuberculosis has a family of 5 resuscitation promoting factors (*rpfs A-E*), first identified in *Micrococcus luteus*, which have the capacity to resuscitate dormant bacilli (Chaves et al., 2015; Rosser et al., 2017; Tufariello et al., 2004). The importance and role of these genes in *Mtb* infection and reactivation were demonstrated by the generation of single and multiple *rpf* gene knockouts in murine and *in vitro* models that provide a growing body of evidence that *rpfs* play a significant part in human TB (Figure 1.2.10) (Rosser et al., 2017). Previous studies demonstrated **s**ingle *rpf* gene knockouts were non-essential for *in vitro* and *in vivo* growth of *Mtb* as no defects in growth or persistence were observed. These findings suggested functional redundancy in strains with only single *rpf* deletions and that these proteins are dispensable for *in vitro* and *in vivo* growth (Downing et al., 2005; Kana et al., 2008; Rosser et al., 2017; Tufariello et al., 2004). However, in contrast to the notion of functional redundancy, gene

expression analysis of *rpf* genes from early exponential into the stationary phase of axenic cultures as well as during acute phase infection and chronic persistence in mice, confirmed *rpf* A-E are differentially expressed (Tufariello et al., 2004). All *rpfs* were expressed in early exponential phase during *in vitro* and *in vivo* growth, but displayed differential, diminishing expression levels as growth continued and persisted, *in vitro* (Tufariello et al., 2004).

Further *rpf* deletions in various combinations showed decreased *Mtb* virulence in the form of reduced growth, dissemination, and persistence, however, the degree of attenuation varies between the different knockouts suggesting they are in fact functionally distinct (Downing et al., 2005; Rosser et al., 2017). In an intraperitoneal infected C57Bl/6 chronic infection model, (Biketov et al., 2007) showed that *Mtb* H37Rv Δ*rpfAC* and Δ*rpfAB* mutant strains were able to establish chronic infection, though infection with the former double mutant displayed higher attenuation. It was also demonstrated that infection with triple *rpf* mutants (Δ*rpfACB* and Δ*rpfACD*) resulted in significant attenuation, with greater attenuation displayed in the triple mutant lacking *rpfD*, and that deletion of *rpfA, rpfC, rpfB* resulted in arrest of cell multiplication after immune suppression with aminoguanidine (AG) carbonate (Tufariello et al., 2004), and were defective in resuscitation *in vitro* (Downing et al., 2005; Kana et al., 2008). These observations indicated the *rpfs* may be differentially significant for *Mtb* proliferation *in vivo* (Biketov et al., 2007; Downing et al., 2005; Tufariello et al., 2004).

Rpf proteins have a conservative domain that is structurally similar to that of lysosymes and transglycosylases and exerts similar enzymatic function in peptidoglycan hydrolysis to initiate early phase resuscitation (Gupta and Srivastava, 2012). Genetic studies revealed Rpf biosynthesis is also active in later stages of resuscitation suggesting they serve as mediators for early and late events of the reactivation process (Tufariello et al., 2004). Thus, each of the *rpf* genes are considered potential therapeutic targets to prevent *Mtb* from exiting dormancy and development of chronic infection (Biketov et al., 2007).

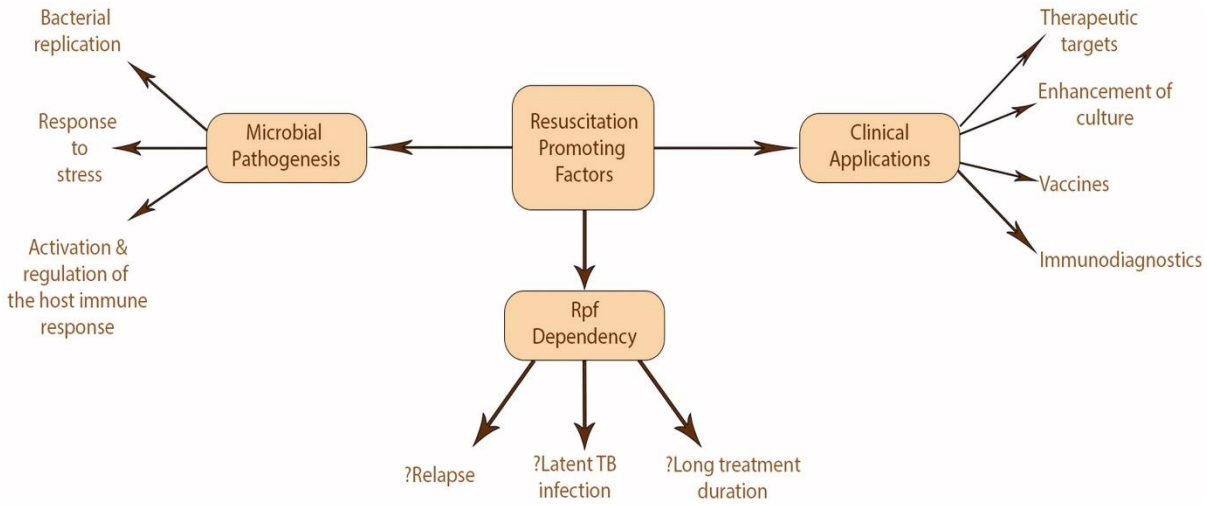

Figure 1.2.10: Role of *rpfs* in *Mtb* pathogenesis, rpf dependency and clinical applications (Rosser et al., 2017).

1.2.11.1 Resuscitation promoting factor B

1.2.11.1.1 Unique structural characteristics

The *rpfB* gene is structurally unique, characterized by its prokaryotic lipoprotein lipid attachment site at its N terminus (Figure 1.2.11), suggesting it may exert functional activity from the cell membrane, while the remaining *rpfs* contain a signal sequence and may therefore be secreted or membrane bound (Tufariello et al., 2004) (Figure 1.2.11). Furthermore, pairwise sequence alignment of the 3D catalytic domain generated by molecular modeling revealed *rpfA* had the highest sequence homology to *rpfB* and that residues 325-327 were common in *rpfB* and *rpfA* but absent in the remaining *rpfs* (Squeglia et al., 2013). Another interesting feature of the *rpfB* catalytic domain is the presence of a large number of glycine residues which are essential for maintaining structure of the domains as six of them present positive φ angles, which are rarely assumed by nonglycine residues (Squeglia et al., 2013).

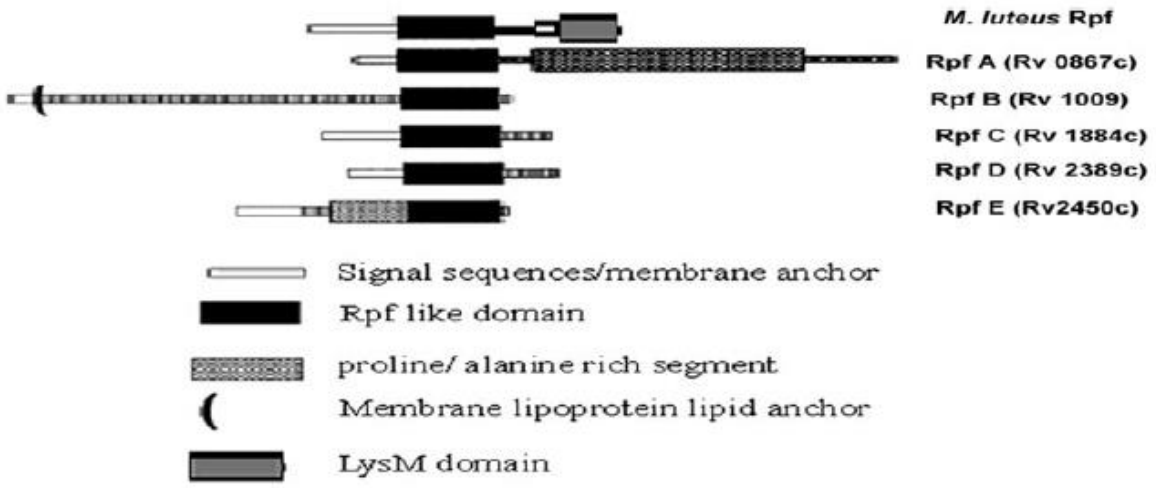

Figure 1.2.11: Domain structure of *Mtb* Rpf A-E relative to *M. luteus* Rpf (Gupta and Srivastava, 2012).

1.2.11.1.2 Role of *rpfB* in growth kinetics, persistence and reactivation, *in vitro* and *in vivo*

Tufariello et al., 2004 demonstrated that from all single *rpf* gene knockout strains grown *in vitro*, only Δ*rpfB* produced an altered, small colony phenotype compared to the wild type strain. It was also shown that *rpfB* (among *rpfA* and *rpfC*) expression peaks at the exponential phase *in vitro*, but diminishes as the bacilli enters the stationary phase, suggesting *rpfB* may be a potential growth factor in *Mtb* proliferation *in vivo* (Tufariello et al., 2004). In contrast to the results obtained by Tufariello et al., 2004, of the two triple mutants, Δ*rpfACB* and Δ*rpfACD* used for infection of mice, the mutant lacking *rpfB* was more attenuated in growth of *Mtb*, suggesting *rpfB* has a greater impact on virulence (Downing et al., 2005). In a high dose infected mice model of chronic infection, reactivation was induced using aminoguanidine (AG). All single Δ*rpf* mutants displayed similar reactivation growth kinetics compared

to the parental strain, except Δ*rpfB* which showed delayed AG-induced reactivation. Complementation of the Δ*rpfB* mutant confirmed that delayed reactivation was due to the gene knockout as reactivation growth kinetics of the complemented strain were restored towards that of the parental strain. The delayed reactivation phenotype was further confirmed in a low dose infection model. This phenotype was accompanied by early pulmonary bacterial burden and worsened pulmonary histopathology in wild type infected mice compared to Δ*rpfB* mutant infected mice. However, this was eventually noticed in Δ*rpfB* infected mice at a much later stage of infection (Tufariello et al., 2006). Russell-Goldman et al., 2008 reinforced the role of *rpfB* in regulating *Mtb* reactivation while also implicating *rpfA* by showing double *rpf* mutants that lacked *rpfB* displayed significant reactivation defects.

1.2.11.1.3 Role of RpfB in regulating immune response

Rpf proteins are potential targets for the host immune system (Commandeur S et al, 2013) and as previously shown are key virulence factors for *Mtb* proliferation and reactivation (Downing et al., 2005; Tufariello., et al, 2006; Russell-Goldman et al., 2008), thus responses targeting *rpfs* may be protective (Rosser et al., 2019). Russell-Goldman et al., 2008 showed that lack of *rpfA* and *rpfB* renders the mutant more pro-inflammatory by demonstrating Δ*rpfAB* induced higher levels of *TNF-α* and *IL-6* pro-inflammatory cytokines at 24 hours post-infection compared to the wild type strain In C57BL/6 bone marrow derived macrophages (Russell-Goldman et al., 2008). Another study showed R*pfB*-induced maturation of DCs resulted in a pro-inflammatory cytokine response by demonstrating recombinant RpfB-stimulated DCs produced high levels of *IL-6*, *TNF-α* and *IL-1* compared to untreated DCs. They went on to show RpfB induced significantly high levels of *IL-12p70* (associated with Th1 cells), but not *IL-10* (associated with Th2 cells) in DCs. Thereafter, it was shown that RpfB has the capacity to induce DC maturation in a *TLR4*-dependent manner which resulted in increased expression of cell surface molecules and pro-inflammatory cytokines (Kim et al., 2013), also shown with *rpfE* (Choi et al., 2015). It was shown that *NF-κB* and *MAPK* signaling pathways were crucial for the induction of pro-inflammatory cytokines and expression of DC maturation markers. Collectively, these findings indicate RpfB induces a pro-inflammatory cytokine response through Th1 polarization in DCs via *TLR4* through *NF-κB* and *MAPK* signaling, in vitro (Kim et al., 2013). The ability to generate a protective immune response against *Mtb* renders RpfB a potential vaccine candidate (Kim et al., 2013; Rosser et al., 2019).

1.2.11.1.4 RpfB in vaccine development and treatment

Romano et al., 2012 evaluated the immunogenicity of plasmid DNA vaccines encoding RpfB and RpfD (p-RpfB/ p-RpfD) proteins in C57BL/6 and BALB/c mice. Vaccination with p-RpfB induced increased levels of specific total IgG antibodies in C57BL/6 and BALB/c mice whereas vaccination with p-RpfD induced weak specific IgG responses in BALB/c mice. P-RpfB-immunized C57BL/6 mice induced increased levels of *IL-2* and *IFN-y* (Th1 response) following stimulation with recombinant RpfB, while

p-RpfD induced low levels of *IFN-y* and no antigen specific *IL-2* production. The same observation was seen in BALB/c mice. Since immunization with p-RpfB produced specific antibody responses and a Th1 type immune response, its protective potential was assessed in an experimental model of pulmonary TB in C57BL/6 mice. At 5 weeks post-infection, p-RpfB immunization resulted in moderate but significant reduction of pulmonary bacterial burden compared to the control group vaccinated with empty vector. However, this response was more pronounced in the spleen rather than in lungs. In conclusion, it was shown both RpfB and RpfD are immunogenic, with RpfB being more immunogenic. Kim et al., 2013 also showed RpfB-mediated DC maturation induced long-lasting Th1 memory in chronic *Mtb* persistence and disease progression (Kim et al., 2013). In theory, in combination with latency antigens, RpfB could induce an immune response that eliminates dormant bacilli enabling long term control of LTBI (Yeremeev et al., 2003; Rosser et al., 2019). However, it is important to note that vaccination with any Rpf also runs the risk of inducing reactivation therefore further evidence is required to interrogate RpfB as a potential component of TB vaccines (Kim et al., 2013). Due to their importance as virulent factors, lack of human homologs ensuring a high degree of drug specificity, and their extracellular nature that eliminates the need for RpfB inhibitors to enter cells, all Rpfs represent inviting targets for the development of new drugs against reactivation of LTBI (Kana et al., 2008; Gupta and Srivastava., 2012). Rpf inhibitors such as 2-nitrophenylthiocyanate, in conjunction with anti-TNF-α inhibitors, could be administered to LTBI patients to prevent reactivation but requires further investigation for validation (Demina et al., 2009).

1.2.12 Gene expression and transcriptome analysis

Transcriptomic technologies permit the interrogation of transcripts from various sample types, conditions and time points which provides biological insight on how the genes are regulated (Lowe et al., 2017). It can be applied to mutant and complemented strains to determine the differences caused by mutants, identification of novel genes, pathways, and disease-associated gene fusions, single nucleotide polymorphisms and allele specific expression (Lowe et al., 2017). This has been instrumental in understanding human disease (Lowe et al., 2017). For decades, the study of gene expression patterns were limited to small scale molecular techniques such as quantitative PCR and microarrays (Wolf JBW., 2013). Recently, with the development of RNA sequencing and maturation of bioinformatics analytical tools, gene expression analysis can now be performed at a global transcriptomic scale (Wolf JBW., 2013).

1.2.12.1 RNA sequencing versus microarray analysis

Microarray analysis has long been used for gene expression quantification but only of predetermined transcripts whereas RNA sequencing captures the entire genome (Lowe et al., 2013; Wolf JBW., 2013). Microarrays are based on hybridization of defined transcripts to complementary probes and permits transcript analysis on a large scale. It is cost effective and less labour intensive (Lowe et al., 2013). In

contrast, RNA sequencing utilises high-throughput technology to sequence cDNA transcripts of the entire genome, and at sufficient coverage is able to capture a wider range of expression values (Lowe et al., 2013; Wolf JBW., 2013). Furthermore, RNA sequencing provides insight on RNA splice events that standard microarrays do not (Wolf JBW., 2013). RNA sequencing has gained increased popularity since the development of Solexa/Illumina sequencing platforms that allow 10^9 transcripts to be sequenced, permitting accurate measurement of entire human transcriptomes (Lowe et al., 2013). Another major advantage of RNA sequencing is the low input of RNA sample (measured in nanograms) required compared to microarrays (Wolf JBW., 2013).

1.2.12.2 Quantitative real-time PCR

Quantitative real-time PCR (qRT-PCR) is one of the most widely used techniques for gene quantification, long before the development of RNA sequencing, attributed to its vast dynamic range, sensitivity, sequence specificity and reproducibility (Costa et al., 2013; Hossain et al., 2019). Despite its single handed use in previous gene expression literature, it is also used as the gold standard for validation of both microarray and RNA sequencing data (Fang and Cui, 2011; VanGuilder et al., 2008).

1.2.13 Cytokine analysis

Cytokines are small proteins produced by various cell types that mediate host immune responses (Young HA, 2009). Therefore, detection and quantification of cytokine expression is crucial to understanding host responses to infections and autoimmunity (Payan RR et al., 2003). Several approaches exist for cytokine detection and quantification, some of which include Enzyme-linked immunosorbent assay (ELISA), Western blots, microarray, qRT-PCR and multiplex assays (Payan RR et al., 2003).

1.2.13.1 ELISA versus Western blots

ELISAs are the traditional and most frequently used method for cytokine quantification, for its rapid turnaround time, specificity, sensitivity and accurate quantification (Whiteside TL., 2002; Selvarajah et al., 2014), however only one cytokine can be analysed per plate. Direct ELISA accurately quantifies a target molecule with high sensitivity from a variety of sample types and has rapid turnaround time, however produces weak signals (Manole et al., 2018). In indirect ELISA, a capture antibody is first added to the plate followed by the targeted cytokine. An enzyme labelled detection body is added to the bound targeted cytokine which is followed by a substrate. The substrate illuminates a colour in the presence of the cytokine with high sensitivity and flexibility. The limitation of this method is production of non-specific signals (Whiteside TL., 2002, Manole et al., 2018). Western blots have diverse applications and can be used to investigate proteins quantities, cellular localization, protein-protein interactions, kinase activity, or tracking of post-translational modifications (Bass et al., 2017) from a

variety of sample types from biological samples or a mixture of proteins. However, the process of western blot is far more tedious, time consuming and labour intensive (Manole et al., 2018).

1.2.13.2 Multiplex bead-based assays

Multiplex assays offer the major advantage of analysing multiple analytes in one sample. In addition, the assay requires small input volumes, is less labour intensive, and ensures reproducibility (Dowall et al., 2019). In the bead-based assays, antibodies are immobilized to fluorescent microsphere beads in suspension, and captured target analytes are detected using the Luminex technology, based on the principle of flow cytometry. This platform offers a robust and flexible way to analyses multiple analytes from different time points under different conditions (Dowall et al., 2019).

1.2.14 Significance of the study

To our knowledge, there have been no reports providing a global transcriptomic view of the host response in the THP-1 macrophage cell line infected with an *Mtb* Δ*rpfB* gene deficient strain using RNA sequencing. This study aims to interrogate the host response at a global transcriptomic level in an attempt to elucidate novel targets and pathways at the exponential phase of *Mtb* infection to provide an overview on the effect of the *Mtb rpfB* gene on the host immune response of macrophages.

1.2.15 Aim

To evaluate the role of the *Mtb rpfB* gene in regulation of host transcriptional response in a THP-1 model by mRNA sequencing, respectively.

1.2.16 Objectives

- To infect THP-1 macrophages with the WT, Δ*rpfB* mutant and *rpfB*-complement strains.
- To isolate mammalian RNA from infected and uninfected THP-1 macrophages at 72 hours post-infection.
- To evaluate *rpfB* gene regulation in THP-1 macrophages at 72 hours post-infection by mRNA sequencing.
- To construct an *rpfB*-complement strain.
- To confirm and quantify *GM-CSF* and *IL-1β* cytokines identified at the transcriptomic level in WT, Δ*rpfB* mutant and *rpfB*-complement infected THP-1 macrophages at 24, 48- and 72 hours post-infection using the Bio-Plex 200 platform.
- To validate RNA sequencing data by qRT-PCR using *GM-CSF* and *IL-1β* cytokine genes in a QuantStudio™ 5 Real-Time PCR System.

References

Agarwal, N., Lamichhane, G., Gupta, R., Nolan, S., and Bishai, W.R. (2009). Cyclic AMP intoxication of macrophages by a *Mycobacterium tuberculosis* adenylate cyclase. Nature *460*, 98-102.

Agrawal, N., Streata, I., Pei, G., Weiner, J., Kotze, L., Bandermann, S., Lozza, L., Walzl, G., du Plessis, N., Ioana, M., *et al.* (2018). Human Monocytic Suppressive Cells Promote Replication of *Mycobacterium tuberculosis* and Alter Stability of *in vitro* Generated Granulomas. Front Immunol *9*, 2417.

Ahmad, S. (2011). Pathogenesis, immunology, and diagnosis of latent *Mycobacterium tuberculosis* infection. Clin Dev Immunol *2011*, 814943.

Ahsan, F., Moura-Alves, P., Guhlich-Bornhof, U., Klemm, M., Kaufmann, S.H., and Maertzdorf, J. (2016). Role of Interleukin 36gamma in Host Defense Against Tuberculosis. J Infect Dis *214*, 464-474.

Almeida Da Silva, P.E., and Palomino, J.C. (2011). Molecular basis and mechanisms of drug resistance in *Mycobacterium tuberculosis*: classical and new drugs. J Antimicrob Chemother *66*, 1417-1430.

Amarante-Mendes, G.P., Adjemian, S., Branco, L.M., Zanetti, L.C., Weinlich, R., and Bortoluci, K.R. (2018). Pattern Recognition Receptors and the Host Cell Death Molecular Machinery. Front Immunol *9*, 2379.

Ansari, A.W., Kamarulzaman, A., and Schmidt, R.E. (2013). Multifaceted Impact of Host C-C Chemokine *CCL2* in the Immuno-Pathogenesis of HIV-1/*M. tuberculosis* Co-Infection. Front Immunol *4*, 312.

Averbakh, M.M., and Ergeshow, A. (2018). Interaction between *Mycobacterium tuberculosis* and Human Host: Role of Cytokines in Pathogenesis and Treatment Monitoring.

Bansal, K., Elluru, S.R., Narayana, Y., Chaturvedi, R., Patil, S.A., Kaveri, S.V., Bayry, J., and Balaji, K.N. (2010). PE_PGRS antigens of *Mycobacterium tuberculosis* induce maturation and activation of human dendritic cells. J Immunol *184*, 3495-3504.

Bass, J.J., Wilkinson, D.J., Rankin, D., Phillips, B.E., Szewczyk, N.J., Smith, K., and Atherton, P.J. (2017). An overview of technical considerations for Western blotting applications to physiological research. Scand J Med Sci Sports *27*, 4-25.

Behar, S.M., Divangahi, M., and Remold, H.G. (2010). Evasion of innate immunity by *Mycobacterium tuberculosis*: is death an exit strategy? Nat Rev Microbiol *8*, 668-674.

Biketov, S., Potapov, V., Ganina, E., Downing, K., Kana, B.D., and Kaprelyants, A. (2007). The role of resuscitation promoting factors in pathogenesis and reactivation of *Mycobacterium tuberculosis* during intra-peritoneal infection in mice. BMC Infect Dis *7*, 146.

Brazier, B., and McShane, H. (2020). Towards new TB vaccines. Semin Immunopathol *42*, 315-331.

Bryson, B.D., Rosebrock, T.R., Tafesse, F.G., Itoh, C.Y., Nibasumba, A., Babunovic, G.H., Corleis, B., Martin, C., Keegan, C., Andrade, P., *et al.* (2019). Heterogeneous *GM-CSF* signaling in macrophages is associated with control of *Mycobacterium tuberculosis*. Nat Commun *10*, 2329.

Brazier, B., and McShane, H. (2020). Towards new TB vaccines. Semin Immunopathol *42*, 315-331.
Bryson, B.D., Rosebrock, T.R., Tafesse, F.G., Itoh, C.Y., Nibasumba, A., Babunovic, G.H., Corleis, B., Martin, C., Keegan, C., Andrade, P., *et al.* (2019). Heterogeneous *GM-CSF* signaling in macrophages is associated with control of *Mycobacterium tuberculosis*. Nat Commun *10*, 2329.

Cambau, E., and Drancourt, M. (2014). Steps towards the discovery of *Mycobacterium tuberculosis* by Robert Koch, 1882. Clin Microbiol Infect *20*, 196-201.

Caminero, J.A., Cayla, J.A., García-García, J.-M., García-Pérez, F.J., Palacios, J.J., and Ruiz-Manzano, J. (2017). Diagnosis and Treatment of Drug-Resistant Tuberculosis. Archivos de Bronconeumología (English Edition) *53*, 501-509.

Chai, Q., Wang, L., Liu, C.H., and Ge, B. (2020). New insights into the evasion of host innate immunity by *Mycobacterium tuberculosis*. Cell Mol Immunol *17*, 901-913.

Chao, W.C., Yen, C.L., Hsieh, C.Y., Huang, Y.F., Tseng, Y.L., Nigrovic, P.A., and Shieh, C.C. (2017). Mycobacterial infection induces higher interleukin-1beta and dysregulated lung inflammation in mice with defective leukocyte NADPH oxidase. PLoS One *12*, e0189453.

Chaves, A.S., Rodrigues, M.F., Mattos, A.M., and Teixeira, H.C. (2015). Challenging *Mycobacterium tuberculosis* dormancy mechanisms and their immunodiagnostic potential. Braz J Infect Dis *19*, 636-642.

Chihota, V.N., Niehaus, A., Streicher, E.M., Wang, X., Sampson, S.L., Mason, P., Kallenius, G., Mfinanga, S.G., Pillay, M., Klopper, M., *et al.* (2018). Geospatial distribution of *Mycobacterium tuberculosis* genotypes in Africa. PLoS One *13*, e0200632.

Choi, H.G., Kim, W.S., Back, Y.W., Kim, H., Kwon, K.W., Kim, J.S., Shin, S.J., and Kim, H.J. (2015). *Mycobacterium tuberculosis* RpfE promotes simultaneous Th1- and Th17-type T-cell immunity via TLR4-dependent maturation of dendritic cells. Eur J Immunol *45*, 1957-1971.

Churchyard, G., Kim, P., Shah, N.S., Rustomjee, R., Gandhi, N., Mathema, B., Dowdy, D., Kasmar, A., and Cardenas, V. (2017). What We Know About Tuberculosis Transmission: An Overview. J Infect Dis *216*, S629-S635.

Cohen, K.A., Abeel, T., Manson McGuire, A., Desjardins, C.A., Munsamy, V., Shea, T.P., Walker, B.J., Bantubani, N., Almeida, D.V., Alvarado, L., *et al.* (2015). Evolution of Extensively Drug-Resistant Tuberculosis over Four Decades: Whole Genome Sequencing and Dating Analysis of *Mycobacterium tuberculosis* Isolates from KwaZulu-Natal. PLoS Med *12*, e1001880.

Commandeur, S., van Meijgaarden, K.E., Lin, M.Y., Franken, K.L., Friggen, A.H., Drijfhout, J.W., Oftung, F., Korsvold, G.E., Geluk, A., and Ottenhoff, T.H. (2011). Identification of human T-cell responses to *Mycobacterium tuberculosis* resuscitation-promoting factors in long-term latently infected individuals. Clin Vaccine Immunol *18*, 676-683.

Cooper, A.M., Mayer-Barber, K.D., and Sher, A. (2011). Role of innate cytokines in mycobacterial infection. Mucosal Immunol *4*, 252-260.

Costa, C., Gimenez-Capitan, A., Karachaliou, N., and Rosell, R. (2013). Comprehensive molecular screening: from the RT-PCR to the RNA-seq. Transl Lung Cancer Res *2*, 87-91.

D'Ambrosio, L., Centis, R., Sotgiu, G., Pontali, E., Spanevello, A., and Migliori, G.B. (2015). New anti-tuberculosis drugs and regimens: 2015 update. ERJ Open Res *1*.

Davenne, T., and McShane, H. (2016). Why don't we have an effective tuberculosis vaccine yet? Expert Rev Vaccines *15*, 1009-1013.

de Martino, M., Lodi, L., Galli, L., and Chiappini, E. (2019). Immune Response to *Mycobacterium tuberculosis*: A Narrative Review. Front Pediatr *7*, 350.

Demina, G.R., Makarov, V.A., Nikitushkin, V.D., Ryabova, O.B., Vostroknutova, G.N., Salina, E.G., Shleeva, M.O., Goncharenko, A.V., and Kaprelyants, A.S. (2009). Finding of the low molecular weight inhibitors of resuscitation promoting factor enzymatic and resuscitation activity. PLoS One *4*, e8174.
Domingo-Gonzalez, R., Prince, O., Cooper, A., and Khader, S.A. (2016). Cytokines and Chemokines in *Mycobacterium tuberculosis* Infection. Microbiol Spectr *4*.

Demina, G.R., Makarov, V.A., Nikitushkin, V.D., Ryabova, O.B., Vostroknutova, G.N., Salina, E.G., Shleeva, M.O., Goncharenko, A.V., and Kaprelyants, A.S. (2009). Finding of the low molecular weight inhibitors of resuscitation promoting factor enzymatic and resuscitation activity. PLoS One *4*, e8174.

Domingo-Gonzalez, R., Prince, O., Cooper, A., and Khader, S.A. (2016). Cytokines and Chemokines in *Mycobacterium tuberculosis* Infection. Microbiol Spectr *4*.

Dowall, S.D., Graham, V.A., Fletcher, T., and Hewson, R. (2019). Use and reliability of multiplex bead-based assays (Luminex) at Containment Level 4. Methods *158*, 17-21.

Downing, K.J., Mischenko, V.V., Shleeva, M.O., Young, D.I., Young, M., Kaprelyants, A.S., Apt, A.S., and Mizrahi, V. (2005). Mutants of *Mycobacterium tuberculosis* lacking three of the five *rpf*-like genes are defective for growth *in vivo* and for resuscitation in vitro. Infect Immun *73*, 3038-3043.

Ehlers, S., and Schaible, U.E. (2012). The granuloma in tuberculosis: dynamics of a host-pathogen collusion. Front Immunol *3*, 411.

Espitia, C., Rodrguez, E., Ramn-Luing, L., Echeverra-Valencia, G., and J, A. (2012). Host–Pathogen Interactions in Tuberculosis.

Falzon, D., Gandhi, N., Migliori, G.B., Sotgiu, G., Cox, H.S., Holtz, T.H., Hollm-Delgado, M.G., Keshavjee, S., DeRiemer, K., Centis, R., *et al.* (2013). Resistance to fluoroquinolones and second-line injectable drugs: impact on multidrug-resistant TB outcomes. Eur Respir J *42*, 156-168.

Fang, Z., and Cui, X. (2011). Design and validation issues in RNA-seq experiments. Brief Bioinform *12*, 280-287.

Gandhi, N.R., Brust, J.C., Moodley, P., Weissman, D., Heo, M., Ning, Y., Moll, A.P., Friedland, G.H., Sturm, A.W., and Shah, N.S. (2014). Minimal diversity of drug-resistant *Mycobacterium tuberculosis* strains, South Africa. Emerg Infect Dis *20*, 426-433.

Gandhi, N.R., Moll, A., Sturm, A.W., Pawinski, R., Govender, T., Lalloo, U., Zeller, K., Andrews, J., and Friedland, G. (2006). Extensively drug-resistant tuberculosis as a cause of death in patients co-infected with tuberculosis and HIV in a rural area of South Africa. The Lancet *368*, 1575-1580.

Gengenbacher, M., and Kaufmann, S.H. (2012). *Mycobacterium tuberculosis*: success through dormancy. FEMS Microbiol Rev *36*, 514-532.

Ghazaei, C. (2018). *Mycobacterium tuberculosis* and lipids: Insights into molecular mechanisms from persistence to virulence. J Res Med Sci *23*, 63.

Gillespie, S.H. (2002). Evolution of drug resistance in *Mycobacterium tuberculosis*: clinical and molecular perspective. Antimicrob Agents Chemother *46*, 267-274.

Gupta, R.K., and Srivastava, R. (2012). Resuscitation promoting factors: a family of microbial proteins in survival and resuscitation of dormant mycobacteria. Indian J Microbiol *52*, 114-121.

Hamilton, J.A. (2019). *GM-CSF*-Dependent Inflammatory Pathways. Front Immunol *10*, 2055.

Harriff, M.J., Cansler, M.E., Toren, K.G., Canfield, E.T., Kwak, S., Gold, M.C., and Lewinsohn, D.M. (2014). Human lung epithelial cells contain *Mycobacterium tuberculosis* in a late endosomal vacuole and are efficiently recognized by CD8(+) T cells. PLoS One *9*, e97515.

Hatherill, M., White, R.G., and Hawn, T.R. (2019). Clinical Development of New TB Vaccines: Recent Advances and Next Steps. Front Microbiol *10*, 3154.

Hett, E.C., and Rubin, E.J. (2008). Bacterial growth and cell division: a mycobacterial perspective. Microbiol Mol Biol Rev *72*, 126-156, table of contents.

Hossain, M.M., and Norazmi, M.N. (2013). Pattern recognition receptors and cytokines in *Mycobacterium tuberculosis* infection--the double-edged sword? Biomed Res Int *2013*, 179174.

Hossain, M.S., Ahmed, R., Haque, M.S., Alam, M.M., and Islam, M.S. (2019). Identification and validation of reference genes for real-time quantitative RT-PCR analysis in jute. BMC Mol Biol *20*, 13.

Hove, P., Molepo, J., Dube, S., and Nchabeleng, M. (2015). Genotypic diversity of *Mycobacterium tuberculosis* in pretoria. Southern African Journal of Epidemiology and Infection *27*, 77-83.

Ignatov, D., Malakho, S., Majorov, K., Skvortsov, T., Apt, A., and Azhikina, T. (2013). RNA-Seq analysis of *Mycobacterium avium* non-coding transcriptome. PLoS One *8*, e74209.

Ito, T., Connett, J.M., Kunkel, S.L., and Matsukawa, A. (2013). The linkage of innate and adaptive immune response during granulomatous development. Front Immunol *4*, 10.

Jee, B., Sharma, P., Katoch, K., Joshi, B., and Awasthi, S.K. (2017). *IL-10* down-regulates the expression of survival associated gene hspX of *Mycobacterium tuberculosis* in murine macrophage. Braz J Infect Dis *21*, 386-390.

Kana, B.D., Gordhan, B.G., Downing, K.J., Sung, N., Vostroktunova, G., Machowski, E.E., Tsenova, L., Young, M., Kaprelyants, A., Kaplan, G., and Mizrahi, V. (2008). The resuscitation-promoting factors of *Mycobacterium tuberculosis* are required for virulence and resuscitation from dormancy but are collectively dispensable for growth in vitro. Mol Microbiol *67*, 672-684.

Kana, B.D., and Mizrahi, V. (2010). Resuscitation-promoting factors as lytic enzymes for bacterial growth and signaling. FEMS Immunol Med Microbiol *58*, 39-50.

Kim, J.S., Kim, W.S., Choi, H.G., Jang, B., Lee, K., Park, J.H., Kim, H.J., Cho, S.N., and Shin, S.J. (2013). *Mycobacterium tuberculosis* RpfB drives Th1-type T cell immunity via a *TLR4*-dependent activation of dendritic cells. J Leukoc Biol *94*, 733-749.

Korb, V.C., Chuturgoon, A.A., and Moodley, D. (2016). *Mycobacterium tuberculosis*: Manipulator of Protective Immunity. Int J Mol Sci *17*, 131.

Kwon, K.W., Kim, W.S., Kim, H., Han, S.J., Hahn, M.Y., Lee, J.S., Nam, K.T., Cho, S.N., and Shin, S.J. (2017). Novel vaccine potential of Rv3131, a DosR regulon-encoded putative nitroreductase, against hyper-virulent *Mycobacterium tuberculosis* strain K. Sci Rep *7*, 44151.

Li, Y., Wang, Y., and Liu, X. (2012). The role of airway epithelial cells in response to mycobacteria infection. Clin Dev Immunol *2012*, 791392.

Liu, C.H., Liu, H., and Ge, B. (2017). Innate immunity in tuberculosis: host defense vs pathogen evasion. Cell Mol Immunol *14*, 963-975.

Lokau, J., Schoeder, V., Haybaeck, J., and Garbers, C. (2019). Jak-Stat Signaling Induced by Interleukin-6 Family Cytokines in Hepatocellular Carcinoma. Cancers (Basel) *11*.

Lotfi, N., Thome, R., Rezaei, N., Zhang, G.X., Rezaei, A., Rostami, A., and Esmaeil, N. (2019). Roles of *GM-CSF* in the Pathogenesis of Autoimmune Diseases: An Update. Front Immunol *10*, 1265.

Lowe, R., Shirley, N., Bleackley, M., Dolan, S., and Shafee, T. (2017). Transcriptomics technologies. PLoS Comput Biol *13*, e1005457.

Lowe, R., Shirley, N., Bleackley, M., Dolan, S., and Shafee, T. (2017). Transcriptomics technologies. PLoS Comput Biol *13*, e1005457.

Maguga-Phasha, N.T.C., Munyai, N.S., Mashinya, F., Makgatho, M.E., and Mbajiorgu, E.F. (2017). Genetic diversity and distribution of *Mycobacterium tuberculosis* genotypes in Limpopo, South Africa. BMC Infect Dis *17*, 764.

Mahamed, D., Boulle, M., Ganga, Y., Mc Arthur, C., Skroch, S., Oom, L., Catinas, O., Pillay, K., Naicker, M., Rampersad, S., *et al.* (2017). Intracellular growth of *Mycobacterium tuberculosis* after macrophage cell death leads to serial killing of host cells. Elife *6*.

Marino, S., Sud, D., Plessner, H., Lin, P.L., Chan, J., Flynn, J.L., and Kirschner, D.E. (2007). Differences in reactivation of tuberculosis induced from anti-*TNF* treatments are based on bioavailability in granulomatous tissue. PLoS Comput Biol *3*, 1909-1924.

Mayer-Barber, K.D., Andrade, B.B., Barber, D.L., Hieny, S., Feng, C.G., Caspar, P., Oland, S., Gordon, S., and Sher, A. (2011). Innate and adaptive interferons suppress IL-1alpha and IL-1beta production by distinct pulmonary myeloid subsets during *Mycobacterium tuberculosis* infection. Immunity *35*, 1023-1034.

Mayer-Barber, K.D., Andrade, B.B., Oland, S.D., Amaral, E.P., Barber, D.L., Gonzales, J., Derrick, S.C., Shi, R., Kumar, N.P., Wei, W., *et al.* (2014). Host-directed therapy of tuberculosis based on interleukin-1 and type I interferon crosstalk. Nature *511*, 99-103.

Meacci, F., Orru, G., Iona, E., Giannoni, F., Piersimoni, C., Pozzi, G., Fattorini, L., and Oggioni, M.R. (2005). Drug resistance evolution of a *Mycobacterium tuberculosis* strain from a noncompliant patient. J Clin Microbiol *43*, 3114-3120.

Meyer-Rath, G., Schnippel, K., Long, L., MacLeod, W., Sanne, I., Stevens, W., Pillay, S., Pillay, Y., and Rosen, S. (2012). The impact and cost of scaling up GeneXpert MTB/RIF in South Africa. PLoS One *7*, e36966.

Migliori, G.B., Lange, C., Centis, R., Sotgiu, G., Mutterlein, R., Hoffmann, H., Kliiman, K., De Iaco, G., Lauria, F.N., Richardson, M.D., *et al.* (2008). Resistance to second-line injectables and treatment outcomes in multidrug-resistant and extensively drug-resistant tuberculosis cases. Eur Respir J *31*, 1155-1159.

Mihret, A. (2012). The role of dendritic cells in *Mycobacterium tuberculosis* infection. Virulence *3*, 654-659.

Mishra, A., Singh, V.K., Actor, J.K., Hunter, R.L., Jagannath, C., Subbian, S., and Khan, A. (2020). *GM-CSF* Dependent Differential Control of *Mycobacterium tuberculosis* Infection in Human and Mouse Macrophages: Is Macrophage Source of GM-CSF Critical to Tuberculosis Immunity? Front Immunol *11*, 1599.

Moreira-Teixeira, L., Mayer-Barber, K., Sher, A., and O'Garra, A. (2018). Type I interferons in tuberculosis: Foe and occasionally friend. J Exp Med *215*, 1273-1285.

Munoz, L., Stagg, H.R., and Abubakar, I. (2015). Diagnosis and Management of Latent Tuberculosis Infection. Cold Spring Harb Perspect Med *5*.

Murray, J.F., Schraufnagel, D.E., and Hopewell, P.C. (2015). Treatment of Tuberculosis. A Historical Perspective. Ann Am Thorac Soc *12*, 1749-1759.

Naidoo, P., Theron, G., Rangaka, M.X., Chihota, V.N., Vaughan, L., Brey, Z.O., and Pillay, Y. (2017). The South African Tuberculosis Care Cascade: Estimated Losses and Methodological Challenges. J Infect Dis *216*, S702-S713.

Ndlovu, H., and Marakalala, M.J. (2016). Granulomas and Inflammation: Host-Directed Therapies for Tuberculosis. Front Immunol *7*, 434.

Ng, A.P., and Alexander, W.S. (2017). Haematopoietic stem cells: past, present and future. Cell Death Discov *3*, 17002.

Ning, S., Pagano, J.S., and Barber, G.N. (2011). *IRF7*: activation, regulation, modification and function. Genes Immun *12*, 399-414.

Nguyen, T.N.A., Anton-Le Berre, V., Banuls, A.L., and Nguyen, T.V.A. (2019). Molecular Diagnosis of Drug-Resistant Tuberculosis; A Literature Review. Front Microbiol *10*, 794.

O'Garra, A. (2013). Systems approach to understand the immune response in tuberculosis: an iterative process between mouse models and human disease. Cold Spring Harb Symp Quant Biol *78*, 173-177.

O'Leary, S., O'Sullivan, M.P., and Keane, J. (2011). *IL-10* blocks phagosome maturation in *Mycobacterium tuberculosis*-infected human macrophages. Am J Respir Cell Mol Biol *45*, 172-180.

Ottenhoff, T.H., and Kaufmann, S.H. (2012). Vaccines against tuberculosis: where are we and where do we need to go? PLoS Pathog *8*, e1002607.

Philips, J.A., and Ernst, J.D. (2012). Tuberculosis pathogenesis and immunity. Annu Rev Pathol *7*, 353-384.

Pillay, M., and Sturm, A.W. (2007). Evolution of the extensively drug-resistant F15/LAM4/KZN strain of *Mycobacterium tuberculosis* in KwaZulu-Natal, South Africa. Clin Infect Dis *45*, 1409-1414.

Rasmussen, S.B., Reinert, L.S., and Paludan, S.R. (2009). Innate recognition of intracellular pathogens: detection and activation of the first line of defense. APMIS *117*, 323-337.

Redford, P.S., Murray, P.J., and O'Garra, A. (2011). The role of *IL-10* in immune regulation during *M. tuberculosis infection*. Mucosal Immunol *4*, 261-270.

Ritz, N., Dutta, B., Donath, S., Casalaz, D., Connell, T.G., Tebruegge, M., Robins-Browne, R., Hanekom, W.A., Britton, W.J., and Curtis, N. (2012). The influence of bacille Calmette-Guerin vaccine strain on the immune response against tuberculosis: a randomized trial. Am J Respir Crit Care Med *185*, 213-222.

Romano, M., Aryan, E., Korf, H., Bruffaerts, N., Franken, C.L., Ottenhoff, T.H., and Huygen, K. (2012). Potential of *Mycobacterium tuberculosis* resuscitation-promoting factors as antigens in novel tuberculosis sub-unit vaccines. Microbes Infect *14*, 86-95.

Romero-Adrian, T.B. (2015). Role of cytokines and other factors involved in the *Mycobacterium tuberculosis* infection. World Journal of Immunology *5*, 16.

Rosser, A., Stover, C., Pareek, M., and Mukamolova, G.V. (2017). Resuscitation-promoting factors are important determinants of the pathophysiology in *Mycobacterium tuberculosis* infection. Crit Rev Microbiol *43*, 621-630.

Russell-Goldman, E., Xu, J., Wang, X., Chan, J., and Tufariello, J.M. (2008). A *Mycobacterium tuberculosis* Rpf double-knockout strain exhibits profound defects in reactivation from chronic tuberculosis and innate immunity phenotypes. Infect Immun *76*, 4269-4281.

Ryndak, M.B., and Laal, S. (2019). *Mycobacterium tuberculosis* Primary Infection and Dissemination: A Critical Role for Alveolar Epithelial Cells. Front Cell Infect Microbiol *9*, 299.

Sakamoto, K. (2012). The pathology of *Mycobacterium tuberculosis* infection. Vet Pathol *49*, 423-439.
Saleh, M., and Longhi, G. (2016). Macrophage Infection by Mycobacteria. Mycobacterial Diseases *06*.

Sasindran, S.J., and Torrelles, J.B. (2011). *Mycobacterium Tuberculosis* Infection and Inflammation: what is Beneficial for the Host and for the Bacterium? Front Microbiol *2*, 2.

Sawai, C.M., Babovic, S., Upadhaya, S., Knapp, D., Lavin, Y., Lau, C.M., Goloborodko, A., Feng, J., Fujisaki, J., Ding, L., *et al.* (2016). Hematopoietic Stem Cells Are the Major Source of Multilineage Hematopoiesis in Adult Animals. Immunity *45*, 597-609.

Sharma, M., Bose, M., Abhimanyu, Sharma, L., Diwakar, A., Kumar, S., Gaur, S.N., and Banavalikar, J.N. (2012). Intracellular survival of *Mycobacterium tuberculosis* in macrophages is modulated by phenotype of the pathogen and immune status of the host. Int J Mycobacteriol *1*, 65-74.

Sia, J.K., Georgieva, M., and Rengarajan, J. (2015). Innate Immune Defenses in Human Tuberculosis: An Overview of the Interactions between *Mycobacterium tuberculosis* and Innate Immune Cells. J Immunol Res *2015*, 747543.

Sia, J.K., and Rengarajan, J. (2019). Immunology of *Mycobacterium tuberculosis* Infections. Microbiol Spectr *7*.

Sloan, D.J., and Lewis, J.M. (2016). Management of multidrug-resistant TB: novel treatments and their expansion to low resource settings. Trans R Soc Trop Med Hyg *110*, 163-172.

Sohn, H., Kim, J.S., Shin, S.J., Kim, K., Won, C.J., Kim, W.S., Min, K.N., Choi, H.G., Lee, J.C., Park, J.K., and Kim, H.J. (2011). Targeting of *Mycobacterium tuberculosis* heparin-binding hemagglutinin to mitochondria in macrophages. PLoS Pathog *7*, e1002435.

Squeglia, F., Romano, M., Ruggiero, A., Vitagliano, L., De Simone, A., and Berisio, R. (2013). Carbohydrate recognition by RpfB from *Mycobacterium tuberculosis* unveiled by crystallographic and molecular dynamics analyses. Biophys J *104*, 2530-2539.

Stamm, C.E., Collins, A.C., and Shiloh, M.U. (2015). Sensing of *Mycobacterium tuberculosis* and consequences to both host and bacillus. Immunol Rev *264*, 204-219.

Stanley, S.A., Johndrow, J.E., Manzanillo, P., and Cox, J.S. (2007). The Type I IFN response to infection with *Mycobacterium tuberculosis* requires ESX-1-mediated secretion and contributes to pathogenesis. J Immunol *178*, 3143-3152.

Syedbasha, M., and Egli, A. (2017). Interferon Lambda: Modulating Immunity in Infectious Diseases. Front Immunol *8*, 119.

Thuong, N.T., Dunstan, S.J., Chau, T.T., Thorsson, V., Simmons, C.P., Quyen, N.T., Thwaites, G.E., Thi Ngoc Lan, N., Hibberd, M., Teo, Y.Y., *et al.* (2008). Identification of tuberculosis susceptibility genes with human macrophage gene expression profiles. PLoS Pathog *4*, e1000229.

Tiberi, S., Munoz-Torrico, M., Duarte, R., Dalcolmo, M., D'Ambrosio, L., and Migliori, G.B. (2018). New drugs and perspectives for new anti-tuberculosis regimens. Pulmonology *24*, 86-98.

Togun, T., Kampmann, B., Stoker, N.G., and Lipman, M. (2020). Anticipating the impact of the COVID-19 pandemic on TB patients and TB control programmes. Ann Clin Microbiol Antimicrob *19*, 21.

Tufariello, J.M., Jacobs, W.R., Jr., and Chan, J. (2004). Individual *Mycobacterium tuberculosis* resuscitation-promoting factor homologues are dispensable for growth *in vitro* and *in vivo*. Infect Immun *72*, 515-526.

Tufariello, J.M., Mi, K., Xu, J., Manabe, Y.C., Kesavan, A.K., Drumm, J., Tanaka, K., Jacobs, W.R., Jr., and Chan, J. (2006). Deletion of the *Mycobacterium tuberculosis* resuscitation-promoting factor Rv1009 gene results in delayed reactivation from chronic tuberculosis. Infect Immun *74*, 2985-2995.

van der Does, A.M., Bogaards, S.J., Ravensbergen, B., Beekhuizen, H., van Dissel, J.T., and Nibbering, P.H. (2010). Antimicrobial peptide hLF1-11 directs granulocyte-macrophage colony-stimulating factor-driven monocyte differentiation toward macrophages with enhanced recognition and clearance of pathogens. Antimicrob Agents Chemother *54*, 811-816.

Van Der Meeren, O., Hatherill, M., Nduba, V., Wilkinson, R.J., Muyoyeta, M., Van Brakel, E., Ayles, H.M., Henostroza, G., Thienemann, F., Scriba, T.J., *et al.* (2018). Phase 2b Controlled Trial of M72/AS01E Vaccine to Prevent Tuberculosis. N Engl J Med *379*, 1621-1634.

Van der Spoel van Dijk, A., Makhoahle, P.M., Rigouts, L., and Baba, K. (2016). Diverse Molecular Genotypes of *Mycobacterium tuberculosis* Complex Isolates Circulating in the Free State, South Africa. Int J Microbiol *2016*, 6572165.

van der Vaart, M., Spaink, H.P., and Meijer, A.H. (2012). Pathogen recognition and activation of the innate immune response in zebrafish. Adv Hematol *2012*, 159807.

VanGuilder, H.D., Vrana, K.E., and Freeman, W.M. (2008). Twenty-five years of quantitative PCR for gene expression analysis. Biotechniques *44*, 619-626.

Vassall, A., Siapka, M., Foster, N., Cunnama, L., Ramma, L., Fielding, K., McCarthy, K., Churchyard, G., Grant, A., and Sinanovic, E. (2017). Cost-effectiveness of Xpert MTB/RIF for tuberculosis diagnosis in South Africa: a real-world cost analysis and economic evaluation. The Lancet Global Health *5*, e710-e719.

Vekemans, J., Gebreselassie, N., Zignol, M., Friede, M., Kasaeva, T., and Swaminathan, S. (2019). A new tuberculosis vaccine: breakthrough, challenges, and a call for collaboration. The Lancet Infectious Diseases *19*, 123-125.

Verrall, A.J., Netea, M.G., Alisjahbana, B., Hill, P.C., and van Crevel, R. (2014). Early clearance of *Mycobacterium tuberculosis*: a new frontier in prevention. Immunology *141*, 506-513.

Wang, Z., Gerstein, M., and Snyder, M. (2009). RNA-Seq: a revolutionary tool for transcriptomics. NatRev Genet *10*, 57-63.

Wolf, J.B. (2013). Principles of transcriptome analysis and gene expression quantification: an RNA-seq tutorial. Mol Ecol Resour *13*, 559-572.

Xing, L., Cheng, Q., Zha, G., and Yi, S. (2017). Transcriptional Profiling at High Temporal Resolution Reveals Robust Immune/Inflammatory Responses during Rat Sciatic Nerve Recovery. Mediators Inflamm *2017*, 3827841.

Yan, K., Gao, L.N., Cui, Y.L., Zhang, Y., and Zhou, X. (2016). The cyclic AMP signaling pathway: Exploring targets for successful drug discovery (Review). Mol Med Rep *13*, 3715-3723.

Yeremeev, V.V., Kondratieva, T.K., Rubakova, E.I., Petrovskaya, S.N., Kazarian, K.A., Telkov, M.V., Biketov, S.F., Kaprelyants, A.S., and Apt, A.S. (2003). Proteins of the Rpf family: immune cell reactivity and vaccination efficacy against tuberculosis in mice. Infect Immun *71*, 4789-4794.

Zager, E.M., and McNerney, R. (2008). Multidrug-resistant tuberculosis. BMC Infect Dis *8*, 10.

Zhang, Y., Chan, J.F., and Cummins, C.L. (2009). Liver X Receptors as Therapeutic Targets for Managing Cholesterol: Implications for Atherosclerosis and Other Inflammatory Conditions. Clin Lipidol *4*, 29-40.

Zhao, S., Song, X., Zhao, Y., Qiu, Y., Mao, F., Zhang, C., Bai, B., Zhang, H., Wu, S., and Shi, C. (2015). Protective and therapeutic effects of the resuscitation-promoting factor domain and its mutants against *Mycobacterium tuberculosis* in mice. Pathog Dis *73*.

2.1 Chapter 2: The *rpfB* gene contributes to the regulation of the host innate immune response in THP- macrophages infected with *Mycobacterium tuberculosis* V9124.

Moti D[1,2], Mvubu N.E[4], Naidoo C. C[1,3], Pillay B[4], Pillay M[1].

[1]Medical Microbiology, School of Laboratory Medicine and Medical Science, University of KwaZulu-Natal, Durban, South Africa.

[2]Current address: Desmond Tutu TB Centre, Department of Paediatrics and Child Health, Faculty of Health Sciences, Tygerberg, Stellenbosch University, Cape Town, South Africa.

[3]Current address: DST/NRF Centre of Excellence in Biomedical Tuberculosis Research, and South African Research Council Centre for Tuberculosis Research, Division of Molecular Biology and Human Genetics, Faculty of Medicine and Health Sciences, Stellenbosch University, Cape Town, South Africa.

[4]Microbiology, School of Life Science, College of Agriculture, Engineering and Science, University of KwaZulu-Natal, Westville 3630, South Africa.

Corresponding author:
Professor Manormoney Pillay
Address: Medical Microbiology, School of Laboratory Medicine and Medical Science, University of KwaZulu-Natal
Phone: 0312604059
Email address: Pillayc@ukzn.ac.za.

Keywords: Macrophages, *M. tuberculosis*, *rpfB*, sequencing, transcriptional regulation, upstream regulators, canonical pathways.

Abstract

Background: Since the initial isolation of *Mycobacterium tuberculosis* (*Mtb*), tuberculosis (TB) remains among the top 10 causes of death. In 2019, 10 million people globally were burdened with TB, of which 25 %were from Africa. A fundamental process in determining the outcome of *Mtb* infection is host-pathogen interactions. These interactions may lead to eradication of bacteria via the innate immune response or latent TB infection (LTBI) in which the bacilli reside in a non-replicating, low metabolic state (dormancy) within AMs. Ten percent of the global population develops LTBI leaving them at greater risk of developing active TB. Initiation of an immune response requires effective antigenic stimulation that induces multiple signalling cascades and the production of pro-inflammatory and anti-inflammatory cytokines, effective against or beneficial to *Mtb*. The pathogen has a family of 5 resuscitation promoting factors (*rfps* A-E) that have been previously characterized in *Mtb* growth, persistence and reactivation, *in vitro* and *in vivo*, using single and multiple *rpf* gene knockouts. Among the other Rpfs proteins, RpfB was shown to be highly antigenic and immunogenic, with the ability to induce a Th1 phenotype immune response in dendritic cells (DC) through binding of toll-like receptor 4 (*TLR4*). Since macrophages are the target cell of *Mtb* and the reservoir of formant bacilli, this study investigated the effect of *rpfB* in THP-1 macrophages at a late phase of replication (72 hours post-infection) using an *Mtb rpfB* gene knockout strain, through global transcriptomic analysis.

Material and Methods: THP-1 macrophages seeded at 7.5 x 105 cells/mL, were infected at an MOI of 1 with wildtype (WT), Δ*rpfB* mutant and *rpfB*-complemented strains. To elucidate host transcriptomic changes attributed to *rpfB*, mammalian RNA was isolated 72 hours post-infection and sequenced using the Illumina High Seq platform. Bioinformatics analysis was performed using the tuxedo suite and Ingenuity Pathway Analysis (IPA). THP-1 cytokine production was analysed at 24-, 48-, and 72 hours post-infection using the human *GM-CSF* and *IL-1β* multiplex panel (Bio-Rad Laboratories) in a Bio-Plex 200 System (Bio-Rad Laboratories). RNA sequencing data were validated using quantitative real-time PCR (qRT-PCR).

Results: Global transcriptomic analysis revealed that *rpfB* induced differential transcriptional regulation in THP-1 macrophages. The total number of significantly enriched genes (SDEGs) induced in by WT strain was 5 times more than the mutant. Furthermore, the WT also induced a greater number of networks and upstream regulators. In addition this study showed *rpfB* stimulates, but is not essential to, IFN signalling, Role of JAK family kinases in IL-6 type cytokine signalling and Activation of IRF by Cytosolic PRRs, enhances IL-10 signalling and DC maturation, and enriches Acute phase response signalling, Phagosome formation, LXR/RXR activation, CAMP-mediated signalling, Gαi signalling and GADD45 signalling. In summary, the findings suggest *rpfB* contributes to the host protective immune response against *Mtb* infection. Upstream regulators induced by both infection models were

all cytokines, however regulated genes that were exclusive to each pathway and mostly interferon stimulated genes (*ISG*s) in WT infected macrophages.

Discussion and conclusion: Transcriptomic analysis showed *rpfB* induced recognition of host immunity and enhanced the THP-1 macrophage host immune response during late stages of *Mtb* infection. These findings provide basic evidence, which requires further interrogation, that *rpfB* regulates the immune response through interferon signalling and possibly plays a role in IL-10 signalling and DC maturation. Collectively, these findings indicate *rpfB* contribute to protective immunity of THP-1 macrophages against *Mtb* and may be used as a recombinant in vaccines against active TB and in combination with LTBI antigens, against LTBI. However, since these observations are reported for the first time, further investigation to validate these findings would be valuable.

Introduction

Tuberculosis (TB) ranks above HIV and is among the top 10 causes of death due to a single infectious agent (**WHO, 2020**). Despite the available treatment regimens (Gillepsie S., 2002; Oggioni et al., 2005; Naidoo et al., 2018), in 2019, 10 million people across the globe were estimated to develop the disease, of which 8.2% were HIV positive. South Africa (SA), one of the top 30 high TB burden countries, was the second country with the highest TB burden (25 %) in 2019 and accounted for 3.6 % of the 10 million incidence cases in 2019 (WHO 2020).

In addition to the poor level of efficacy of the only FDA approved vaccine, Bacillus Calmette-Guerin (BCG), to provide protective immunity against active TB in adolescence and adults (Kim *et al*., 2013; Bonavia et al., 2015; Davenne and McShane., 2016), the failure to efficiently control and maintain TB is attributed to the evolution of drug resistant strains that are more complex to treat (Gillepsie S, 2002; Oggioni et al., 2005; Naidoo et al., 2018). Furthermore, 23 % of the global population have latent TB infection, and are carriers of dormant *Mycobacterium tuberculosis* (*Mtb*) bacilli (Commandeur et al., 2011), leaving them with a greater risk of developing active TB (WHO, 2020). Collectively, these concerns highlight the necessity for extensive research targeting elucidation of novel biomarkers and approaches to improve the existing treatment regimen (Ottenfoff and Kaufmann., 2012).

The determining factor of the outcome of *Mtb* infection is the early interactions between the host and pathogen (Davenne and McShane, 2016; Sohn et al., 2011). Alveolar macrophages are the preferred target for *Mtb* invasion since they express multiple pathogen recognition receptors (PRR) that interact with *Mtb* pathogen associated molecular patterns (PAMP) during invasion (Sohn et al., 2011; Davenne and McShane., 2016). The interaction between the two leads to activation of multiple intracellular signalling pathways that induces production of a variety of cytokines and chemokines, which are

essential for initiating adaptive immunity (Downing et al., 2004; Sasindran and Torelles., 2011; Norazmi and Hossain., 2013; Valecillo et al., 2015; McShane and Davenne., 2016; Saleh *et al*., 2016; Baoxue Ge et al., 2017; Chiappini et al., 2019; Liu et al., 2019). However, *Mtb* has developed strategies to evade intracellular eradication by manipulating and influencing the function of immune cells as well as their cytokine and chemokine production (Du et al., 2016; Davenne and McShane., 2016; Saleh *et al*., 2016; Baoxue Ge et al., 2017; Liu et al., 2019)) (Valecillo et al., 2015; McShane and Davenne., 2016; Baoxue Ge et al., 2017 Chiappini et al., 2019, thus facilitating its survival and persistence (McShane and Davenne., 2016; Liu et al., 2019).

Given the role of macrophages in *Mtb* pathogenesis, its maturation and differentiation are pivotal to its protective function against *Mtb*. *GM-CSF* is a cytokine produced during inflammation by multiple cells, including macrophages, that exerts a wide range of effects on myeloid cells such as survival, activation, differentiation, and mobilization (Lotfi et al., 2019). Its expression is induced by members of the *IL-1* family, *TNF-α*, and *IL-12*, and supressed by *IL-4*, *IFN-γ* and *IL-10*. Previous studies (Hamilton, 2019; Lotfi et al., 2019) have shown *GM-CSF* is required for maturation and differentiation of macrophages to the pro-inflammatory phenotype and promotes its survival. Another cytokine that contributes to macrophage differentiation, and enhances their phagocytic and antigen presenting abilities, is *IL-1β* (Averbakh and Ergeshow, 2018). *IL-1β* is a potent regulator of inflammation and immune response and is required for host resistance (Chao et al., 2017; Cooper et al., 2011). Overall, it has been implicated in direct killing of *Mtb*, recruitment of anti-microbial effector cells, and macrophage response against *Mtb* (Romero-Adrian, 2015).

The role of *rpfB* has been well characterized in *Mtb* growth, persistence and reactivation (Tufariello et al., 2004; Downing et al., 2005; Tufariello., et al, 2006; Russell-Goldman et al., 2008). Analysis of host immune recognition revealed RpfB is highly antigenic and immunogenic and is therefore a potential target of the host immune response (Romano et al., 2011; Yeremeev et al., 2003). Some cellular and *in vivo* studies have demonstrated that exposure to the RpfB protein leads to the development of T cell immunity, specifically the Th1 phenotype (Kim et al., 2013). In addition, cytokine profiles of murine bone marrow derived macrophages (Russell-Goldman et al., 2008) and dendritic cells (Kim et al., 2013) show increased levels of pro-inflammatory cytokines when infected with mycobacterial *rpfB* deficient strains compared to wild type strains and uninfected controls**.** Studies also reported that RpfB regulates innate immunity and activates adaptive immunity, assessed specifically through binding of RpfB to TLR4 of DCs (Kana et al., 2008; Gupta and Srivastava, 2012; Romano et al., 2012; Kim et al., 2013).

Narrowing down the analysis of the immune response to specific pathogenic determinants may elucidate integral biomarkers and therapeutic targets in controlling TB. Transcriptomic studies can be used to elucidate novel antigens expressed during *Mtb* infection that are capable of eliciting an immune response against the pathogen. The majority of research studies (Tufariello et al., 2004; Downing et al.,

2005; Tufariello et al., 2006; Russell-Goldman et al., 2008) associated with *rpfB* have focused mainly on its role in growth, persistence and resuscitation of *Mtb*. There is limited information on its contribution to, and effect on, macrophage host gene regulation using global transcriptomics. In this study, the global transcriptomic response of THP-1 macrophages infected with *rpfB*-proficient and deficient strains were analysed by RNA sequencing and validated with *GM-CSF* and *IL-1β* multiplex assays, and qRT-PCR.

Materials and Methods

Ethics approval

The study was approved by the Biomedical Research and Ethics Committee (BREC), University of KwaZulu-Natal (UKZN), reference number: BE271/15 (Approval letter shown in Appendix A).

Bacterial strains and growth conditions

M. tuberculosis V9124, a drug-susceptible clinical isolate of the F15/LAM4/KZN family (wild type) (provided by Medical Microbiology, University of KwaZulu-Natal) was used to generate the previously constructed unmarked Δ*rpfB* mutant (Dr. C. C. Naidoo, PhD student, Medical Microbiology, UKZN, South Africa, unpublished) (Generation of strain shown in Appendix B) and *rpfB*-complemented strain. Briefly, an allelic exchange substrate (AES) (provided by Dr. William Jacobs Jr, Albert Einstein College of Medicine, New York, United States of America) containing a hygromycin resistance (hyg^R)-sacB cassette (screening marker) was used to replace the *rpfB* gene in the genome of the WT strain by specialized transduction. Following confirmation of the Δ*rpfB* mutant strain, unmarking was performed using a γδ-resolvase encoded phAE280 phage to remove the hyg^R-sacB cassette from the AES. Unmarking was confirmed on 7H10 agar (DIFO, Becton Dickinson, South Africa) containing 3 % sucrose by the pick and patch method and PCR (Confirmation shown in Appendix B). Frozen stocks of each strain were revived and propagated in Middlebrook 7H9 broth (Difco, Becton Dickinson), with hygromycin (75 µg/mL, Roche) and kanamycin (50 µg/mL, Sigma) for the mutant and complement strain, respectively, and supplemented with 0.5 % (v/v) Glycerol (Merck, South Africa), 0.05 % (v/v) Tween-80 (Sigma, Merck) and 10 % (v/v) oleic acid dextrose catalase enrichment (OADC) (Becton Dickinson). Cultures were incubated at 37 °C with agitation (100 rpm) (New Brunswick Scientific, South Africa) to exponential phase (OD_{600nm} ~1) (WPA, Lightwave II, Labotec, South Africa). Stocks of 1 mL were stored at -80 °C until further use.

Construction of the *Mtb rpfB*-complemented strain

Cloning of the *Mtb rpfB* gene into the pMV261 plasmid vector

Amplification and digestion

M. tuberculosis rpfB gene (1089 bp) was amplified using whole gene primers (Table 2.1). The PCR master mix contained: 10 x PCR buffer with $MgCl_2$, 0.5 mM $MgCl_2$, 200 µM dNTPs, 10 µM of each primer, 1 U Taq polymerase (Roche, Merck), and 60 ng wild type DNA per 50 µL total volume reaction. Thermal cycling conditions were as follows: 94 °C for 2 minutes, 30 cycles of 94 °C for 30 seconds, annealing at 63 °C for 30 seconds, 72 °C for 1 minute, and a final extension at 72 °C for 7 minutes (MultiGene Optimax, Labnet, Whitehead Scientific, South Africa). The resulting amplicons were electrophoresed before and after purification (QIAquick PCR Purification Kit, Qiagen, Whitehead Scientific) in addition to extracted pMV261 plasmid DNA vector containing the *hsp60* promoter, (plasmid mini prep kit, Qiagen), at 70 volts for 1 hour. Purified amplicons and plasmid DNA were double digested using fast digest EcoRI and HindIII restriction enzymes (Fermentas, ThermoFisher Scientific, South Africa) at 37°C for 1 hour. The reaction mixture contained: 10X universal buffer, 1 µL of each restriction enzyme, and either *rpfB* PCR product or pMV261 DNA in a final volume of 20 µL. Digestion enzymes were inactivated at 80 °C for 10 minutes. Digestion was confirmed via electrophoresis at 70V for 1 hour.

Ligation of digested pMV261 plasmid DNA and *rpfB* amplicon and transformation into *E. coli* DH5α competent cells Digested fragments were ligated using T4 DNA ligase (ThermoFisher Scientific) at 16 °C for ~16 hours in a thermal cycler (MultiGene Optimax, Labnet, Whitehead Scientific). The reaction mixture contained the following: 10 X ligation buffer, 1 µL ligase, either 50, 75 or 100 ng *rpfB* insert to 25 ng plasmid, and nuclease-free water in a final volume of 20 µL. Ligation mixtures were transformed into chemically competent DH5-α *E. coli* cells at 37 °C at 300 rpm for 1 hour. Plasmid DNA from transformant colonies grown overnight on Luria Bertani-Kanamycin (LB-Kan, 1 µL/mL) agar at 37°C were screened by PCR for the kanamycin and the *rpfB* genes.

Electro-transformation into *Mtb* Δ*rpfB* mutant cultures

Plasmid DNA was extracted from PCR confirmed pMV261-*rpfB* transformants, and the pMV261-rpfB construct was electroporated into electrocompetent *Mtb* Δ*rpfB* mutant cultures at 2500 Hv, 1000 Ω, capacitor 25 uF (ECM 630, BTX Harvard Apparatus, South Africa), followed by overnight incubation at 37°C. Putative transformants were selected from 7H11-Kan (50 µg/mL) agar after incubation at 37°C for 3 weeks and plasmid DNA screened by PCR for the *rpfB* gene and kanamycin cassette.

Confirmation of the *Mtb rpfB*-complemented strain

Polymerase chain reaction

Plasmid DNA from potential *Mtb* transformed cells was isolated (Plasmid mini prep kit, Qiagen) and amplified using *rpfB* gene specific primers (Table 1). The PCR master mix contained: 10 x PCR buffer with MgCl2, 0.5 mM MgCl2, 200 µM dNTPs, 10 µM of each primer, 1 U Taq polymerase (Roche, Merck), and 1 µL of plasmid DNA per 10 µL total reaction volume. Thermal cycling conditions were as follows: 94 ℃ for 2 minutes, 30 cycles of 94 ℃ for 30 seconds, annealing at 63 ℃ for 30 seconds, 72 ℃ for 1 minute, and a final extension at 72 ℃ for 7 minutes (MultiGene Optimax, Labnet). Amplification of the kanamycin cassette in transformed colonies was performed using primers, Kan-F and Kan-R (Table 2.1) (Inqaba Biotec, South Africa) with the same PCR master mix components and thermal cycling conditions, apart from 53 ℃ for annealing.

NGS sequencing

Purified (QIAquick PCR Purification Kit, Qiagen) gene specific amplicons and gene specific primers (Table 2.1) were sent to Inqaba Biotec for Sanger sequencing. Chromatogram and sequence analysis were performed using a trial version of Geneious Prime (v2019.0.4). Forward and reverse primers were pairwise aligned to the *Mycobacterium tuberculosis* H37Rv complete genome, selected from the software database.

Table 2.1: Primers used for PCR and NGS complement confirmation, and qRT-PCR.

Name	Sequence	Product size (bp)	Application
rpfB-EcoRI_F	5'-TTTTTTGAATTCATGTTGCGCCTGGTAGTCG- 3'	1089	Amplification of *rpfB* sequence
rpfB-HindIII_R	5'-TTTTTTAAGCTTTCAGCGCGCACCCGCTCGT-3'		
Kan_F	5'-TTATGCCTCTTCCGACCATC-3'	223	PCR confirmation of complement transformants and complement strain
Kan_R	5'-GCCTGAGCGAGACGAAATAC-3'		
*rpfB*_F	5'-ATGTTGCGCCTGGTAGTCG -3'	1089	PCR confirmation of complement transformants and complement strain PCR and NGS sequencing confirmation of complement
*rpfB*_R	5'-TCAGCGCGCACCCGCTCGT-3'		
IL-1B_F	5'- CTCTTCAGCCAATCTTCAT-3'	333	qRT-PCR validation of RNA sequencing results
IL-1B_R	5'- AGATGAAGGGAAAGAAGGTGC-3'		
GM-CSF_F	5'- TGGCTGCAGAGCCTGCTGCTC-3'	432	qRT-PCR validation of RNA sequencing results
GM-CSF_R	5'- TCACTCCTGGACTGGCTCCC-3'		
GAPDH_F	5'-GAGTCAACGGATTTGGTCGT-3'	262	qRT-PCR validation of RNA sequencing results
GAPDH_R	5'-AAATGAGCCCCAGCCTTCT-3'		

Propagation of THP-1 cells

Frozen stocks of human monocytic THP-1 cells were propagated in RPMI 1640 media with 2 mM L-glutamine (Lonza, Whitehead Scientific), supplemented with 20% fetal bovine serum (FBS) (Biowest, Celtic Molecular Diagnostics, South Africa) at 37 °C with 5 % CO_2 and 95 % humidity (CO_2 Series, Shel Lab, United Scientific, South Africa). Cell suspensions were seeded in triplicate in 25 cm^2 flasks (NEST, Biotechnology, Whitehead Scientific) at a density of 7.5 x 10^5 cells/mL. Cells were differentiated into macrophages with 50 ng/mL phorbol-myristate-acetate (PMA) (Sigma, Merck) at 37 °C with 5 % CO_2 and 95 % humidity. Following overnight incubation, monolayers were washed with 10 X PBS (Oxoid, Thermofisher Scientific) to remove non-adherent cells and PMA.

THP-1 macrophage infection

M. tuberculosis cultures were grown to logarithmic phase (OD_{600nm} = ~1) and centrifuged at 2000 x g for 10 minutes (Heraeus Multifuge 3S-R centrifuge, Thermo Electron Corporation, Separations Scientific, South Africa) following resuspension of pellets in fresh RPMI media. To dissociate and prevent clumping, bacterial suspensions were homogenized several times using a 26-gauge needle (Healthease Plus, United Scientific). For both RNA and cytokine/chemokine profiling experiments, monolayers were infected at a multiplicity of infection (MOI) of 1:1 at 37 °C with 5 % CO_2 for 4 hours. Post-incubation spent media was discarded and monolayers were washed once in an equal volume of 10 X PBS to remove extracellular bacteria. Flasks were replaced with fresh RPMI media and incubated at 37°C with 5% CO_2 for the required time intervals. At 48 hours post-infection, spent media was discarded from flasks and replaced with fresh media for re-incubation. For all infection experiments, uninfected macrophages were included as a negative control and each of the three biological assays were performed in triplicate, independent of each other. To confirm a MOI of 1, 100 µL of the bacterial inoculum was serially diluted 10-fold in 7H9 broth and plated (100 µL) in triplicate on Middlebrook 7H11 agar (DIFCO, Becton Dickinson) supplemented with 10 % OADC and 0.5 % glycerol. To determine the intracellular bacterial load at each interval post-infection, monolayers were washed once with an equal volume of 10 X PBS and lysed with 1 % (v/v) triton X-100 (Sigma, Merck) for 20 minutes at 37°C with 5% CO_2. Cells were serially diluted 10-fold for plating (100 µL) in triplicate on 7H11 agar. All plates were incubated at 37 °C with 5 % CO_2 for 3 weeks. Dilutions that produced 20 – 200 colonies were used for colony forming units per mL (CFU/mL) quantification (Raw CFU/mL data shown in Appendix D).

GM-CSF and *IL-1B* Luminex human magnetic assay

At 24-, 48- and 72-hours post-infection, infected and uninfected cell culture supernatants were removed and filtered through a 0.22 µm sterile filter (Lasec) into 2.0 mL microcentrifuge tubes (Merck) containing 50 µL bovine serum albumin (BSA) (0.1 g/mL) (Roche, Merck). Supernatants were stored

at -80°C until further use. *GM-CSF* and *IL-1B* human cytokine/chemokine analytes (R n D systems, Whitehead Scientific) were used for quantification, in duplicate, in a Bio-Plex 200 instrument for 1.5 hours at a five-parameter logistic regression algorithm (5PL) (Bio-Rad Laboratories, Lasec, South Africa), according to the manufacturer's instructions. The analyte concentrations in the standards and samples were normalized against the background using RPMI media. All wash steps were performed using the Bio-Plex Pro ™ wash station (Bio-Rad Laboratories, Lasec) (Raw data shown in Appendix I).

Mammalian RNA harvesting and isolation from infected and uninfected THP-1 macrophages 72 hours post-infection

Infected and uninfected monolayers were washed once with an equal volume of 10 X PBS. Cells were detached by treatment with 2 mL Trypsin-Versene (Lonza) for 5 minutes at 37 °C with 5 % CO_2. Cell scrapers (NEST Biotechnology) were used to remove any remaining adhered cells by gently scraping the surface of the flasks. Harvested cells were centrifuged at 300 x g for 5 minutes and pellets were resuspended in RLT lysis buffer (RNeasy mini kit, Qiagen) with 1 % β-mercaptoethanol (Sigma, Merck) and stored at -80 °C until further use. Thawed lysates were homogenized using a 21-gauge needle (Healthease Plus, United Scientific) and RNA was isolated using the RNeasy mini kit (Qiagen) according to manufacturer's instructions. DNA digestion was performed using 80 µL DNase I (10 µL stock solution added to 70 µL RDD buffer) (Qiagen). RNA was eluted in 30 µL of RNase-free water and aliquoted in 0.2 mL microcentrifuge tubes (Lasec) for storage at -80 °C until used for downstream analysis (Raw RNA extraction data shown in Appendix E).

RNA quantification and integrity analysis

Quantity and quality of RNA was evaluated using the Nanodrop 2000c Spectrophotometer (ThermoFisher Scientific). RNA with a value of 2 for both the A260/280 and A260/230 purity ratios was considered good quality (Shown in Appendix C). Integrity of RNA was assessed by 1 x RNA 3-(N-morpholino) propanesulfonic acid (MOPS) (Sigma, Merck) gel electrophoresis for 3 hours at 60V. Prior to library preparation, RNA concentration was further analysed by Omega Bioservices (Norcross, GA, United States of America) using the Nanodrop 2000c spectrophotometer (ThermoFisher Scientific, Waltham, MA, United States of America), and integrity was assessed using Agilent 2200 Tape station instrument (Agilent Technologies, Santa Clara, CA, United States of America). All samples attained RNA integrity numbers (RIN) of 9 and above (RNA quality analysis shown in Appendix E).

TruSeq stranded mRNA sequencing and quality assessment

Sequencing libraries were prepared using the TruSeq Stranded mRNA Library Prep Kit (Illumina, San Diego, CA) according to manufacturer's instructions. The Promega QuantiFluor dsDNA system was used to quantify the libraries on a Quants Fluorometer (Promega, Madison, WI) and the size and purity were assessed using the High Sensitivity D1000 Screen Tape on an Agilent 2200 Tape Station instrument. Pair end read sequencing of RNA samples was performed using a HiSeq 4000 platform (Illumina, San Diego) at 50 million reads in 2 x 150 base pair reads format (25M reads in each direction) for 150 cycles.

Upstream bioinformatics analysis

Post mRNA sequencing, adaptor sequences were trimmed off using Trimmomatic 0.36 (Linux, Ubuntu software). The quality of the adaptor trimmed mRNA sequenced reads were assessed using the online Babraham Bioinformatics FastQc (v0.11.7) tool. The sequenced reads were aligned to the *homo sapiens* HG38 reference genome (University of California Santa Cruz (UCSC) browser) using *Tophat* (v2.1.0, in conjunction with *Bowtie2* (v2.2.1) (Alignment and mapping data shown in Appendix E). Transcript assembly, merging of assembled transcripts and differential gene expression analysis was analysed using *cuffmerge* and *cuffdiff* implemented within a *cufflinks* pipeline (v 2.2) (Trapnell *et al*, 2012). The significantly differentially expressed genes (SDEGs) were identified using log fold changes of greater than and less than 1.5 (Trapnell *et al*, 2012) which were used for downstream analysis.

Downstream analysis

Data visualization and global transcriptome statistical analysis

SDEGs were categorised into three groups using Venny (Oliveros, J.C. (2007-2015) Venny. An interactive tool for comparing lists with Venn's diagrams. https://bioinfogp.cnb.csic.es/tools/venny/index.html). SDEGs commonly induced by the WT and mutant and those exclusive to either, relative to uninfected host cells. Heat maps were generated to visualize commonly induced SDEGs by log fold change using MultiExperiment Viewer (V4.9.0). Global transcriptome statistical analysis and visualization of the statistics were analysed and generated using a Bioconductor package, cummeRbund, within R (v3.4.3) and R studio software (v2.20.0).

Gene ontology (GO) and functional enrichment analysis

Functional profiles of *Mtb* wild type and Δ*rpfB* mutant induced SDEGs were generated using Molecular Signatures Database (MSigDB). To identify and analyse biological functions associated with the SDEGs, compute overlaps C5 (GO gene sets) was selected which included GO biological process (BP), GO cellular components (CC) and GO molecular functions (MF). A false discovery rate (FDR) *q*-value < 0.05 was used as a statistical cut-off.

Ingenuity Pathway Analysis (IPA)

Core analysis within IPA (v7.0, Ingenuity Systems, USA) was performed to interpret SDEGs in the context of biological processes, pathways and networks. The software was used to provide biological insight into canonical pathways, upstream regulators, mechanistic networks, and diseases and functions associated with the input data set.

Canonical Pathways

Significance values (*p*-value and z-score) were calculated by Fisher's exact test right-tailed. The pathways are first represented in a bar graph chart with the tallest bars equating to increased significance (*p*-value <0.05). The orange (activated) and blue (inhibited) bars represent the predicted activation/inhibition state of the pathway (z-score), whereas the white bars indicate a z-score close to or equal to 0, and grey bars are ineligible for prediction. When viewing the same graph as stacked bar graph, red and green bars represent the number of up- and down-regulated genes, respectively. The grey bars represent unchanged molecules. In a canonical pathway, dataset genes are highlighted in pink, up-regulated and down-regulated genes in red and green, respectively, and double bordered molecules represent a complex or groups that have other associated members.

Upstream regulator analysis

Upstream regulator analysis identifies a variety of different types of molecules that may be responsible for the changes in gene expression observed (regulators). A *p*-value <0.05 and Fisher's exact test was used to calculate significant overlapping genes in the dataset and genes regulated by upstream molecules. An activation z-score ≥ 2 (increased function) and ≤ 2 (decreased function) was considered significant in determining the activation state of the regulators.

Mechanistic networks

For each upstream regulator of interest, a mechanistic network was generated displaying plausible sets of associated regulators that may collectively be responsible for gene expression changes observed in the dataset. The guiding statistical parameters were Fisher's exact test *p*-value and z-score.

Diseases and functions

To further visualize and explore biological trends in the dataset, the diseases and functions category provides both a heat map and bar graph of the most enriched biological processes, diseases and toxicological functions based on associated gene expression changes. The prediction of increased or decreased function is based on the comparison of expected causal effects and the actual effect observed in the data. The statistical parameters guiding these predictions are a *p*-value <0.05 and a z-score ≥ 2 (increased function) and ≤ 2 (decreased function).

Quantitative real-time PCR (qRT-PCR)

Validation of the RNA sequencing results was completed using *IL-1B, GM-CSF*, and *GAPDH* (reference) genes from two independent biological replicates. These two analytes were selected for validation based on their frequent appearance in canonical pathways indicated in the results section. Total RNA was synthesised into cDNA using the High Capacity cDNA RT kit (Thermo Scientific). In a 10 µL reaction, the master mix contained 10 X RT buffer, 25 X dNTP mix, 10 x RT random primers, 1 µL multiscribe reverse transcriptase, 1 µL RNase inhibitor and 500 ng total RNA. The cDNA synthesis thermal cycling conditions were followed as per manufacturer's instructions. The reverse transcription master mix included 2X SYBR green supermix (Bio-Rad), 10 µM µL forward and reverse primers (Table 1), and 50 ng cDNA in a total volume of 10 µL. Quantification was performed at 95°C for 10 min, 95°C for 30 s, annealing at 60°C for 30 s, extension at 72°C for 30 s at 45 cycles; Melt curve: 95°C for 15 s, 60°C for 1 min, 95°C for 15 s using the QuantStudio™ 5 Real-Time PCR System (Thermofisher Scientific). For each target gene, a melt curve analysis was generated to confirm amplification specificity using serially diluted cDNA to generate standard curves (Melt and standard curves is shown in Appendix H).

Statistical analysis

The ANOVA and Tukey Post-hoc test statistical analysis was used to determine the significant difference in bacterial load between samples infected with the respective strains at different time intervals. A p <0.05 and a confidence interval of 95 % were equated to statistical significance. Samples displaying the least significant difference ($p < 0.05$) in bacterial load were selected for RNA sequencing and the multiplex magnetic bead-based assay. SPSS (V22.0) was used to analyse cytokine and qRT-PCR results and generate graphs.

Results

Confirmation of the *Mtb* Δ*rpfB* mutant and complemented strain

PCR screening

Mtb Δ*rpfB* mutant strain (Dr. C. C Naidoo, Unpublished).

Construction of the Δ*rpfB* mutant strain was achieved by specialized transduction. A 600 bp product size was amplified in the WT and 500 bp in the mutant (Figure 2.1), thus confirming deletion of the *rpfB* gene.

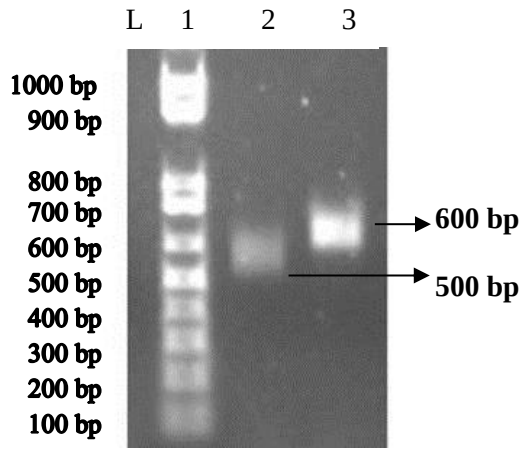

Figure 2.1: PCR confirmation of the *Mtb* Δ*rpfB* mutant strain. The *rpfB* gene was amplified using *rpfB*_L and uni_uptag primers in the mutant strain (lane 2) to yield a 500 bp product, and *rpfB*_right and uni_uptag primers in the WT strain (lane 3) to yield a 600 bp product. The amplicon size was verified against a 100 bp molecular weight marker (lane 1). PCR products were resolved on a 1.5 % agarose gel and viewed using a UV-transilluminator at 80 ms.

Mtb rpfB-complemented strain

The pMV261 plasmid contained the promoter region to allow for *rpfB* expression. Complementation was achieved via electro-transformation of transformed *rpfB*-pMV261 constructs into the Δ*rpfB* mutant strain. A 223 bp region of the kanamycin cassette was amplified in 5 randomly selected putative transformed colonies and the pMV261 positive control, confirming the presence of the pMV261 (Figure 2.2A). The same 5 colonies were then screened for the *rpfB* gene insert (1089 bp). Four of the 5 colonies were successfully complemented with the *rpfB* gene (Figure 2.2B).

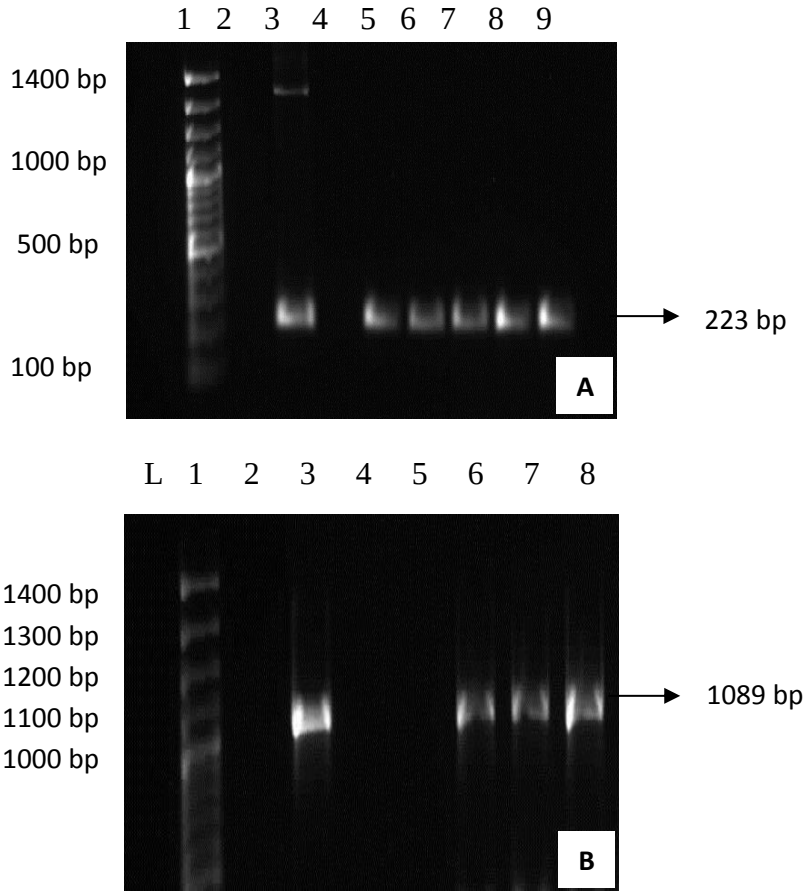

Figure 2.2: PCR confirmation of the *rpfB*-complement strain. (A) Amplification of a 223 bp region of the kanamycin cassette in the positive pMV261 control (lane 3) and all 5 putative transformed replicates (lanes 5-9) against a 100 bp molecular weight marker (lane 1). **(B)** *rpfB* whole gene amplification produced an amplicon size of 1089 bp in the WT positive control (lane 3) and 3 of the 5 kanamycin positive replicates (lanes 6-8). All PCR products were resolved on a 1.5 % agarose gel and viewed using the UV-transilluminator at 80 ms**Next Generation Sequencing**

Mtb Δ*rpfB* mutant strain (Dr. C. C Naidoo, Unpublished).

In correlation with PCR confirmation, the chromatogram shows the primer sequences shared sequence similarity of the uptag and right primer to the reference *Mtb* H37Rv *rpfB* gene sequence, thereby confirming the loss of the gene (Figure 2.3) (Dr. C. C Naidoo, Unpublished).

Figure 2.3: **Chromatogram illustration of confirmatory Sanger sequence alignment of the *Mtb* Δ*rpfB* mutant strain. (Upper)** The *rpfB*_left primer shares sequence similarity of 3 bp to the reference *Mtb* H37Rv *rpfB* gene sequence, confirming the *rpfB* gene knockout. **(Lower)** As expected, the universal_uptag primer shares greater sequence similarity, approximately 48 bp to the reference. All chromatogram images were generated using the online trial Geneious software.(Dr. C. C Naidoo, Unpublished)

Mtb rpfB complemented strain

PCR confirmatory amplicons were purified using the QIAquick PCR Purification kit (Qiagen, Whitehead Scientific) and subjected to Sanger sequencing at Inqaba Biotec (Johannesburg) using *rpfB*_F and *rpfB*_R whole gene primers (Table 2.1). The generated consensus sequence was aligned against the *Mtb* H37Rv *rpfB* reference gene using the Geneious Prime software (2020.1.2) (Figure 2.4).

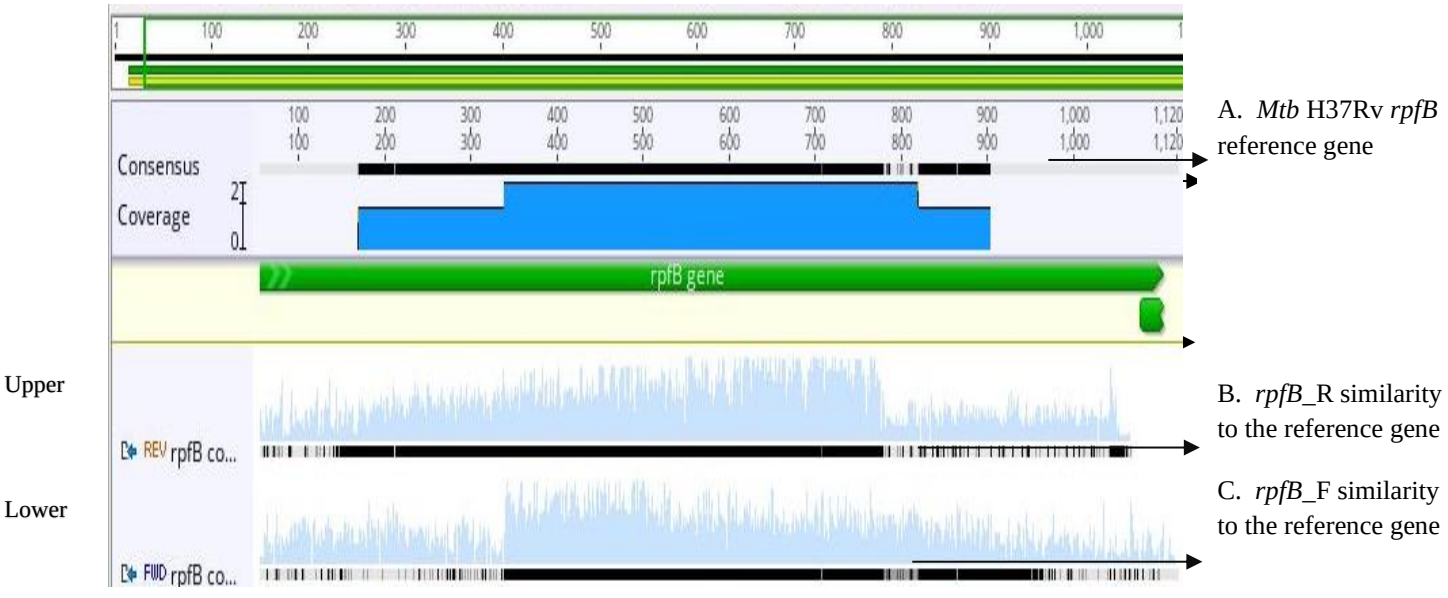

Figure 2.4: Chromatogram illustration of confirmatory Sanger sequence alignment. A. The consensus sequence displays approximately 80% alignment and coverage to the *Mtb* H37Rv *rpfB* gene sequence serving as confirmation of *rpfB* complementation. **B and C**. Alignment of the *rpfB*_F and *rpfB*_R whole gene primers displays the regions that made up the consensus sequence.

RNA expression analysis

Global transcriptome analysis of WT and Δ*rpfB* infected THP-1 cells, 72 hours post-infection.

At 72 hours post-infection, RNA from uninfected and WT and Δ*rpfB* infected THP-1 cells were sequenced in duplicate using the HiSeq 4000 Illumina platform. Sequenced reads were trimmed, analysed via FastQC and aligned to the HG38 human genome using Linux (Quality analysis and mapping data shown in Appendix E). Downstream analysis was performed using Venny (V2.1), MeV (V4.9.0) and IPA software for differential gene expression, statistical and functional enrichment, and pathway and network analysis. Sequencing results were supported by cytokine analysis and validated by qRT-PCR. Relative to the uninfected host, a total of 22 914 host genes was expressed in response to *Mtb* infection, and filtered to include only those with a minimum log1.5-fold change (SDEGs), which were used for further analysis (Differential expression FPKM plots shown in Appendix E). Overall, 629 SDEGs were identified of which 289 and 52 were exclusively induced by the WT and mutant infection, respectively (Figure 2.5) (Genes with fold changes shown in Appendix F). Exclusively induced WT and mutant SDEGs were not enriched in the same biological processes. The WT induced SDEGs were associated with biological processes such as Cellular response to lipid, Response to oxygen containing compound, Defence response, Inflammatory response, and Cellular response to biotic stimulus and Secretion, whereas the mutant induced SDEGs were associated with Response to cytokine, Response to biotic stimulus, Cytokine mediated signalling pathway, Innate immune response, Immune effector process and Response to type I interferon. Of the 288 commonly induced SDEGs (Genes with fold changes shown in Appendix F), 150 SDEGs were upregulated and 138 SDEGs were downregulated (Figure 2.6). Differential expression patterns of commonly induced SDEGs between the WT and mutant infected host were similar such that the regulation state (up- or downregulated) for any given SDEG is the same but at different levels of expression (Figure 2.7).

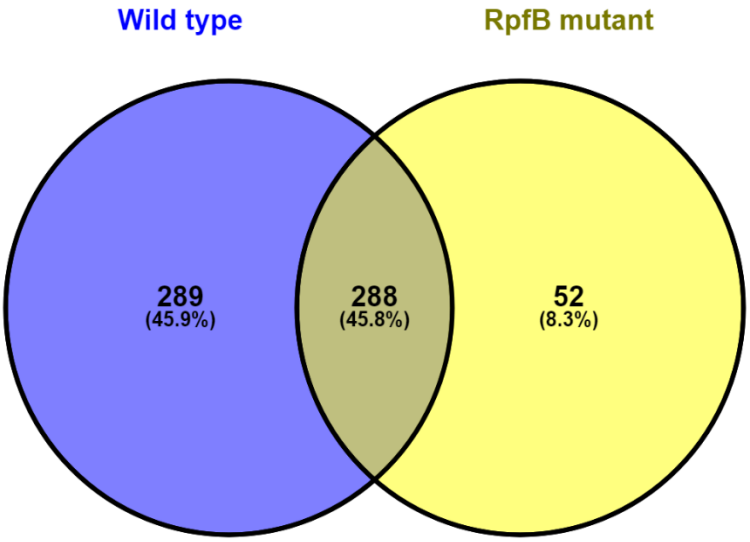

Figure 2.5: Total number of SDEGs with a log1.5-fold change induced at 72 hours post-infection by WT and Δ*rpfB* mutant infection, relative to the uninfected host. Blue. Number of WT induced SDEGs, relative to the uninfected host. **Yellow**. Number of mutant induced SDEGs, relative to the uninfected host. **Intersection**. Number of commonly induced SDEGs, relative to the uninfected host. **Wild type**: Induced by WT infection. Δ***RpfB*** **mutant**: Induced by mutant infection.

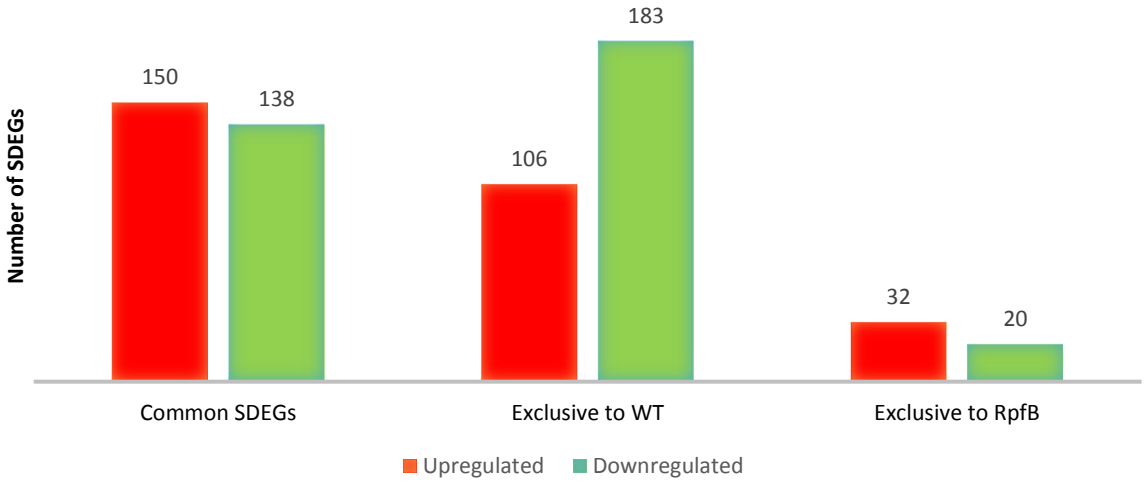

Figure 2.6: Number and the regulation state of commonly and exclusively induced SDEGs by WT and Δ*rpfB* infection. Commonly induced SDEGs and SDEGs exclusively induced by mutant infection expressed a higher number of upregulated than downregulated genes. The opposite pattern was observed in SDEGs exclusively induced by the WT infection with almost a 2-fold higher number of downregulated genes than upregulated genes. **Red**. Represents upregulation. **Green.** Represents downregulation.

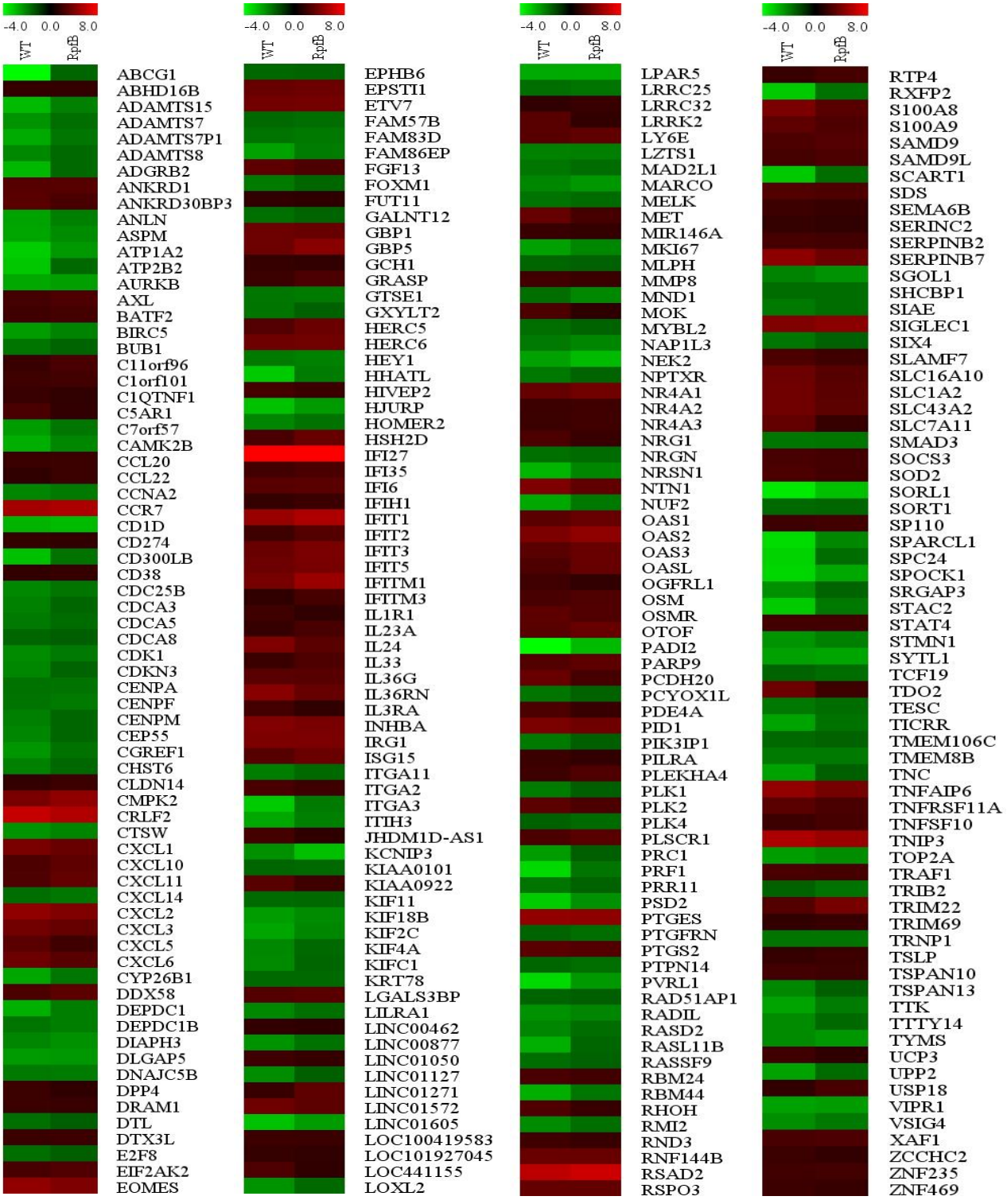

Figure 2.7: Differential expression patterns of commonly induced SDEGs. The difference in expression levels of commonly induced SDEGs between the WT and Δ*rpfB* experimental conditions is depicted on a two-way colour scale using MeV. All SDEGs were expressed in the same regulation state at varying levels, however, *ABCG1* and *PADI2* showed a significantly greater level of downregulation in the WT infected host compared to the mutant infected host, and *IFI27* was the most upregulated

SDEG in the WT and mutant infected hosts of all commonly induced SDEGs. **Green**. Downregulation. **Red.** Upregulation. **WT**: SDEGs induced by WT infection. ***rpfB***: SDEGs induced by mutant infection.

Significantly up- and down-regulated SDEGs

Seven of the top 10 significantly upregulated SDEGs were common but were differentially expressed (highlighted in red) in the respective WT and Δ*rpfB* mutant infected host (Table 2.2). These SDEGs, with fold changes of 4.5 and above, included cytokines, transmembrane receptors, G-protein coupled receptors, enzymes and kinases (Table 2.2). *IFI27*, located in the cytoplasm, had the highest level of expression of all SDEGs induced by *Mtb* infection, however, was induced at higher levels by the WT (log fold 9.709) than Δ*rpfB* mutant (log fold 8.719). The remaining 3 significantly upregulated SDEGs, *TNFAIP6* (fold change 4.645) (unidentified by IPA), *CXCL2* (fold change 4.589) (cytokine) and *EOMES* (fold change 4.577) (transcription regulator) were induced only by the WT infection, and *CMPK2* (fold change 4.591) (kinase), *OAS2* (fold change 4.546) (enzyme) and *IFITM1* (fold change 5.505) (transmembrane receptor) were induced only by Δ*rpfB* mutant infection (Table 2.2). Only 3 significantly downregulated host SDEGs, *PADI2* (WT fold change -4.098, Δ*rpfB* mutant fold change -2.934) (enzyme), *SORL1* (WT fold change -3.689, Δ*rpfB* fold change -3.042) (transporter) and *SPOCK1* (WT fold change -3.384, Δ*rpfB* fold change -2.655) (unknown molecule) (highlighted in green) were common to both infection models. The most downregulated SDEG of the WT infected host was *PADI2* (fold change -4.098) and *SORL1* (fold change -3.042) of the Δ*rpfB* mutant infected host. The remaining 7 were unique to each infection model and consisted of transmembrane receptors, G-protein coupled receptors and enzymes with fold changes between -2.4 to -4. Overall, WT infection induced higher expression levels of downregulated SDEGs (Table 2.3).

Table 2.2: Top 10 upregulated host SDEGs induced by WT and Δ*rpfB* mutant infection. Upregulated SDEGs were identified by Ingenuity Pathway Analysis (IPA). SDEGs commonly upregulated by both strains are highlighted in red. *P*-value refers to the fold change by IPA.

WT infected host				Δ*rpfB* mutant infected host			
Gene ID	**Molecule type**	**Location**	***p*-value**	**Gene ID**	**Molecule Type**	**Location**	***p*-value**
IFI27	Other	Cytoplasm	9.079	***IFI27***	Other	Cytoplasm	8.719
CRLF2	Transmembrane receptor	Plasma membrane	6.266	***CRLF2***	Transmembrane receptor	Plasma membrane	5.569
RSAD2	Enzyme	Cytoplasm	5.953	***RSAD2***	Enzyme	Cytoplasm	6.476
TNIP3	Other	Cytoplasm	5.503	***TNIP3***	Other	Cytoplasm	4.895
CCR7	G-protein coupled receptor	Plasma membrane	5.228	***CCR7***	G-protein coupled receptor	Plasma membrane	5.472
IFIT1	Other	Cytoplasm	4.841	***IFIT1***	Other	Cytoplasm	4.529
PTGES	Enzyme	Cytoplasm	4.655	***PTGES***	Enzyme	Cytoplasm	4.863
TNFAIP6	Other	Extracellular space	4.645	***CMPK2***	Kinase	Cytoplasm	4.591
CXCL2	Cytokine	Extracellular space	4.589	***OAS2***	Enzyme	Cytoplasm	4.546
EOMES	Transcription regulator	Nucleus	4.577	***IFITM1***	Transmembrane receptor	Plasma membrane	5.505

NB: Molecules highlighted in red represent commonly induced differentially upregulated SDEGs.

Table 2.3: **Top 10 downregulated host SDEGs induced by WT and Δ*rpfB* infection.** Downregulated SDEGs were identified by Ingenuity Pathway Analysis (IPA). SDEGs commonly downregulated by both strains are highlighted in green. *P*-value refers to the fold change by IPA.

WT infected host				**Δ*rpfB* mutant infected host**			
Gene ID	**Molecule type**	**Location**	***p*-value**	**Gene ID**	**Molecule Type**	**Location**	***p*-value**
PADI2	Enzyme	Cytoplasm	-4.098	***PADI2***	Enzyme	Cytoplasm	-2.934
ABCG1	Transporter	Plasma membrane	-3.961	*KCNIP3*	Transcription regulator	Nucleus	-3.015
SORL1	Transporter	Cytoplasm	-3.689	***SORL1***	Transporter	Cytoplasm	-3.042
SPARCL1	Other	Extracellular space	-3.439	*NEK2*	Kinase	Cytoplasm	-2.964
PRF1	Transporter	Cytoplasm	-3.434	*CD1D*	Other	Plasma membrane	-2.952
NECTIN1	Other	Plasma membrane	-3.426	*LPAR5*	G-protein coupled receptor	Plasma membrane	-2.689
SPOCK1	Other	Extracellular space	-3.384	***SPOCK1***	Other	Extracellular space	-2.655
SPC24	Other	Cytoplasm	-3.314	*SYTL1*	Enzyme	Cytoplasm	-2.610
ATP1A2	Transporter	Plasma membrane	-3.235	*AURKB*	Kinase	Nucleus	-2.524
PSD2	Other	Plasma membrane	-3.219	*LINC01605*	Other	Other	-2.458

NB: Molecules highlighted in green represent commonly induced differentially downregulated SDEGs.

Gene enrichment analysis

Gene enrichment was used to identify biological processes, cellular components and molecular functions induced in response to WT and Δ*rpfB* mutant infection. The 150 commonly upregulated SDEGs were associated with response to cytokines, response to biotic stimulus, defense response, inflammatory response, innate immune response and regulation of innate immune processes (Table 2.4). The commonly downregulated SDEGs (138) were associated with cell cycle processes, cell cycle, mitotic cell cycle, cell division and regulation of cell cycle (Table 2.4).

Table 2.4: Top 10 gene ontology functions associated with WT and Δ*rpfB* mutant commonly induced up- and down-regulated SDEGs. Enrichment analysis was done using Gene Set Enrichment Analysis (GSEA) with a FDR *q*-value < (0.05). Gene overlap indicates the number of experimental genes overlapping MSigDB currated genes.

Upregulated SDEGs			**Downregulated SDEGs**		
Function	**Gene overlap**	**FDR *q*-value**	**Function**	**Gene overlap**	**FDR *q*-value**
Response to cytokine	66	4.08E-54	Cell cycle process	50	8.43E-32
Defence response	73	2.70E-53	Cell cycle	55	1.30E-31
Response to biotic stimulus	60	2.69E-50	Mitotic cell cycle	43	6.31E-30
Cytokine mediated signalling pathway	54	2.69E-48	Organelle fission	29	9.54E-24
Defence response to other organism	38	1.54E-32	Cell division	31	2.54E-23
Defence response to virus	29	2.04E-31	Mitotic nuclear division	24	1.65E-22
Response to virus	31	1.30E-30	Chromosome segregation	24	2.20E-21
Inflammatory response	39	9.31E-30	Sister chromatid segregation	20	2.13E-20
Innate immune response	43	1.89E-29	Regulation of cell cycle	36	1.65E-19
Regulation of immune system process	49	9.78E-27	Mitotic sister chromatid segregation	18	3.37E-19

One hundred and six of the exclusive WT induced SDEGs were upregulated and 183 downregulated. The most significantly enriched GO function associated with the WT induced upregulated SDEGs was the defence response (FDR q-value 2.21E-06), and negative regulation of secretion (1.37E-05) by downregulated SDEGs. Overall, both upregulated and downregulated WT SDEGs were associated with mostly biological processes and 1 cellular component (intrinsic component of plasma membrane-upregulated, extracellular matrix -downregulated) (Table 2.5). All 32 Δ*rpfB* mutant induced upregulated SDEGs were associated with only biological processes related to immune response. The downregulated SDEGs (20) were also associated with only biological processes, none of which were related to immune response (Table 2.6).

Table 2.5: Top 10 gene ontology functions associated with exclusively induced WT up- and down-regulated SDEGs. Enrichment analysis was done using Gene Set Enrichment Analysis (GSEA) with a statistical significance of FDR *q*-value < (0.05). Gene overlap indicates the number of experimental genes overlapping MSigDB currated genes.

Upregulated			**Downregulated**		
Function	**Gene overlap**	**FDR *q*-value**	**Function**	**Gene overlap**	**FDR *q*-value**
Defence response	23	2.21E-06	Negative regulation of secretion	12	1.37E-05
Aging	9	1.43E-03	Organelle fission	15	3.99E-05
Intrinsic component of plasma membrane	18	3.23E-03	Chromosome segregation	12	1.26E-04
Response to oxygen containing compound	17	3.36E-03	Neurogenesis	26	1.26E-04
Metal ion homeostasis	11	3.36E-03	Nuclear chromosome segregation	11	1.26E-04
Cellular ion homeostasis	11	3.36E-03	Secretion	26	1.41E-04
Cellular response to oxygen containing compound	14	3.36E-03	Mitotic nuclear division	11	1.90E-04
Circulatory system process	10	3.36E-03	Extracellular matrix	14	3.38E-04
Response to bacterium	11	3.36E-03	Sister chromatid segregation	9	3.98E-04
Chemical homeostasis	14	4.39E-03	Mitotic cell cycle	19	4.39E-04

Table 2.6: Top 10 gene ontology functions associated with exclusively induced Δ*rpfB* mutant up- and down-regulated SDEGs. Enrichment analysis was done using Gene Set Enrichment Analysis (GSEA) with a statistical significance of FDR *q*-value < (0.05). Gene overlap indicates the number of experimental genes overlapping MSigDB currated genes.

Upregulated			**Downregulated**		
Function	Gene overlap	FDR *q*-value	Function	Gene overlap	FDR *q*-value
Response to virus	10	1.85E-09	Negative regulation of relaxation of muscle	5	1.09E-02
Defense response to virus	9	2.99E-09	Thorax and anterior abdomen determination	5	1.09E-02
Response to biotic stimulus	13	6.51E-09	Vestibulocochlear nerve morphogenesis	6	1.09E-02
Response to cytokine	13	3.30E-08	Zygotic determination of anterior posterior axis embryo	6	1.09E-02
Defense response to other organism	10	7.69E-08	Regulation of saliva secretion	7	1.22E-02
Cytokine mediated signalling pathway	10	1.89E-06	Cranial nerve formation	8	1.35E-02
Immune effector process	11	9.61E-06	Vestibulocochlear nerve development	9	1.45E-02
Innate immune response	10	1.19E-05	Learned vocalization behaviour or vocal learning	10	1.45E-02
Defense response	12	1.57E-05	Peristalsis	10	1.45E-02
Response to type I interferon	5	2.41E-05	Regulation of relaxation of muscle	12	1.59E-02

Ingenuity Pathway and Network Analysis

To further interrogate the biological impact of *Mtb rpfB* gene deficiency in macrophage immune responses, IPA analysis was performed to identify canonical pathways, networks and upstream regulators regulated by WT and Δ*rpfB* mutant induced SDEGs. All WT and Δ*rpfB* mutant SDEGs were associated with 51 significantly enriched WT canonical pathways and 64 mutant canonical pathways, respectively (Data not shown). Of these pathways, Activation of IRF by cytosolic pattern recognition receptors, Acute phase response signalling, Agranulocyte adhesion and diapedesis, Crosstalk between DC and NK cells, DC maturation, IL-10 signalling, Interferon signalling, LXR/RXR, Phagosome formation, Role of JAK family kinases in IL-6 type cytokine signalling were common in WT and Δ*rpfB* mutant infected macrophages (Figure 2.8).

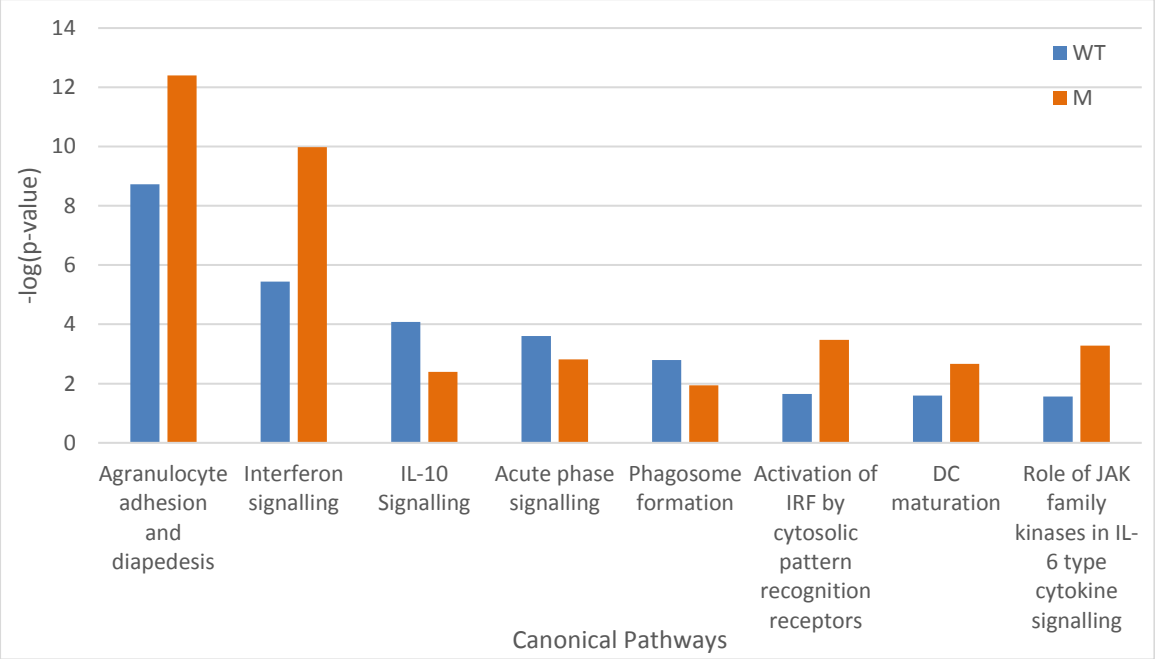

Figure 2.8: Significantly enriched canonical pathways in THP-1 macrophages commonly induced by WT and Δ*rpfB* mutant infection 72 hours post-infection. Canonical pathways are plotted against enrichment levels (-log (*p*-value). A (blue). WT induced pathways. **B (orange).** Mutant induced pathways.

A total number of 288 SDEGs were commonly induced by infection with *Mtb*. Of the total number of 288 commonly induced canonical pathways, 54 were significantly enriched (Shown in Appendix G). Only 16 networks and 44 upstream regulators were commonly induced (Table 2.7). Overall, even though the number of SDEGs induced exclusively by the Δ*rpfB* mutant infection were almost 6 times less than that exclusively induced by the WT infection, the number of significantly enriched canonical pathways based on -log(*p*-value) were greater in the Δ*rpfB* infected host (21) than the WT infected host (17) (Shown in Appendix G). The total number of enriched canonical pathways were higher in the

WT infected host (241) than the mutant infected host (115). The WT infection also induced enrichment of more networks and upstream regulators than the mutant infection (Table 2.7).

Table 2.7: Comparison of the SDEGs, canonical pathways, networks and upstream regulators commonly and exclusively induced by the WT and Δ*rpfB* mutant infection.

	Commonly induced	WT induced	Δ*rpfB* induced
SDEGs	288	289	52
Canonical pathways	54/288	17/241	21/115
Networks	16	20	8
Upstream regulators	44	190	143

Immune pathways

Agranulocyte adhesion and diapedesis

This pathway was expressed at higher significance, -log (12.4), in mutant infected macrophages compared to WT infected macrophages, – log (8.73).The WT infection induced 22 SDEGs associated with the pathway, including *MYH14*, *IL36B*, *CX3CL1* that were exclusive to this infection model. Of the 21 mutant associated SDEGs, *PODXL* and *MMP17* were exclusive to mutant infected macrophages. Both strains induced upregulation of *IL-1*, *C5AR1*, *IL-1R*, *CLDN* (Figure 2.9A and 2.9B). The WT infection induced downregulation of Myosin (Figure 2.9A) whereas the mutant infection induced downregulation of *PNAd* and *MMP* (Figure 2.9B), however, the latter was upregulated in WT infected hosts (Figure 2.9A).

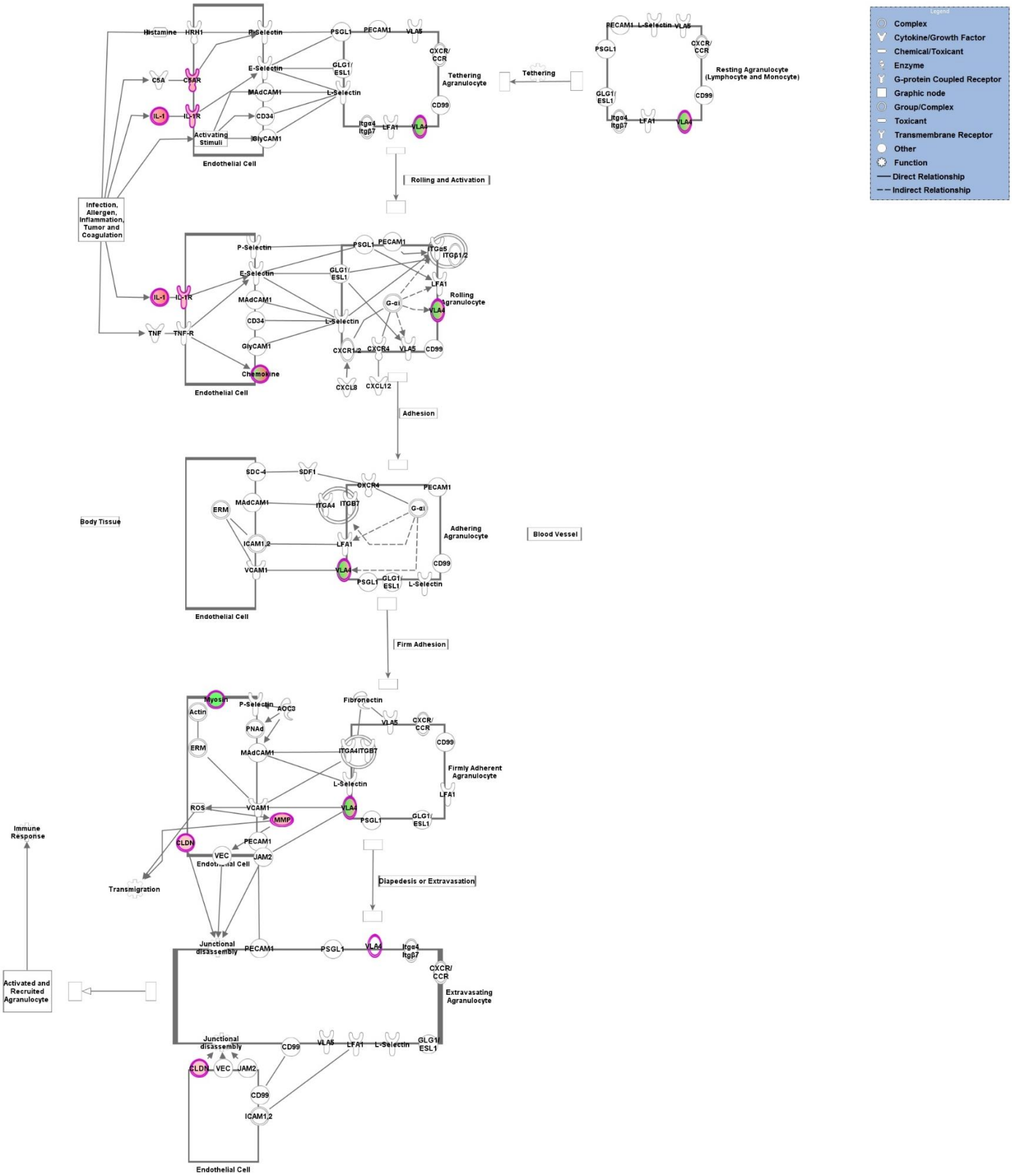

A. WT induced canonical pathway

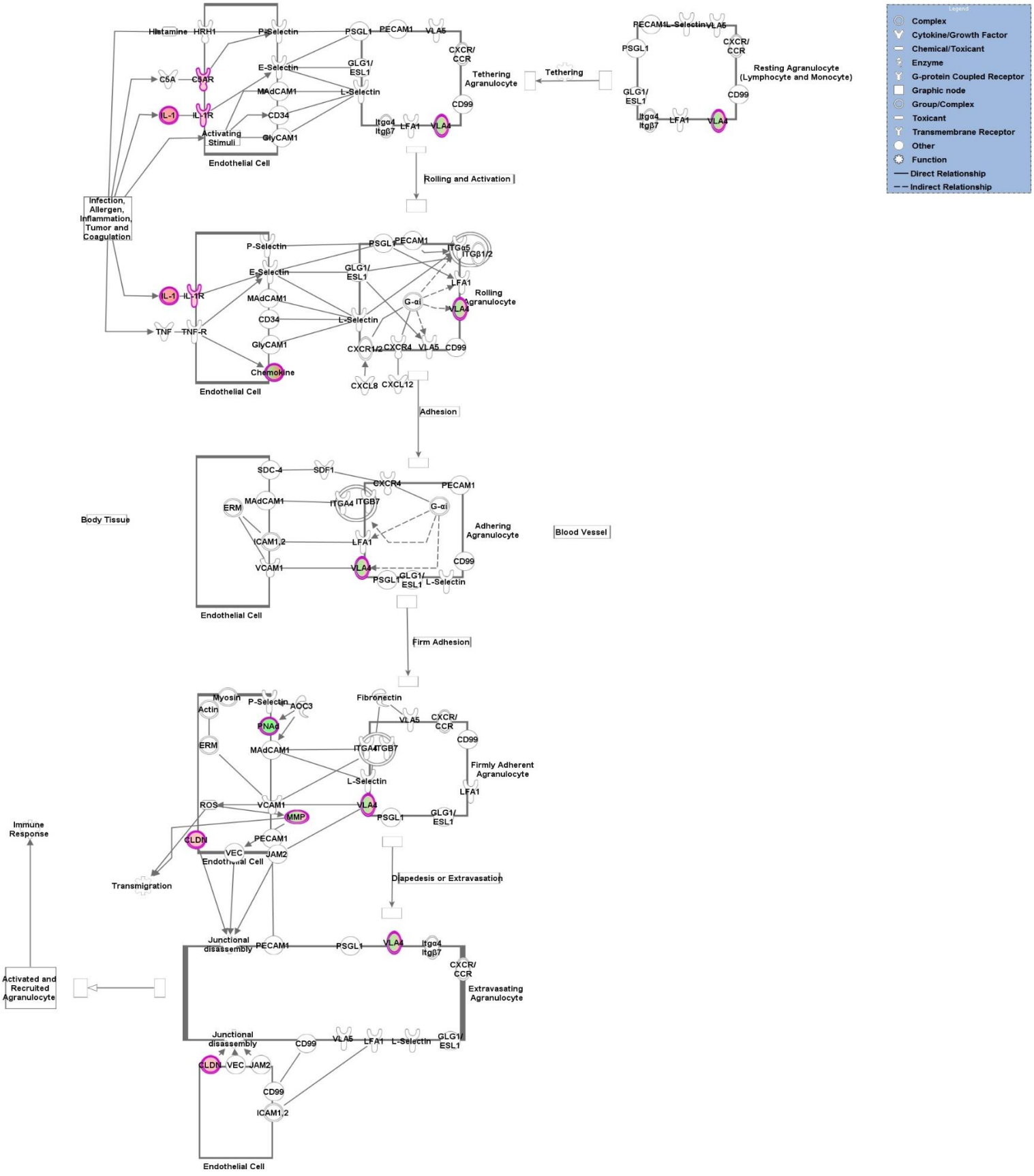

B. Δ*rpfB* mutant induced canonical pathway

Figure 2.9: Agranulocyte adhesion and diapedesis. A. WT induced pathway. **B.** Δ*rpfB* mutant induced pathway. Upregulated SDEGs are represented in pink and downregulated SDEGs in green. The colour intensity corresponds with the level of expression. White molecules are IPA curated genes and purple double lined shapes represent groups of SDEGs. SDEGs, *PODXL* and *MMP17* were exclusive to mutant infected macrophages whereas *MYH14, IL36B, CX3CL1* were exclusive to WT infected macrophages. Both strains induced upregulation of *IL-1*, *C5AR1*, *IL-1R*, *CLDN*. The mutant infection induced downregulation of *PNAd* and *MMP*, however, the latter was upregulated in WT infected hosts.

Interferon signalling

This pathway was the second highest expressed by infection with both strains but was expressed at higher significance in mutant infected macrophages (– log (9.98) relative to the WT infected macrophages (-log (5.44). The WT and mutant infection commonly induced upregulation of *IFITM3*, *IFITM1*, *IFI35*, *IFIT1*, *OAS1*, *G1P2* (Figure 2.10A and 2.10B). However, the WT infection induced upregulation of one more SDEG, *G1P3* (Figure 2.10A), and the mutant infection induced upregulation of 3 more SDEGs, *STAT1*, *MX1* and *IFIT3* (Figure 2.10B). No SDEGs were downregulated. The interferon signalling pathway was also the second highest expressed pathway exclusively induced in response to the mutant infection. To further support the pathway induced by the mutant strain, Figure 2.10C shows the influence of *STAT1* on *IFITM1, IFI35*, *IFIH1*, *OAS1* and *IFIT3* gene expression, as shown in the pathway. All molecules in the pathway are upregulated by *STAT1* at varying levels of expression depicted by the intensity of the red colour.

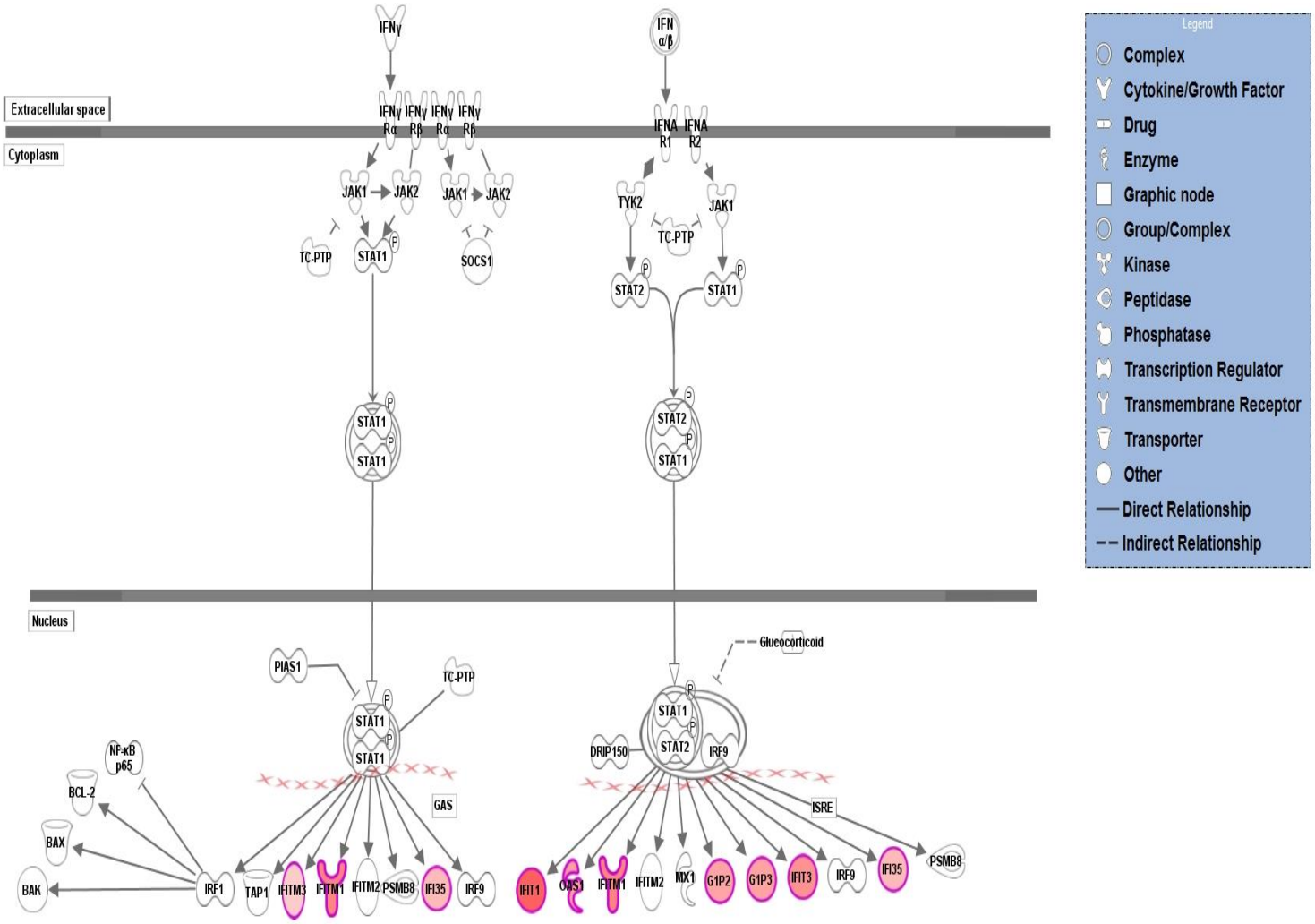

A. WT induced canonical pathway

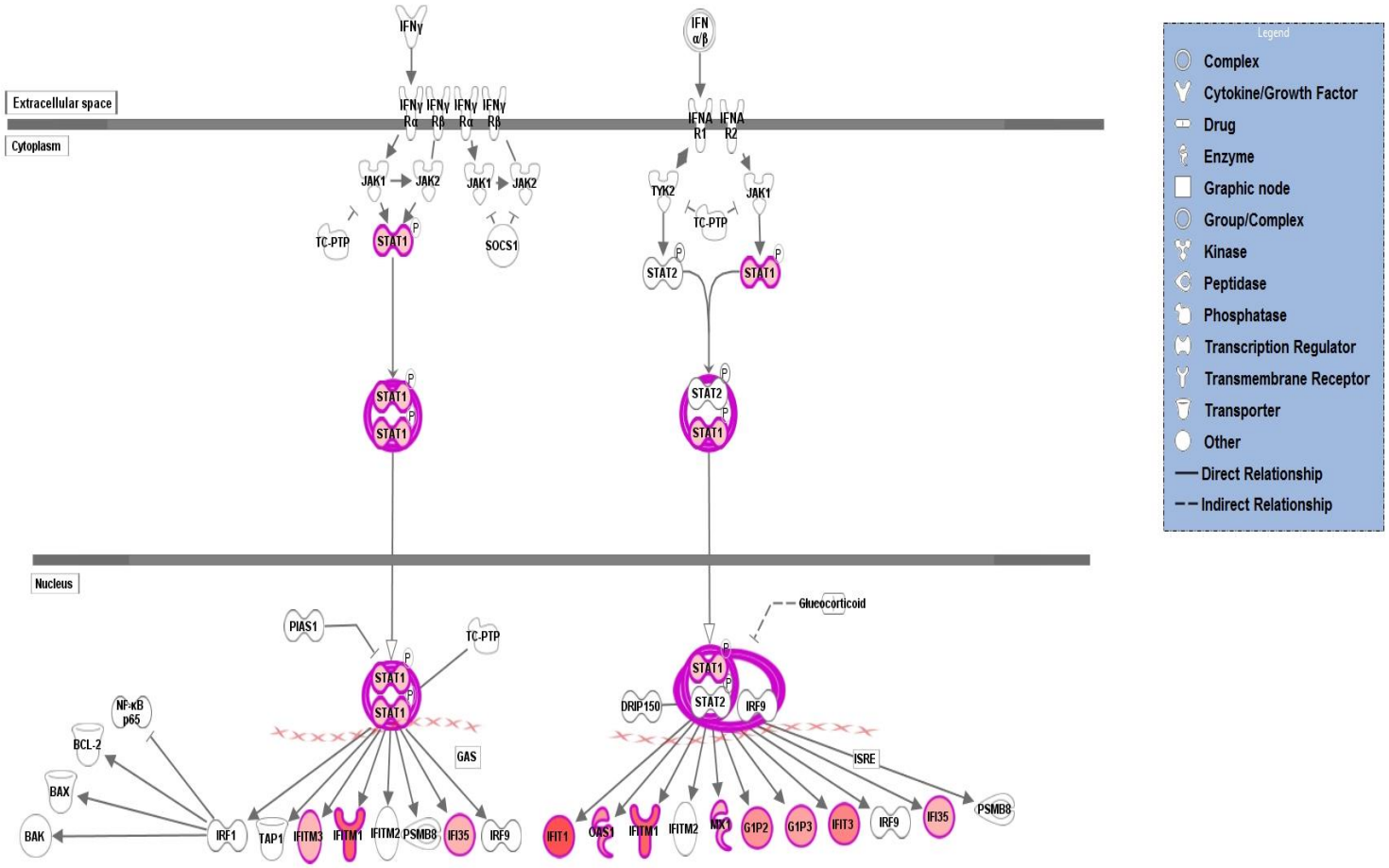

B. Δ*rpfB* mutant induced canonical pathway

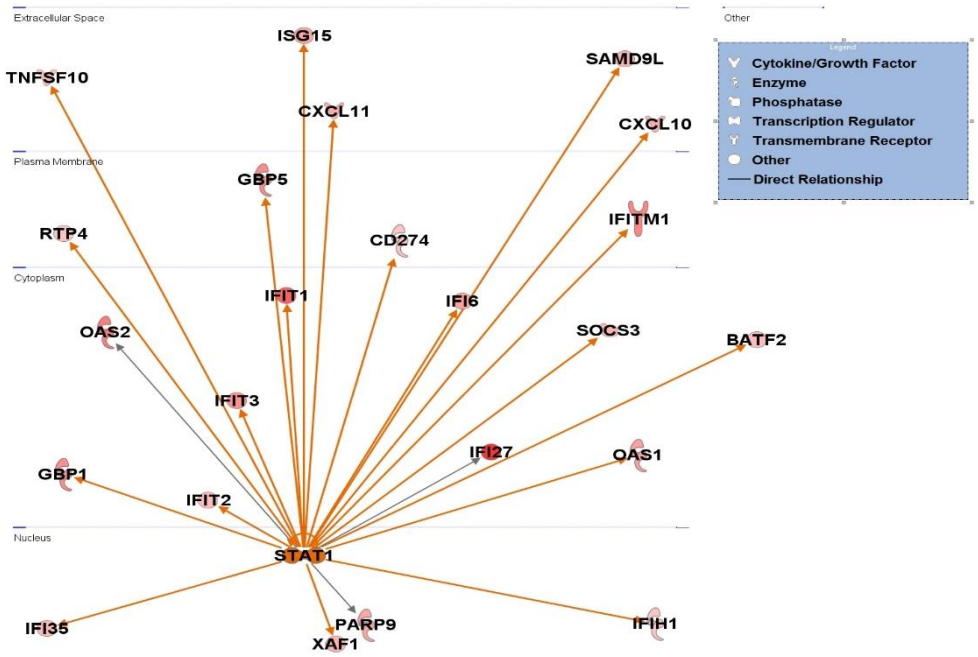

C. STAT1

Figure 2.10: Interferon signalling. A. WT induced pathway. **B.** Δ*rpfB* mutant induced pathway. Upregulated SDEGs are represented in pink and downregulated SDEGs in green. The colour intensity corresponds with the level of expression. White molecules are IPA curated genes and purple double lined shapes represent groups of SDEGs. **C.** *STAT1* network. Upregulated SDEGs are represented in red and downregulated SDEs in green. WT and mutant infection commonly induced upregulation of *IFITM3*, *IFITM1*, *IFI35*, *IFIT1*, *OAS1*, *G1P2*. *GIP3* was exclusively induced by WT and *STAT1*, *MX1* and *IFIT3* exclusively induced by the mutant. No SDEGs were downregulated. *STAT1* influences differential upregulation of all molecules shown in the network.

IL-10 signalling

In association with the IL-10 signalling pathway, the mutant infection induced *IL33*, *SOCS3*, *IL36G*, *IL36RN* and *IL1R1* SDEGs whereas in addition to these, the WT infection induced 4 more SDEGs than the mutant infection, *SOCS3*, *IL10*, *FCGR2B* and *IL36B*. *IL-1*, *IL-1R* and *SOCS3* were commonly upregulated by both strains (Figure 2.11A and 2.11B) whereas *IL-10* and *HMOX1* were exclusively upregulated by infection with the WT (Figure 2.11A). Only one SDEG was downregulated in infected macrophages, *FCGRII*, induced by the WT infection (Figure 2.11A). The IL-10 signalling pathway also appeared as the sixth highest expressed pathway exclusively induced in response to the WT infection**.**

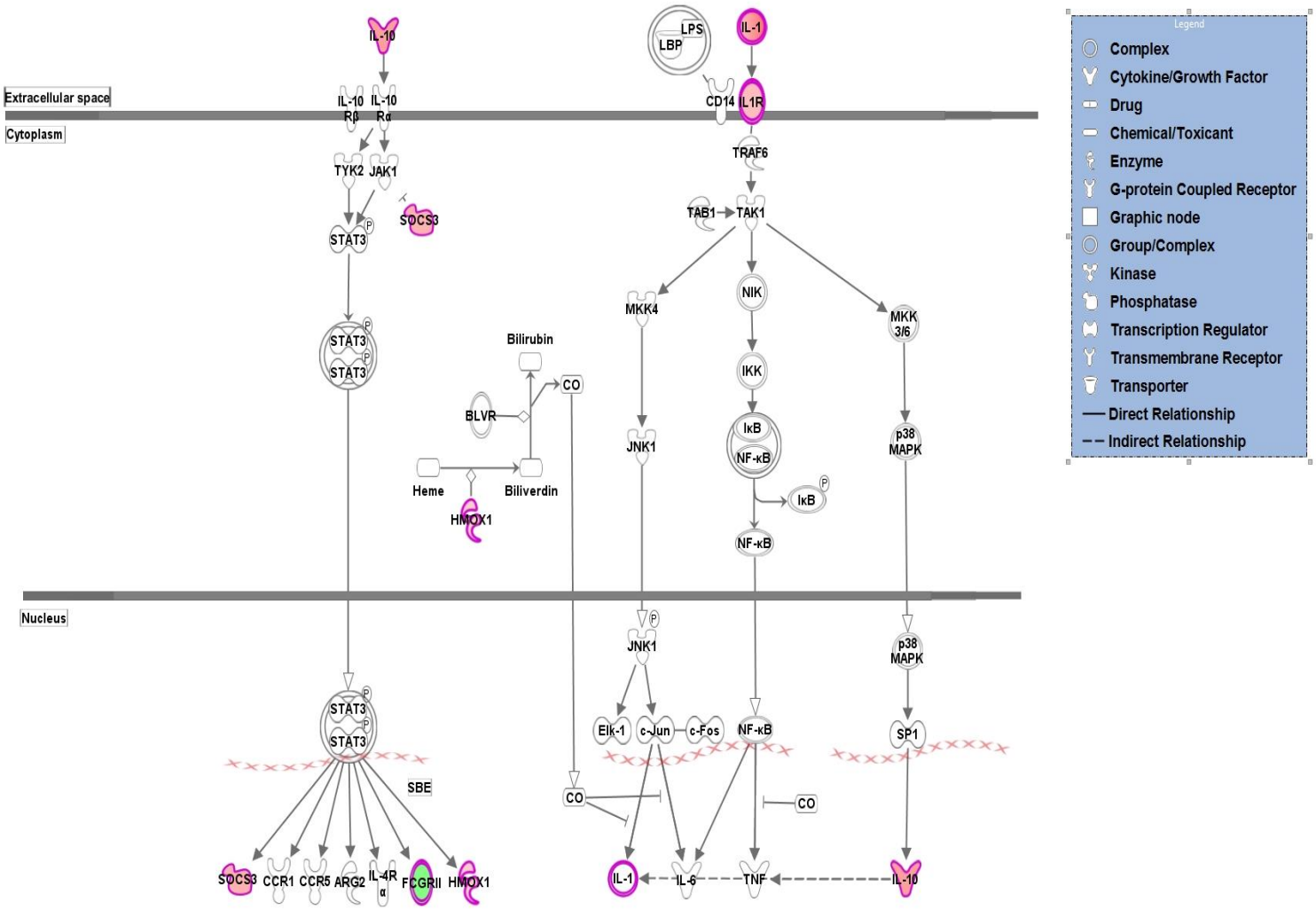

A. WT induced canonical pathway

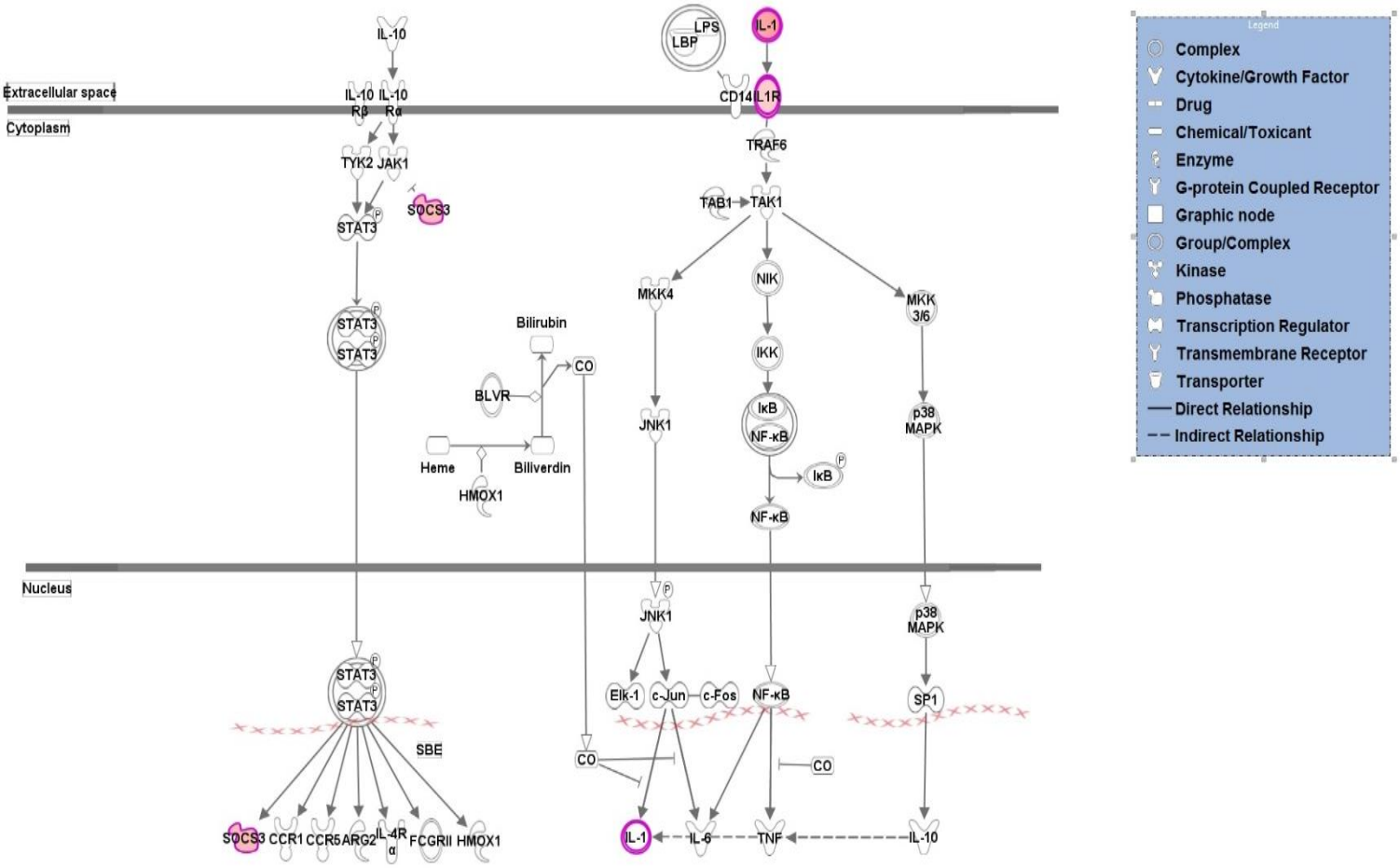

B. Δ*rpfB* mutant induced canonical pathway

Figure 2.11: IL-10 signalling. A. WT induced pathway. **B.** Δ*rpfB* mutant induced pathway. Upregulated SDEGs are represented in pink and downregulated SDEGs in green. The colour intensity corresponds with the level of expression. White molecules are IPA curated genes and purple double lined shapes represent groups of SDEGs. The mutant infection induced *IL33*, *SOCS3*, *IL36G*, *IL36RN* and *IL1R1* SDEGs whereas in addition to these, the WT infection induced 4 more SDEGs than the mutant infection, *SOCS3*, *IL10*, *FCGR2B* and *IL36B. IL36B. IL-1*, *IL-1R* and *SOCS3* were commonly upregulated by both strains. *IL-10* and *HMOX1* were exclusively upregulated by infection with the WT. Only one SDEG was downregulated in infected macrophages, *FCGRII*, induced by the WT infection.

Acute phase response signalling

In addition to the SDEGs (*IL-1*, *IL-1R*, *OSM*, *OSMR*, *SOCS3*, *SOCS*, *SOD2*) induced by both infections (Figure 2.12A and 2.12B), the WT induced two more SDEGs, *HMOX1* and *SERPING1* (Figure 2.12A), not induced in mutant infected macrophages. *ITIH3* was downregulated in WT and mutant infected macrophages (Figure 2.12A and 2.12B) but the WT induced downregulation of two more SDEGs, *VWF* and *SERPINE1* (Figure 2.12A).

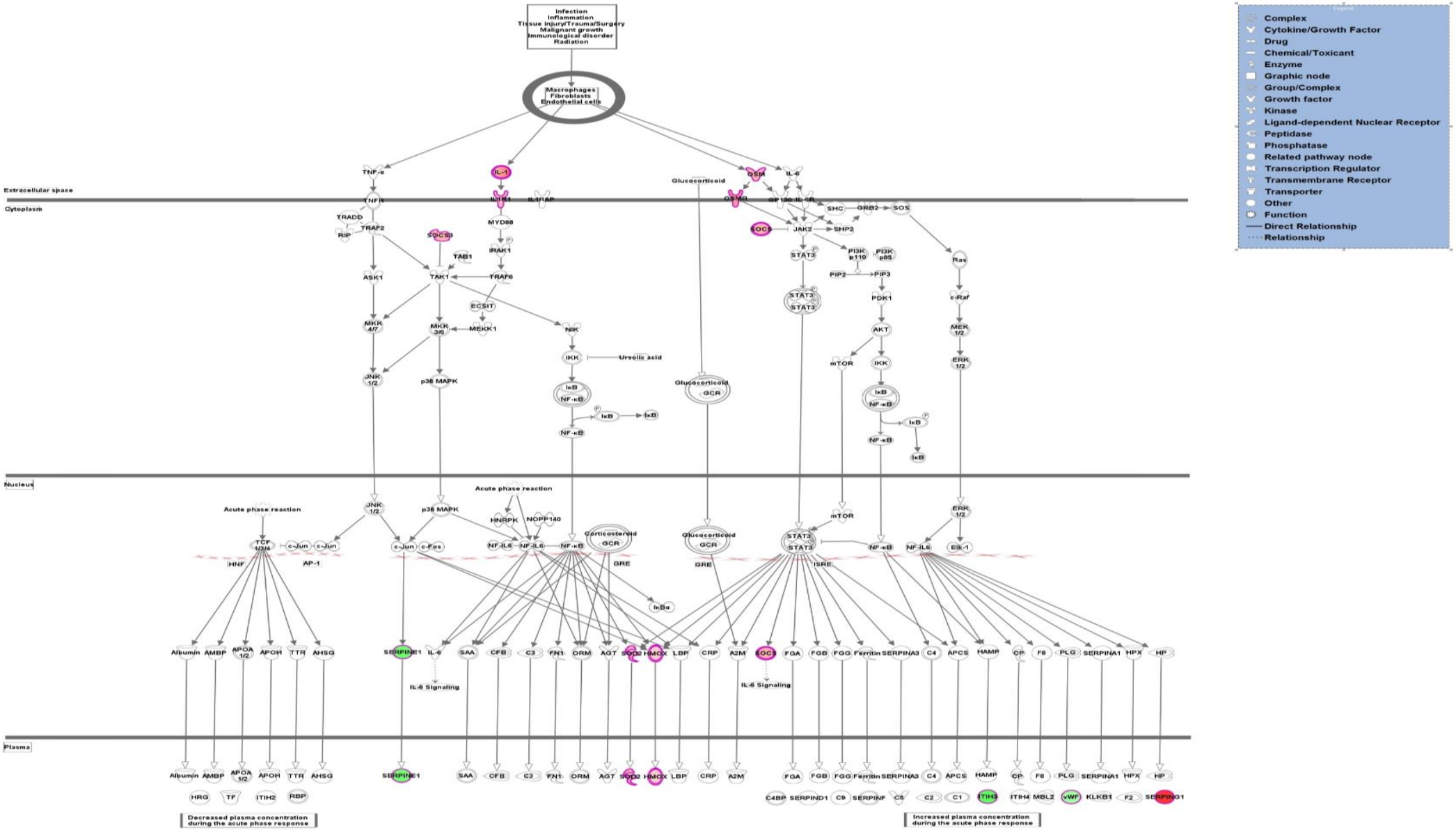

A. WT induced canonical pathway

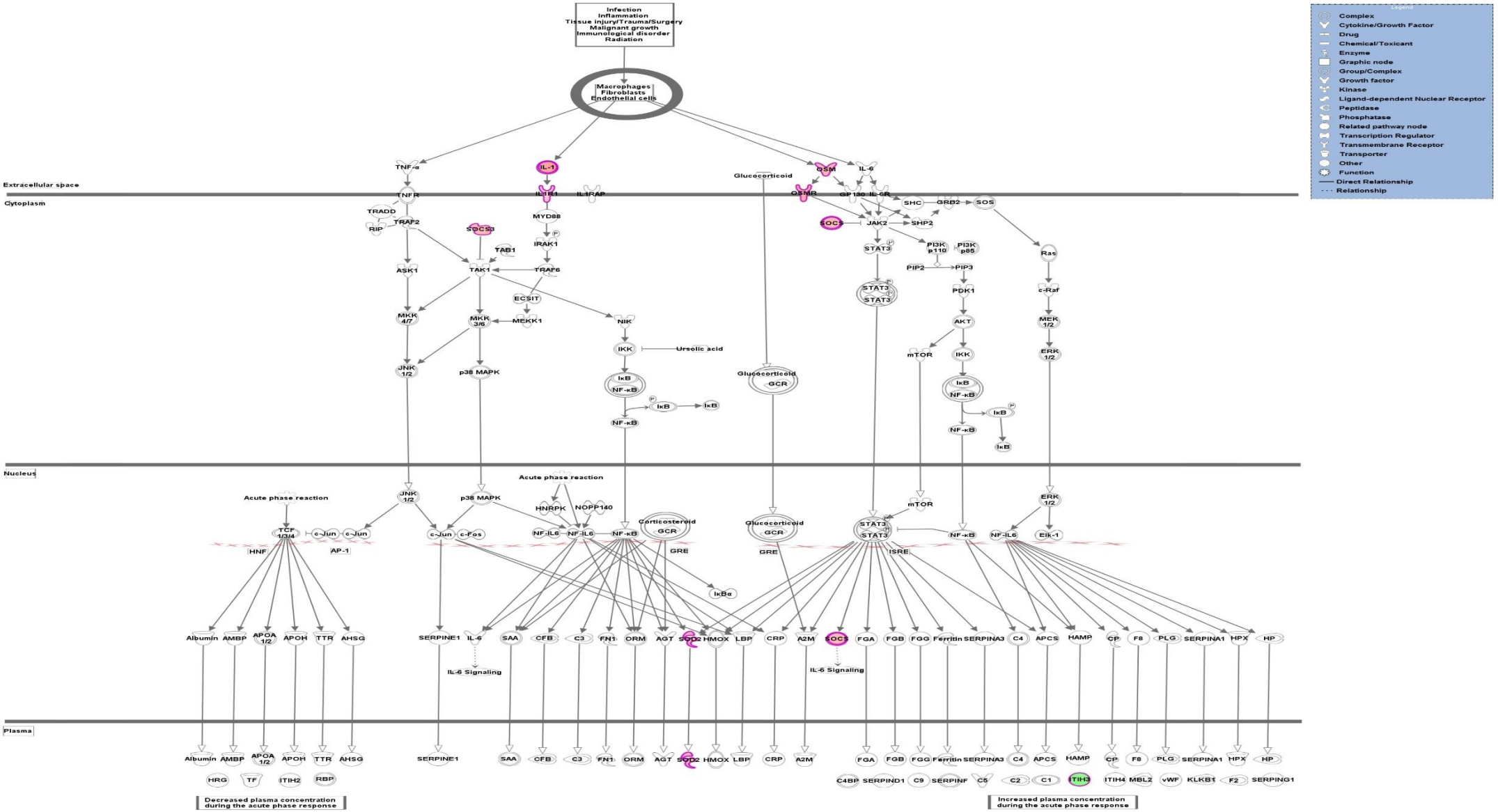

B. Δ*rpfB* mutant induced canonical pathway

Figure 2.12: Acute phase response signalling. A. WT induced pathway. **B.** Δ*rpfB* mutant induced pathway. Upregulated SDEGs are represented in pink and downregulated SDEGs in green. The colour intensity corresponds with the level of expression. White molecules are IPA curated genes and purple double lined shapes represent groups of SDEGs. *IL-1*, *IL-1R*, *OSM*, *OSMR*, *SOCS3*, *SOCS*, *SOD* induced by both infections. The WT exclusively induced *HMOX1* and *SERPING1*. *ITIH3* was downregulated in WT and mutant infected macrophages. *VWF* and *SERPINE1* were exclusively downregulated by WT infection.

Phagosome formation

The WT and Δ*rpfB* mutant infection commonly induced upregulation of *complement receptor* and *Rho-GTPase* (Figure 2.13A and 2.13B). However, WT infected macrophages also showed upregulation of *MSR* (Figure 2.13A), not shown in mutant infected macrophages (Figure 2.13B). Infection with both strains induced downregulation of *marco* and *integrin* (Figure 2.13A and 2.13B), but the WT infection induced downregulation of two more SDEGs, *FcRS* and *TRL* (Figure 2.13A).

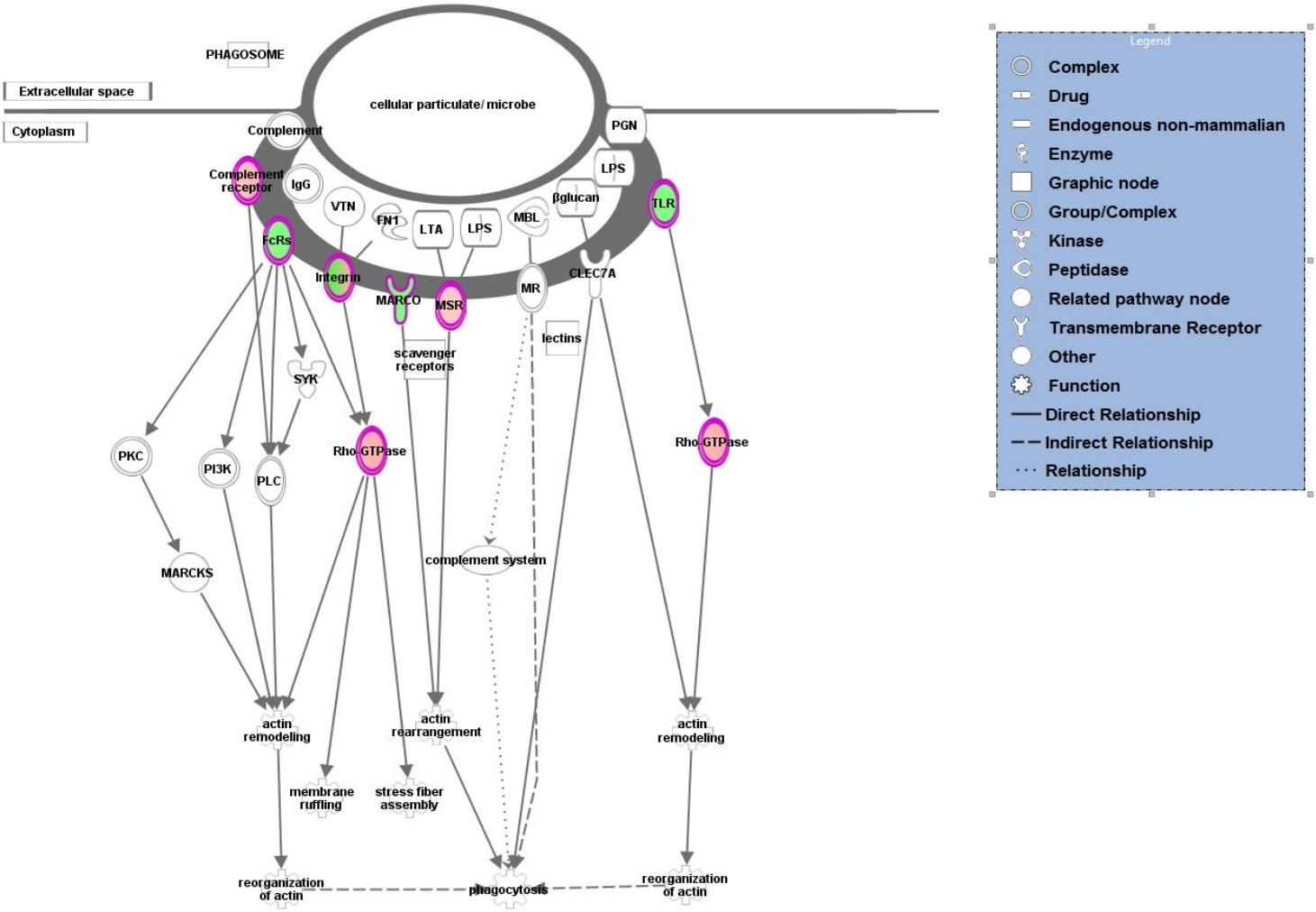

A. WT induced canonical pathway

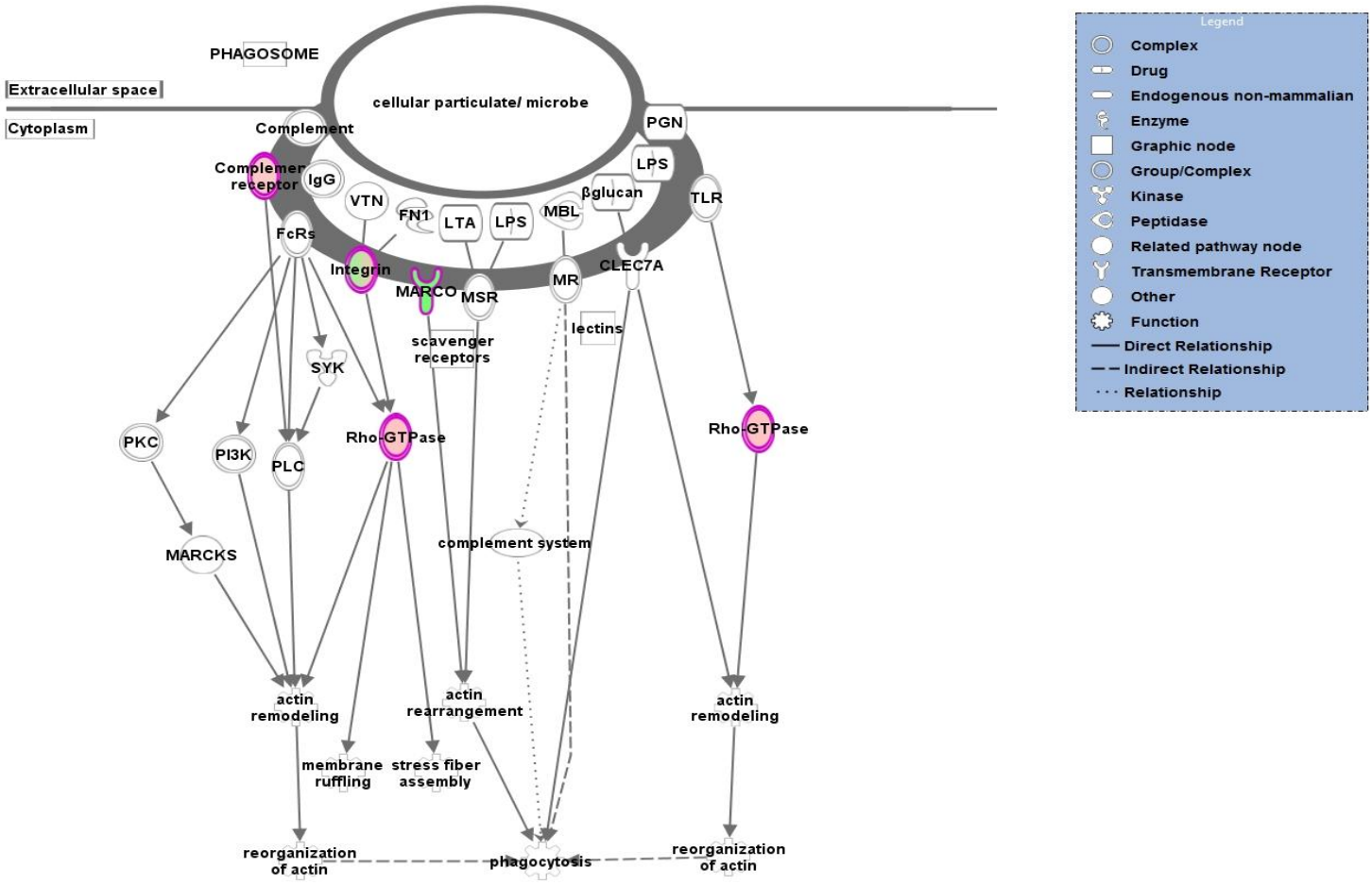

B. Δ*rpfB* mutant induced canonical pathway

Figure 2.13: Phagosome formation. A. WT induced pathway. **B.** Δ*rpfB* mutant induced pathway. Upregulated SDEGs are represented in pink and downregulated SDEGs in green. The colour intensity corresponds with the level of expression. White molecules are IPA curated genes and purple double lined shapes represent groups of SDEGs. WT and mutant infection commonly induced upregulation of *complement receptor* and *Rho-GTPase.* WT exclusively induced upregulation of *MSR* and downregulation *FcRS* and *TRL*. Infection with both strains induced downregulation of *marco* and *integrin.*

Activation of IRF by cytosolic pattern recognition receptors

Macrophages infected with the Δ*rpfB* mutant strain revealed a higher level of expression of the pathway (- log (3.48) relative to WT infected macrophages (-log (1.65). Both strains induced upregulation of *RIG-I*, *ISG15*, *MDA5* and *ISG54* (Figure 2.14A and 2.14B). Additional SDEGs were upregulated exclusively to the WT infected host (*IL-0*) (Figure 2.14A) and mutant infected host (*IRF7* and *STAT4*) (Figure 2.14B). No SDEGs were downregulated. This pathway also appeared as the fourth highest expressed pathway exclusively induced in response to the mutant infection.

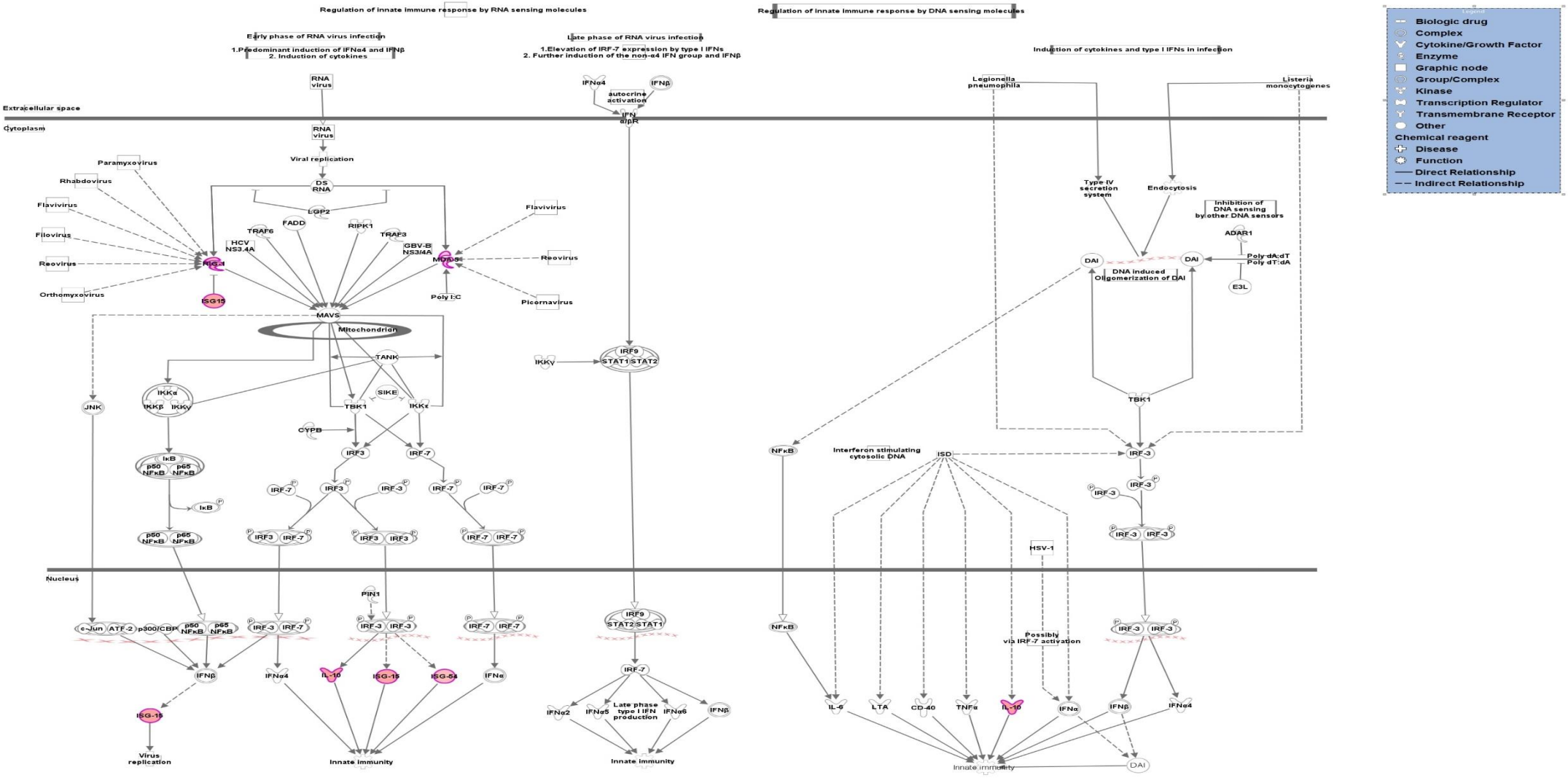

A. WT induced canonical pathway

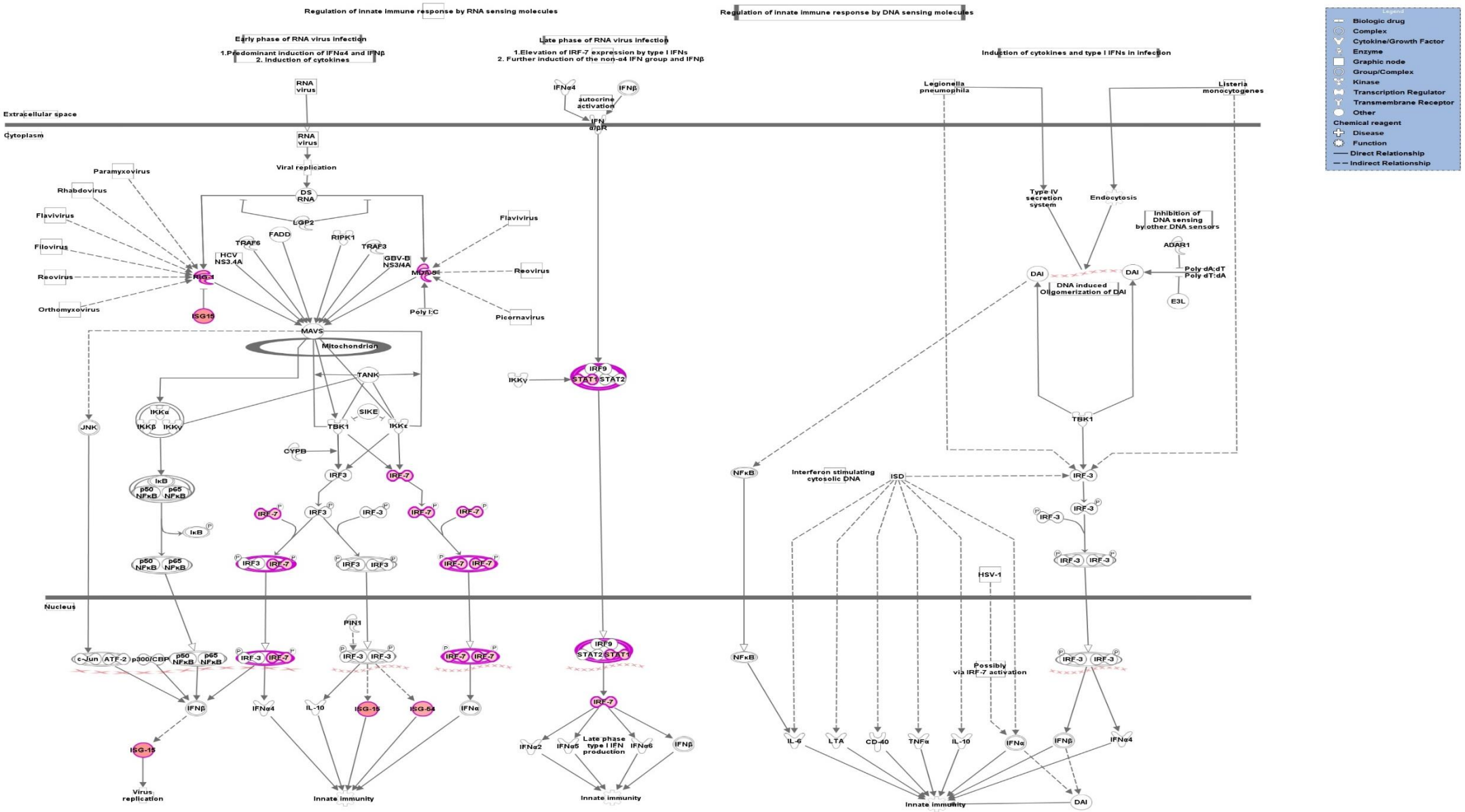

B. Δ*rpfB* mutant induced canonical pathway

Figure 2.14: Activation of IRF by cytosolic pattern recognition receptors. A. WT induced pathway. **B.** Δ*rpfB* mutant induced pathway. Upregulated SDEGs are represented in pink and downregulated SDEGs in green. The colour intensity corresponds with the level of expression. White molecules are IPA curated genes and purple double lined shapes represent groups of SDEGs. Both strains induced upregulation of *RIG-1*, *ISG15*, *MDA-5* and *ISG-54.* Additional SDEGs were upregulated exclusively to the WT infected host (*IL-10*) and mutant infected host (*IRF-7* and *STAT4*). No SDEGs were downregulated.

Dendritic cell maturation

This pathway was also expressed at a higher level of –log (2.66) in mutant infected macrophages compared to –log (1.59) in WT infected macrophages.Molecules *IL-23p19*, *IL-1*, *CCR7*, *IL-1F9*, *STAT1* and *STAT4* were commonly upregulated in WT and mutant infected macrophages (Figure 2.15A and 2.15B). WT infection exclusively induced upregulation of *IL-10* and *IL-1F8* (Figure 2.15A). The mutant infection exclusively induced upregulation of *GM-CSF* and *STAT1α* (Figure 2.15B). Four SDEGs were downregulated (*CD32*, *CD1*, *FcγR* and *FcγRII*) in response to the WT strain (Figure 2.15A) whereas only *CD1* was downregulated in response to the mutant strain (Figure 2.15B).

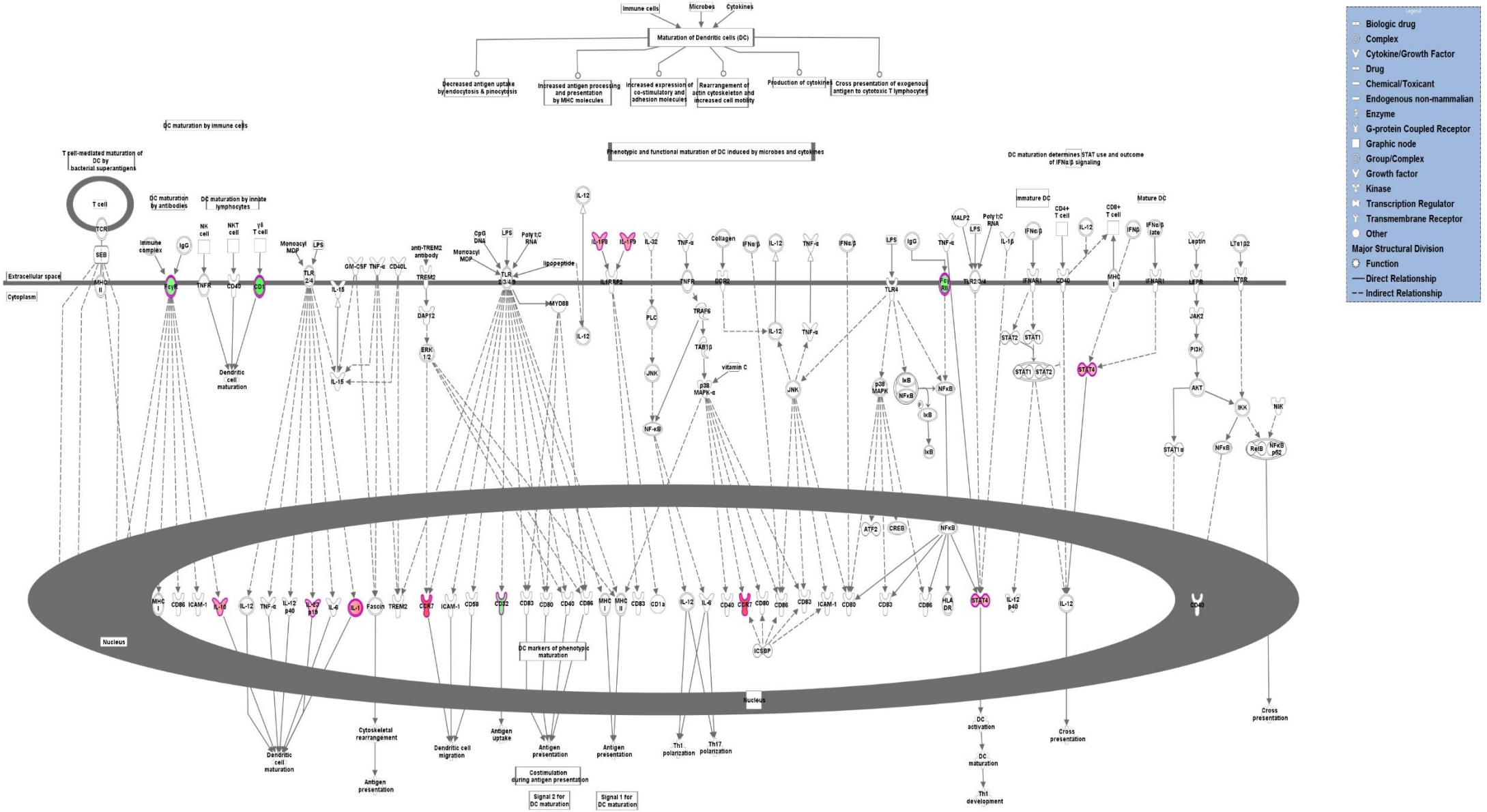

A. WT induced canonical pathway

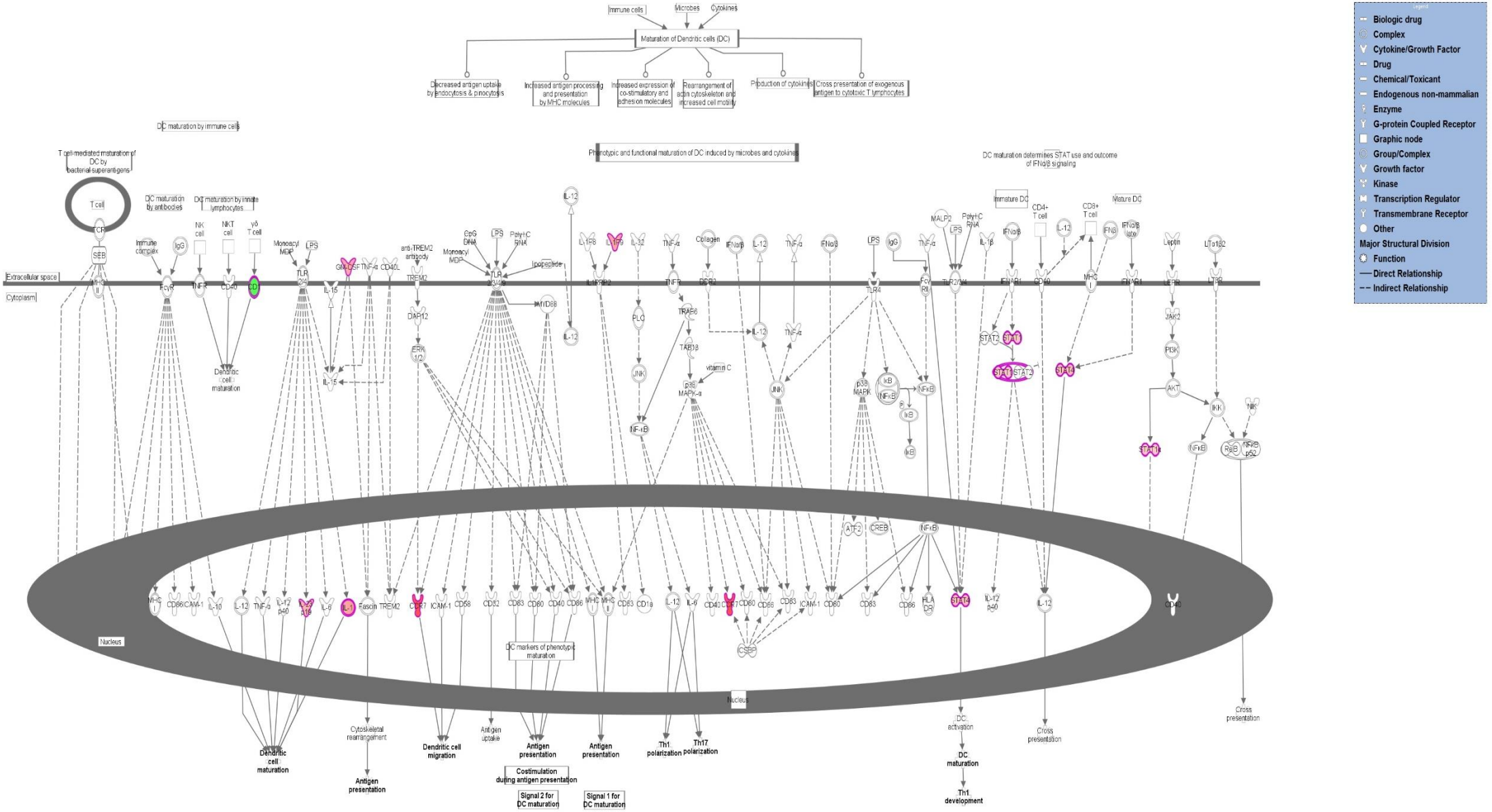

B. Δ*rpfB* mutant induced canonical pathway

Figure 2.15: Dendritic cell maturation. A. WT induced pathway. **B.** Δ*rpfB* mutant induced pathway. Upregulated SDEGs are represented in pink and downregulated SDEGs in green. The colour intensity corresponds with the level of expression. White molecules are IPA curated genes and purple double lined shapes represent groups of SDEGs. Molecules *IL-23p19*, *IL-1*, *CCR7*, *IL-1F9*, *STAT1* and *STAT4* were commonly upregulated in WT and mutant infected macrophages. The WT infection exclusively induced upregulation of *IL-10* and *IL-1F8* and the mutant infection exclusively induced upregulation of *GM-CSF* and *STAT1α.* Four SDEGs were downregulated (*CD32*, *CD1*, *FcγR* and *FcγRII*) in response to the WT strain whereas only *CD1* was downregulated in response to the mutant strain.

Role of JAK family kinases in IL-6-type cytokine signalling

Infection with the WT and Δ*rpfB* mutant strain induced upregulation of *OSM* and *OSMRβ* (Figure 2.16A and 2.16B). Infection with the WT exclusively induced upregulation of one more SDEG, *SOCS3* (Figure 2.16A). In response to the mutant infection, additional molecules were also upregulated (*STAT1*, *STAT3* and *STAT5*) (Figure 2.16B). No SDEGs were downregulated.

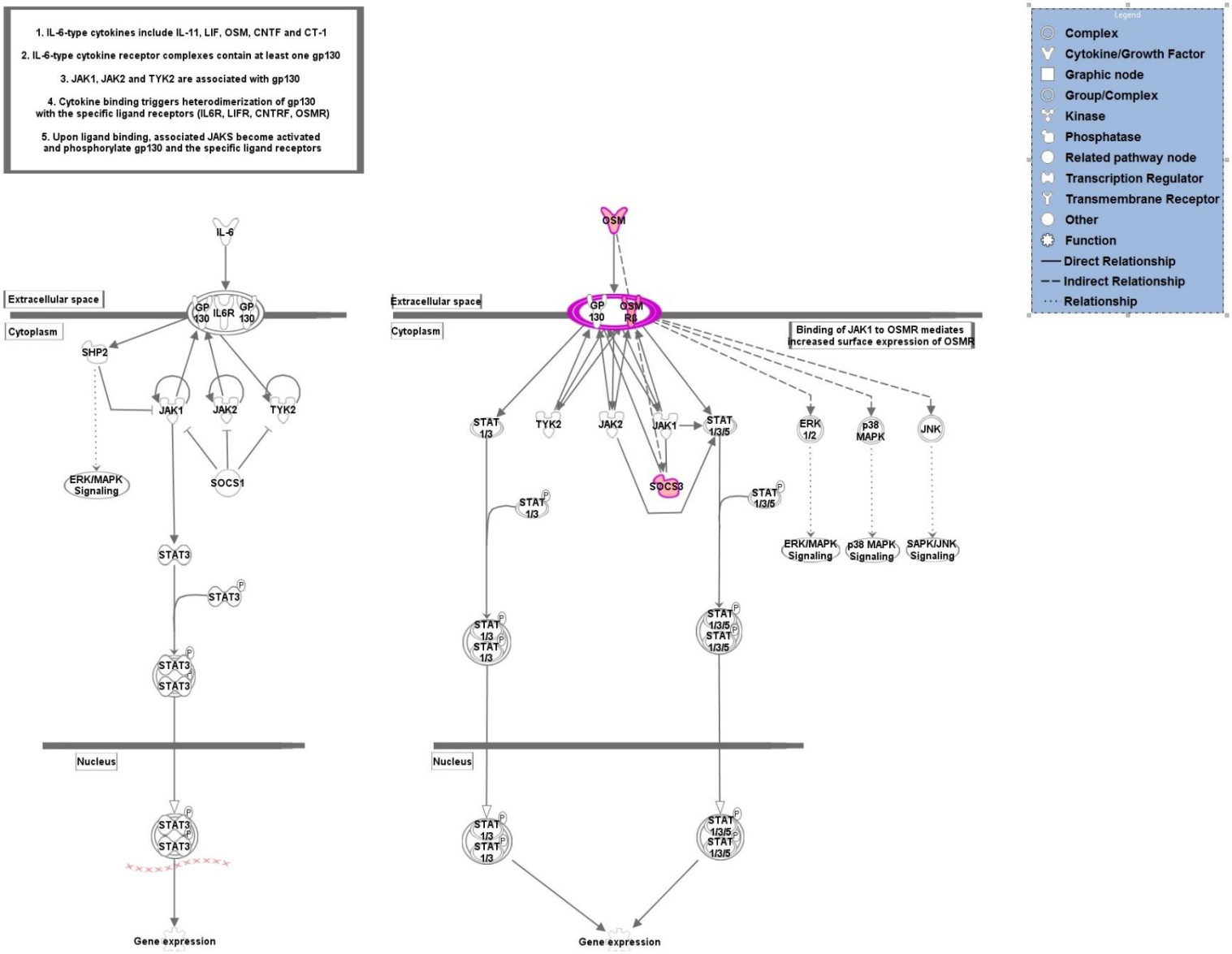

A. WT induced canonical pathway

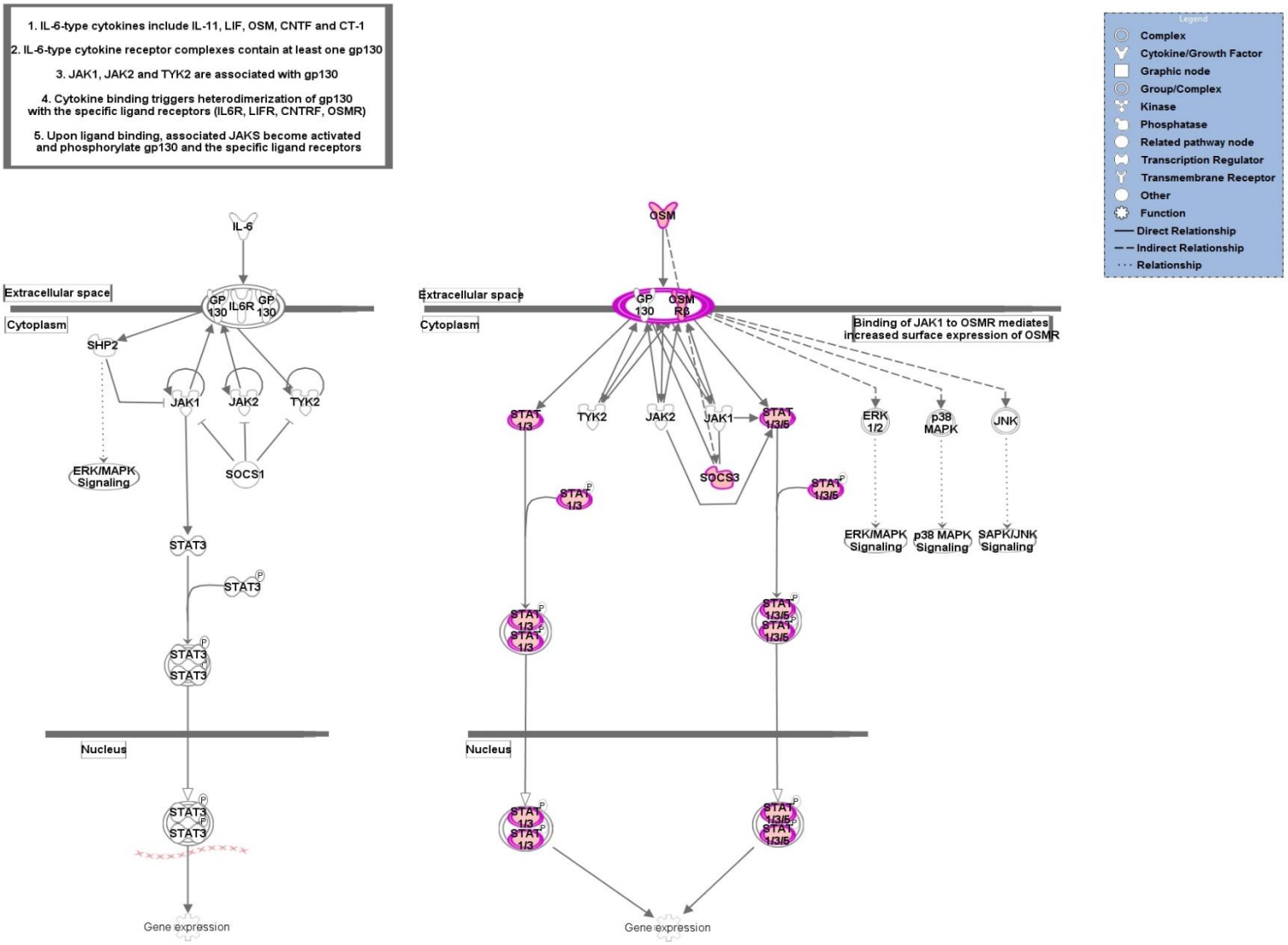

B. Δ*rpfB* induced canonical pathway

Figure 2.16: Role of JAK family kinases in IL-6 – type signalling. A. WT induced pathway. **B.** Δ*rpfB* mutant induced pathway. Upregulated SDEGs are represented in pink and downregulated SDEGs in green. The colour intensity corresponds with the level of expression. White molecules are IPA curated genes and purple double lined shapes represent groups of SDEGs. WT and mutant infection induced upregulation of *OSM* and *OSMRβ.* The WT exclusively induced upregulation of *SOCS3* and *STAT1*, *STAT3* and *STAT5* were exclusively induced by the mutant infection. No SDEGs were downregulated.

The top 10 canonical pathways exclusively induced by the WT infection were associated with intracellular signalling pathways (cAMP-mediated signalling, Gαi Signalling, GADD45 Signalling and EphrinB Signalling), anti-inflammatory immune response (IL-10 signalling), inflammation (LXR/RXR Activation), and biosynthetic processes (Choline Biosynthesis III, Methylglyoxal Degradation VI and Alanine Degradation III) (Figure 2.17A). Some of the biological processes associated with the top 10 canonical pathways induced by the mutant infection were innate immunity (Role of Pattern Recognition Receptors in Recognition of Bacteria and Viruses, Hematopoiesis from Pluripotent Stem Cells, Hematopoiesis from Multipotent Stem Cells), cytokine immune response (Interferon Signalling, Activation of IRF by Cytosolic Pattern Recognition Receptors, GM-CSF Signalling) and inflammation (Leukotriene Biosynthesis) (Figure 2.17B).

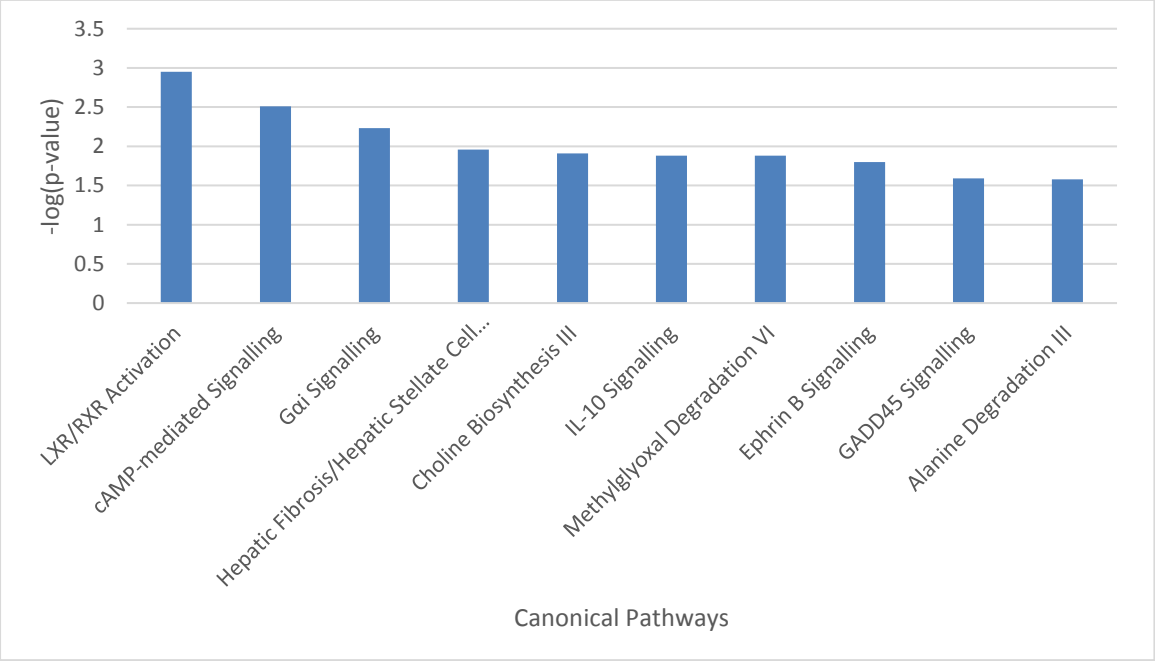

A. WT induced canonical pathways

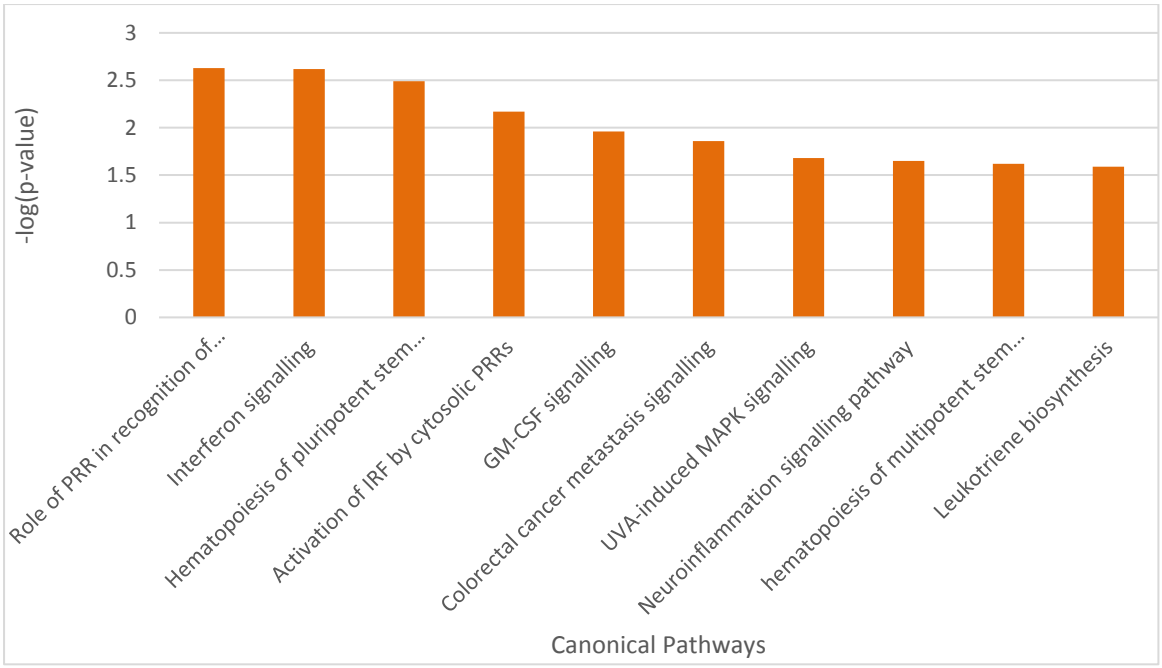

B. Δ*rpfB* mutant induced canonical pathways

Figure 2.17: Top 10 canonical pathways exclusively enriched by *Mtb* WT and Δ*rpfB* mutant infection. Canonical pathways are plotted against enrichment levels (-log (*p*-value). **A (blue).** WT induced pathways. **B (orange).** Mutant induced pathways.

Canonical pathways exclusively expressed in WT infected THP-1 macrophages 72 hours post-infection.

LXR/RXR activation

This pathway had the highest significance level of -log (2.95) of all exclusively induced WT canonical pathways (Figure 2.17A). In the pathway, most of the SDEGs (*HADH*, *HDL*, *LDL*, *LXR*, *SOD1* and *IDOL*) were downregulated compared to *SR-A* and *IL-1* that were the only two that were upregulated (Figure 2.18).

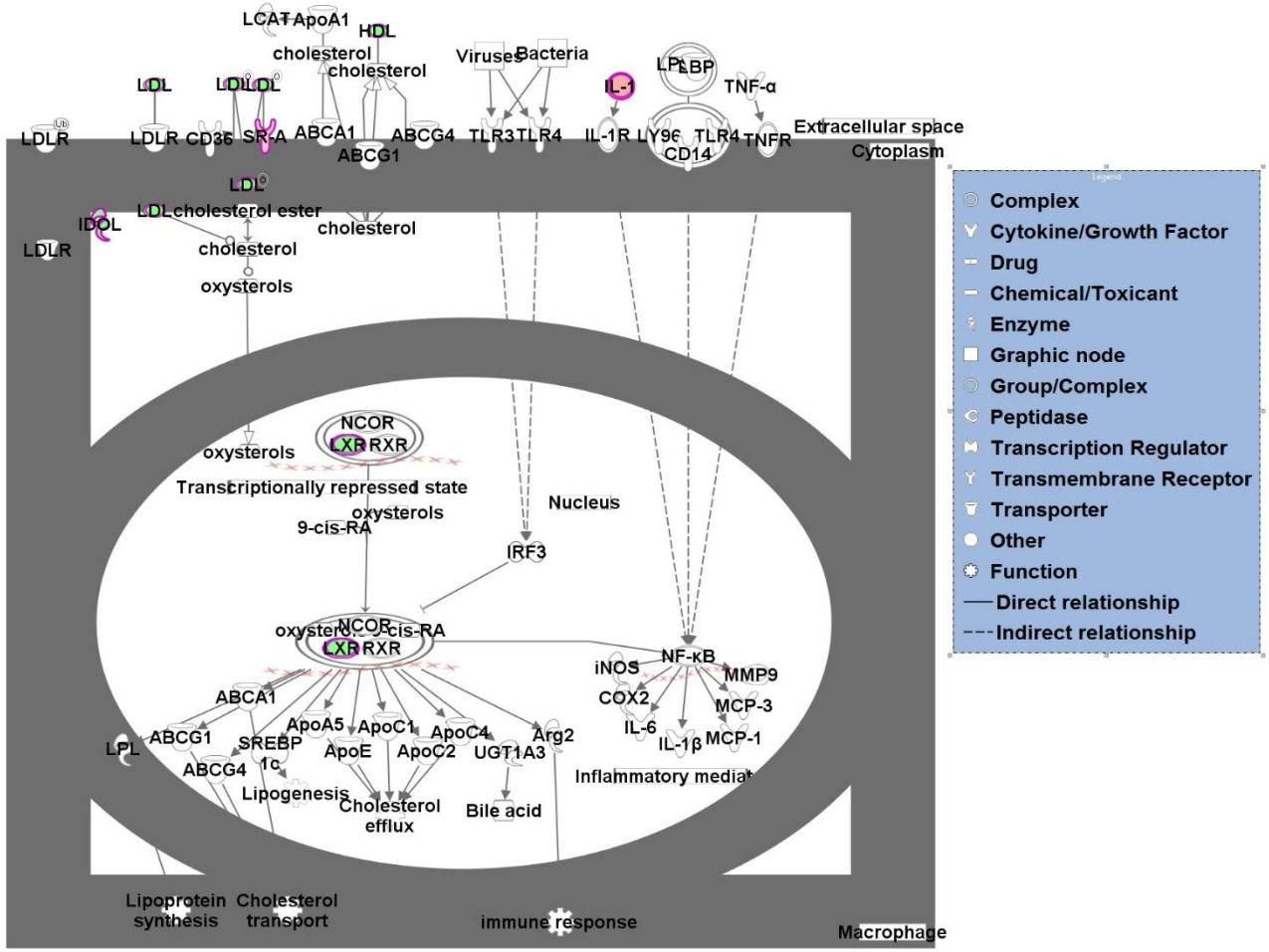

Figure 2.18: LXR/RXR activation pathway induced by WT infection. Upregulated SDEGs are represented in pink and downregulated SDEGs in green. The colour intensity corresponds with the level of expression. White molecules are IPA curated genes and purple double lined shapes represent groups of SDEGs. SDEGs *HADH*, *HDL*, *LDL*, *LXR*, *SOD1* and *IDOL* were downregulated compared to *SR-A* and *IL-1* that were the only two upregulated SDEGs.

cAMP - mediated, GαI signalling and GADD45 signalling

cAMP-mediated signalling, GαI signalling and GADD45 signalling are among the top 10 canonical pathways exclusively induced by WT infected macrophages at -log (2.51), -log (2.23) and -log (1.59), respectively (Figure 2.17A). In the cAMP - mediated and Gαi signalling pathway, *Gi-coupled receptor*, *Rap1Gap* and *AC* are commonly downregulated (Figure2.19A and 2.19B). *PDE* and *ICER* are slightly upregulated in the cAMP – mediated signalling pathway (Figure 2.19A) whereas no SDEGs were upregulated in the Gαi signalling pathway (Figure 2.19B). In the GADD45 signalling pathway, *CYCLIN D* and *CYCLIN B1* are downregulated, with no upregulated SDEGs (Figure 2.19C). In mutant infected macrophages, cAMP-mediated signalling and GαI signalling were expressed below the acceptable fold change of –log (1.5), at –log (0.4537) and –log (0.658), respectively. GADD45 signalling had a zero-fold change in mutant infected macrophages (Data not shown).

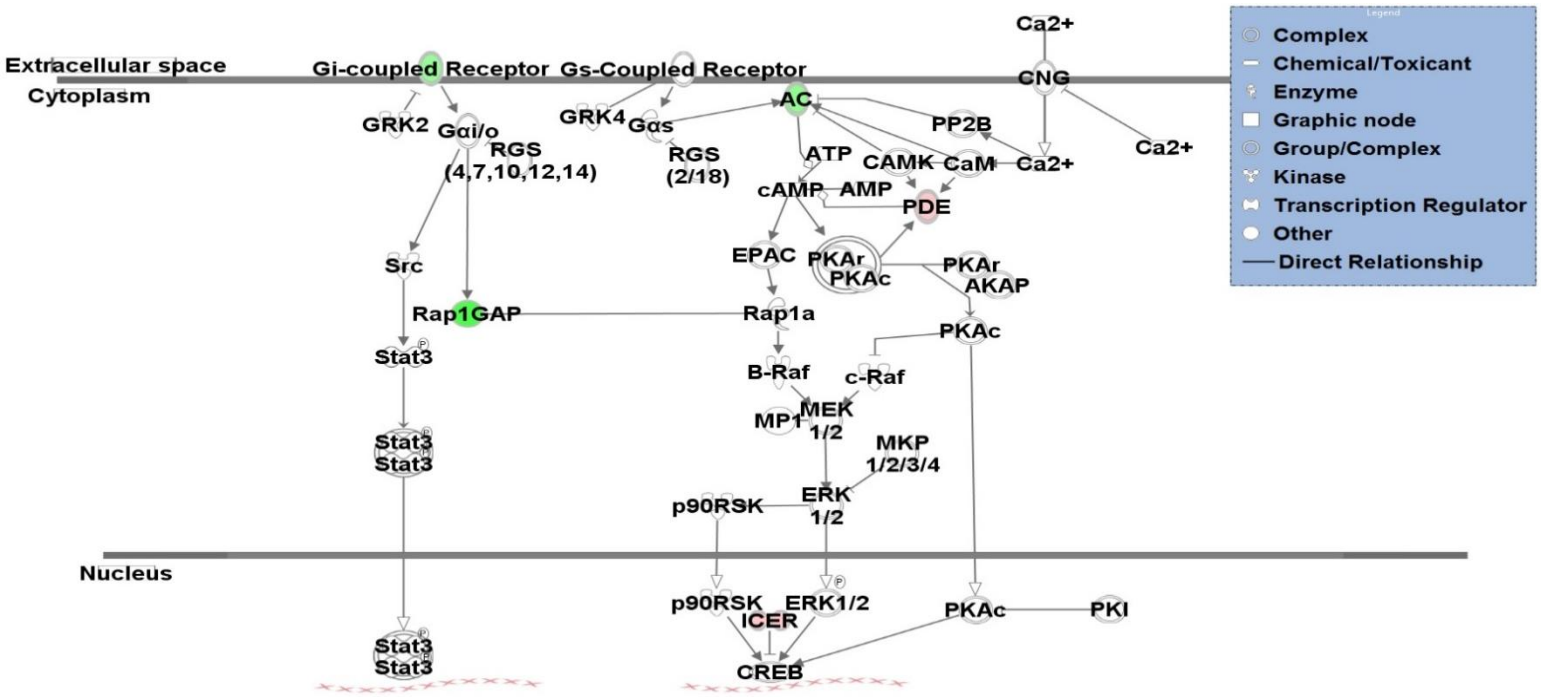

A. WT induced c-AMP mediated signalling pathway

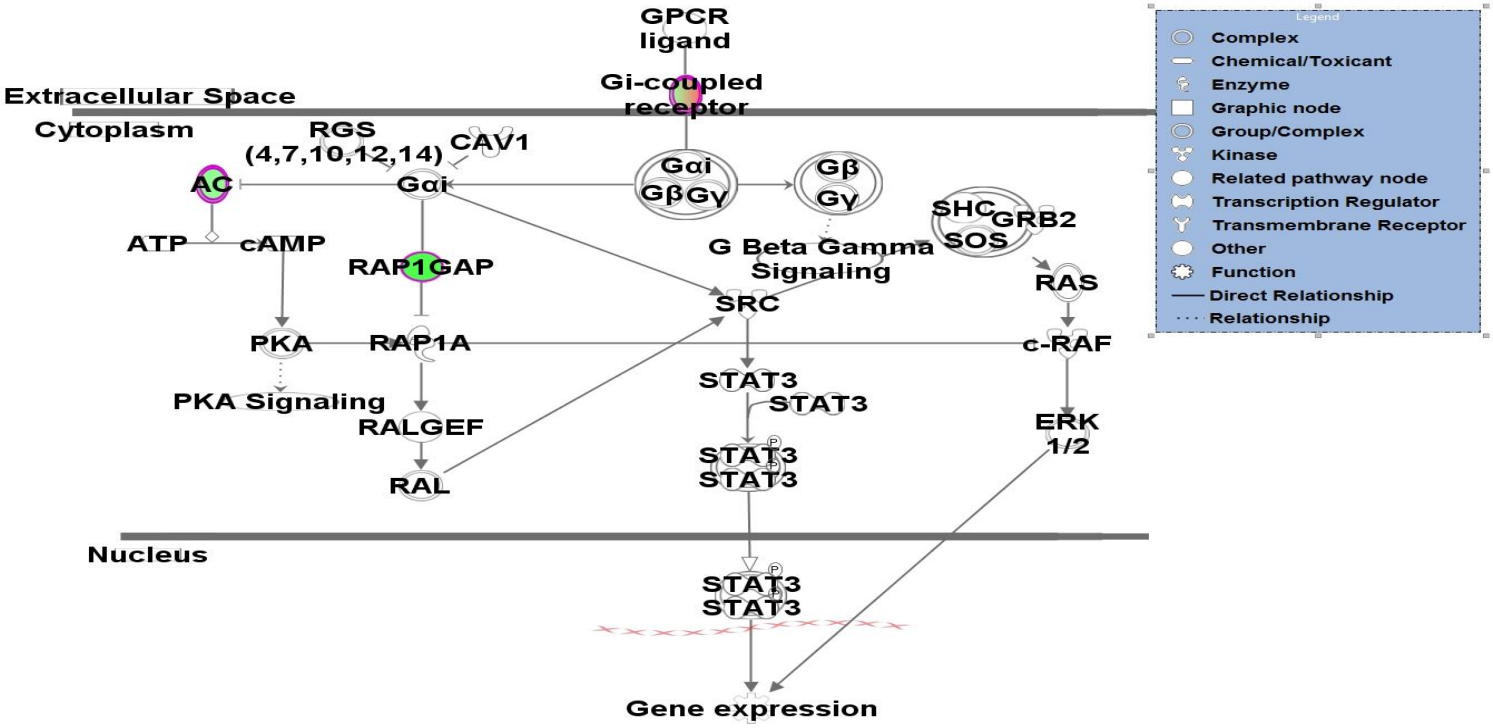

B. WT induced Gαi Signalling pathway

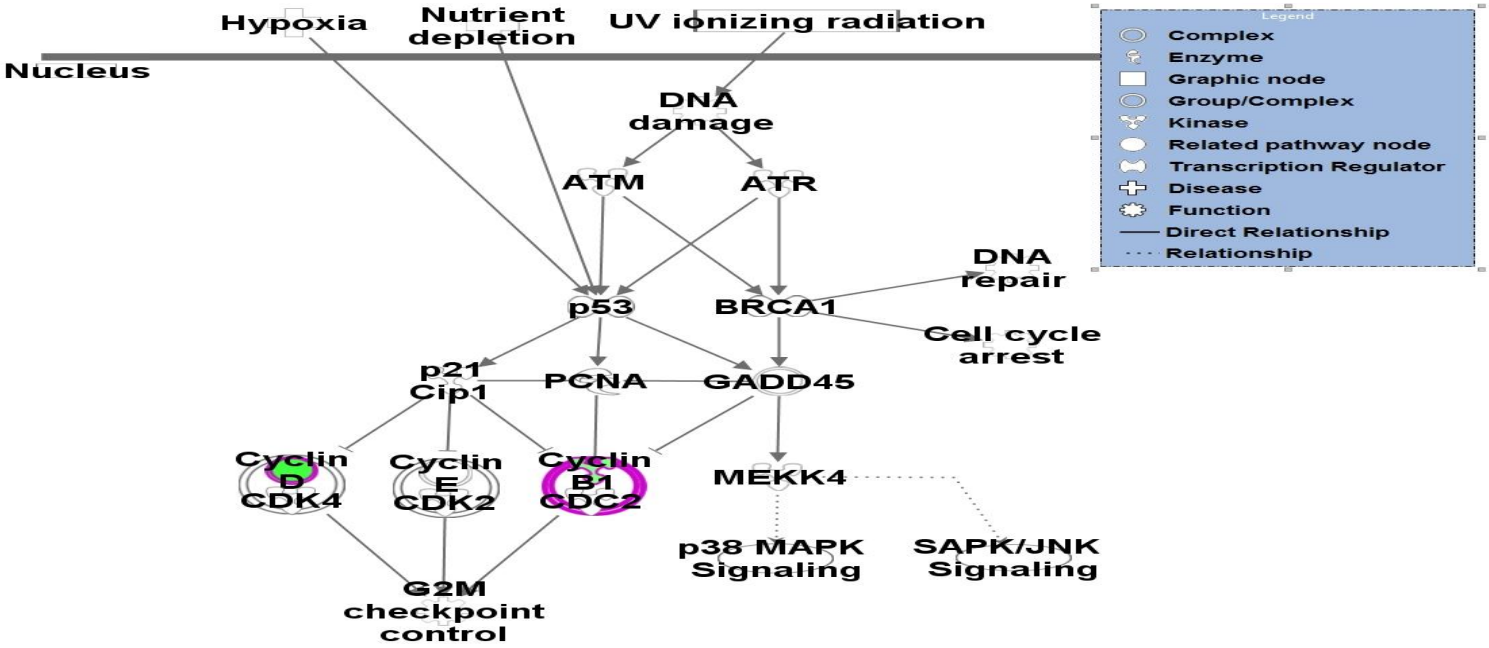

C. WT induced GADD45 signalling pathway

Figure 2.19: Second messenger signalling pathways induced by WT infection. A. cAMP – mediated signalling. **B.** Gαi signalling. **C.** GADD45 signalling. Upregulated SDEGs are represented in pink and downregulated SDEGs in green. The colour intensity corresponds with the level of expression. White molecules are IPA curated genes and purple double lined shapes represent groups of SDEGs. In the cAMP - mediated and Gαi signalling pathway, *Gi-coupled receptor*, *Rap1Gap* and *AC* are commonly downregulated. *PDE* and *ICER* are slightly upregulated in the cAMP – mediated signalling pathway whereas no SDEGs were upregulated in the Gαi signalling pathway. In the GADD45 signalling pathway, *CYCLIN D* and *CYCLIN B1* are downregulated, with no upregulated SDEGs.

Ephrin B signalling

With a z-score of -1, this was the only inhibited pathway of the exclusively induced WT pathways. SDEGs, *Gα*, *RGS3* and *EPHB* were highly downregulated (Figure 2.20). No SDEGs were upregulated.

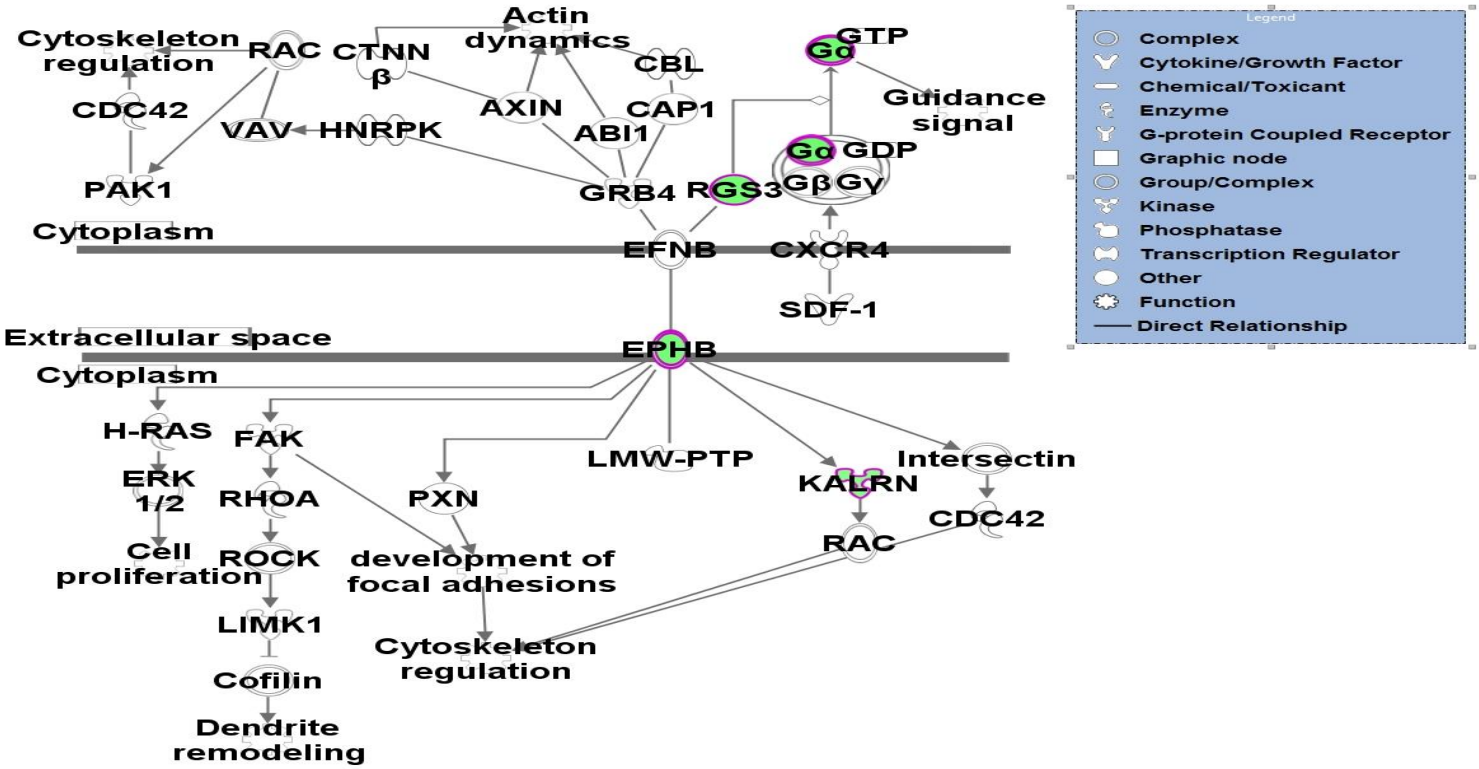

Figure 2.20: Ephrin B signalling pathway induced by WT infection. Upregulated SDEGs are represented in pink and downregulated SDEGs in green. The colour intensity corresponds with the level of expression. White molecules are IPA curated genes and purple double lined shapes represent groups of SDEGs. This was the only inhibited pathway of the exclusively induced WT pathways. SDEGs, *Gα*, *RGS3* and *EPHB* were highly downregulated while no SDEGs were upregulated.

Canonical pathways exclusively expressed in Δ*rpfB* mutant infected THP-1 macrophages 72 hours post-infection.

Role of pattern recognition receptors in recognition of bacteria and viruses

This pathway was the highest expressed from all mutant induced pathways (Figure 2.17B), however only three SDEGs (*IRF7*, *LIF*, *CSF2*) were involved. Interestingly, none of the SDEGs were up – or downregulated (Figure 2.21). In WT infected macrophages the pathway is expressed below the acceptable log fold change of log (1.5), at 0.286.

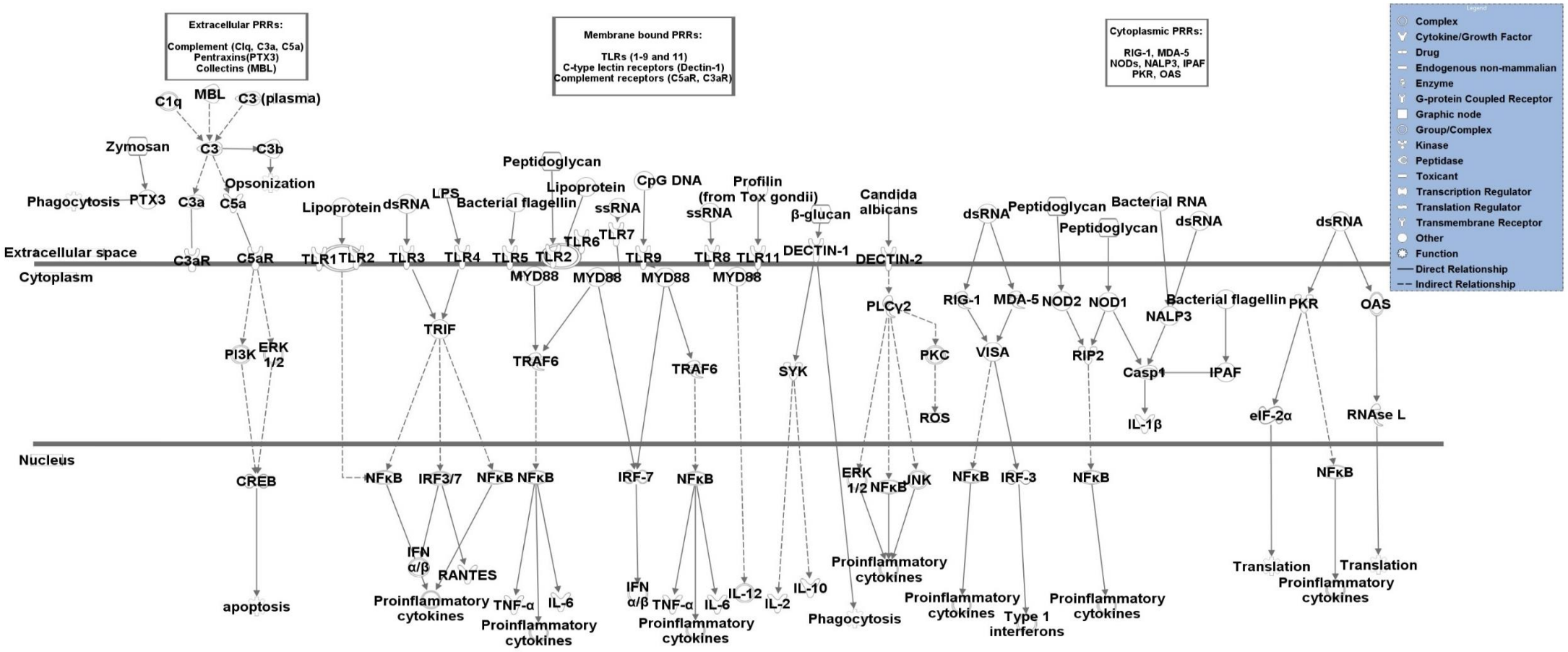

Figure 2.21: Role of pattern recognition receptors in recognition of bacteria and viruses pathway induced by Δ*rpfB* mutant infection. Upregulated SDEGs are represented in pink and downregulated SDEGs in green. The colour intensity corresponds with the level of expression. White molecules are IPA curated genes and purple double lined shapes represent groups of SDEGs. Only three SDEGs (*IRF7*, *LIF*, and *CSF2*) were involved according to IPA. Interestingly, none of the SDEGs were up – or downregulated.

Hematopoiesis of pluripotent and multipotent stem cells

Even though these pathways ranked in the top 10 canonical pathways exclusively induced by the mutant infection, hardly any SDEGs were induced and differentially expressed within the pathways. In the hematopoiesis of pluripotent stem cells pathway, the mutant infection induced expression of only two SDEGs, *LIF* and *CSF2*, whereas in the hematopoiesis of multipotent stem cells, only *CSF2* was induced. No SDEGs were up- or downregulated in the latter pathway (Figure 2.22B). In the former pathway, *GM-CSF* and *LIF* were upregulated, with no downregulated SDEGs (Figure 2.22A). In WT infected macrophages, the hematopoiesis of pluripotent stem cells pathway was expressed below the acceptable log fold change of log (1.5), at 0.369.

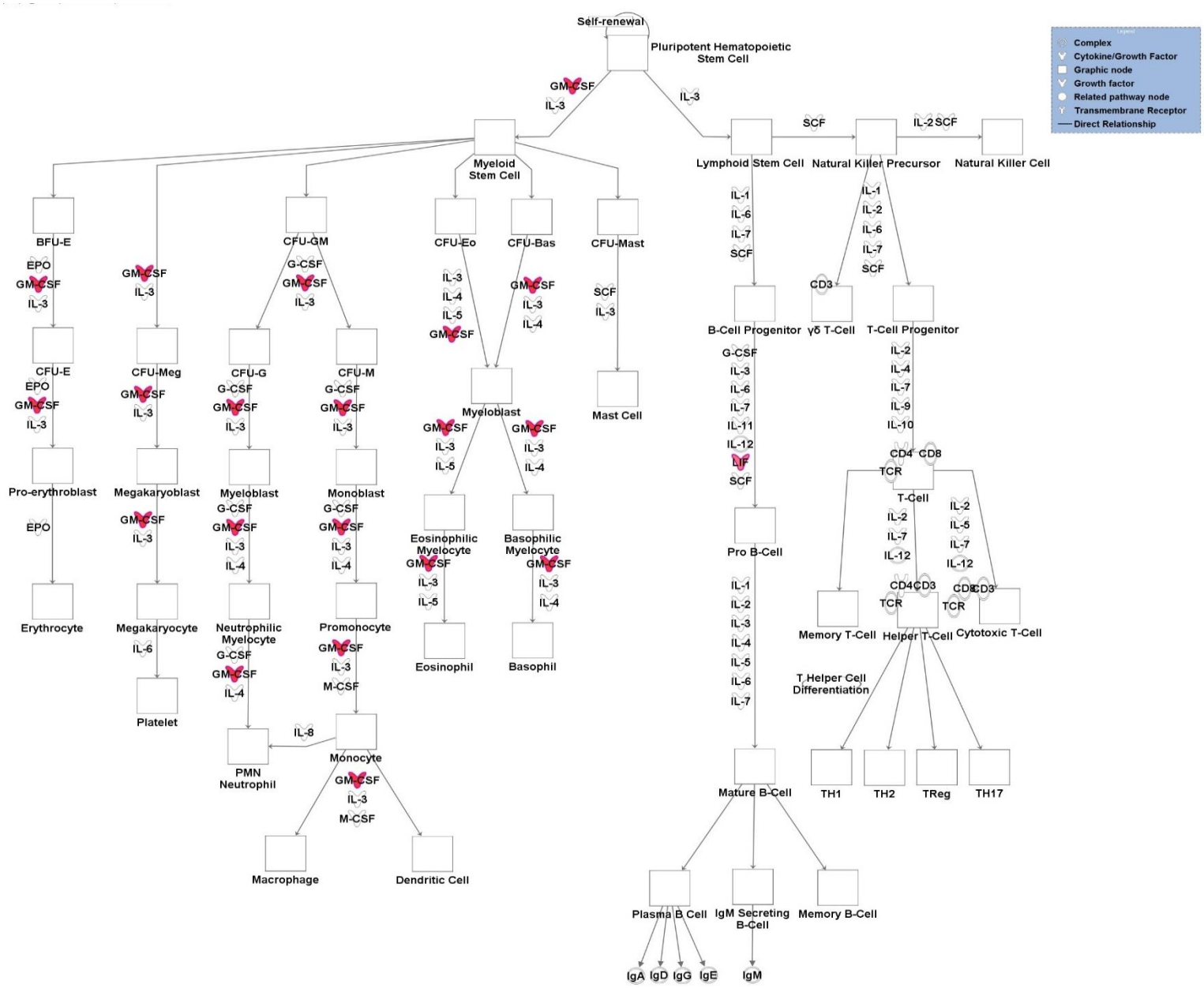

A. Hematopoiesis of pluripotent stem cells pathway

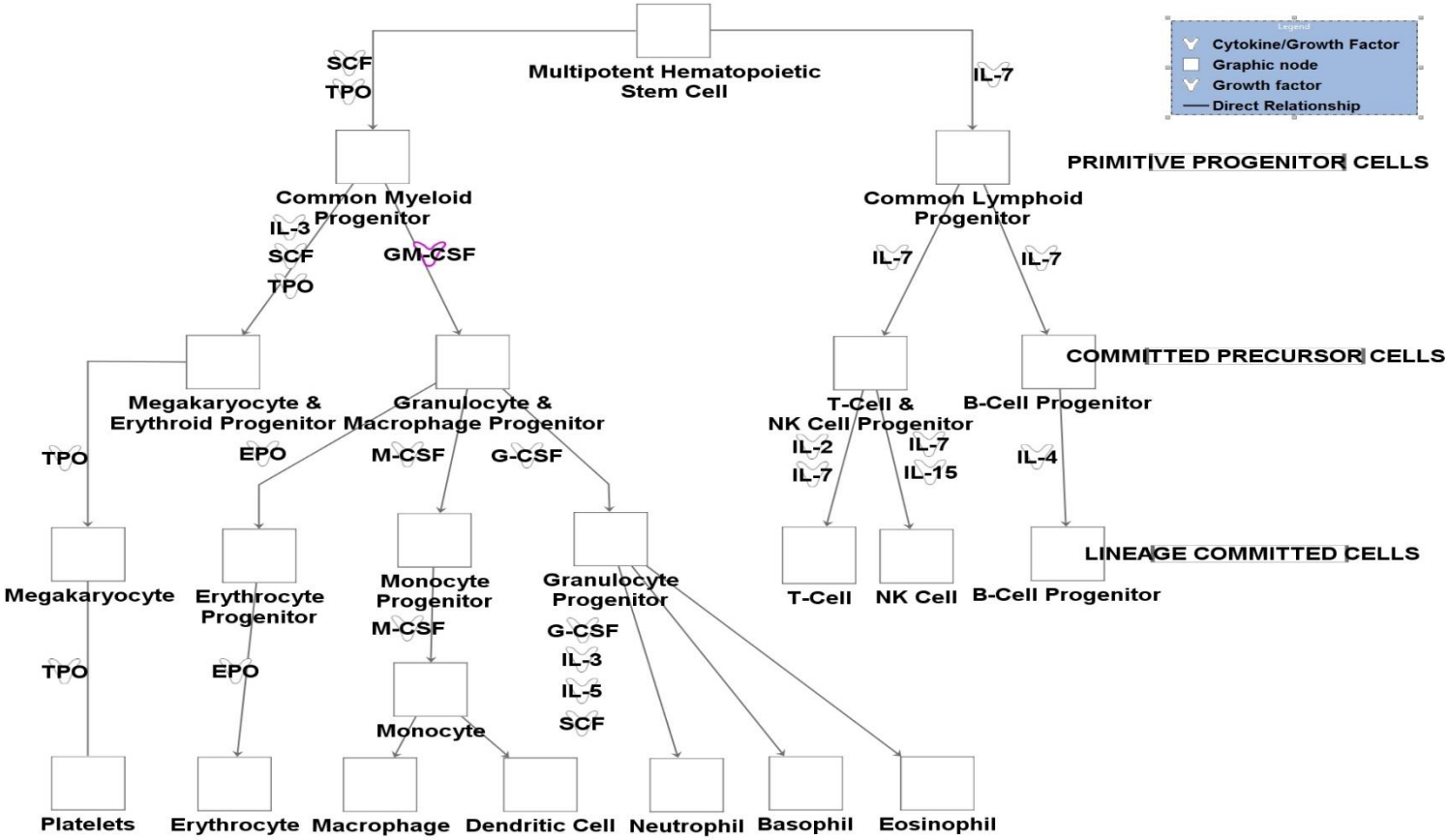

B. Hematopoiesis of multipotent stem cells pathway

Figure 2.22: Hematopoiesis of pluri – and multipotent stem cells induced by Δ*rpfB* mutant infection. A. Hematopoiesis of pluripotent stem cells. **B.** Hematopoisesis of multipotent stem cells. Upregulated SDEGs are represented in pink and downregulated SDEGs in green. The colour intensity corresponds with the level of expression. White molecules are IPA curated genes and purple double lined shapes represent groups of SDEGs. In the hematopoiesis of pluripotent stem cells pathway, the mutant infection induced expression of *LIF* and *CSF2*, whereas in the hematopoiesis of multipotent stem cells, only *CSF2* was induced. No SDEGs were up- or downregulated in the latter pathway. In the former pathway, *GM-CSF* and *LIF* were upregulated, with no downregulated SDEGs.

GM-CSF signalling

This pathway shows expression of only two SDEGs induced by the mutant infection, *GM-CSF* and *STAT1*, both of which were highly upregulated (Figure 2.23). A third SDEG associated with the pathway was *CSF2*, which was neither up - nor downregulated. The pathway was also induced in WT infected macrophages but had zero-fold change (Data not shown).

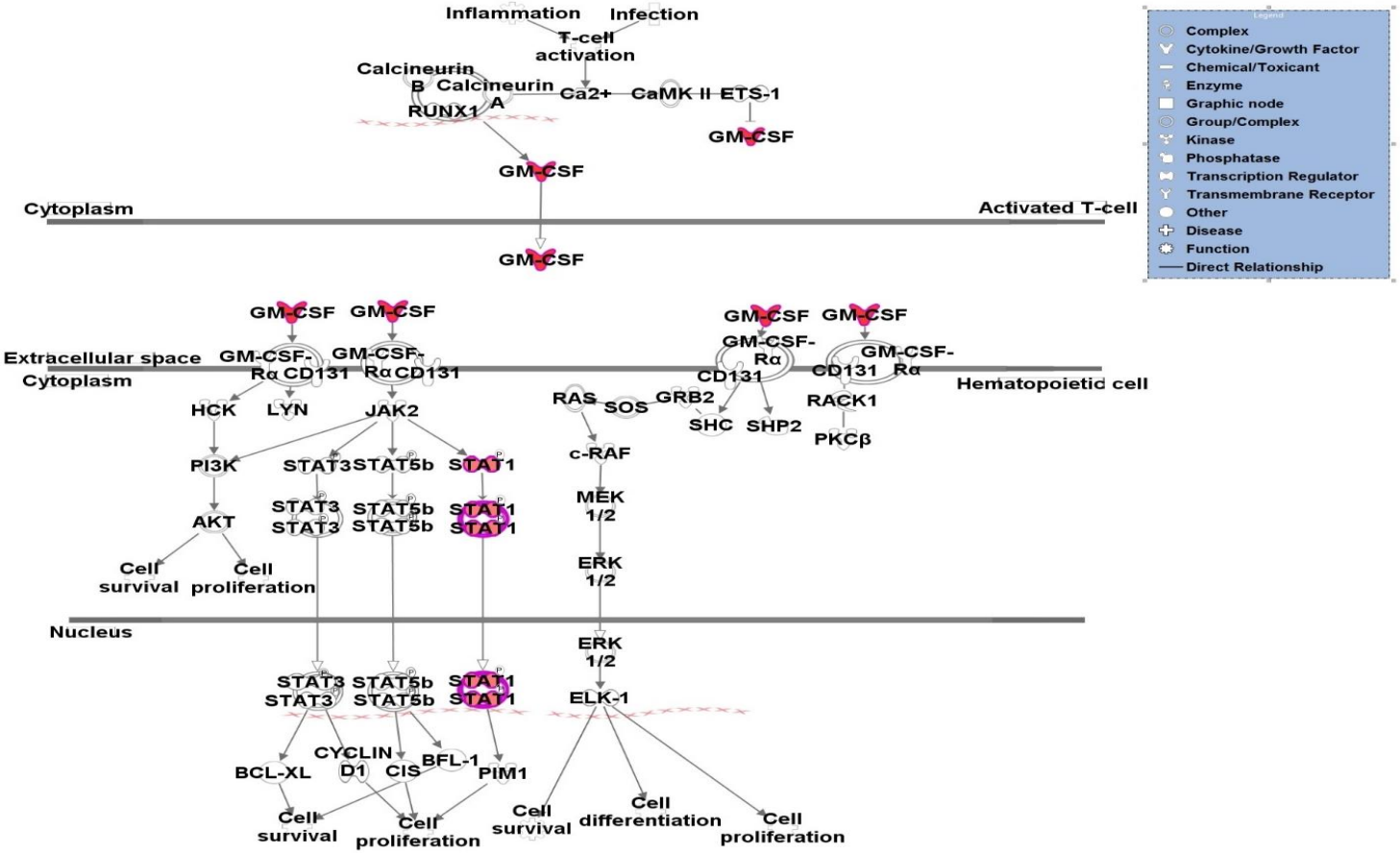

Figure 2.23: GM-CSF signalling pathway induced by Δ*rpfB* mutant infection. Upregulated SDEGs are represented in pink and downregulated SDEGs in green. The colour intensity corresponds with the level of expression. White molecules are IPA curated genes and purple double lined shapes represent groups of SDEGs. Only two SDEGs were induced by the mutant infection, *GM-CSF* and *STAT1*, both of which were highly upregulated**.** A third SDEG associated with the pathway was *CSF2*, which was neither up - nor downregulated

Upstream regulators

Based on statistical significance (*p*-value), the top 5 upstream regulators commonly induced by the WT and Δ*rpfB* mutant infection were all cytokines (*IFNL1, IFNA2, PRL, IFN-γ*, TNF, *IFN-α*) with high activated prediction scores (Table 2.8). These upstream regulators were found associated with biological processes such as STAT signalling and the negative regulation of IL-13 and IL-5 production (Table 2.8).

The WT infection induced almost a 6-fold higher number of SDEGs (289) compared to the mutant infection (52) (Figure 2.5). The top 5 upstream regulators exclusively induced by the WT infection were a combination of ligand-dependent nuclear receptor (*RARA*), growth factor (*TGFB1*), kinase (*ERRB*) and two molecules unidentified by IPA (*VIPAS39*, *NEDD9*). These were enriched at *p*-values within a range of 1.04E-04 – 4.12E-05 (Table 2.9). The top 5 upstream regulators exclusively induced by the Δ*rpfB* mutant infection were a combination of a group of interferons (*IFN-α*), transmembrane receptor (*TLR3*) and regulator (*SPI1*, activated), and cytokines (*IFNA2*, *PRL*, both activated). These were enriched at a higher level than the WT induced upstream regulators, within a *p*-value range of 8.40E-07 – 5.48E-08. (Table 2.9). Biological processes associated with WT induced upstream regulators were associated with cell differentiation and regulation of cellular processes whereas those induced by the mutant were associated with transcription and gene expression, and cytokine production (Table 2.9).

Table 2.8: Top 5 upstream regulators commonly induced by WT and Δ*rpfB* mutant infection in association with biological processes. Upstream regulators were identified by Ingenuity Pathway Analysis (IPA) and biological processes by MSigDB. The *p*-value represents level of enrichment by IPA and false discovery rate (FDR) q-value by MSigDB. Z-score represents predicted activation score.

Upstream regulator	*p*-value	Z-score	Function	FDR q-value
IFNL1	1.15E-43	5.672	Positive regulation of receptor signalling pathway via STAT	1.37E-04
IFNA2	1.78E-35	5.336	Regulation of receptor signalling pathway via STAT	1.74E-04
PRL	2.72E-35	5.376	Receptor signalling pathway via STAT	1.74E-04
IFN-γ	2.87E-34	5.764	Negative regulation of IL-13 production	1.74E-04
IFN-α	7.19E-26	2.854	Negative regulation of IL-5 production	1.74E-04

Table 2.9: **Top 5 upstream regulators exclusively induced by WT and Δ*rpfB* mutant infection in association with GO functions.** Upstream regulators were identified by Ingenuity Pathway Analysis (IPA) and biological processes by MSigDB. The *p*-value represents level of enrichment by IPA and false discovery rate (FDR) *q*-value by MSigDB.

WT induced				**Δ*rpfB* induced**			
Upstream regulator	*p*-value	Function	FDR *q*-value	Upstream regulator	*p*-value	Function	FDR *q*-value
RARA	1.07E-05	Positive regulation of cell adhesion	6.02E-04	*Interferon-α*	2.23E-08	Positive regulation of RNA biosynthetic process	1.34E-02
TGFB1	1.15E-05	Ensheathment of neurons	1.27E-03	*TLR3*	2.69E-08	Positive regulation of pri-miRNA transcription by RNA polymerase II	1.34E-02
VIPAS39	4.12E-05	Regulation of T cell differentiation	1.27E-03	*SPI1*	5.48E-08	Positive regulation of gene expression	1.34E-02
ERRB2	1.04E-04	Regulation of cell adhesion	1.27E-03	*IFNA2*	8.40E-07	Leukocyte differentiation	1.34E-02
NEDD9	1.07E-04	Regulation of lymphocyte differentiation	1.68E-03	*PRL*	8.91E-07	Regulation of cytokine production involved in immune response	2.88E-02

Transcripts *IFNA2*, *PRL* and *IFN-α* were significantly enriched upstream regulators common to macrophages infected with both strains and to those exclusively infected by the mutant. The difference here can be seen in the network of each of these regulators that influence a different number of SDEGs and their expression levels (Figure 2.24 A-F). In the commonly induced *IFNA2* network, all 32 molecules are upregulated and have a predicted activated state influenced by *IFNA2* except *TNFRSF-10D* and *BIRC* which are downregulated, and the latter had a predicted inhibited state. The same network induced by the mutant infection influenced upregulated and predicted activation of only 5 molecules (*MX1, IRF7, DDX60, STAT1, ISG20*) that cannot be seen in the former network (Figure 2.24 1A and 1B). The commonly induced interferon alpha network showed upregulation and predicted activation of all 33 molecules except *TRIB2* which was downregulated, however in the mutant induced interferon alpha network, only 8 molecules were upregulated, and none had predicted states (Figure 2.24 2C and 2D). The *PRL* commonly and exclusively induced network had no downregulated molecules, but the commonly induced network showed upregulation and predicted activation of 31 molecules compared 5 induced by the mutant infection (Figure 2.24 3E and 3F). All molecules influenced by the respective upstream regulators in Figure 24 1B, 2D and 3F are not found in WT induced macrophages.

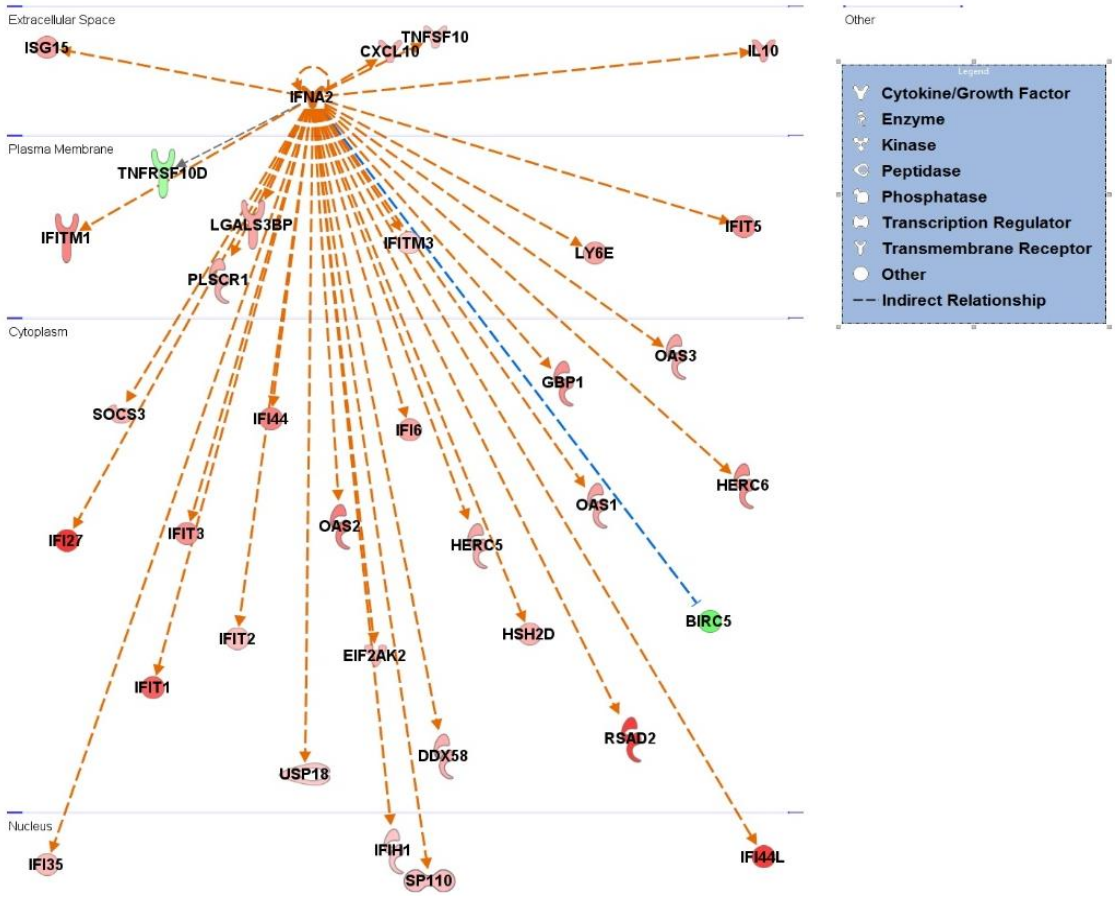
Extracellular Space
Plasma Membrane
Cytoplasm
Nucleus
ISG15
CXCL10
TNFSF10
IL10
IFNA2
TNFRSF10D
IFITM1
LGALS3BP
PLSCR1
IFITM3
LY6E
IFIT5
OAS3
GBP1
SOCS3
IFI44
IFI6
HERC6
OAS1
IFI27
IFIT3
OAS2
HERC5
BIRC5
IFIT2
HSH2D
EIF2AK2
IFIT1
RSAD2
DDX58
USP18
IFI35
IFIH1
SP110
IFI44L
Other
Legend
Cytokine/Growth Factor
Enzyme
Kinase
Peptidase
Phosphatase
Transcription Regulator
Transmembrane Receptor
Other
Indirect Relationship

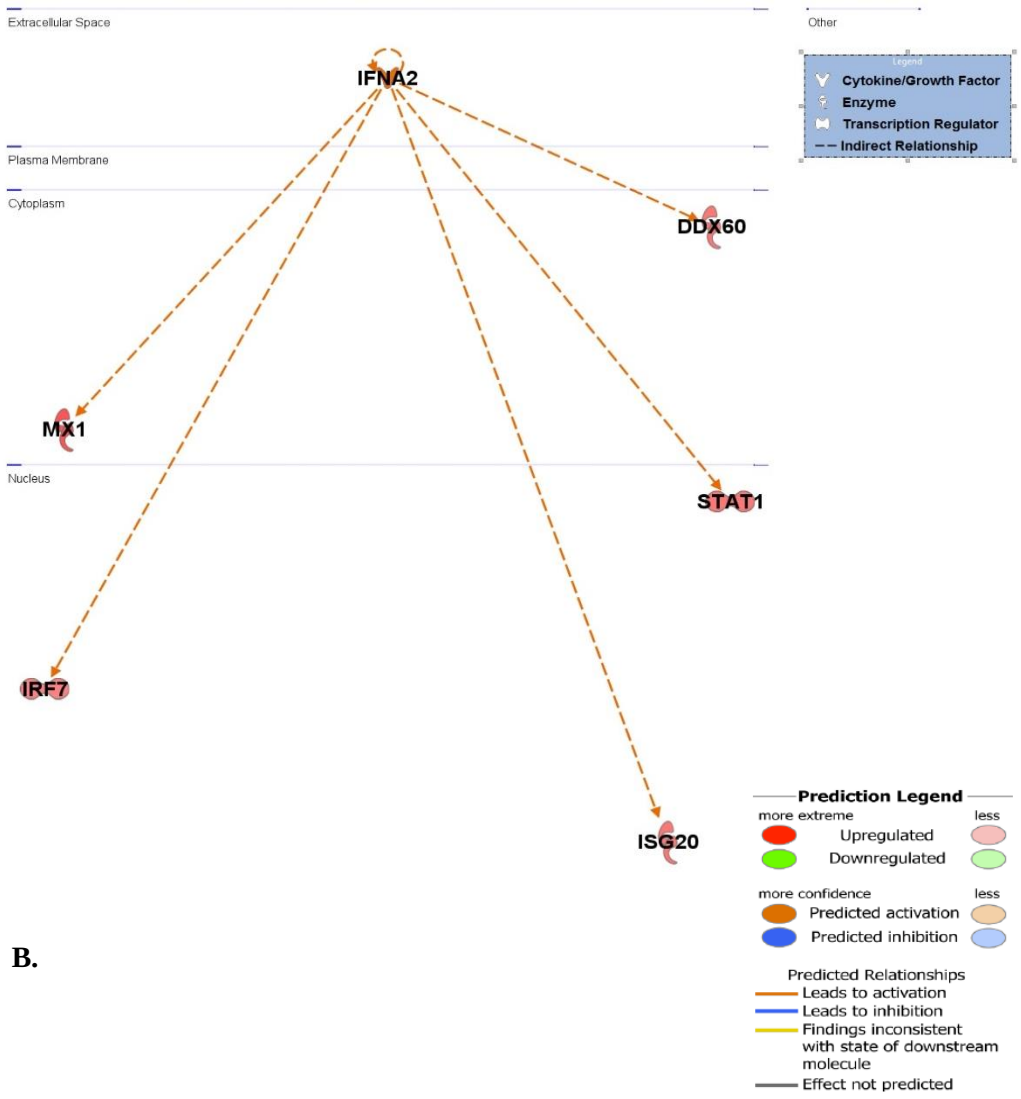
Extracellular Space
Plasma Membrane
Cytoplasm
Nucleus
IFNA2
DDX60
MX1
STAT1
IRF7
ISG20
Other
Legend
Cytokine/Growth Factor
Enzyme
Transcription Regulator
Indirect Relationship
Prediction Legend
more extreme
less
Upregulated
Downregulated
more confidence
less
Predicted activation
Predicted inhibition
Predicted Relationships
Leads to activation
Leads to inhibition
Findings inconsistent with state of downstream molecule
Effect not predicted

1 **A.** **B.**

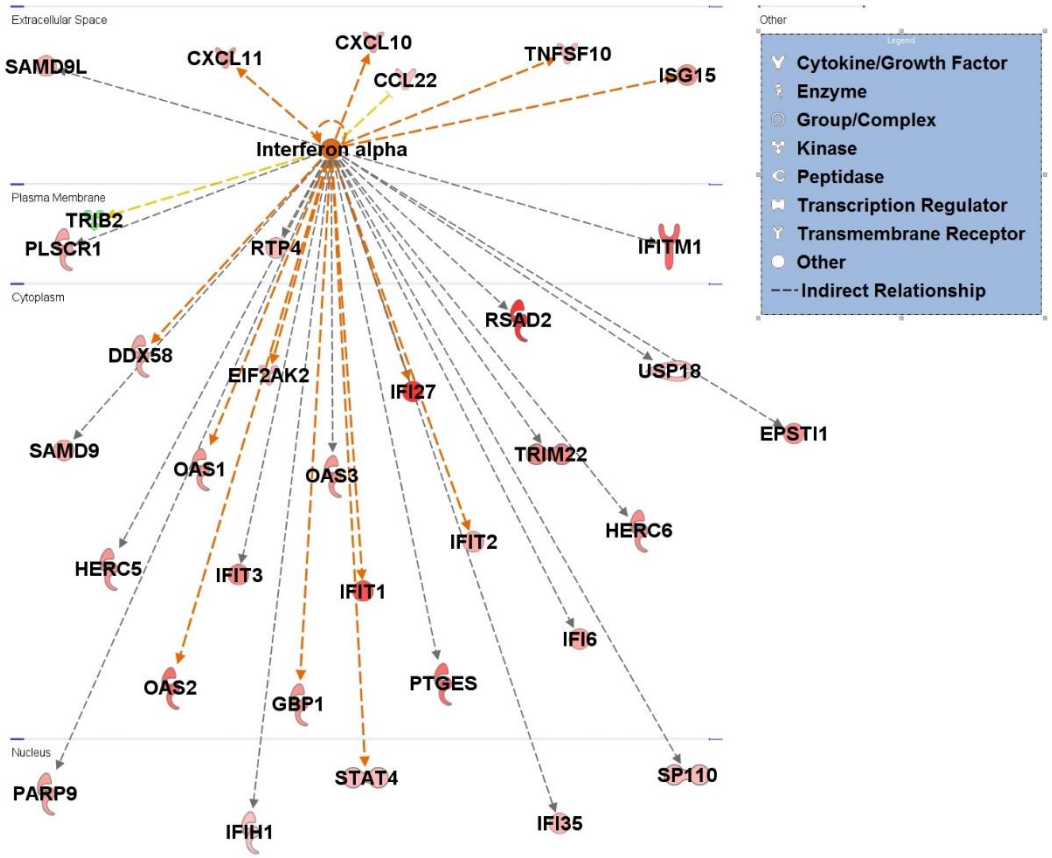
Extracellular Space
Plasma Membrane
Cytoplasm
Nucleus
SAMD9L
CXCL11
CXCL10
CCL22
TNFSF10
ISG15
Interferon alpha
TRIB2
PLSCR1
RTP4
IFITM1
RSAD2
DDX58
EIF2AK2
IFI27
USP18
EPSTI1
SAMD9
OAS1
OAS3
TRIM22
HERC6
HERC5
IFIT3
IFIT2
IFIT1
IFI6
OAS2
GBP1
PTGES
PARP9
STAT4
SP110
IFIH1
IFI35
Other
Cytokine/Growth Factor
Enzyme
Group/Complex
Kinase
Peptidase
Transcription Regulator
Transmembrane Receptor
Other
Indirect Relationship

2 C.

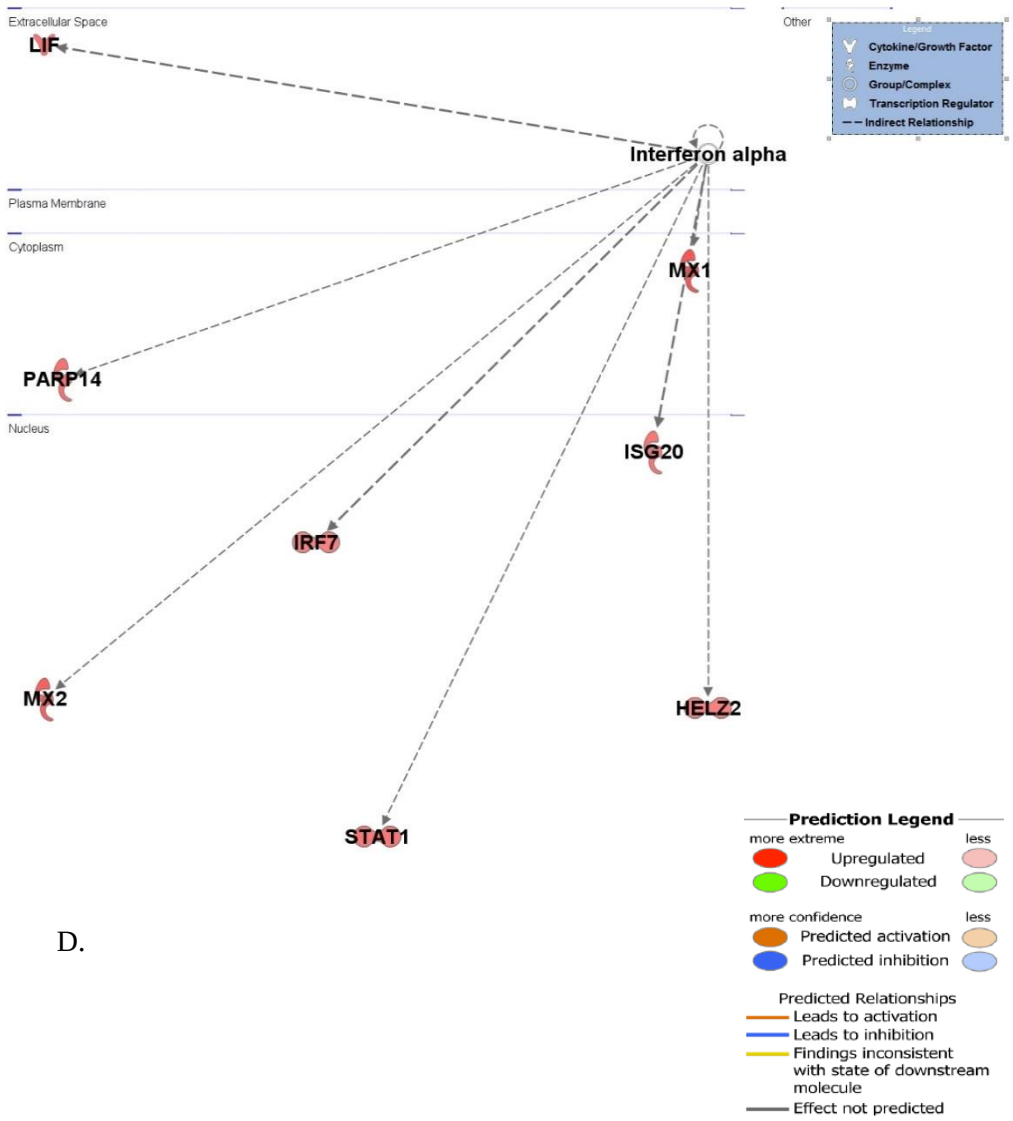
Extracellular Space
Plasma Membrane
Cytoplasm
Nucleus
LIF
Interferon alpha
MX1
PARP14
ISG20
IRF7
MX2
HELZ2
STAT1
Other
Cytokine/Growth Factor
Enzyme
Group/Complex
Transcription Regulator
Indirect Relationship
Prediction Legend
more extreme
less
Upregulated
Downregulated
more confidence
less
Predicted activation
Predicted inhibition
Predicted Relationships
Leads to activation
Leads to inhibition
Findings inconsistent with state of downstream molecule
Effect not predicted

D.

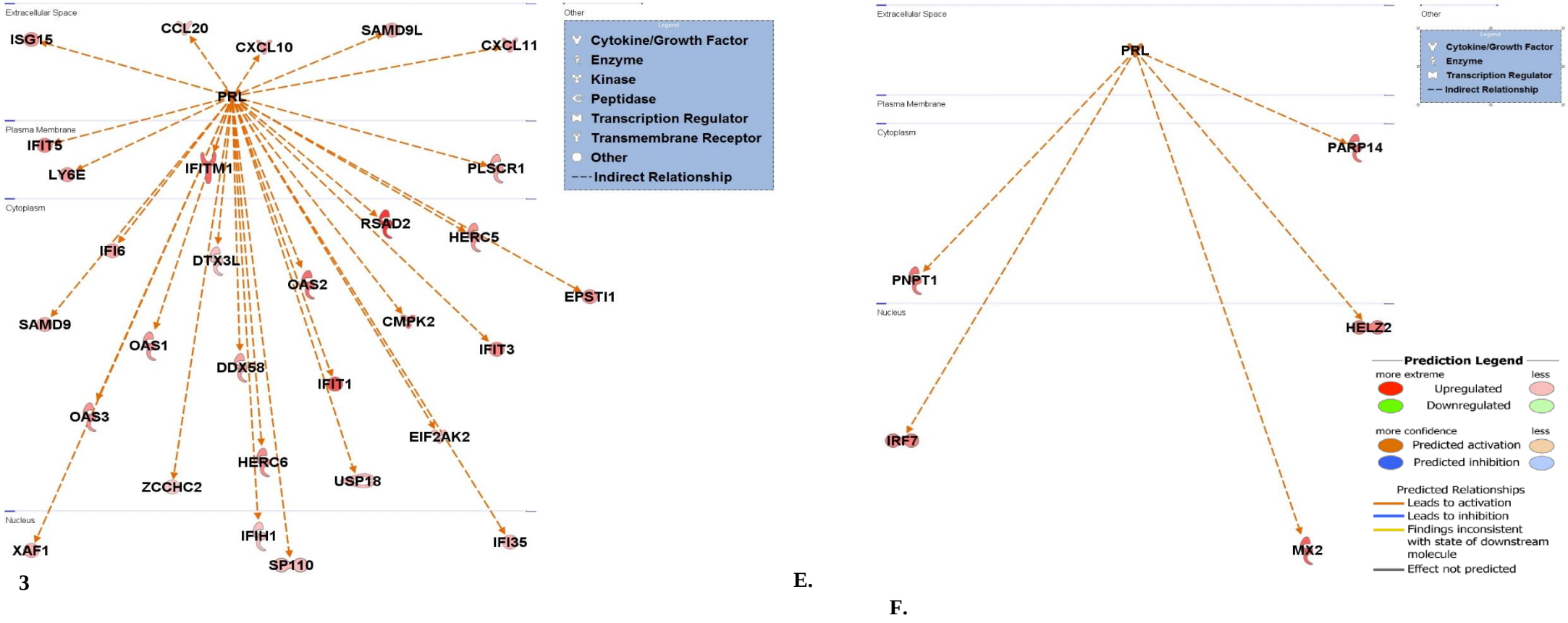

Figure 2.24: Networks of IFNA2 (1), Interferon alpha (2) and PRL (3) upstream regulators commonly and exclusively induced by *Mtb* infection. **A, C, E**. Induced by infection with *M. tuberculosis* WT and mutant strains. **B, E, F.** Induced exclusively by Δ*rpfB* mutant infection. Upregulated molecules are represented in red and downregulated molecules in green. The level of expression varies with colour intensity. Orange and blue broken lines indicate predicted activation and inhibition, respectively, by the upstream regulator on another molecule. Yellow broken lines represent findings inconsistent with state of downstream molecule and grey represents no effect predicted.

Diseases and functions

Overall, the WT infection induced higher scores of diseases and functions compared to the mutant infection. Table 2.11 shows the top 5 diseases and functions induced by both strains based on the highest scores (Top 5 enriched networks shown in Appendix G). At the highest score of 41, Lipid metabolism, Molecular transport and Small molecule biochemistry was elicited in response to WT infection compared to Cellular development, Hematological system development and function, Lymphoid tissue structure and development at the highest score of 37, elicited by the mutant infection.

Infection with both strains induced 16 diseases and functions some of which were associated with an innate immune response (Table 2.10). Interestingly, antimicrobial response, inflammatory response and infectious diseases appeared twice in the list of the top 5 as the first highest (Score = 43) with 28 associated molecules and the fourth highest (Score = 32) with 23 associated molecules (Table 2.10, Figure 2.25A and 2.25B). Even though the networks are the same, they both share a wide range of commonly and exclusively induced SDEGs. (Figure 2.25A and B). *ISG15, IFITM3, NTN1, CXCL10, DPP4, SIGLEC1, S100A8, HERC5, S100A9, SOCS3, IFIT2, USP18, DDX58, IFIT3, EIF2AK2, OAS3, IFI27, PARP9, IFI35* (all upregulated) and *TNC, AT1A2* and *KIF2C* (all downregulated) are exclusive to Figure 2.23A. Molecules *CCR7, RTP4, PLSCR1, IFIT5, TRIM22, HSH2D, SAMD9, HERC6, OAS2, STAT4, ETV7, SPI10* (all upregulated) and *SPOCK1, VIPR1, TRIB2* and *ASPM* (All downregulated) are exclusive to Figure 2.25B.

Table 2.10: Top 5 diseases and functions based on Ingenuity Pathway Analysis (IPA) scores and number of molecules elicited in THP-1 macrophages in response to *Mtb* infection.

Diseases and functions	Scores/Number of molecules
Antimicrobial Response, Inflammatory Response, Infectious Diseases	43/28
Cell Cycle, Nutritional Disease, Cellular Assembly and Organization	43/28
Connective Tissue Disorders, Inflammatory Disease, Inflammatory Response	36/25
Antimicrobial Response, Inflammatory Response, Infectious Diseases	32/23
Cellular Assembly and Organization, Hair and Skin Development and Function, Cellular Development	22/18

Table 2.11: Top 5 diseases and functions induced by WT and Δ*rpfB* mutant infection and number of molecules, based on Ingenuity Pathway Analysis (IPA) scores.

WT induced		**Δ*rpfB* mutant induced**	
Diseases and functions	**Score/Number of molecules**	**Diseases and functions**	**Score/Number of molecules**
Lipid metabolism, Molecular Transport, Small Molecule Biochemistry	41/26	Cellular Development, Hematological System Development and Function, Lymphoid Tissue Structure and Development	37/17
Connective Tissue Development and Function, Tissue Development, Cancer	32/22	Cellular Growth and Proliferation, Cell Death and Survival, Cancer	18/10
Cell Cycle, Connective Tissue Development and Function, DNA Replication, Recombination, and Repair	26/19	Skeletal and Muscular System Development and Function, Cancer, Cardiovascular System Development and Function	2/1
Cellular Development, Cellular Growth and Proliferation, Hematological System Development and Function	24/18	Carbohydrate Metabolism, Cancer, Cellular Development	2/1
Cell-To-Cell Signaling and Interaction, Hematological System Development and Function, Cellular Development	22/17	Cancer, Organismal Injury and Abnormalities, Reproductive System Disease	2/1

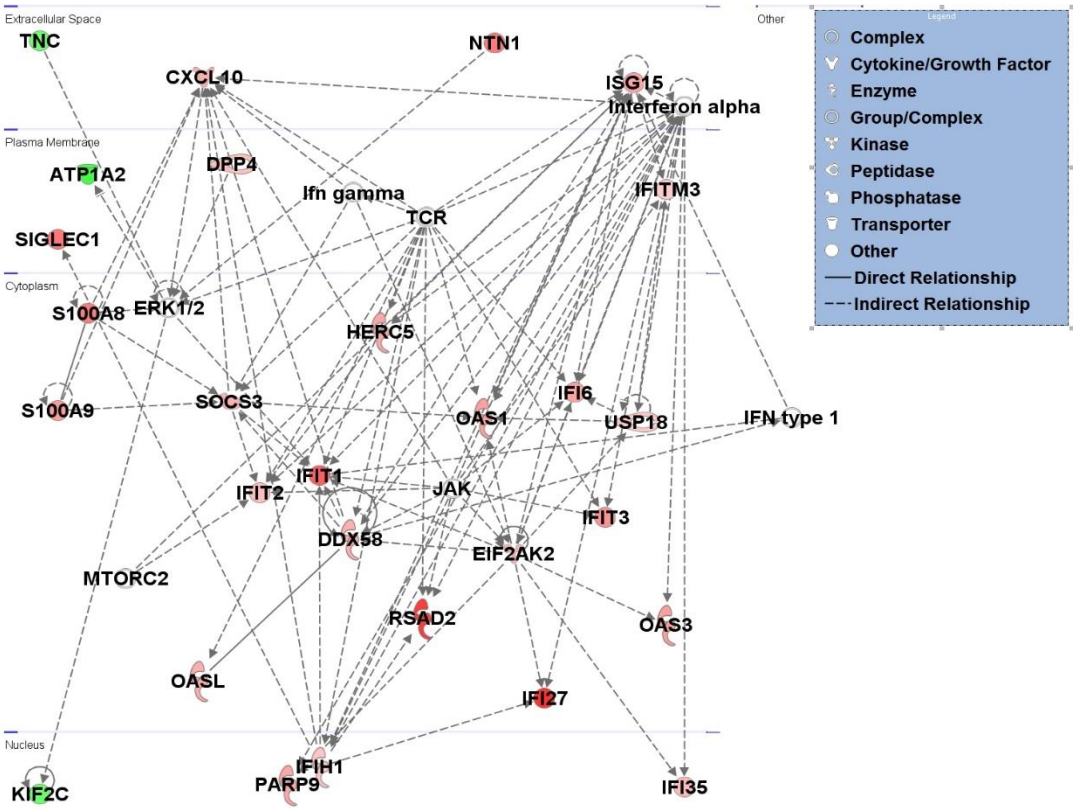

A.Score = 43

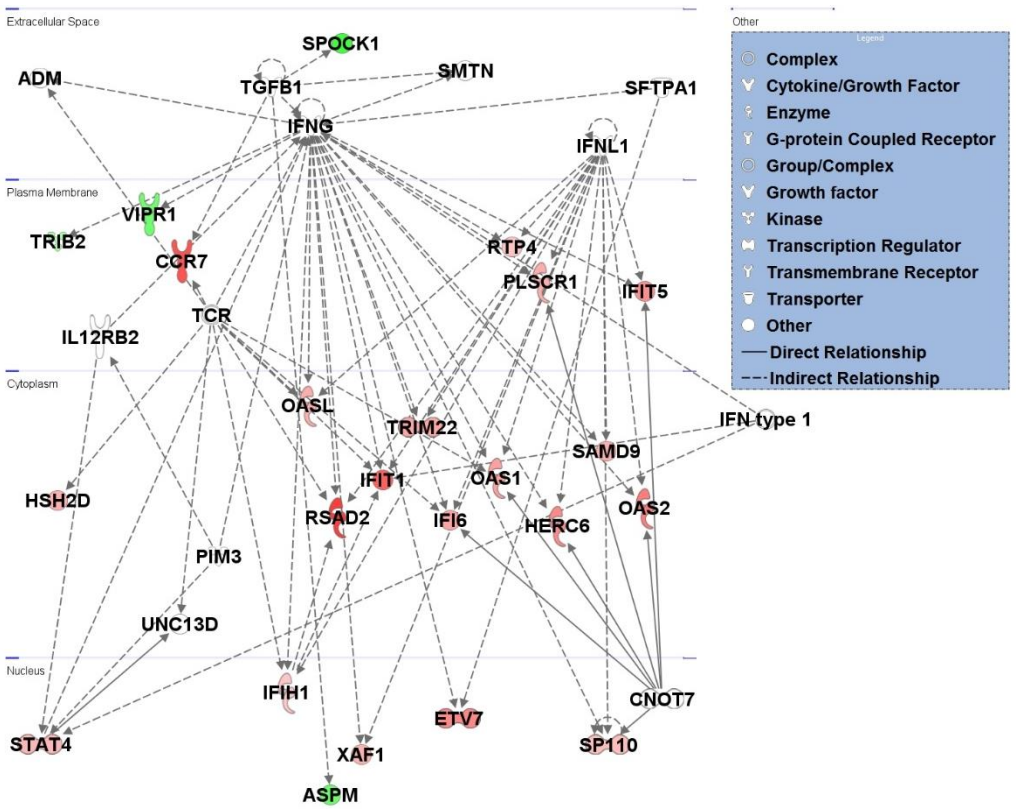

B. Score = 32

Figure 2.25: Diseases and functions network of Antimicrobial response, Inflammatory response and Infectious diseases induced by *Mtb* infection. A. Highest ranking of the top 5 at score 43. **B.** Fourth highest ranking of the top 5 at score 32. Upregulated molecules are represented in red and downregulated molecules in green. The level of expression varies with the intensity of the colour.

Overall, comparison of the expression analysis of all WT and Δ*rpfB* mutant induced SDEGs revealed that, 29 were specific to tuberculosis disease. The networks below show the SDEGs and its regulation state induced by infection with the WT and Δ*rpfB* mutant strain (Figure 2.26A) and the heat map shows a direct comparison of the regulation state with an expression log ratio range of -3.820 – 6.476 (Figure 2.26B). Both strains induced downregulation of only 2 of these SDEGs, *TYMS* and *TOP2A* (Figure 2.26A and 2.26B). *CSF2, MX1, IRF7, STAT1* and *IFI16* were exclusive to the Δ*rpfB* infected host and *IFI44L* and *IFI44* to the WT infected host (Figure 2.26A and 2.26B).

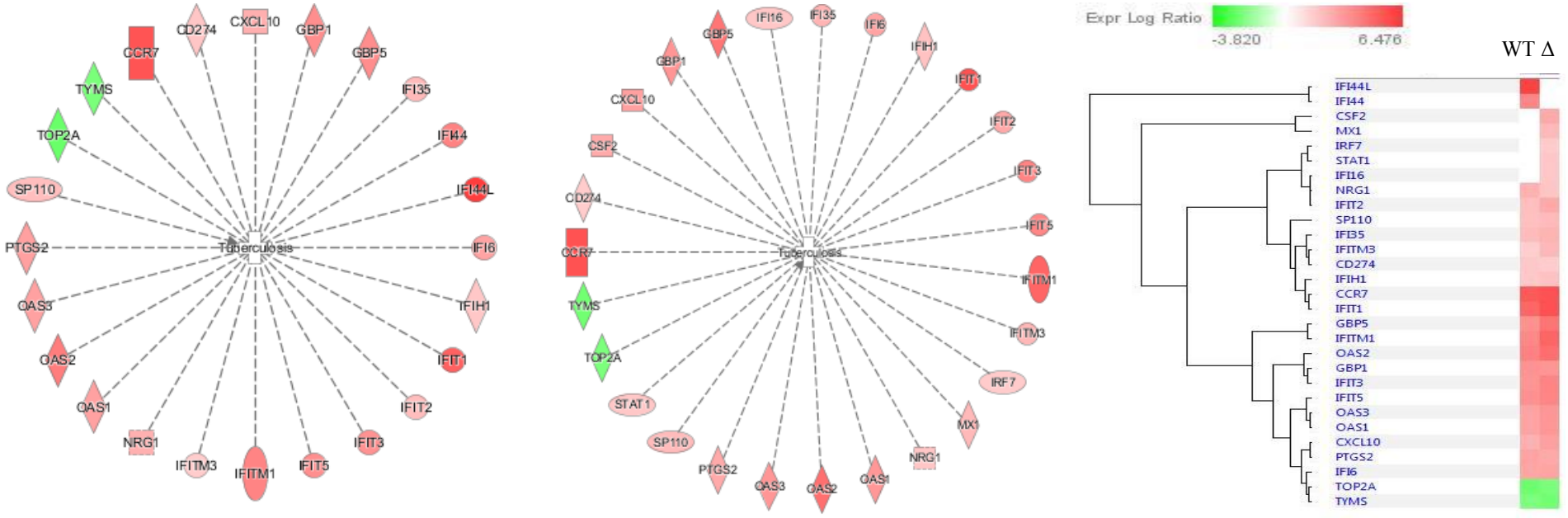

A. WT **B. Δ*rpfB*** **C. Heat map**

Figure 2.26: Network and gene expression heat map of WT and Δ*rpfB* mutant induced SDEGs associated with tuberculosis disease. A WT induced SDEGs associated with tuberculosis disease network. **B Δ*rpfB* mutant induced** SDEGs associated with tuberculosis disease network. The regulation state of SDEGs is displayed in green (downregulated) or red (upregulated) and the degree of expression is indicated by the intensity of the colour.

Validation of RNA sequencing

Cytokine genes *GM-CSF* and *IL1B* were used for validation of RNA sequencing results using qRT-PCR, normalized against *GAPDH*. Overall, qRT-PCR results showed the same gene expression trend for all genes in that the WT infection induced higher levels of expression, relative to the mutant infection (Figure 2.27A, 2.27C). The same trend can be seen in RNA sequencing expression results (Figure 2.27A, 2.27C) except for *CSF2* where the mutant induced slightly higher levels (2.68) of expression than the WT (2.59) (Figure 2.27C). (Raw expression values and statistical analysis shown in Appendix H).

Human *IL-1B* and *GM-CSF* multiplex magnetic bead-based assay

An exponential increase in the level of *GM-CSF* was induced by the uninfected, WT, mutant and complement strains from 24 hours to 72 hours post-infection. At each time point, the mutant displayed the highest level of *GM-CSF* production (Figure 2.27B). In contrast to the qPCR data at 72 hours post-infection, *GM-CSF* cytokine levels elicited in WT infected macrophages were lower than in mutant infected macrophages (Figure 2.27B). At 24, 48 and 72 hours post-infection, similar levels of *IL-1B* were induced by all 3 infections. At 24 hours, slightly lower levels of *IL-1B* were induced by the WT compared to the mutant and complemented strains (Figure 2.27D). At 48- and 72-hours post-infection, all 3 infections induced similar levels of *IL-1B* levels, with the exception of the slight decrease induced by the mutant and complemented compared to the WT strains at the former interval (Figure 2.27D).

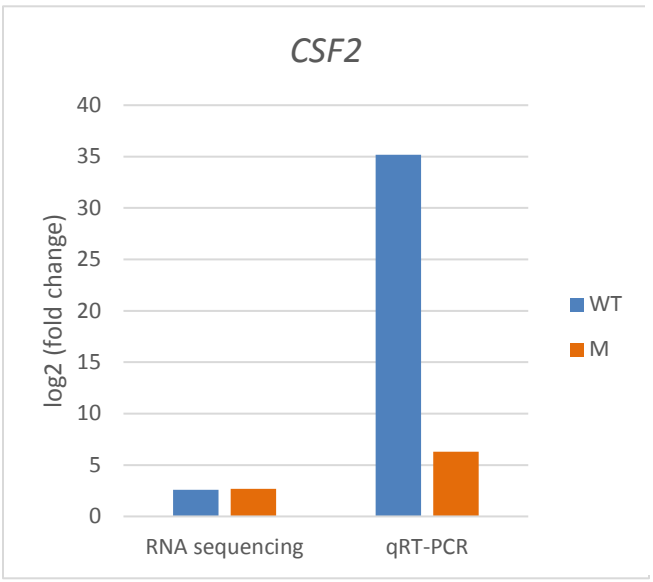

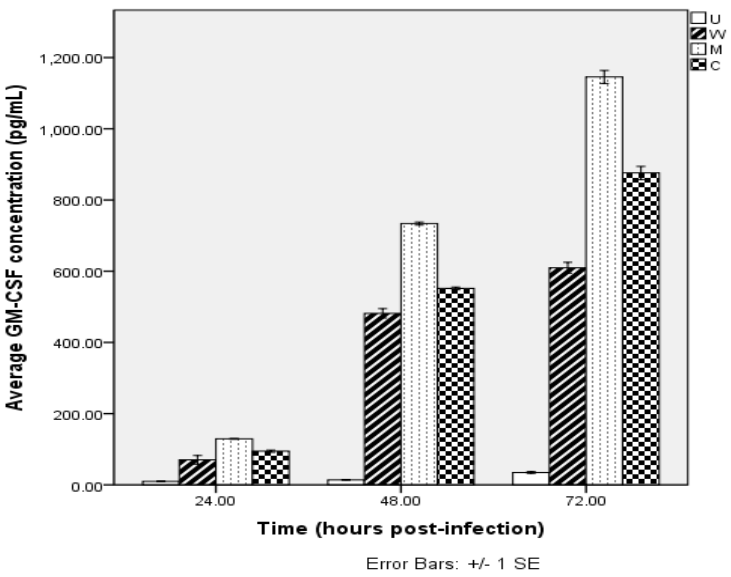

A. **B.**

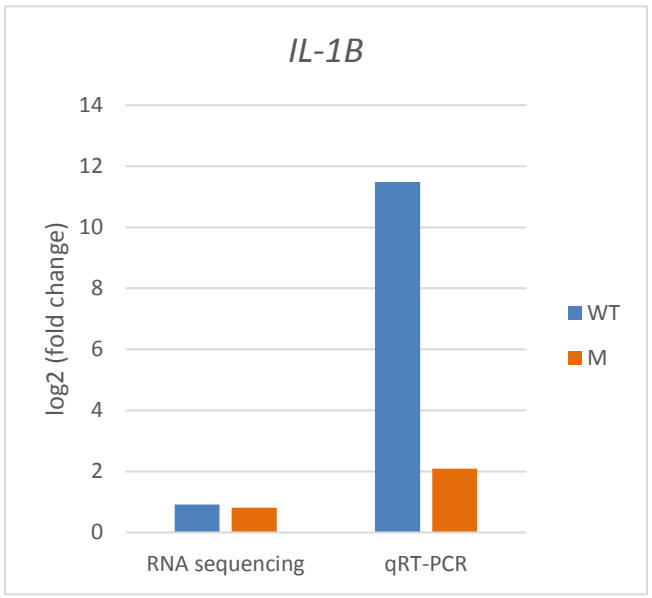

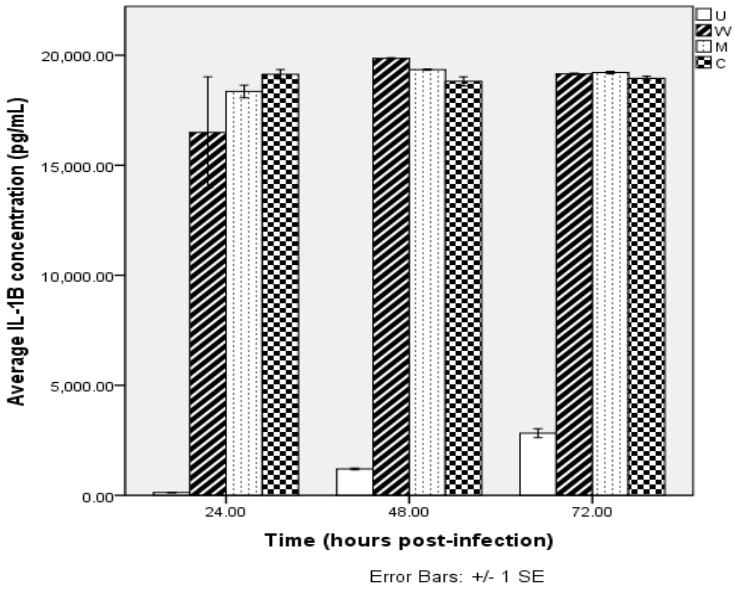

C. **D.**

Figure 2.27: Validation of RNA sequencing mRNA levels by quantitative real-time PCR and cytokine production. A and B. *CSF2*quantified by RNA sequencing and qPCR, and Multiplex, respectively. **C.** and **D.** *IL-1B* quantified by RNA sequencing and qPCR, and Multiplex, respectively.. RNA sequencing and qPCR expression levels were displayed as log fold changes and as pg/mL in the Multiplex assay.

Discussion

Previous studies have provided limited understanding of the role of *rpfB* on global transcriptome response against *Mtb*. In this study, global transcriptional host immune response to *Mtb* WT and Δ*rpfB* mutant infection was assessed using RNA sequencing. Recognition of *Mtb* by macrophages leads to initiation of the innate immune response and eventually adaptive immunity (Verrall et al., 2014; Brazzier and McShane., 2020). Eradication and restriction of *Mtb* replication requires a successful Th1 response (Kaushal et al., 2013). In this study, transcriptomic analysis of infected THP-1 macrophages showed *rpfB* contributes to the host protective immune response in macrophages and may play a role in DC maturation and anti-inflammatory modulation.

The *rpfB* gene induced differential expression and enrichment patterns in THP-1 macrophages at 72 hours P.I

Infection with the *Mtb* WT and Δ*rpfB* mutant strains induced a total of 629 SDEGs identified with a minimum fold change of log (1.5) of which 288 genes were differentially expressed between the infection models. A total of 289 SDEGs were exclusively enriched by the WT infection, of which more than 50 % were downregulated. In contrast, of the 52 SDEGs exclusively induced by the Δ*rpfB* mutant infection, more than 50 % were upregulated. In contrast, Rampersadh et al., 2019 (unpublished) showed, at 4 hours P.I, THP-1 macrophages elicit only 1 % of total genes analysed in downstream analysis, in response to the *Mtb* V9124 WT strain. The difference between the exclusively induced WT SDEGs between the studies may be attributed to the time points at which RNA sequencing was performed. Even though the WT infection in this study induced almost 6 times more significantly expressed SDEGs than the mutant, the mutant infection induced enrichment of more canonical pathways (64) than the WT infection (51), with highest significance based on –log (*p*-value). However, a greater number of networks and upstream regulators were induced in response to WT infection. In summary, this suggests *rpfB* is capable of inducing substantial differential expression of genes associated with differential enrichment of canonical pathways and networks. Enumeration of bacterial loads at 4 hours P.I between the WT and mutant infected macrophages showed no statistical difference, therefore the observations in differential expression and enrichment is attributed to deletion of the *rpfB* gene and not bacterial load.

Seven of the top 10 upregulated SDEGs were common to both infection models and were identified as Interferon stimulated genes (*IFI27, RSAD2, and IFIT1*) (Zhang et al., 2019), macrophage immune response genes (*TNIP3*) (Thuong et al., 2008) and others associated with cell proliferation and development of haematopoietic systems (*CRLF2*), DC migration and T cell priming (*CCR7*) and regulation of macrophage apoptosis (*PTGES*) (Behar et al., 2010). The SDEGs induce similar gene ontology biological processes;

Response to cytokine, Defence response, Cytokine-mediated signalling pathway, Inflammatory response, Innate immune response and Regulation of immune system process, as previously reported in other studies (Thuong et al., 2008; Behar et al., 2010; Zhang et al., 2019) through gene enrichment analysis. Despite the differential gene regulation induced by *Mtb* infection, both *rpfB* proficient and deficient strains were capable of inducing genes associated in the above-mentioned gene ontology functions, characteristic of a protective immune response.

RpfB does not play a significant role in the regulation of Agranulocyte Adhesion and Diapedesis, Role of Pattern Recognition Receptors in Recognition of Bacteria and Viruses, Haematopoiesis of Pluripotent and Multipotent Stem Cells, GM-CSF Signalling

Agranulocyte Adhesion and Diapedesis

The Agranulocyte (and granulocyte) adhesion and diapedesis pathway is involved in the cellular immune response (Dorr et al., 2015). In addition to granulocytes, agranulocyte adhesion and diapedesis are initiators of host defence against infections, essential for recruitment of agranulocytes to the site of infection or injury (Xing et al., 2017). The WT infection exclusively induced *MYH14*, *IL36B*, *CX3CL1* and higher levels of expression of *IL-1* and *IL-1R* than the mutant infection. *IL36B* is a pro-inflammatory cytokine that elicits a Th1 immune response which is crucial for control of intracellular *Mtb* (Ahsan et al., 2016). However, the mutant infection elicited higher levels of expression of the pathway (– log (12.4) compared to the WT infection (- log (8.73). Compared to the mutant infection, WT induced downregulation of *Mysosin*, while *MMP* was upregulated. The mutant infection induced downregulation of *PNAd* and *MMP* infection. The Agranulocyte adhesion and diapedesis pathway was more significantly enriched in the mutant infection with similar SDEGs than the WT. Absence of the *rpfB* gene made no difference in inducing this pathway, which has not been previously reported.

Role of Pattern Recognition Receptors in Recognition of Bacteria and Viruses

Macrophages express cell surface proteins, PRRs that interact with specific PAMPs on the *Mtb* cell surface. Recognition and binding culminates in phagocytosis, production of pro-inflammatory cytokines, recruitment of additional immune cells, and eventually the initiation of the adaptive immune response. These processes occur via a series of signalling transduction cascades, that results from the initial host-pathogen recognition and binding (Amarante-Mendes et al., 2018; Stamm et al., 2015). The Role of pattern recognition receptors in recognition of bacteria and viruses pathway was the highest enriched from all those induced by mutant infection, however only three SDEGs, (*IRF7, LIF* and *CSF2*) were associated with the

pathway. None of these SDEGs were up- or downregulated. *IRF7* is a pivotal regulator of type I *IFN*. When stimulated by pathogenic infections, *IRF7* triggers signalling cascades (Ning et al., 2011). Leukemia inhibitory factor (*LIF*) modulates activation of *IFN-γ* and *GM-CSF* plays a role in innate resistance against *Mtb* (Mishra et al., 2020). The pathway was induced below the acceptable log fold change of log (1.5), at 0.286 in the WT infection. Collectively, it seems *rpfB* does not affect the Role of PRRs in Recognition of Bacteria and Viruses pathway. To our knowledge there are no previous studies that report this.

Haematopoiesis of Pluripotent and Multipotent Stem Cells

Haematopoiesis refers to a process of continuous blood development (Ng and Alexander, 2017; Sawai et al., 2016). Throughout an individual's lifespan, haematopoietic stem cells (HSC) are responsible for the daily production and replenishment of all blood types from the bone marrow (Ng and Alexander, 2017; Sawai et al., 2016). These range from red blood cells that carry oxygen, megakaryotes that regulate clotting, to innate and adaptive immune cells that work against microbial infection (Ng and Alexander, 2017). The HSCs express surface molecules that mediates signalling to influence the immune system. Stimulatory infection and inflammation signals activate and induce HSCs surface receptors of TLRs, *IFN* and *TNF-α* (Zhang CC, 2012). Even though these pathways were ranked in the top 10 canonical pathways induced by the mutant infection, hardly any SDEGs were induced and differentially expressed within the pathways. In the hematopoiesis of pluripotent stem cells pathway, the mutant infection induced the upregulation of only two SDEGs (*LIF* and *CSF2*). In the hematopoiesis of multipotent stem cells, only *CSF2* was induced. No SDEGs were downregulated in either pathway. In the WT infection, the hematopoiesis of pluripotent stem cells pathway was expressed below the acceptable log fold change of log (1.5), at 0.369, whereas Rampersadh et al, 2019 showed at 4 hours P.I, WT infection did not enrich this pathway. In this study, the haematopoiesis of multipotent stem cells pathway was not enriched at all. Collectively, these findings indicate that *rpfB* may not be required for stimulation of the Haematopoiesis of pluripotent and multipotent stem cell pathway.

GM-CSF signalling

Apart from acting as a critical haematopoietic growth factor, *GM-CSF* also plays a role in homeostatic and inflammatory settings (Bryson et al., 2019), and its role in differentiation of monocytes to macrophages is critical for increased macrophages response against microbial pathogens (Mishra et al., 2020). Upon encountering pathogens, tissue damage or other danger signals, macrophages produce *GM-CSF* and directs differentiation of monocytes towards a pro-inflammatory response, which includes production of *IL12p40* and *TNF-α* (van der Does et al., 2010). Mutant infection induced upregulation of *GM-CSF* and *STAT1* in

the *GM-CSF* signalling pathway. This pathway had a zero fold change in the WT infection (Data not shown). These findings suggest that *rpfB* is not essential for *GM-CSF* signalling.

RpfB stimulates, but is not essential to, IFN signalling, Role of JAK family kinases in IL-6 type cytokine signalling and Activation of IRF by Cytosolic PRRs.

IFN signalling

Type I *IFN*s include multiple *IFN-α* and *IFN-β* cytokine subtypes that signal via the type I *IFNAR1* and *IFNAR2* receptors (Moreira-Teixeira et al., 2018; Stanley et al., 2007). It was initially thought that the role of type I *IFN*s were limited to promotion of bacterial virulence and exacerbation of growth (Mayer-Barber et al., 2014) through *STAT1* dependent signalling pathways (Mayer-Barber et al., 2011), but they are now well characterized in inhibition of cellular growth, control of apoptosis and modulation of the immune response (Stanley et al., 2007). Upon stimulation, type I *IFN*s activate a family of *ISG*s that either enhance or inhibit immune functions and therefore provides either a protective or detrimental effect in host immune responses in multiple species, including *Mtb* (Stanley et al., 2007; Moreira-Teixeira et al., 2018) (Figure 2.28). This pathway was expressed in both infection models but higher in the mutant infection at – log (9.98) compared to the WT infection at -log (5.44).The mutant infection induced 12 upregulated SDEGs of which *STAT1*, *MX1* and *IFIT3* were exclusive to this infection model. The WT infection induced 10 upregulated SDEGs of which only *GIP3* was exclusive to this model. No SDEGs were downregulated. In this study, the mutant infection upregulates *ISG*s (*IFITM1*, *IFI35*, *IFIH1*, *OAS1* and *IFIT3*). In both infection models, IFN signalling is enriched and induces upregulated expression of ISGs. We conclude that *rpfB* stimulates *ISG* production in a non-*STAT* dependent manner in the *IFN* pathway but is not essential to its stimulation as shown in the mutant infection.

Role of JAK family kinases in IL-6 type cytokine signalling

IL-6, produced by multiple cells that include monocytes and macrophages, fibroblasts, hepatocytes and endothelial cells, regulates cell activation, differentiation and proliferation (Lokau et al., 2019) (Figure 2.28). It has both pro- and anti-inflammatory properties and acts by activating the family of *JAK* kinases (*JAK1*, *JAK2* and *TYK2*) leading to activation of transcription factors of the STAT family (Lokau et al., 2019). All *IL-6* type cytokines (*IL-11*, *LIF*, *OSM*, *CNTF*, *CT1*) are potent activators of *STAT3* and to a lesser extent, *STAT1*. The primary inhibitor of *IL-6* signaling is *SOCS3* (Lokau et al., 2019). In this study, the mutant infection induced higher enrichment of the pathway (– log (3.28) than the WT infection (– log (1.56). The mutant infection induced and upregulated more SDEGs (*OSM, OSMRβ, STAT1, STAT3* and *STAT5*) compared to the WT infection (*OSM, OSMRβ, SOCS3*). In the mutant infection, *OSM* mediates

gene expression by upregulating *STAT1, STAT3* and *STAT5.* This study shows *rpfB* is not essential for the activation of transcription factors through *STAT* and that other molecules are present during *Mtb* infection that activate these pathways.

Activation of IRF by Cytosolic PRRs

DNA-dependent cytosolic PRRs recognize components such as DNA of internalized microbes or intracellular cytosolic pathogens (Rasmussen et al., 2009; van der Vaart et al., 2012). Cytosolic double stranded DNA (dsDNA) induces a type I *IFN* response, referred to as DNA-dependent activation of *IFN* regulatory factors (*IRF*s) (Rasmussen et al., 2009). The exit of *Mtb* from the phagosome into the cytosol exposes mycobacterial extracellular DNA to recognition by host cytosolic PRRs (Chai et al., 2020) (Figure 2.28)Previous studies (Mayer-Barber et al., 2011) reported unique blood transcriptional signatures in patients with active TB that were associated with type I IFN signalling through the activation of cytosolic surveillance pathway, which produces type I *IFN*s. Macrophages infected with *Mtb* can also deliver exosomes composed of mycobacterial RNA to recipient cells, implying that *Mtb* RNA can stimulate and trigger RNA-dependent cytosolic PRRs. A well conserved cytosolic PRR in mammalian cells, retinoid acid-inducible gene I (*RIG-I*), activates downstream immune pathways leading to type I *IFN* and pro-inflammatory cytokine production. Initially, its role was limited to recognition of viral RNAs but was thereafter shown to also participate in host immune response to bacterial pathogens, including *Mtb*, which was accounted for by increased RIG-I and melanoma differentiation-associated protein 5 (*MDA5*) expression in macrophages infected with *Mtb* (Chai et al., 2020). Mutant infected macrophages revealed a higher level of expression of the pathway (- log (3.48)) relative to WT infected macrophages (-log (1.65). Six upregulated SDEGs (*RIG-I, ISG15, MDA5* and *ISG54, IRF7* and *STAT4*) were induced by the mutant infection of which *IRF7* and *STAT4* were exclusive to this model, compared to 5 upregulated (*RIG-I, ISG15, MDA5, ISG54, IL-10*) by the WT infection, of which *IL-10* was exclusive. This pathway shows both infection models upregulate *RIG-1* and *MDA5* that play a role in cytosolic PRRs to stimulate virus replication and innate immunity through *ISG15* and *IL10, ISG15,* and *ISG45* respectively, in WT infected macrophages, and *IRF7* in mutant infected macrophages. In both models, ISGs that contribute to virus replication and innate immunity are highly upregulated. Our findings suggest *rpfB* stimulates, but is not essential to, activation of *IRF*s by cytosolic PRRs.

RpfB enhances IL-10 signalling and DC maturation

IL-10 signalling

Infection with *Mtb* induces rapid production of *TNF-α* and *IL-10* from monocytes and macrophages (O'Leary et al., 2011). *IL-10,* representative of Th2 cytokines (Jee et al., 2017), acts as a modulator of the

inflammatory immune response by inhibiting production of pro-inflammatory cytokines such as *TNF-α* and the Th1 polarizing *IL-12* cytokine from macrophages and DCs (Jee et al., 2017; Redford et al., 2011) (Figure 2.28)Decreased production of pro-inflammatory cytokines leads to prevention of reactive oxygen and nitrogen intermediates that results in inhibition of phagocytosis and microbial killing (O' Leary et al., 2011; Redford et al., 2011), thereby promoting survival of *Mtb* within the host (Jee et al., 2017). When bound to its respective receptors, *IL-10* transduces signals through the JAK-STAT pathway via *JAK1* and *TYK2* that leads to phosphorylation and activation of *STAT1* and *STAT3* (Redford et al., 2011). In this study, the WT infection induced 9 SDEGs (*IL33, SOCS3, IL36G, IL36RN* and *IL1R1, SOCS3, IL10, FCGR2B* and *IL36B*) of which *IL-10* and *HMOX1* were exclusive to this, compared to 5 SDEGs (*IL33, SOCS3, IL36G, IL36RN* and *IL1R1*) that were induced by the mutant infection. *HMOX1* is induced in response to an array of cellular stress, including hypoxia, starvation, *TLR* and cytokine mediated cellular activation (O' Leary et al., 2011; Jee et al., 2017), and infections. (Mihret, 2012). Only one SDEG was downregulated, *FCGRII*, by the WT infection. This pathway was more enriched by WT infection suggesting *rpfB* may play a role in *IL-10* signalling, that modulates inflammation.

DC maturation

DCs are key mediators in the switch between innate to adaptive immunity and the most important APCs for naïve T cell priming, and primary source of *IL-12* (Bansal et al., 2010; Korb et al., 2016; Mihret, 2012). They express a diverse range of cell surface markers, important for recognition and internalization of antigens, and cytokine receptors, important for an enhanced inflammatory response (Bansal et al., 2010), both of which are essential in initiating the adaptive immune response and secretion of Th1 polarizing cytokines (Sia et al., 2015) (Figure 2.28). Although enriched by both infection models, DC maturation showed higher enrichment in the mutant infection (–log (2.66) relative to the WT infection (–log (1.59), however the WT induced regulation of 12 SDEGs and 9 were induced by the mutant. The WT infection induced downregulation of 4 SDEGs (*CD32, CD1, FcγR* and *FcγRII*), whereas only 1 SDEG (*CD1*) was downregulated in the mutant infection. These findings show *rpfB* may play a dual role by downregulating DC maturation, antigen uptake and DC activation through *CD32*, *CD1*, *FcγR* and *FcγRII* while also upregulating *IL-1, IL-10 IL-23p19* and *CCR7* involved in DC maturation, migration and activation.

Other pathways enriched by *rpfB*

Acute phase response signalling

In response to *Mtb*, an inflammatory reaction is induced that results in the production of pro-inflammatory cytokines. These cytokines stimulate a potent systemic acute phase response characterized by fever and the production of acute phase proteins mainly of hepatic origin (Peresi E, 2008; Martins et al., 2014; Abdelrhman et al., 2018; Kathamuthu et al., 2020) (Figure 2.28). In this study, 5 SDEGs were commonly upregulated in both infection models (*IL-1*, *IL-1R*, *OSM*, *OSMR*, *SOCS3*, *SOCS*, *SOD2*), but the WT induced two more upregulated SDEGs, *HMOX1* and *SERPING1*, than the mutant infection. The WT infection also induced downregulation of two more SDEGs, *VWF* and *SERPINE1*, than the mutant. *HMOX1* is induced in response to an array of cellular stress (McMahon et al., 2017), including hypoxia, starvation, *TLR* a cytokine mediated cellular activation, and infections (McMahon et al., 2017, Batra et al., 2020). Rockwood N et al, 2017 reported *HMOX-1* is induced by murine and human macrophages in response to *Mtb*, and that *HMOX-1* deficient mice show increased susceptibility to mycobacterial infection. *SERPING1* is a negative regulator of complement activation and is transcriptionally regulated by *IFN-y* activated *STAT1* (Hausberg et al., 2021). Its expression was identified in granulomas of WT infected C57BL/6 mice, and upregulated in *Mtb* infected lungs, but revealed no difference in bacterial burden between *SERPING1*-proficient and deficient infected mice. However, increased inflammation of *SERPING1* deficient mice was observed (Mushtaq A, 2020). This reveals that the WT infection enhanced expression of SDEGs that are induced in response to cellular stress and inflammation, which correlates with other studies performed by members of this research group who showed increased enrichment of the acute phase response signalling pathway in response to *Mtb* infection. The pathway was more enriched in the WT infection (- log 3.61) than the mutant infection (- log 2.82). These findings suggest that *rpfB* may influence the acute phase response which ultimately facilitates initial control of *Mtb*.

Phagosome formation

Following macrophage phagocytosis, *Mtb* becomes entrapped within phagosomes that undergo sequential fusion with lysosomes and acquires microbicidal and degradation properties through maturation (Queval et al., 2017; Zhaiet et al., 2019). Phagosome maturation is regulated via a network of *Rab GTPases* proteins that facilitate phagosome maturation from its early stages to late stages. These proteins are recruited through maturation and are responsible for the biological changes observed throughout maturation that lead to final clearance of *Mtb* (Zhaiet al., 2019) (Figure 2.28). Two transcripts were commonly upregulated by both infection models, *complement receptor* and *Rho-GTPase* but the WT additionally induced upregulation of *MSR*. The WT infection also induced downregulation of 2 more SDEGs, *FcRS* and *TRL*, than the mutant.

Complement receptors and complement mediated opsonisation are essential in facilitating entry of *Mtb* into macrophages. These receptors, among others such as mannose receptor, surfactant protein A, scavenger receptors, Fcy receptors are implicated in *Mtb* phagocytosis and internalization (Liu et al., 2017; Syedbasha and Egli, 2017). The *Rho GTPase* family controls F-actin re-organization that is required for all types of phagocytosis, regardless of the phagocytic cell. Previous reports have demonstrated its role in acidification of phagosomes in macrophages by inhibiting Rho signalling that resulted in decreased acidification rates (de Martino et al., 2019). *MSR* plays a role in binding varying forms of lipids in Gram negative and gram positive bacteria. The class A scavenger receptors were shown to be important for the attachment of *Mtb* Erdman on macrophages (Joel D. Ernst, 1998). Beyond opsonisation, antibodies also mediate antimicrobial activity by signalling through Fc receptors (Mayer-Barber et al., 2014). In this study, the WT infection shows upregulation of more SDEGs than the mutant, and SDEGs exclusive to the WT, associated with binding and internalisation of *Mtb*, These findings suggest that *rpfB* may enhance the process of phagocytosis, which is a critical even in intracellular killing of *Mtb*.

LXR/RXR activation

During *Mtb* persistence, host cholesterol serves as one of the primary sources of carbon, therefore interrogating modulators of cholesterol metabolism may provide a strategy to control *Mtb* (Figure 2.28) *LXR*s have been identified as key regulators of macrophage cholesterol, fatty acid and glucose homeostasis, and contributes to resistance against TB in mice and humans by potentiating *LPS* induced responses (Korf et al, 2009; Ahsan et al., 2018). Hannelie Korf et al, 2009 showed *LXR* contributes to protective immunity against intracellular *Mtb* via aerogenic infection. This study showed the LXR/RXR pathway was the most enriched by the WT infection, with downregulation of *HADH*, *HDL*, *LDL*, *LXR*, *SOD1* and *IDOL*. Only 2 SDEGs, *SR-A* and *IL-1* were upregulated. Cholesterol can be transported through high and low density lipoproteins, which is *HDL* and *LDL* and its uptake is facilitated by molecules such as inducible degrader of the *LDLR* (*IDOL*), as well as SR-A that also binds lipopolysaccharides (Jean-Marc Zingg, Roberta Ricciarelli, and Angelo Azzi 2000, Yuan Zhang, Jessica F. Chan, and Carolyn L. Cummins 2009; Bo Wang and Peter Tontonoz, 2018). In this study, the WT infection downregulated SDEGs involved in processes of cholesterol uptake and transport. This suggests *rpfB* may downregulate host lipid metabolism thereby limiting cholesterol as a source of carbon for *Mtb*.

CAMP-mediated signalling, G*α*i signalling and GADD45 signalling

Macrophages produce intracellular *cAMP*, a key second messenger in multiple signal transduction pathways (Zhou, 2016), through G-protein coupled receptors (*GPCR*s) activated adenylate cyclases (*AC*s) (Agarwal et al., 2009). An increase in *cAMP* stimulates protein kinase A production which ultimately results in transcriptional and cytokine expression changes. *cAMP* regulates multiple cellular functions including

growth, differentiation, transcription and protein expression (Yan et al., 2016) *Mtb* uses multiple second messenger molecules, including *cAMP*, for regulation of its own physiology under stress and to hinder host cell signaling (Yan et al., 2016) (Figure 2.28). In this study, pathways with *cAMP*, *Gαi* and *GADD45* were enriched by the WT infection. cAMP-mediated signaling and Gαi signalling were expressed below the acceptable fold change of –log (1.5), at –log (0.4537) and –log (0.658), respectively. GADD45 signalling had no fold change in mutant infections (Data not shown). In the former pathways, *Gi-coupled receptor*, *Rap1Gap* and *AC* are commonly downregulated, and in cAMP-mediated signalling, *PDE* and *ICER* were slightly upregulated. *GPCR*s as mentioned above is important in inducing signal transduction via *cAMP*. Binding of *GPCR* activates *AC*s that concert ATP into cAMP (Agarwal et al., 2009). *PDE*s are the only enzymes that function in hydrolysis of *cAMP* (Fertig and George, 2018), and *Rap1Gap* plays a pivotal role in cell biology by coupling signals generated in intracellular effectors. In this study, WT infection induced downregulation of *cyclin D* and *cyclin B1*. GADD45 signalling is induced in response to physiological and environmental pressure that results in cell cycle arrest, cell survival, DNA repair and apoptosis. *Cyclin B1* regulates the transition of cells from G2 to the M phase, leading to G2/M checkpoint (Hoffman and Lieberman, 2008). In the presence of DNA damage, cell cycle arrests at the above checkpoints (Zhan Q, 2002). Collectively, these findings show the THP-1 macrophages elicit downregulation of SDEGs associated with second messenger signaling and cellular processes in response to WT infection, and that *rpfB* may play a role in increasing host DNA damage.

CAMP-mediated signalling

Gαi signalling

GADD45 signalling

IFN signalling

Role of JAK family kinases in IL-6 type cytokine signalling

Activation of IRF by Cytosolic PRRs

IL-10 signalling

DC maturation

Acute phase response signalling

Phagosome formation

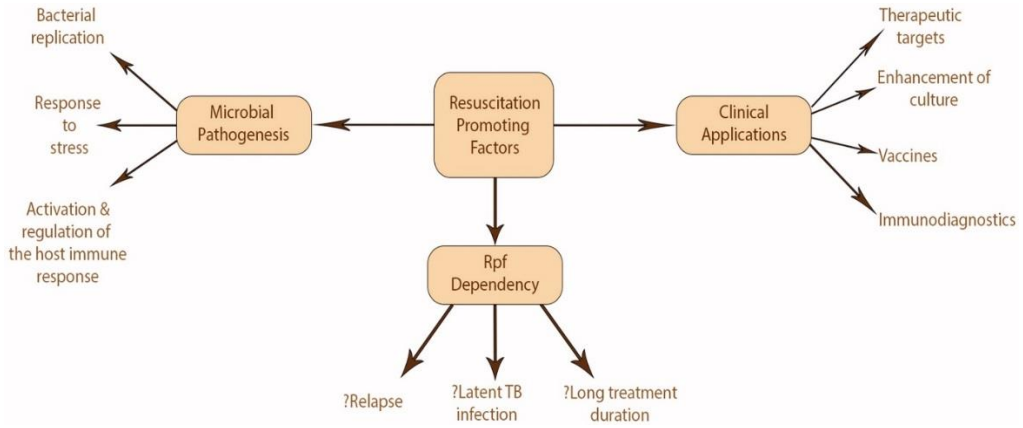

RpfB protein as a recombinant, in addition to LTBI proteins, against LTBI

IL-10 signalling

DC maturation

RpfB protein recombinant against *Mtb* infection

Figure 2.28: Association of pathways induced in this study with the role of rpfs/*rpfB* in Microbial pathogenesis, Rpf redundancy and clinical applications.

RpfB induces upstream regulators

The top 5 upstream regulators induced by WT and Δ*rpfB* mutant infection were all cytokines, *IFNL1*, *IFNA2*, *PRL*, *IFN-γ*, TNF, *IFN-α,* with high activated prediction scores. Other upstream regulators induced by both infection models were *CFS-2* and *IL-1B*.

Type II *IFN* include *IFNA2, IFN-α* and *IFNL1* is a type *III IFN*. *IFNL1* is expressed in a wide array of cell types by PRRs including *TLR*s, but is primarily produced in type 2 myeloid DC cells in response to bacterial components, including *Mtb* lipopolysaccharide (Syedbasha and Egli, 2017). *IFNA2* and *IFN-α* are essential in the cytosolic cascade of signal transduction toward the activation of ISGs (Gonzalez et al., 2016). In this study, *IFNA2*, *IFN-α, IFNL1* and *PRL* were highly expressed in the mutant strain compared to the WT strain, however, their respective upstream regulator networks show the WT network regulated a greater number of genes. The genes upregulated by these upstream regulators were mainly *ISG*s (*OAS2, IFIHI1, OAS1, IFI44L, IFI6, IFITM3, IFITM1, IFIT1, IFI35, IFIT3, OAS3, IFIT2*, and *IFI44*), which can be seen as upregulated in the WT infection pathways displayed above. These ISGs were also the same ISGs associated with the WT network in connection with tuberculosis disease. Interestingly, in the mutant infection, the *IFNA2*, *IFN-α, IFNL1* and *PRL* cytokines did not regulate the same SDEGs, but rather *MX1, IRF7, DDX60, STAT1, ISG20* and *MX2*, which were exclusive to the mutant strain, and its network associated with tuberculosis disease. Based on these finding and the role of these genes displayed above, *rpfB* may play a role in protective immunity by enhancing expression of ISGs. In addition, the lack of expression of *MX1, IRF7, DDX60, ISG20* and *MX2* shows its production is not essential in *Mtb* infection.

GM-CSF (also called *CSF2*) is a cytokine produced during inflammation by multiple cells, including macrophages, that exerts a wide range of effects on myeloid cells such as survival, activation, differentiation, and mobilization (Lotfi et al., 2019). In this study, *GM-CSF* was exponentially expressed at 24-, 48- and 72 hours P.I in each infected model, but the mutant infection expressed the highest levels at all three time points. However, qRT-PCR analysis showed a higher level of expression at 72 hours P.I in the WT, and similar levels between strains in RNA sequencing, possibly due to technical error. *IL-1β* is a potent regulator of inflammation and immune response and is required for host resistance (Cooper et al., 2011). Overall, it has been implicated in direct killing of *Mtb*, recruitment of anti-microbial effector cells, and macrophage response against Mtb (Romero-Adrian, 2015). This study showed enhanced *IL-1β* expression in WT infected macrophages at 24 h and 48 h P.I, compared to mutant infected macrophages. RNA sequencing and qRT-PCR also showed enhanced expression enhanced expression at 72 h P.I, but cytokine analysis showed similar levels of expression. RNA sequencing and qRT-PCR expression values point to a possible role of *rpfB* in *GM-CSF* and *IL-1β* but this requires further validation.

Limitations

One of the limitations of this study was the use of a low MOI. This may have attributed to the low number of global transcripts induced at –log (1.5) and above, and cytokine expression levels. Prior to performing main experiments, trial experiments were conducted to determine the optimal MOI for RNA sequencing experiments using various MOIs. An MOI of 1 showed optimal macrophage cell recovery required for RNA sequencing analysis and was therefore selected. Using a higher MOI may be promising in these strains inducing a more potent immune response. The differences observed between the expression levels of cytokines between RNA sequencing, qPCR and cytokine quantification may be due to technical error as two different experiments were performed for the RNA sequencing and qPCR, and cytokine analysis, and the cytokine analysis was done in duplicate instead of triplicate due to the small volume of samples left after performing trial experiments. Including more replicates may have allowed for the removal of outliers. Sequencing did not include the complemented strain. To ensure accuracy, reproducibility and consistency, the samples were sequenced in duplicate for each strain, ie a total of six, which was very expensive. Therefore, the complemented strain was not sequenced. Inclusion of the complemented strain would have further improved our understanding and validated the findings of the role of *rpfB* in host immune response. Cytokine analysis was performed on two cytokines. Induction of the immune response induces an array of pro- and anti-inflammatories. Including additional cytokines would provide a global overview of how *rpfB* influences cytokine production during *Mtb* infection.

Conclusion

Global transcriptomic analysis revealed *rpfB* induces differential expression of genes associated with important type I associated immune response canonical pathways, confirmed by qRT-PCR. Despite these the inconsistent observations noted in cytokine analysis, there are no studies that show the role of *rpfB* in THP-1 macrophage immune response against *Mtb* using transcriptomic studies. This study provides basic evidence, based on transcriptomic studies only, that *rpfB* enhances protective immunity, and may play a role in DC maturation, and anti-inflammatory modulation.

Future work

Based on our findings that *rpfB* contributes to a protective immune response in macrophages against *Mtb*, including all 5 *rpf* gene deficient strains in the same study design, including the complemented strain in all types of analysis,may further validate the potential of Rpf inclusion in recombinant vaccines. In addition, since *rpfB* may play a role in DC maturation and IL-10 signalling, studies using RpfB proteins to stimulate dendritic cells and IL-10 may elucidate the mechanism through which it plays a role. If RpfB plays a direct

role in DC maturation and IL-10 signalling, employing anti-Rpf agents in the same study design may be useful in identifying its significance or functional redundancy of its role in these pathways.

Conflicts of interest

The authors declare no conflicts of interest.

Author contributions

Experimental work: DM

Data Analysis: DM

Presentation of results: DM, MP, NEM

Drafting of Manuscript: DM, NEM, MP

Formulation of the study design: DM, CCN, MP

Funding: MP

Review of the Manuscript: NEM, MP

Acknowledgments

The authors would like to acknowledge the National Research foundation of South Africa (MP-CPRR 105841) and the College of Health Science for financial support. We also thank Dr. Ravesh Singh for assistance with the qRT-PCR analysis.

References

Agarwal, N., Lamichhane, G., Gupta, R., Nolan, S., and Bishai, W.R. (2009). Cyclic AMP intoxication of macrophages by a *Mycobacterium tuberculosis* adenylate cyclase. Nature *460*, 98-102.

Agrawal, N., Streata, I., Pei, G., Weiner, J., Kotze, L., Bandermann, S., Lozza, L., Walzl, G., du Plessis, N., Ioana, M., *et al.* (2018). Human Monocytic Suppressive Cells Promote Replication of *Mycobacterium tuberculosis* and Alter Stability of in vitro Generated Granulomas. Front Immunol *9*, 2417.

Ahmad, S. (2011). Pathogenesis, immunology, and diagnosis of latent *Mycobacterium tuberculosis* infection. Clin Dev Immunol *2011*, 814943.

Ahsan, F., Moura-Alves, P., Guhlich-Bornhof, U., Klemm, M., Kaufmann, S.H., and Maertzdorf, J. (2016). Role of Interleukin 36gamma in Host Defense Against Tuberculosis. J Infect Dis *214*, 464-474.

Almeida Da Silva, P.E., and Palomino, J.C. (2011). Molecular basis and mechanisms of drug resistance in Mycobacterium tuberculosis: classical and new drugs. J Antimicrob Chemother *66*, 1417-1430.

Amarante-Mendes, G.P., Adjemian, S., Branco, L.M., Zanetti, L.C., Weinlich, R., and Bortoluci, K.R. (2018). Pattern Recognition Receptors and the Host Cell Death Molecular Machinery. Front Immunol *9*, 2379.

Ansari, A.W., Kamarulzaman, A., and Schmidt, R.E. (2013). Multifaceted Impact of Host C-C Chemokine CCL2 in the Immuno-Pathogenesis of HIV-1/*M. tuberculosis* Co-Infection. Front Immunol *4*, 312.

Averbakh, M.M., and Ergeshow, A. (2018). Interaction between *Mycobacterium tuberculosis* and Human Host: Role of Cytokines in Pathogenesis and Treatment Monitoring.

Bansal, K., Elluru, S.R., Narayana, Y., Chaturvedi, R., Patil, S.A., Kaveri, S.V., Bayry, J., and Balaji, K.N. (2010). PE_PGRS antigens of *Mycobacterium tuberculosis* induce maturation and activation of human dendritic cells. J Immunol *184*, 3495-3504.

Bass, J.J., Wilkinson, D.J., Rankin, D., Phillips, B.E., Szewczyk, N.J., Smith, K., and Atherton, P.J. (2017). An overview of technical considerations for Western blotting applications to physiological research. Scand J Med Sci Sports *27*, 4-25.

Behar, S.M., Divangahi, M., and Remold, H.G. (2010). Evasion of innate immunity by Mycobacterium tuberculosis: is death an exit strategy? Nat Rev Microbiol *8*, 668-674.

Biketov, S., Potapov, V., Ganina, E., Downing, K., Kana, B.D., and Kaprelyants, A. (2007). The role of resuscitation promoting factors in pathogenesis and reactivation of *Mycobacterium tuberculosis* during intra-peritoneal infection in mice. BMC Infect Dis *7*, 146.

Brazier, B., and McShane, H. (2020). Towards new TB vaccines. Semin Immunopathol *42*, 315-331.

Bryson, B.D., Rosebrock, T.R., Tafesse, F.G., Itoh, C.Y., Nibasumba, A., Babunovic, G.H., Corleis, B., Martin, C., Keegan, C., Andrade, P., *et al.* (2019). Heterogeneous *GM-CSF* signaling in macrophages is associated with control of *Mycobacterium tuberculosis*. Nat Commun *10*, 2329.

Cambau, E., and Drancourt, M. (2014). Steps towards the discovery of *Mycobacterium tuberculosis* by Robert Koch, 1882. Clin Microbiol Infect *20*, 196-201.

Caminero, J.A., Cayla, J.A., García-García, J.-M., García-Pérez, F.J., Palacios, J.J., and Ruiz-Manzano, J. (2017). Diagnosis and Treatment of Drug-Resistant Tuberculosis. Archivos de Bronconeumología (English Edition) *53*, 501-509.

Chai, Q., Wang, L., Liu, C.H., and Ge, B. (2020). New insights into the evasion of host innate immunity by *Mycobacterium tuberculosis*. Cell Mol Immunol *17*, 901-913.

Chao, W.C., Yen, C.L., Hsieh, C.Y., Huang, Y.F., Tseng, Y.L., Nigrovic, P.A., and Shieh, C.C. (2017). Mycobacterial infection induces higher interleukin-1beta and dysregulated lung inflammation in mice with defective leukocyte NADPH oxidase. PLoS One *12*, e0189453.

Chaves, A.S., Rodrigues, M.F., Mattos, A.M., and Teixeira, H.C. (2015). Challenging *Mycobacterium tuberculosis* dormancy mechanisms and their immunodiagnostic potential. Braz J Infect Dis *19*, 636-642.

Chihota, V.N., Niehaus, A., Streicher, E.M., Wang, X., Sampson, S.L., Mason, P., Kallenius, G., Mfinanga, S.G., Pillay, M., Klopper, M., *et al.* (2018). Geospatial distribution of *Mycobacterium tuberculosis* genotypes in Africa. PLoS One *13*, e0200632.

Choi, H.G., Kim, W.S., Back, Y.W., Kim, H., Kwon, K.W., Kim, J.S., Shin, S.J., and Kim, H.J. (2015). *Mycobacterium tuberculosis* RpfE promotes simultaneous Th1- and Th17-type T-cell immunity via TLR4-dependent maturation of dendritic cells. Eur J Immunol *45*, 1957-1971.

Churchyard, G., Kim, P., Shah, N.S., Rustomjee, R., Gandhi, N., Mathema, B., Dowdy, D., Kasmar, A., and Cardenas, V. (2017). What We Know About Tuberculosis Transmission: An Overview. J Infect Dis *216*, S629-S635.

Cohen, K.A., Abeel, T., Manson McGuire, A., Desjardins, C.A., Munsamy, V., Shea, T.P., Walker, B.J., Bantubani, N., Almeida, D.V., Alvarado, L., *et al.* (2015). Evolution of Extensively Drug-Resistant Tuberculosis over Four Decades: Whole Genome Sequencing and Dating Analysis of *Mycobacterium tuberculosis* Isolates from KwaZulu-Natal. PLoS Med *12*, e1001880.

Commandeur, S., van Meijgaarden, K.E., Lin, M.Y., Franken, K.L., Friggen, A.H., Drijfhout, J.W., Oftung, F., Korsvold, G.E., Geluk, A., and Ottenhoff, T.H. (2011). Identification of human T-cell responses to *Mycobacterium tuberculosis* resuscitation-promoting factors in long-term latently infected individuals. Clin Vaccine Immunol *18*, 676-683.

Cooper, A.M., Mayer-Barber, K.D., and Sher, A. (2011). Role of innate cytokines in mycobacterial infection. Mucosal Immunol *4*, 252-260.

Costa, C., Gimenez-Capitan, A., Karachaliou, N., and Rosell, R. (2013). Comprehensive molecular screening: from the RT-PCR to the RNA-seq. Transl Lung Cancer Res *2*, 87-91.

D'Ambrosio, L., Centis, R., Sotgiu, G., Pontali, E., Spanevello, A., and Migliori, G.B. (2015). New anti-tuberculosis drugs and regimens: 2015 update. ERJ Open Res *1*.

Davenne, T., and McShane, H. (2016). Why don't we have an effective tuberculosis vaccine yet? Expert Rev Vaccines *15*, 1009-1013.

de Martino, M., Lodi, L., Galli, L., and Chiappini, E. (2019). Immune Response to *Mycobacterium tuberculosis*: A Narrative Review. Front Pediatr *7*, 350.

Demina, G.R., Makarov, V.A., Nikitushkin, V.D., Ryabova, O.B., Vostroknutova, G.N., Salina, E.G., Shleeva, M.O., Goncharenko, A.V., and Kaprelyants, A.S. (2009). Finding of the low molecular weight inhibitors of resuscitation promoting factor enzymatic and resuscitation activity. PLoS One *4*, e8174.

Domingo-Gonzalez, R., Prince, O., Cooper, A., and Khader, S.A. (2016). Cytokines and Chemokines in *Mycobacterium tuberculosis* Infection. Microbiol Spectr *4*.

Dowall, S.D., Graham, V.A., Fletcher, T., and Hewson, R. (2019). Use and reliability of multiplex bead-based assays (Luminex) at Containment Level 4. Methods *158*, 17-21.

Downing, K.J., Mischenko, V.V., Shleeva, M.O., Young, D.I., Young, M., Kaprelyants, A.S., Apt, A.S., and Mizrahi, V. (2005). Mutants of *Mycobacterium tuberculosis* lacking three of the five rpf-like genes are defective for growth *in vivo* and for resuscitation *in vitro*. Infect Immun *73*, 3038-3043.

Ehlers, S., and Schaible, U.E. (2012). The granuloma in tuberculosis: dynamics of a host-pathogen collusion. Front Immunol *3*, 411.

Espitia, C., Rodrguez, E., Ramn-Luing, L., Echeverra-Valencia, G., and J, A. (2012). Host–Pathogen Interactions in Tuberculosis.

Falzon, D., Gandhi, N., Migliori, G.B., Sotgiu, G., Cox, H.S., Holtz, T.H., Hollm-Delgado, M.G., Keshavjee, S., DeRiemer, K., Centis, R., *et al.* (2013). Resistance to fluoroquinolones and second-line injectable drugs: impact on multidrug-resistant TB outcomes. Eur Respir J *42*, 156-168.

Fang, Z., and Cui, X. (2011). Design and validation issues in RNA-seq experiments. Brief Bioinform *12*, 280-287.

Gandhi, N.R., Brust, J.C., Moodley, P., Weissman, D., Heo, M., Ning, Y., Moll, A.P., Friedland, G.H., Sturm, A.W., and Shah, N.S. (2014). Minimal diversity of drug-resistant *Mycobacterium tuberculosis* strains, South Africa. Emerg Infect Dis *20*, 426-433.

Gandhi, N.R., Moll, A., Sturm, A.W., Pawinski, R., Govender, T., Lalloo, U., Zeller, K., Andrews, J., and Friedland, G. (2006). Extensively drug-resistant tuberculosis as a cause of death in patients co-infected with tuberculosis and HIV in a rural area of South Africa. The Lancet *368*, 1575-1580.

Gengenbacher, M., and Kaufmann, S.H. (2012). *Mycobacterium tuberculosis*: success through dormancy. FEMS Microbiol Rev *36*, 514-532.

Ghazaei, C. (2018). *Mycobacterium tuberculosis* and lipids: Insights into molecular mechanisms from persistence to virulence. J Res Med Sci *23*, 63.

Gillespie, S.H. (2002). Evolution of drug resistance in *Mycobacterium tuberculosis*: clinical and molecular perspective. Antimicrob Agents Chemother *46*, 267-274.

Gupta, R.K., and Srivastava, R. (2012). Resuscitation promoting factors: a family of microbial proteins in survival and resuscitation of dormant mycobacteria. Indian J Microbiol *52*, 114-121.

Hamilton, J.A. (2019). *GM-CSF*-Dependent Inflammatory Pathways. Front Immunol *10*, 2055.

Harriff, M.J., Cansler, M.E., Toren, K.G., Canfield, E.T., Kwak, S., Gold, M.C., and Lewinsohn, D.M. (2014). Human lung epithelial cells contain *Mycobacterium tuberculosis* in a late endosomal vacuole and are efficiently recognized by CD8(+) T cells. PLoS One *9*, e97515.

Hatherill, M., White, R.G., and Hawn, T.R. (2019). Clinical Development of New TB Vaccines: Recent Advances and Next Steps. Front Microbiol *10*, 3154.

Hett, E.C., and Rubin, E.J. (2008). Bacterial growth and cell division: a mycobacterial perspective. Microbiol Mol Biol Rev *72*, 126-156, table of contents.

Hossain, M.M., and Norazmi, M.N. (2013). Pattern recognition receptors and cytokines in *Mycobacterium tuberculosis* infection--the double-edged sword? Biomed Res Int *2013*, 179174.

Hossain, M.S., Ahmed, R., Haque, M.S., Alam, M.M., and Islam, M.S. (2019). Identification and validation of reference genes for real-time quantitative RT-PCR analysis in jute. BMC Mol Biol *20*, 13.

Hove, P., Molepo, J., Dube, S., and Nchabeleng, M. (2015). Genotypic diversity of *Mycobacterium tuberculosis* in pretoria. Southern African Journal of Epidemiology and Infection *27*, 77-83.

Ignatov, D., Malakho, S., Majorov, K., Skvortsov, T., Apt, A., and Azhikina, T. (2013). RNA-Seq analysis of *Mycobacterium avium* non-coding transcriptome. PLoS One *8*, e74209.

Ito, T., Connett, J.M., Kunkel, S.L., and Matsukawa, A. (2013). The linkage of innate and adaptive immune response during granulomatous development. Front Immunol *4*, 10.

Jee, B., Sharma, P., Katoch, K., Joshi, B., and Awasthi, S.K. (2017). IL-10 down-regulates the expression of survival associated gene hspX of *Mycobacterium tuberculosis* in murine macrophage. Braz J Infect Dis *21*, 386-390.

Kana, B.D., Gordhan, B.G., Downing, K.J., Sung, N., Vostroktunova, G., Machowski, E.E., Tsenova, L., Young, M., Kaprelyants, A., Kaplan, G., and Mizrahi, V. (2008). The resuscitation-promoting factors of *Mycobacterium tuberculosis* are required for virulence and resuscitation from dormancy but are collectively dispensable for growth *in vitro*. Mol Microbiol *67*, 672-684.

Kana, B.D., and Mizrahi, V. (2010). Resuscitation-promoting factors as lytic enzymes for bacterial growth and signaling. FEMS Immunol Med Microbiol *58*, 39-50.

Kim, J.S., Kim, W.S., Choi, H.G., Jang, B., Lee, K., Park, J.H., Kim, H.J., Cho, S.N., and Shin, S.J. (2013). *Mycobacterium tuberculosis* RpfB drives Th1-type T cell immunity via a TLR4-dependent activation of dendritic cells. J Leukoc Biol *94*, 733-749.

Korb, V.C., Chuturgoon, A.A., and Moodley, D. (2016). *Mycobacterium tuberculosis*: Manipulator of Protective Immunity. Int J Mol Sci *17*, 131.

Kwon, K.W., Kim, W.S., Kim, H., Han, S.J., Hahn, M.Y., Lee, J.S., Nam, K.T., Cho, S.N., and Shin, S.J. (2017). Novel vaccine potential of Rv3131, a DosR regulon-encoded putative nitroreductase, against hyper-virulent *Mycobacterium tuberculosis* strain K. Sci Rep *7*, 44151.

Li, Y., Wang, Y., and Liu, X. (2012). The role of airway epithelial cells in response to mycobacteria infection. Clin Dev Immunol *2012*, 791392.

Liu, C.H., Liu, H., and Ge, B. (2017). Innate immunity in tuberculosis: host defense vs pathogen evasion. Cell Mol Immunol *14*, 963-975.

Lokau, J., Schoeder, V., Haybaeck, J., and Garbers, C. (2019). Jak-Stat Signaling Induced by Interleukin-6 Family Cytokines in Hepatocellular Carcinoma. Cancers (Basel) *11*.

Lotfi, N., Thome, R., Rezaei, N., Zhang, G.X., Rezaei, A., Rostami, A., and Esmaeil, N. (2019). Roles of GM-CSF in the Pathogenesis of Autoimmune Diseases: An Update. Front Immunol *10*, 1265.

Lowe, R., Shirley, N., Bleackley, M., Dolan, S., and Shafee, T. (2017). Transcriptomics technologies. PLoS Comput Biol *13*, e1005457.

Maguga-Phasha, N.T.C., Munyai, N.S., Mashinya, F., Makgatho, M.E., and Mbajiorgu, E.F. (2017). Genetic diversity and distribution of *Mycobacterium tuberculosis* genotypes in Limpopo, South Africa. BMC Infect Dis *17*, 764.

Mahamed, D., Boulle, M., Ganga, Y., Mc Arthur, C., Skroch, S., Oom, L., Catinas, O., Pillay, K., Naicker, M., Rampersad, S., *et al.* (2017). Intracellular growth of *Mycobacterium tuberculosis* after macrophage cell death leads to serial killing of host cells. Elife *6*.

Marino, S., Sud, D., Plessner, H., Lin, P.L., Chan, J., Flynn, J.L., and Kirschner, D.E. (2007). Differences in reactivation of tuberculosis induced from anti-TNF treatments are based on bioavailability in granulomatous tissue. PLoS Comput Biol *3*, 1909-1924.

Mayer-Barber, K.D., Andrade, B.B., Barber, D.L., Hieny, S., Feng, C.G., Caspar, P., Oland, S., Gordon, S., and Sher, A. (2011). Innate and adaptive interferons suppress IL-1alpha and IL-1beta production by distinct pulmonary myeloid subsets during *Mycobacterium tuberculosis* infection. Immunity *35*, 1023-1034.

Mayer-Barber, K.D., Andrade, B.B., Oland, S.D., Amaral, E.P., Barber, D.L., Gonzales, J., Derrick, S.C., Shi, R., Kumar, N.P., Wei, W., *et al.* (2014). Host-directed therapy of tuberculosis based on interleukin-1 and type I interferon crosstalk. Nature *511*, 99-103.

Meacci, F., Orru, G., Iona, E., Giannoni, F., Piersimoni, C., Pozzi, G., Fattorini, L., and Oggioni, M.R. (2005). Drug resistance evolution of a *Mycobacterium tuberculosis* strain from a noncompliant patient. J Clin Microbiol *43*, 3114-3120.

Meyer-Rath, G., Schnippel, K., Long, L., MacLeod, W., Sanne, I., Stevens, W., Pillay, S., Pillay, Y., and Rosen, S. (2012). The impact and cost of scaling up GeneXpert MTB/RIF in South Africa. PLoS One *7*, e36966.

Migliori, G.B., Lange, C., Centis, R., Sotgiu, G., Mutterlein, R., Hoffmann, H., Kliiman, K., De Iaco, G., Lauria, F.N., Richardson, M.D., *et al.* (2008). Resistance to second-line injectables and treatment outcomes in multidrug-resistant and extensively drug-resistant tuberculosis cases. Eur Respir J *31*, 1155-1159.

Mihret, A. (2012). The role of dendritic cells in *Mycobacterium tuberculosis* infection. Virulence *3*, 654-659.

Mishra, A., Singh, V.K., Actor, J.K., Hunter, R.L., Jagannath, C., Subbian, S., and Khan, A. (2020). GM-CSF Dependent Differential Control of *Mycobacterium tuberculosis* Infection in Human and Mouse Macrophages: Is Macrophage Source of *GM-CSF* Critical to Tuberculosis Immunity? Front Immunol *11*, 1599.

Moreira-Teixeira, L., Mayer-Barber, K., Sher, A., and O'Garra, A. (2018). Type I interferons in tuberculosis: Foe and occasionally friend. J Exp Med *215*, 1273-1285.

Munoz, L., Stagg, H.R., and Abubakar, I. (2015). Diagnosis and Management of Latent Tuberculosis Infection. Cold Spring Harb Perspect Med *5*.

Murray, J.F., Schraufnagel, D.E., and Hopewell, P.C. (2015). Treatment of Tuberculosis. A Historical Perspective. Ann Am Thorac Soc *12*, 1749-1759.

Naidoo, P., Theron, G., Rangaka, M.X., Chihota, V.N., Vaughan, L., Brey, Z.O., and Pillay, Y. (2017). The South African Tuberculosis Care Cascade: Estimated Losses and Methodological Challenges. J Infect Dis *216*, S702-S713.

Ndlovu, H., and Marakalala, M.J. (2016). Granulomas and Inflammation: Host-Directed Therapies for Tuberculosis. Front Immunol *7*, 434.

Ng, A.P., and Alexander, W.S. (2017). Haematopoietic stem cells: past, present and future. Cell Death Discov *3*, 17002.

Nguyen, T.N.A., Anton-Le Berre, V., Banuls, A.L., and Nguyen, T.V.A. (2019). Molecular Diagnosis of Drug-Resistant Tuberculosis; A Literature Review. Front Microbiol *10*, 794.

Ning, S., Pagano, J.S., and Barber, G.N. (2011). IRF7: activation, regulation, modification and function. Genes Immun *12*, 399-414.

O'Garra, A. (2013). Systems approach to understand the immune response in tuberculosis: an iterative process between mouse models and human disease. Cold Spring Harb Symp Quant Biol *78*, 173-177.

O'Leary, S., O'Sullivan, M.P., and Keane, J. (2011). IL-10 blocks phagosome maturation in *Mycobacterium tuberculosis*-infected human macrophages. Am J Respir Cell Mol Biol *45*, 172-180.

Ottenhoff, T.H., and Kaufmann, S.H. (2012). Vaccines against tuberculosis: where are we and where do we need to go? PLoS Pathog *8*, e1002607.

Philips, J.A., and Ernst, J.D. (2012). Tuberculosis pathogenesis and immunity. Annu Rev Pathol *7*, 353-384.

Pillay, M., and Sturm, A.W. (2007). Evolution of the extensively drug-resistant F15/LAM4/KZN strain of *Mycobacterium tuberculosis* in KwaZulu-Natal, South Africa. Clin Infect Dis *45*, 1409-1414.

Rasmussen, S.B., Reinert, L.S., and Paludan, S.R. (2009). Innate recognition of intracellular pathogens: detection and activation of the first line of defense. APMIS *117*, 323-337.

Redford, P.S., Murray, P.J., and O'Garra, A. (2011). The role of IL-10 in immune regulation during *M. tuberculosis* infection. Mucosal Immunol *4*, 261-270.

Ritz, N., Dutta, B., Donath, S., Casalaz, D., Connell, T.G., Tebruegge, M., Robins-Browne, R., Hanekom, W.A., Britton, W.J., and Curtis, N. (2012). The influence of bacille Calmette-Guerin vaccine strain on the immune response against tuberculosis: a randomized trial. Am J Respir Crit Care Med *185*, 213-222.

Romano, M., Aryan, E., Korf, H., Bruffaerts, N., Franken, C.L., Ottenhoff, T.H., and Huygen, K. (2012). Potential of *Mycobacterium tuberculosis* resuscitation-promoting factors as antigens in novel tuberculosis sub-unit vaccines. Microbes Infect *14*, 86-95.

Romero-Adrian, T.B. (2015). Role of cytokines and other factors involved in the *Mycobacterium tuberculosis* infection. World Journal of Immunology *5*, 16.

Rosser, A., Stover, C., Pareek, M., and Mukamolova, G.V. (2017). Resuscitation-promoting factors are important determinants of the pathophysiology in *Mycobacterium tuberculosis* infection. Crit Rev Microbiol *43*, 621-630.

Russell-Goldman, E., Xu, J., Wang, X., Chan, J., and Tufariello, J.M. (2008). A *Mycobacterium tuberculosis* Rpf double-knockout strain exhibits profound defects in reactivation from chronic tuberculosis and innate immunity phenotypes. Infect Immun *76*, 4269-4281.

Ryndak, M.B., and Laal, S. (2019). Mycobacterium tuberculosis Primary Infection and Dissemination: A Critical Role for Alveolar Epithelial Cells. Front Cell Infect Microbiol *9*, 299.

Sakamoto, K. (2012). The pathology of *Mycobacterium tuberculosis* infection. Vet Pathol *49*, 423-439.
Saleh, M., and Longhi, G. (2016). Macrophage Infection by Mycobacteria. Mycobacterial Diseases *06*.

Sasindran, S.J., and Torrelles, J.B. (2011). Mycobacterium Tuberculosis Infection and Inflammation: what is Beneficial for the Host and for the Bacterium? Front Microbiol *2*, 2.

Sawai, C.M., Babovic, S., Upadhaya, S., Knapp, D., Lavin, Y., Lau, C.M., Goloborodko, A., Feng, J., Fujisaki, J., Ding, L., *et al.* (2016). Hematopoietic Stem Cells Are the Major Source of Multilineage Hematopoiesis in Adult Animals. Immunity *45*, 597-609.

Sharma, M., Bose, M., Abhimanyu, Sharma, L., Diwakar, A., Kumar, S., Gaur, S.N., and Banavalikar, J.N. (2012). Intracellular survival of *Mycobacterium tuberculosis* in macrophages is modulated by phenotype of the pathogen and immune status of the host. Int J Mycobacteriol *1*, 65-74.

Sia, J.K., Georgieva, M., and Rengarajan, J. (2015). Innate Immune Defenses in Human Tuberculosis: An Overview of the Interactions between *Mycobacterium tuberculosis* and Innate Immune Cells. J Immunol Res *2015*, 747543.

Sia, J.K., and Rengarajan, J. (2019). Immunology of Mycobacterium tuberculosis Infections. Microbiol Spectr *7*.

Sloan, D.J., and Lewis, J.M. (2016). Management of multidrug-resistant TB: novel treatments and their expansion to low resource settings. Trans R Soc Trop Med Hyg *110*, 163-172.

Sohn, H., Kim, J.S., Shin, S.J., Kim, K., Won, C.J., Kim, W.S., Min, K.N., Choi, H.G., Lee, J.C., Park, J.K., and Kim, H.J. (2011). Targeting of *Mycobacterium tuberculosis* heparin-binding hemagglutinin to mitochondria in macrophages. PLoS Pathog *7*, e1002435.

Squeglia, F., Romano, M., Ruggiero, A., Vitagliano, L., De Simone, A., and Berisio, R. (2013). Carbohydrate recognition by RpfB from *Mycobacterium tuberculosis* unveiled by crystallographic and molecular dynamics analyses. Biophys J *104*, 2530-2539.

Stamm, C.E., Collins, A.C., and Shiloh, M.U. (2015). Sensing of *Mycobacterium tuberculosis* and consequences to both host and bacillus. Immunol Rev *264*, 204-219.

Stanley, S.A., Johndrow, J.E., Manzanillo, P., and Cox, J.S. (2007). The Type I IFN response to infection with *Mycobacterium tuberculosis* requires ESX-1-mediated secretion and contributes to pathogenesis. J Immunol *178*, 3143-3152.

Syedbasha, M., and Egli, A. (2017). Interferon Lambda: Modulating Immunity in Infectious Diseases. Front Immunol *8*, 119.

Thuong, N.T., Dunstan, S.J., Chau, T.T., Thorsson, V., Simmons, C.P., Quyen, N.T., Thwaites, G.E., Thi Ngoc Lan, N., Hibberd, M., Teo, Y.Y., *et al.* (2008). Identification of tuberculosis susceptibility genes with human macrophage gene expression profiles. PLoS Pathog *4*, e1000229.

Tiberi, S., Munoz-Torrico, M., Duarte, R., Dalcolmo, M., D'Ambrosio, L., and Migliori, G.B. (2018). New drugs and perspectives for new anti-tuberculosis regimens. Pulmonology *24*, 86-98.

Togun, T., Kampmann, B., Stoker, N.G., and Lipman, M. (2020). Anticipating the impact of the COVID-19 pandemic on TB patients and TB control programmes. Ann Clin Microbiol Antimicrob *19*, 21.

Tufariello, J.M., Jacobs, W.R., Jr., and Chan, J. (2004). Individual *Mycobacterium tuberculosis* resuscitation-promoting factor homologues are dispensable for growth *in vitro* and *in vivo*. Infect Immun *72*, 515-526.

Tufariello, J.M., Mi, K., Xu, J., Manabe, Y.C., Kesavan, A.K., Drumm, J., Tanaka, K., Jacobs, W.R., Jr., and Chan, J. (2006). Deletion of the *Mycobacterium tuberculosis* resuscitation-promoting factor Rv1009 gene results in delayed reactivation from chronic tuberculosis. Infect Immun *74*, 2985-2995.

van der Does, A.M., Bogaards, S.J., Ravensbergen, B., Beekhuizen, H., van Dissel, J.T., and Nibbering, P.H. (2010). Antimicrobial peptide hLF1-11 directs granulocyte-macrophage colony-stimulating factor-driven monocyte differentiation toward macrophages with enhanced recognition and clearance of pathogens. Antimicrob Agents Chemother *54*, 811-816.

Van Der Meeren, O., Hatherill, M., Nduba, V., Wilkinson, R.J., Muyoyeta, M., Van Brakel, E., Ayles, H.M., Henostroza, G., Thienemann, F., Scriba, T.J., *et al.* (2018). Phase 2b Controlled Trial of M72/AS01E Vaccine to Prevent Tuberculosis. N Engl J Med *379*, 1621-1634.

Van der Spoel van Dijk, A., Makhoahle, P.M., Rigouts, L., and Baba, K. (2016). Diverse Molecular Genotypes of *Mycobacterium tuberculosis* Complex Isolates Circulating in the Free State, South Africa. Int J Microbiol *2016*, 6572165.

van der Vaart, M., Spaink, H.P., and Meijer, A.H. (2012). Pathogen recognition and activation of the innate immune response in zebrafish. Adv Hematol *2012*, 159807.

VanGuilder, H.D., Vrana, K.E., and Freeman, W.M. (2008). Twenty-five years of quantitative PCR for gene expression analysis. Biotechniques *44*, 619-626.

Vassall, A., Siapka, M., Foster, N., Cunnama, L., Ramma, L., Fielding, K., McCarthy, K., Churchyard, G., Grant, A., and Sinanovic, E. (2017). Cost-effectiveness of Xpert MTB/RIF for tuberculosis diagnosis in South Africa: a real-world cost analysis and economic evaluation. The Lancet Global Health *5*, e710-e719.

Vekemans, J., Gebreselassie, N., Zignol, M., Friede, M., Kasaeva, T., and Swaminathan, S. (2019). A new tuberculosis vaccine: breakthrough, challenges, and a call for collaboration. The Lancet Infectious Diseases *19*, 123-125.

Verrall, A.J., Netea, M.G., Alisjahbana, B., Hill, P.C., and van Crevel, R. (2014). Early clearance of *Mycobacterium tuberculosis*: a new frontier in prevention. Immunology *141*, 506-513.

Wang, Z., Gerstein, M., and Snyder, M. (2009). RNA-Seq: a revolutionary tool for transcriptomics. Nat Rev Genet *10*, 57-63.

Wolf, J.B. (2013). Principles of transcriptome analysis and gene expression quantification: an RNA-seq tutorial. Mol Ecol Resour *13*, 559-572.

Xing, L., Cheng, Q., Zha, G., and Yi, S. (2017). Transcriptional Profiling at High Temporal Resolution Reveals Robust Immune/Inflammatory Responses during Rat Sciatic Nerve Recovery. Mediators Inflamm *2017*, 3827841.

Yan, K., Gao, L.N., Cui, Y.L., Zhang, Y., and Zhou, X. (2016). The cyclic AMP signaling pathway: Exploring targets for successful drug discovery (Review). Mol Med Rep *13*, 3715-3723.

Yeremeev, V.V., Kondratieva, T.K., Rubakova, E.I., Petrovskaya, S.N., Kazarian, K.A., Telkov, M.V., Biketov, S.F., Kaprelyants, A.S., and Apt, A.S. (2003). Proteins of the Rpf family: immune cell reactivity and vaccination efficacy against tuberculosis in mice. Infect Immun *71*, 4789-4794.

Zager, E.M., and McNerney, R. (2008). Multidrug-resistant tuberculosis. BMC Infect Dis *8*, 10.
Zhang, Y., Chan, J.F., and Cummins, C.L. (2009). Liver X Receptors as Therapeutic Targets for Managing Cholesterol: Implications for Atherosclerosis and Other Inflammatory Conditions. Clin Lipidol *4*, 29-40.

Zhao, S., Song, X., Zhao, Y., Qiu, Y., Mao, F., Zhang, C., Bai, B., Zhang, H., Wu, S., and Shi, C. (2015). Protective and therapeutic effects of the resuscitation-promoting factor domain and its mutants against *Mycobacterium tuberculosis* in mice. Pathog Dis *73*.

Appendices

Appendix A: BREC approval

UNIVERSITY OF KWAZULU-NATAL
INYUVESI YAKWAZULU-NATALI

04 September 2020

Ms D Moti (210553293)
School of Laboratory Medicine and Medical Sciences
Health Sciences
210553293@stu.ukzn.ac.za

Dear Ms Moti

PROTOCOL: Global transcriptome analysis of THP-1 cells infected with an rpfB gene knockout strain of Mycobacterium tuberculosis.
Degree: MMedSc
BREC reference number: BE271/15

RECERTIFICATION APPLICATION APPROVAL NOTICE

Approved:	**03 July 2020**
Expiration of Ethical Approval:	**02 July 2021**

I wish to advise you that your application for recertification received on 01 September 2020 for the above study has been **noted and approved** by a subcommittee of the Biomedical Research Ethics Committee (BREC). The start and end dates of this period are indicated above.

If any modifications or adverse events occur in the project before your next scheduled review, you must submit them to BREC for review. Except in emergency situations, no change to the protocol may be implemented until you have received written BREC approval for the change.

The committee will be notified of the above approval at its next meeting to be held on 13 October 2020.

Yours sincerely

[redacted]

Ms A Marimuthu
(for) Prof D Wassenaar
Chair: Biomedical Research Ethics Committee

Appendix B: Generation and confirmation of the Δ*rpfB* mutant strain (Dr. C. C Naidoo, unpublished)

Construction and unmarking of the Δ*rpfB* mutant strain

High titre phage lysate preparation

Mycobacterium smegmatis mc^2 155 (*M. smegmatis*) was grown in Luria Bertani (LB) broth (Becton Dickinson) overnight at 37 °C. Following incubation, mycobacteriophage was added the *M. smegmatis* culture. Phage was mixed with top agar, poured onto 7H10 agar plates and incubated at 30 °C for 2 days. Mycobacteriophage (MP) buffer was added to the plates and left for shaking at room temperature for 2 hours, followed by filtration of the lysate through 0.22 µm filter units. Ten-fold serial dilutions were set up using MP buffer in a 96 well plate. A spot of each dilution including a control was done on 7H10 agar plates. Plates were incubated at 30 °C for 2 days.

Specialized transduction

Wild type culture was grown in 20 mL 7H9 to OD_{600nm} ~1. Culture was transferred in 10 mL volumes into 2 x 50 mL conical tubes. MP buffer was added to each tube, mixed and centrifuged at 3000 rpm at 4 °C for 10 minutes, and the supernatant discarded. The pellet was resuspended in MP for the control and in high titre phage lysate for the mutant. Tubes were incubated overnight at 37 °C. The suspension was centrifuged at 3000 rpm at 4 °C for 10 minutes, and 500 µL of the supernatant was discarded. The pellet was dissolved in the remaining supernatant by pipetting. The suspension was plated in duplicate onto 7H10 agar containing 75 µg/mL hygromycin. Plates were incubated at 37 °C for 3 weeks. Half a colony from transduction plates was inoculated in 5 mL 7H9 and incubated at 37 °C with agitation for 1-2 weeks until turbid. Stocks were made in 1 mL aliquots and stored at -80 °C. The other half of the colony was resuspended in 100 µL of Instagene matrix. The suspension was boiled at 95 °C for 45 minutes and centrifuged at maximum speed for 1 minute. The supernatant was transferred to a fresh tube and stored at -20 °C for. The unmarked Δ*rpfB* mutant strain was confirmed by PCR and NGS sequencing.

Unmarking of the Δ*rpfB* mutant strain

Frozen stocks of the Δ*rpfB* strain was revived in 7H9 to OD_{600nm} ~0.6. The strain was subcultured once more to OD_{600nm} ~0.6 and pelleted by centrifugation at 3000 rpm for 10 minutes at room temperature. The supernatant was discarded, and the pellet washed with the MP buffer and centrifuged again at 4000 rpm for 10 minutes at room temperature. The wash step was repeated, and the supernatant was discarded and the residual buffer was removed. The pellet was resuspended in the MP buffer and the cell suspension was

transferred to a 15 mL tube. phAE280 (10^9-10^{11} pfu/mL) was added and incubated at 37 °C for 3 days without shaking. After 3 days, the cells were centrifuged at 300 rpm for 10 minutes at room temperature. The pellet was resuspended in 7H9 and plated (10, 50, 440 µL) onto 7H10 agar containing 3 % sucrose. The plates were incubated at 37 °C for 4 weeks or until colonies appear.

Unmarking

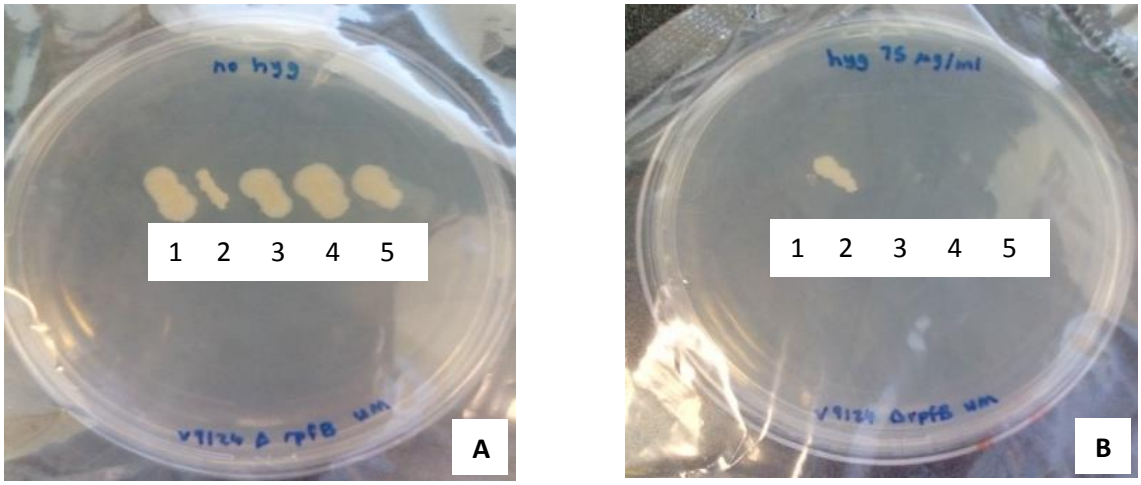

Figure B1: **Confirmation of unmarking of the Δ*rpfB* mutant strain using the pick and patch method**. **(A)** 4 of the 5 colonies (colonies 1 and 3-5) selected from the 7H10 – 3% sucrose agar plates were confirmed as unmarked visible by growth on 7H11 agar without hygromycin. Colony 2 appeared on both 7H11 agar with and without hygromycin. **(B)** Only 1 of the 5 replicates (colony 2) plated on 7H11 agar with hygromycin grew and was therefore not considered unmarked.

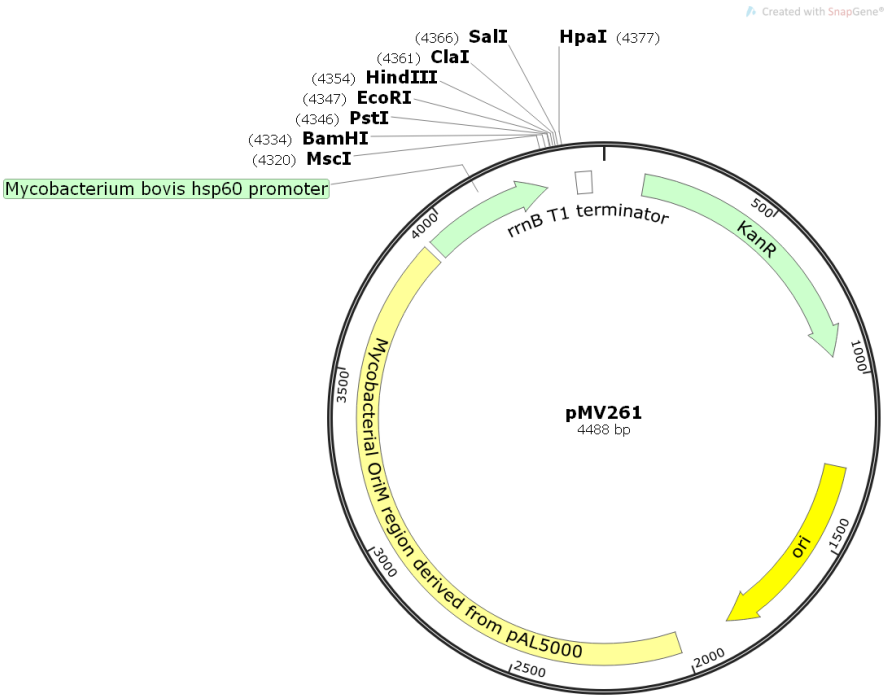

Figure B2: pMV261 vector map showing the promoter region and restriction sites (https://www.lifescience-market.com/plasmid-c-94/pmv261-p-108774.html).

Appendix C: Media and reagents

Propagation, construction and confirmation of bacterial strains

Middlebrook 7H9 broth (1L)

4.7 g Middlebrook 7H9 powder

900 mL distilled water

10 mL 50% (w/v) glycerol

100 mL OADC

2.5 mL 20% Tween 80

4.7 g Middlebrook 7H9 broth was dissolved in 900 mL distilled water and autoclaved at 121°C for 15mins. 10 mL 50% glycerol, 100 mL OADC and 2.5 mL 20% Tween 80 was added aseptically after cooling at 56°C in a water bath. Media was mixed well and stored at 4°C.

Middlebrook 7H11 media (1L)

21 g Middlebrook 7H11 powder

900 mL distilled water

10 mL 50% glycerol

100 mL OADC

75 µg/mL Hygromycin

50 µg /mL Kanamycin

21 g of Middlebrook 7H11 powder was dissolved in 900mL distilled water and autoclaved at 121°C for 15min. Glycerol and OADC were added aseptically after cooling at 56°C in a water bath. Relevant antibiotics were added after cooling. 12.5 mL was aliquoted into sterile 65 mm petri dishes.

50% Glycerol

50 mL glycerol

50 mL autoclaved distilled water

50 mL glycerol was dissolved in 50 mL autoclaved distilled water. The solution was filter-sterilized with a 0.2 µm pore membrane filter into a sterile container.

20% Tween-80

20 mL Tween-80 into

80 mL distilled water

Tween-80 was dissolved in water and filter sterilized through a 0.2 µm membrane.

10 X TBE buffer (500 mL)

54 g Trizma base

27.5 g Boric acid

4.65 g EDTA

All powders were dissolved in 500 mL distilled water.

LB broth (1 L)

20 g LB powder

1000 mL distilled water

LB powder dissolved in distilled water and autoclaved at 121°C for 15min.

LB agar (1 L)

20 g LB powder

15 g Bacto agar powder

1000 mL distilled water

LB and Bacto agar powder were dissolved in the distilled water autoclaved at 121°C for 15min. The agar was cooled at 56°C in a water bath. 12.5 mL was aliquoted into sterile 65 mm petri dishes.

1.5 % large/ small Agarose gel

2.1/ 0.6 g agarose

140/ 40 mL 10 X TBE

Propagation of THP-1 cell line

Phosphate buffered saline (PBS)

10 PBS tablets (Oxoid)

1000 mL distilled water

10 PBS tablets were dissolved in 1L of distilled water. The solution was autoclaved at 121°C for 15 min, and thereafter decanted into 20 mL aliquots and stored at 4°C.

MOPS gel electrophoresis

DEPC

1 mL 0.1% DEPC

1 L distilled water

1 mL of 0.1% DEPC was added to 1 L of distilled water, mixed well and left at room temperature overnight. Thereafter, autoclaved at 121°C for 15 min and allowed to cool prior to use.

10 X MOPs Buffer (1 L)

41.9 g MOPS

8.2 g Sodium acetate. $3H_20$

3.72 g EDTA

DEPC-treated water

41.9 g MOPS, 8.2 g Sodium acetate and 3.72 g EDTA was dissolved in 800 mL DEPC-treated water, and made up to 1 L with DEPC-treated water. The solution was autoclaved for 121°C for 15 min.

MOPS gel

2 g agarose

144 mL DEPC-treated water

20 mL 10 x MOPS buffer

36 mL 37% Formaldehyde

2 g agarose was heat dissolved in 144 mL DEPC-treated water with gently swirling to mix. The mixture was cooled to 60°C followed by the addition of 20 mL of 10 x MOPS buffer. Thereafter, 36 mL 37% formaldehyde was added in a fume hood. The gel was poured into a casting tray, avoiding air bubbles, and allowed to set for 30 minutes.

Appendix D: Raw data of CFU counts from bacterial infections

Table D1. Colony forming units (CFUs) of inoculum and MOI of each strain from three independent biological assays done in triplicate for RNA sequencing and qRT-PCR.

Biological assay	Strain	Dilution	CFUs			Average CFU	MOI
			Replicate 1	Replicate 2	Replicate 3		
1	WT	10^{-4}	61	58	56	58	1.7
2		10^{-4}	29	44	32	35	1.1
3		10^{-4}	33	26	29	29	0.9
1	M	10^{-4}	55	55	48	53	1.6
2		10^{-4}	36	35	31	34	1.0
3		10^{-4}	34	23	30	29	0.9

MOI calculation

$$\frac{\text{Average CFU counts} \times \text{Dilution factor } (10^5) \times \text{volume of inoculum used}(2.25)}{\text{THP} - 1 \text{ Seeded } (7.5 \times 10^5 \times \text{Total volume } (10)}$$

Table D2: CFU from three independent biological assays done in triplicate at 4 hours post-infection, for RNA sequencing and qRT-PCR

Biological assay	Strain	Dilution	CFUs			Average CFU	CFU/mL
			Replicate 1	Replicate 2	Replicate 3		
1	WT	10^{-3}	32	42	26	33	3.33×10^5
		10^{-3}	23	13	21	19	1.90×10^5
		10^{-3}	41	45	29	38	3.83×10^5
2		10^{-4}	12	9	19	13	1.33×10^6
		10^{-4}	22	29	30	27	2.7×10^6
		10^{-4}	28	33	24	28	2.83×10^6
3		10^{-4}	33	33	34	33	3.33×10^6
		10^{-4}	24	32	21	26	2.57×10^6
		10^{-4}	33	24	29	29	2.87×10^6
1	M	10^{-3}	29	29	26	28	2.80×10^5
		10^{-3}	31	33	38	34	3.40×10^5
		10^{-3}	28	25	27	27	2.67×10^5
2		10^{-4}	24	36	29	30	2.97×10^6
		10^{-4}	27	24	23	25	2.47×10^6
		10^{-4}	30	35	32	32	3.23×10^6
3		10^{-4}	35	31	36	34	3.40×10^6
		10^{-4}	24	22	22	23	2.27×10^6
		10^{-4}	31	30	28	30	2.97×10^6

Table D3: CFU from three independent biological assays done in triplicate at 72 hours post-infection, for RNA sequencing and qRT-PCR

Biological assay	Strain	Dilution	CFUs			Average CFU	CFU/mL
			Replicate 1	Replicate 2	Replicate 3		
1	WT	10^{-3}	90	81	116	96	9.57×10^5
		10^{-3}	113	126	115	118	1.18×10^6
		10^{-3}	84	142	74	100	1.00×10^6
2		10^{-3}	52	52	62	55	5.53×10^5
		10^{-3}	31	44	20	32	3.17×10^5
		10^{-3}	19	28	19	22	2.20×10^5
3		10^{-3}	71	65	99	78	7.83×10^5
		10^{-3}	119	75	74	89	8.93×10^5
		10^{-3}	92	58	71	74	7.37×10^5
1	M	10^{-3}	59	98	96	84	8.43×10^5
		10^{-3}	112	92	98	101	1.01×10^6
		10^{-3}	109	86	90	95	9.50×10^5
2		10^{-3}	43	52	42	46	4.57×10^5
		10^{-3}	48	33	53	45	4.47×10^5
		10^{-3}	41	34	53	43	4.26×10^5
3		10^{-3}	90	67	103	87	8.67×10^5
		10^{-3}	39	65	65	56	5.63×10^5
		10^{-3}	66	95	106	89	8.90×10^5

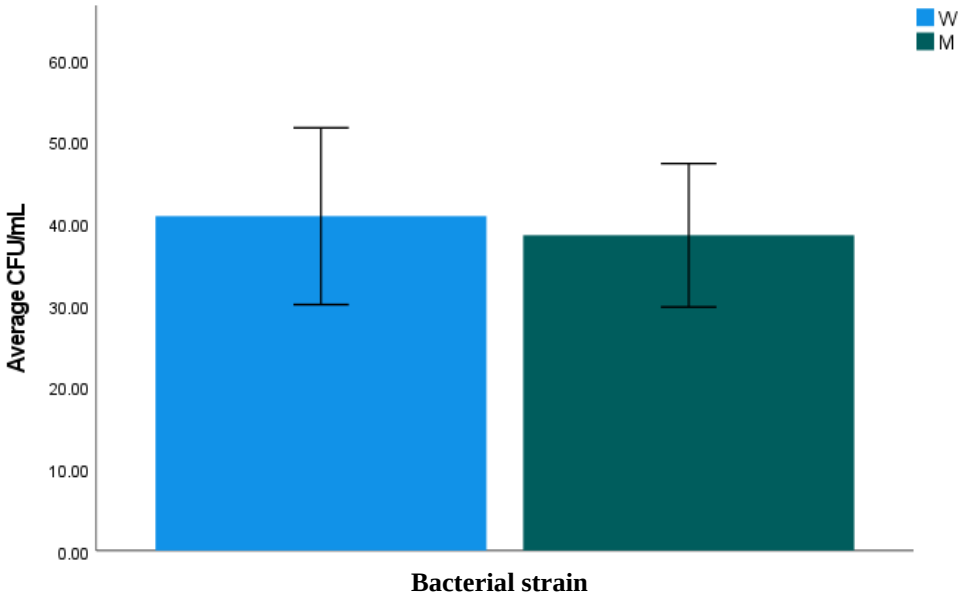

Figure D1: Graphical representation of WT and *rpfB* mutant bacterial inoculum (CFU/mL) used to infect THP-1 macrophages in RNA sequencing and qRT-PCR assays. Following infection of THP-1 macrophages with the WT and *rpfB* mutant strains for 4 hours, spent media was discarded and macrophage monolayers detached and lysed. The lysate was plated onto 7H11 agar to determine the bacterial load and the difference between in bacterial load between the two strains. There were no significant differences in CFU/mL between the WT and mutant infected macrophages at 4 hours post-infection as the P value of 0.201 was above the statistical cut-off, 0.05.

Table D4. Colony forming units (CFUs) of inoculum and MOI of each strain from three independent biological assays done in triplicate at 4 hours post-infection, for cytokine validation.

Biological assay	Strain	Dilution	CFUs			Average CFU	MOI
			Replicate 1	Replicate 2	Replicate 3		
1	WT	10^{-4}	14	19	21	18	0.5
2		10^{-4}	23	36	37	32	0.96
3		10^{-4}	21	29	35	28	0.8
1	M	10^{-4}	19	21	13	18	0.5
2		10^{-4}	69	36	31	45	1.3
3		10^{-4}	58	41	26	42	1.2
1	C	10^{-4}	11	19	29	20	0.6
2		10^{-4}	60	67	59	62	1.9
3		10^{-4}	36	42	29	36	1.1

Table D5: CFU from three independent biological assays done in triplicate at 24 hours post-infection, for cytokine validation

Biological assay	Strain	Dilution	CFUs			Average CFU	CFU/mL
			Plate 1	Plate 2	Plate 3		
1	WT	10^{-3}	18	35	38	30	3.03×10^5
		10^{-3}	42	30	28	33	3.33×10^5
		10^{-3}	39	48	32	40	3.97×10^5
2		10^{-3}	42	50	59	50	5.03×10^5
		10^{-3}	60	59	55	58	5.80×10^5
		10^{-3}	72	63	54	63	6.30×10^5
3		10^{-3}	64	73	81	73	7.27×10^5
		10^{-3}	80	75	60	72	7.17×10^5
		10^{-3}	69	62	78	70	6.97×10^5
1	M	10^{-3}	19	31	33	28	2.78×10^5
		10^{-3}	28	35	40	34	3.43×10^4
		10^{-3}	45	50	41	45	4.53×10^5
2		10^{-3}	73	74	77	75	7.47×10^5
		10^{-3}	69	65	76	70	7.00×10^5
		10^{-3}	80	71	68	73	7.30×10^5
3		10^{-3}	62	64	99	75	7.50×10^5
		10^{-3}	70	79	83	77	7.73×10^5
		10^{-3}	66	72	80	73	7.27×10^5
1	C	10^{-3}	21	29	45	32	3.17×10^5
		10^{-3}	31	43	29	34	3.43×10^5
		10^{-3}	48	50	35	44	4.43×10^5
2		10^{-3}	67	68	73	69	6.93×10^5
		10^{-3}	61	75	71	69	6.90×10^5
		10^{-3}	59	70	65	65	6.47×10^5
3		10^{-3}	64	65	78	69	6.90×10^5
		10^{-3}	73	62	79	71	7.13×10^5
		10^{-3}	80	75	69	75	7.47×10^5

Table D6: CFU from three independent biological assays in triplicate at 48 hours post-infection, for cytokine validation

Biological assay	Strain	Dilution	CFUs			Average CFU	CFU/mL
			Plate 1	Plate 2	Plate 3		
1	WT	10^{-3}	20	25	25	23	2.33×10^5
		10^{-3}	32	45	29	35	3.53×10^5
		10^{-3}	52	39	40	44	4.37×10^5
2		10^{-3}	32	38	50	40	4.00×10^5
		10^{-3}	36	42	51	43	4.30×10^5
		10^{-3}	45	49	53	49	4.90×10^5
3		10^{-3}	75	81	89	82	8.17×10^5
		10^{-3}	64	52	76	64	6.40×10^5
		10^{-3}	59	45	60	55	5.47×10^5
1	M	10^{-3}	20	21	24	22	2.17×10^5
		10^{-3}	42	49	33	41	4.13×10^5
		10^{-3}	36	43	55	45	4.47×10^5
2		10^{-3}	29	44	48	40	4.03×10^5
		10^{-3}	59	49	65	58	5.77×10^5
		10^{-3}	38	46	61	48	4.83×10^5
3		10^{-3}	60	65	67	64	6.40×10^5
		10^{-3}	50	59	42	50	5.03×10^5
		10^{-3}	37	40	57	45	4.47×10^5
1	C	10^{-3}	26	30	20	25	2.53×10^5
		10^{-3}	50	45	38	44	4.43×10^5
		10^{-3}	29	36	50	38	3.83×10^5
2		10^{-3}	57	65	75	66	6.57×10^5
		10^{-3}	72	60	55	62	6.23×10^5
		10^{-3}	41	56	69	55	5.53×10^5
3		10^{-3}	75	78	81	78	7.80×10^5
		10^{-3}	63	72	59	65	6.47×10^5
		10^{-3}	70	66	75	70	7.03×10^5

Table D7: CFU from three independent biological assays done in triplicate at 72 hours post-infection, for cytokine validation

Biological assay	Strain	Dilution	CFUs			Average CFU	CFU/mL
			Plate 1	Plate 2	Plate 3		
1	WT	10^{-3}	40	64	59	54	5.43 X 10^5
		10^{-3}	50	53	48	50	5.03 X 10^5
		10^{-3}	55	61	50	55	5.53 X 10^5
2		10^{-3}	52	50	62	55	5.47 X 10^5
		10^{-3}	69	65	51	62	6.17 X 10^5
		10^{-3}	63	53	59	58	5.83 X 10^5
3		10^{-3}	56	65	49	57	5.67 X 10^5
		10^{-3}	60	69	65	65	6.47 X 10^5
		10^{-3}	58	51	69	59	5.93 X 10^5
1	M	10^{-3}	62	53	59	58	5.80 X 10^5
		10^{-3}	60	65	57	61	6.07 X 10^5
		10^{-3}	70	63	61	65	6.47 X 10^5
2		10^{-3}	82	76	90	83	8.27 X 10^5
		10^{-3}	74	64	60	66	6.60 X 10^5
		10^{-3}	75	84	79	79	7.93 X 10^5
3		10^{-3}	96	84	82	87	8.73 X 10^5
		10^{-3}	70	87	90	82	8.23 X 10^5
		10^{-3}	80	79	78	79	7.90 X 10^5
1	C	10^{-3}	61	50	42	51	5.10 X 10^5
		10^{-3}	55	63	60	59	5.93 X 10^5
		10^{-3}	72	69	61	67	6.73 X 10^5
2		10^{-3}	77	80	80	79	7.90 X 10^5
		10^{-3}	85	75	69	76	7.63 X 10^5
		10^{-3}	60	65	70	65	6.50 X 10^5
3		10^{-3}	105	94	95	98	9.80 X 10^5
		10^{-3}	85	91	79	85	8.50 X 10^5
		10^{-3}	88	80	71	80	1.58 X 10^5

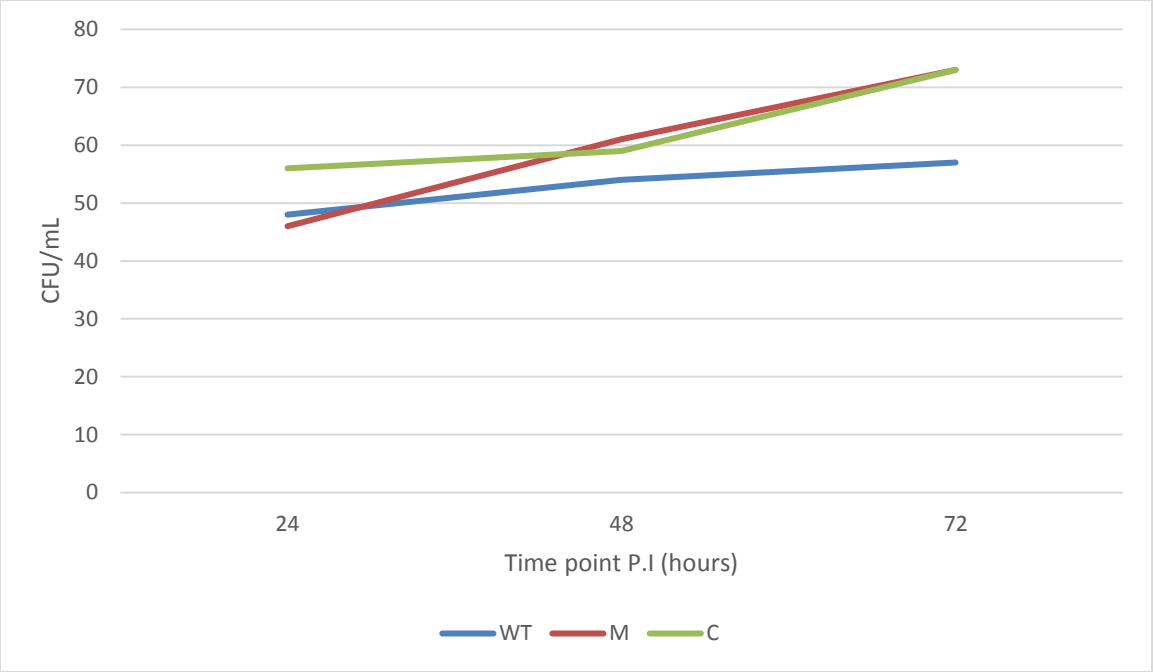

Figure D2: Average CFU/mL from cytokine experiments of *Mtb* WT, Δ*rpfB* mutant and *rpfB*-complemented strain at 24, 48 and 72 hours P.I. This figure shows the highest CFU/mL for all three strains was obtained at 72 hours P.I, late phase of *Mtb* growth. The complemented strain showed restoration of growth but was slightly higher than the WT. At 48 and 72 hours P.I, there is a visible difference in CFU/mL between the WT and mutant.

Appendix E: Quality of alignment of RNA extracted and sequenced reads.

Table E1: Raw extraction data of mammalian RNA used for RNA sequencing at 72 hours post-infection.

Samples	Concentrations ng/µl	260/280	260/230	RIN
WT1	140.6	2.12	1.48	9.5
WT2	279.2	2.12	2.11	9.3
MUT1	557.4	2.07	2.19	9.1
MUT2	1062.1	2.12	2.23	9.7
UN1	2239.4	2.11	2.14	9.6
UN2	1885.7	2.12	2.21	9.4

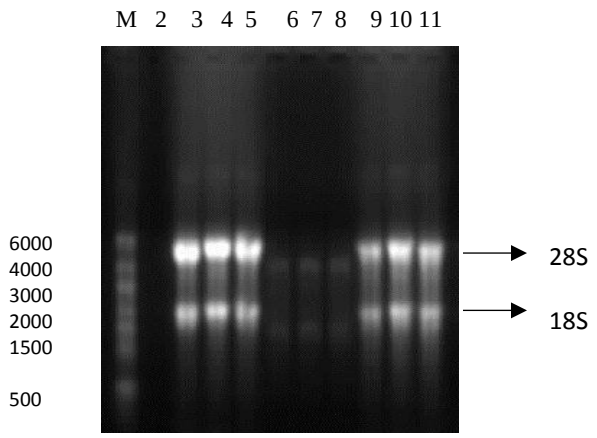
M 2 3 4 5 6 7 8 9 10 11
6000
4000
3000
2000
1500
500
28S
18S

A.

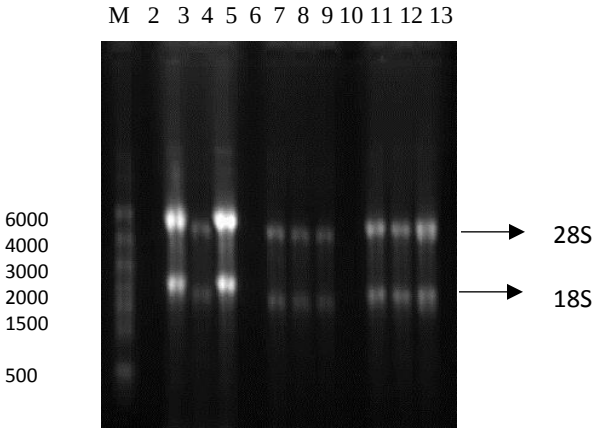
M 2 3 4 5 6 7 8 9 10 11 12 13
6000
4000
3000
2000
1500
500
28S
18S

B.

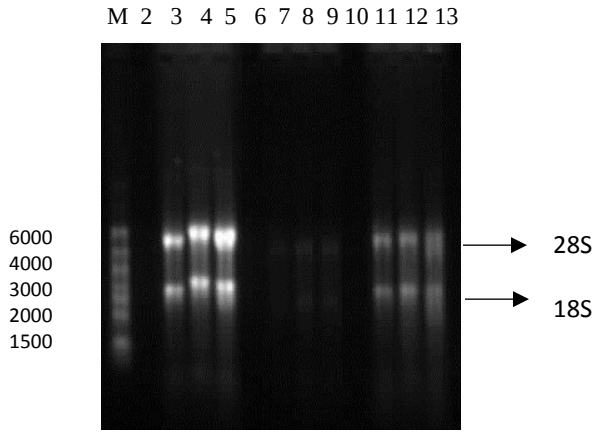
M 2 3 4 5 6 7 8 9 10 11 12 13
6000
4000
3000
2000
1500
28S
18S

C.

Figure E1: MOPs gel image of mammalian RNA extracted from uninfected, WT, and Δ*rpfB* mutant infected THP-1 macrophages 72 hours post-infection. RNA samples from triplicate, independent biological assays were electrophoresed. Each gel image shows the desired 28S and 18S bands of mammalian RNA against the Riboruler RNA marker. **A**. Lanes: M (Riboruler- RNA marker), 3-4: RNA extracted from Uninfected macrophages, 6-8: RNA extracted from WT infected macrophages, 9-10: RNA extracted from Δ*rpfB* mutant infected macrophages. Lanes: 8: WT1 (RNA sequencing), 9: M1 (RNA sequencing). **B.** Lanes: M (Riboruler- RNA marker), 3-5: RNA extracted from uninfected macrophages, 7 -9: RNA extracted from WT infected macrophages, 11 – 13: RNA extracted from Δ*rpfB* mutant infected macrophages. Lanes: 5: U1 (RNA sequencing), 7: WT2 (RNA sequencing), 11: M2 (RNA sequencing). **C**. Lanes: M (Riboruler- RNA marker), 3-5: RNA extracted from uninfected macrophages, 7 -9: RNA extracted from WT infected macrophages, 11 – 13: RNA extracted from Δ*rpfB* mutant infected macrophages. Lane 5: U2 (RNA sequencing).

Adaptor trimming and FASTQC per base quality analysis

Quality of forward and reverse RNA sequenced reads of raw RNA sequenced reads and after adaptor trimming were assessed using FastQC (V0.11.7). This tool provided per base sequence quality, per tile sequence quality, per sequence quality scores, per base sequence content, per sequence GC content, per base N content, sequence length distribution, sequence duplication levels, overrepresented sequences and adaptor content. Each of the above were ranked into either 1 of 3 categories, pass (green), warning (orange) or fail (red). Adaptor sequences added during library preparation prior to RNA sequencing were trimmed using Trimmomatic 0.36. Trimmomatic removed approximately 20 % of the total read (Figure D1). The results show all sequenced reads generated were 150-151 bp. The mean of the per base sequence quality score for all R1 reads for each sample were above 20 but slightly below 20 for all R2 reads (Figure D1).

UN1 R1

Adaptor trimming

Input Read Pairs: 28496683 Both Surviving: 25393145 (89.11%) Forward Only Surviving: 2997997 (10.52%) Reverse Only Surviving: 61119 (0.21%) Dropped: 44422 (0.16%).

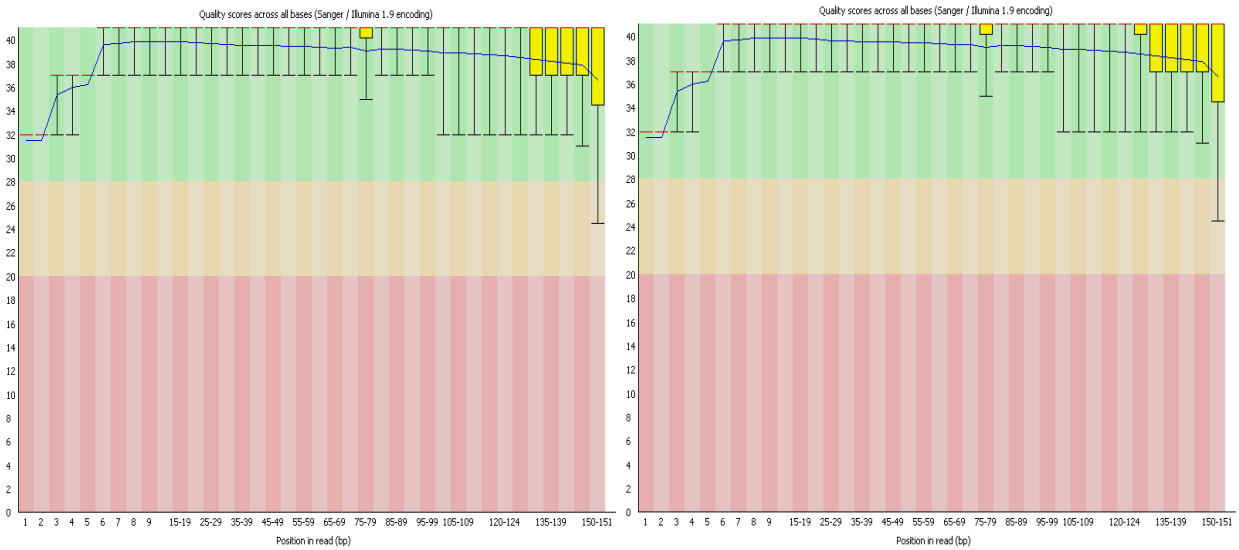

A. Raw data B. Adapter trimmed reads

UN1 R2

Adapter trimming plus additional arguments (results):
UN1: Input Read Pairs: 28496683 Both Surviving: 25393145 (89.11%) Forward Only Surviving: 2997997 (10.52%) Reverse Only Surviving: 61119 (0.21%) Dropped: 44422 (0.16%).

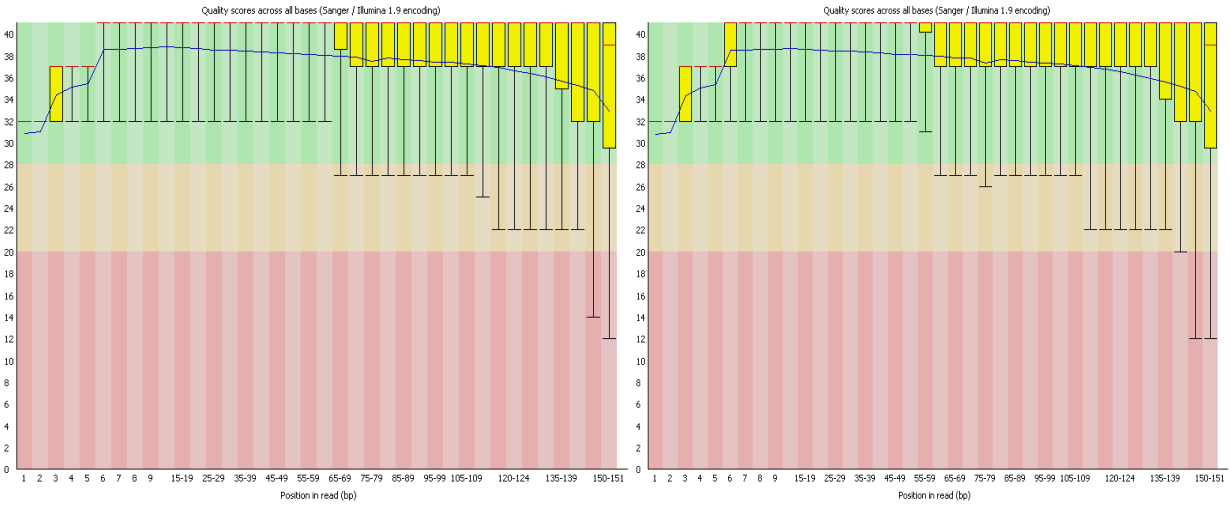

A. Raw data B. Adapter trimmed reads

UN2 R1

Adapter trimming (results):
Input Read Pairs: 44186820 Both Surviving: 37878312 (85.72%) Forward Only Surviving: 6153364 (13.93%) Reverse Only Surviving: 93042 (0.21%) Dropped: 62102 (0.14%).

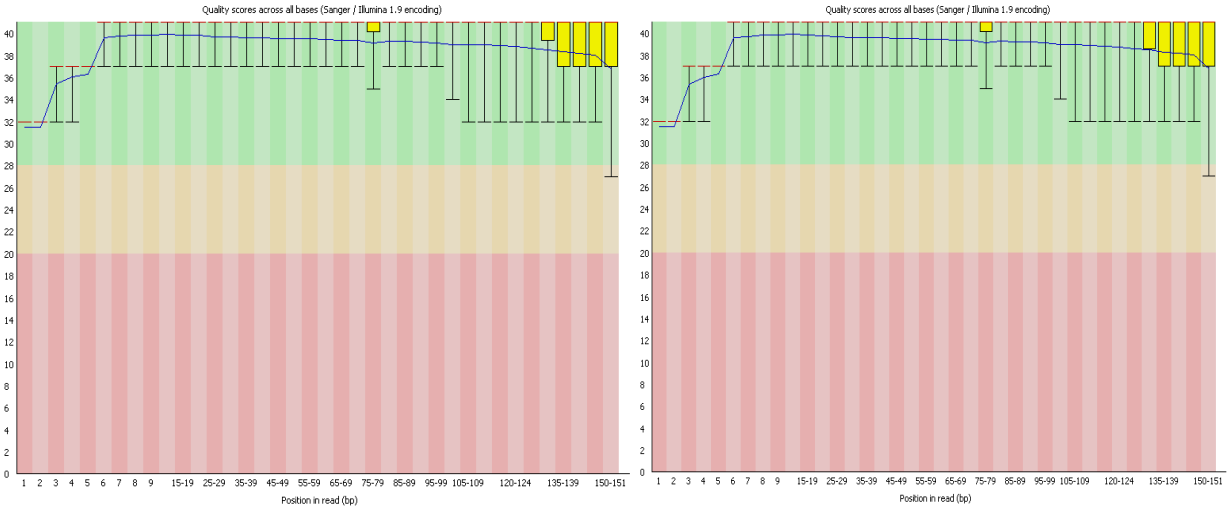

A. Raw data B. Adapter trimmed reads

UN2 R2

Adapter trimming plus additional arguments (results):
Input Read Pairs: 44186820 Both Surviving: 37878312 (85.72%) Forward Only Surviving: 6153364 (13.93%) Reverse Only Surviving: 93042 (0.21%) Dropped: 62102 (0.14%).

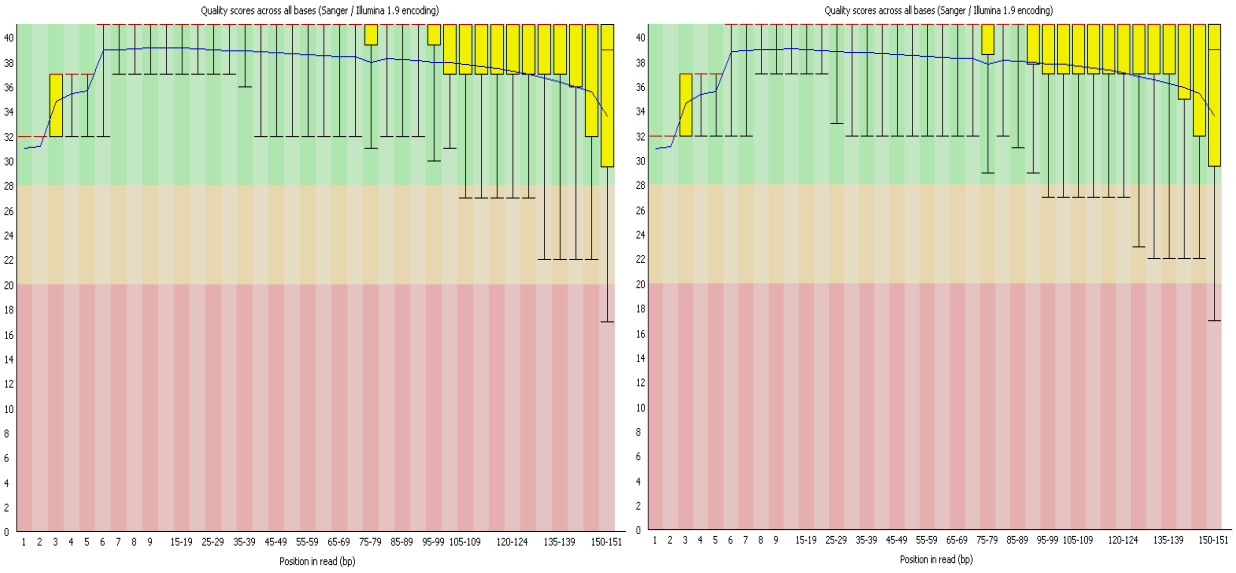

A. Raw data B. Adapter trimmed reads

WT1 R1

Adapter trimming plus additional arguments (results):
Input Read Pairs: 39868784 Both Surviving: 35279795 (88.49%) Forward Only Surviving: 4443287 (11.14%) Reverse Only Surviving: 86119 (0.22%) Dropped: 59583 (0.15%).

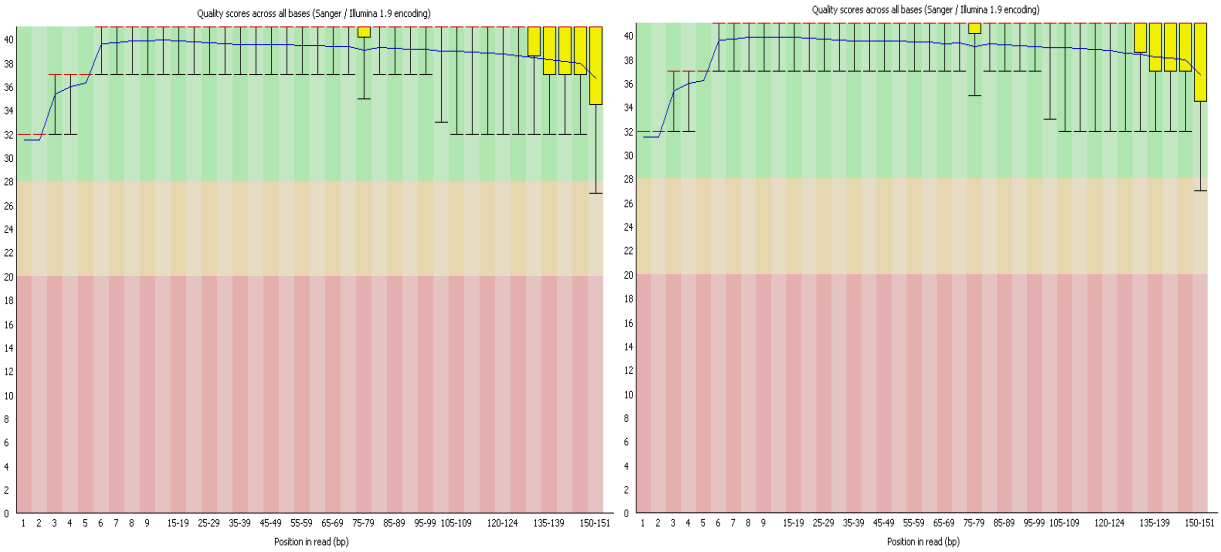

A. Raw data B. Adapter trimmed reads

WT1 R2

Adapter trimming plus additional arguments (results):
Input Read Pairs: 39868784 Both Surviving: 35279795 (88.49%) Forward Only Surviving: 4443287 (11.14%) Reverse Only Surviving: 86119 (0.22%) Dropped: 59583 (0.15%).

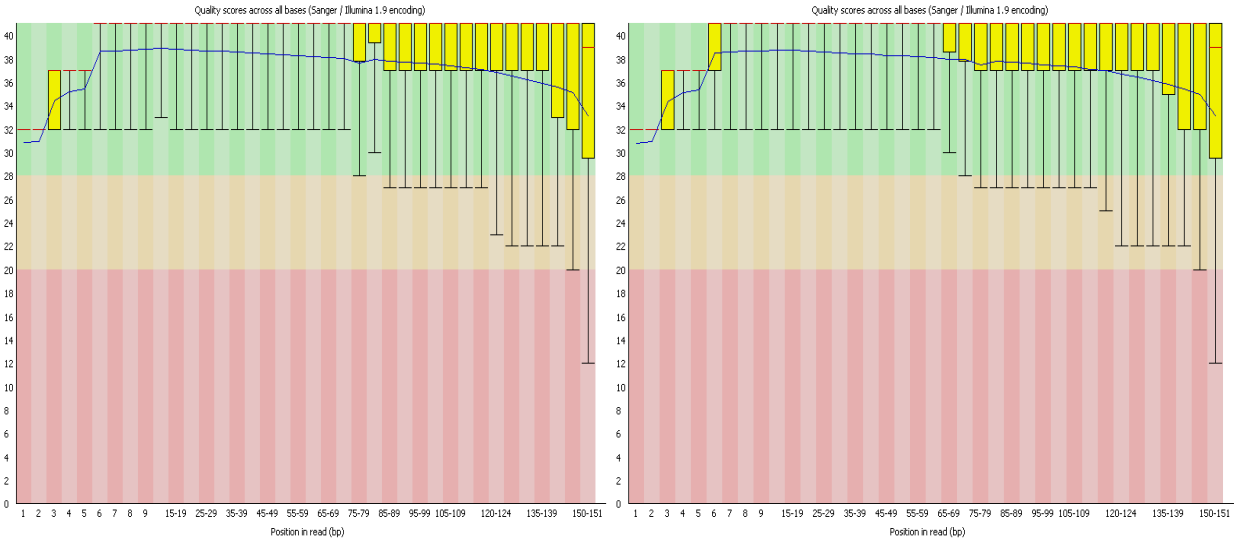

A. Raw data B. Adapter trimmed reads

WT2 R1

Adapter trimming plus additional arguments (results):
Input Read Pairs: 35263514 Both Surviving: 31502310 (89.33%) Forward Only Surviving: 3633031 (10.30%) Reverse Only Surviving: 73910 (0.21%) Dropped: 54263 (0.15%).

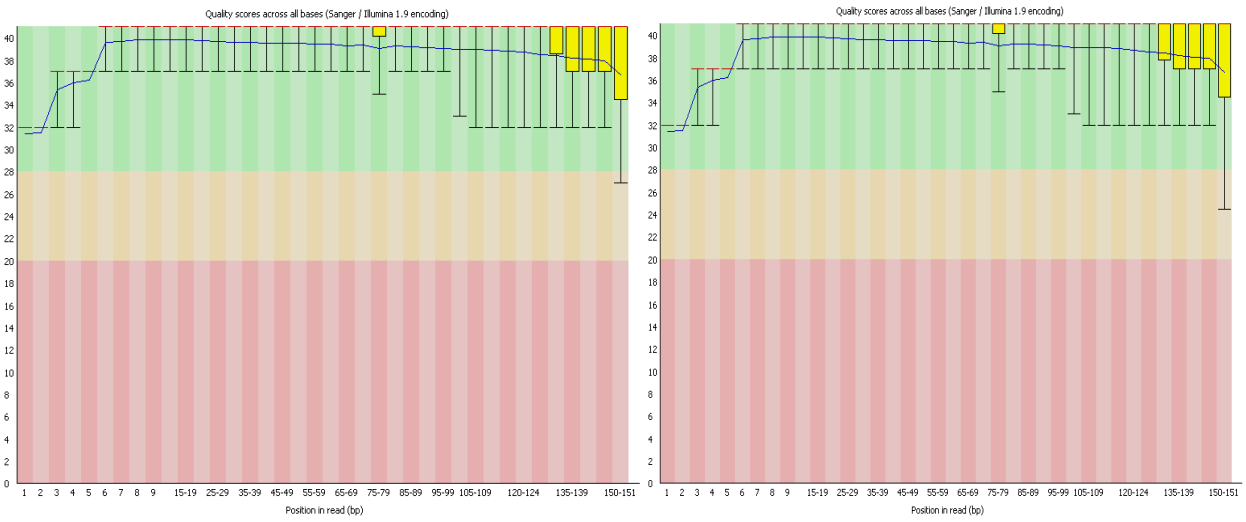

A. Raw data B. Adapter trimmed reads

WT2 R2

Adapter trimming plus additional arguments (results):
Input Read Pairs: 35263514 Both Surviving: 31502310 (89.33%) Forward Only Surviving: 3633031 (10.30%) Reverse Only Surviving: 73910 (0.21%) Dropped: 54263 (0.15%).

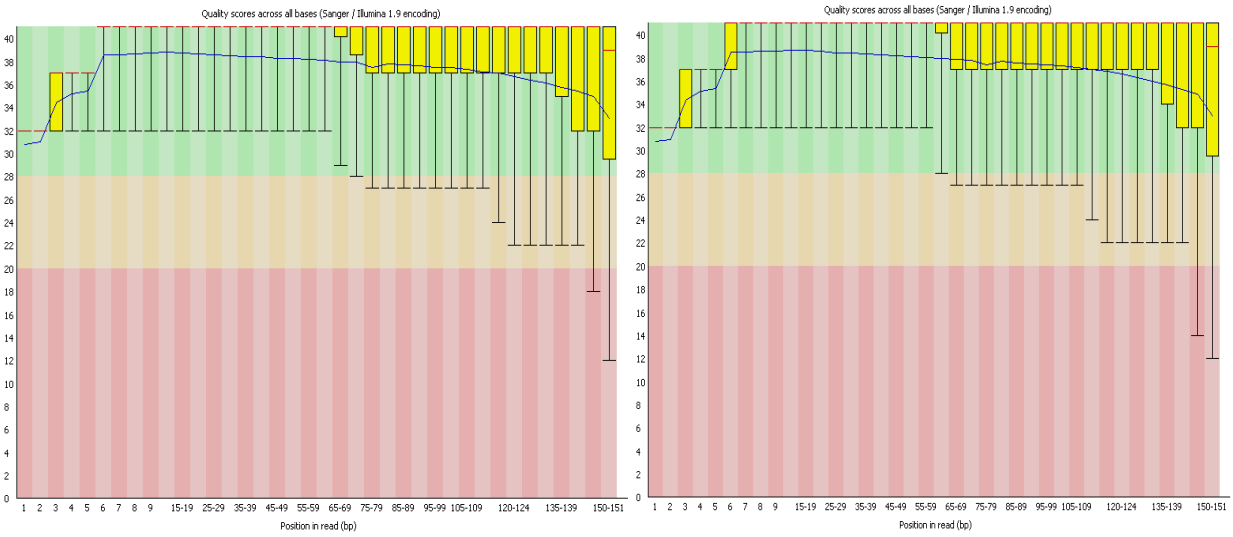

A. Raw data B. Adapter trimmed reads

rpfB1 R1

Adapters trimming plus additional arguments (results):
Input Read Pairs: 35911261 Both Surviving: 32624109 (90.85%) Forward Only Surviving: 3158290 (8.79%) Reverse Only Surviving: 75222 (0.21%) Dropped: 53640 (0.15%).

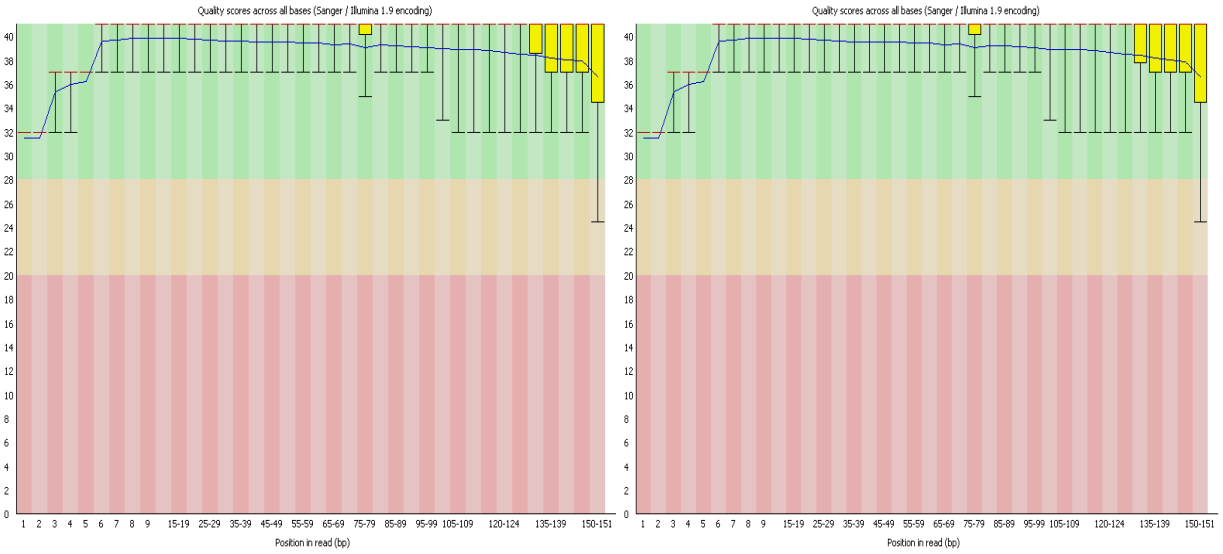

A. Raw data B. Adapter trimmed reads

rpfB1 R2

Adapters trimming plus additional trimming (results):
Input Read Pairs: 35911261 Both Surviving: 32624109 (90.85%) Forward Only Surviving: 3158290 (8.79%) Reverse Only Surviving: 75222 (0.21%) Dropped: 53640 (0.15%).

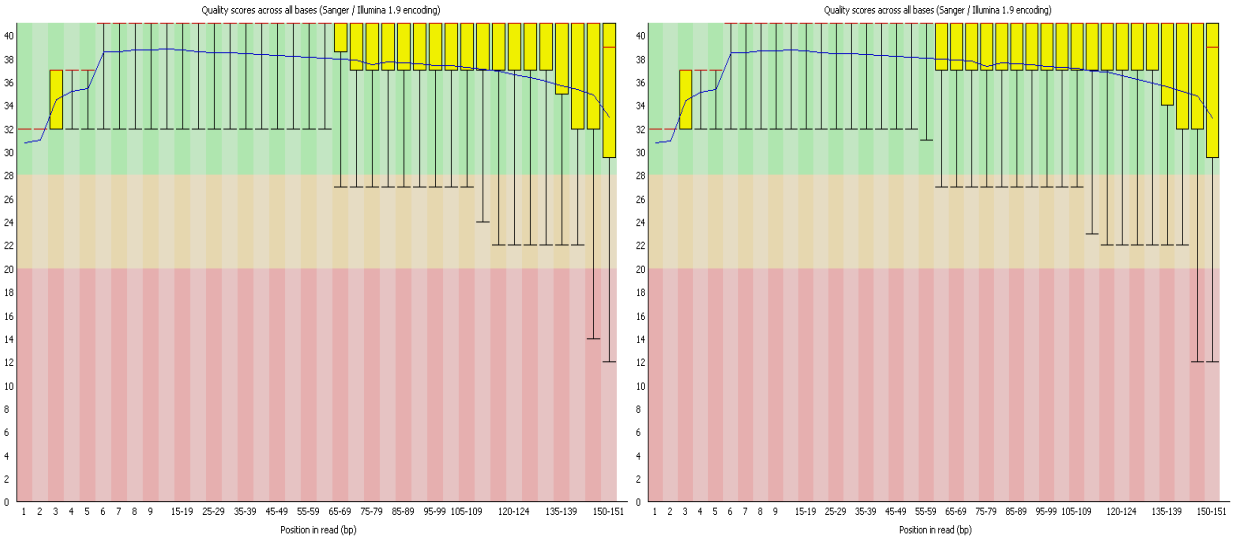

A. Raw data B. Adapter trimmed reads

rpfB2 R1

Adapters trimming plus additional arguments (results):
Input Read Pairs: 34683627 Both Surviving: 31275318 (90.17%) Forward Only Surviving: 3283551 (9.47%) Reverse Only Surviving: 74831 (0.22%) Dropped: 49927 (0.14%).

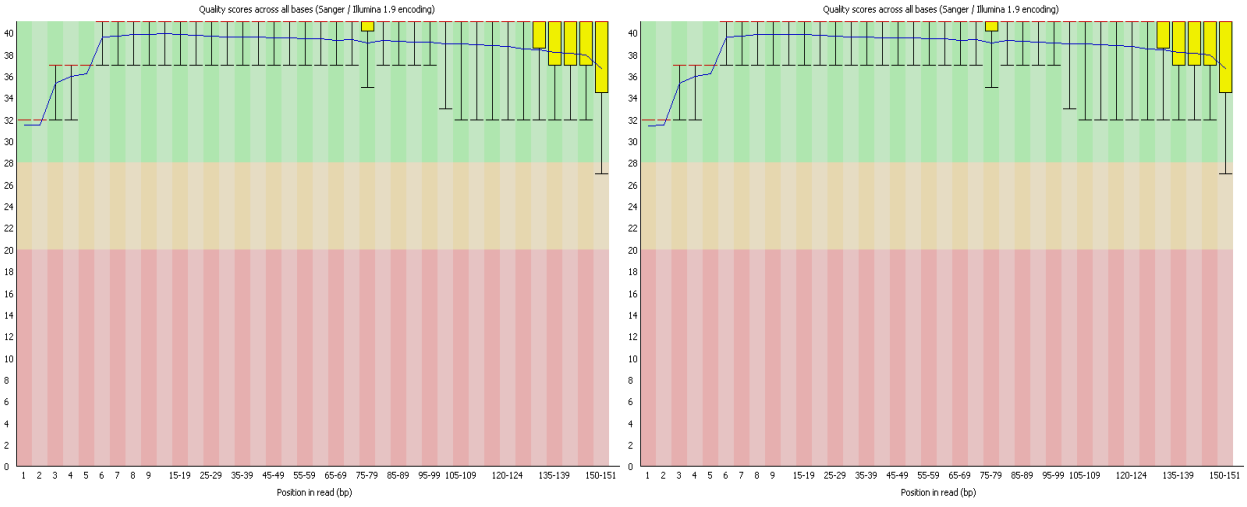

A. Raw data B. Adapter trimmed reads

rpfB2 R2

Adapters trimming plus additional arguments (results):
Input Read Pairs: 34683627 Both Surviving: 31275318 (90.17%) Forward Only Surviving: 3283551 (9.47%) Reverse Only Surviving: 74831 (0.22%) Dropped: 49927 (0.14%)

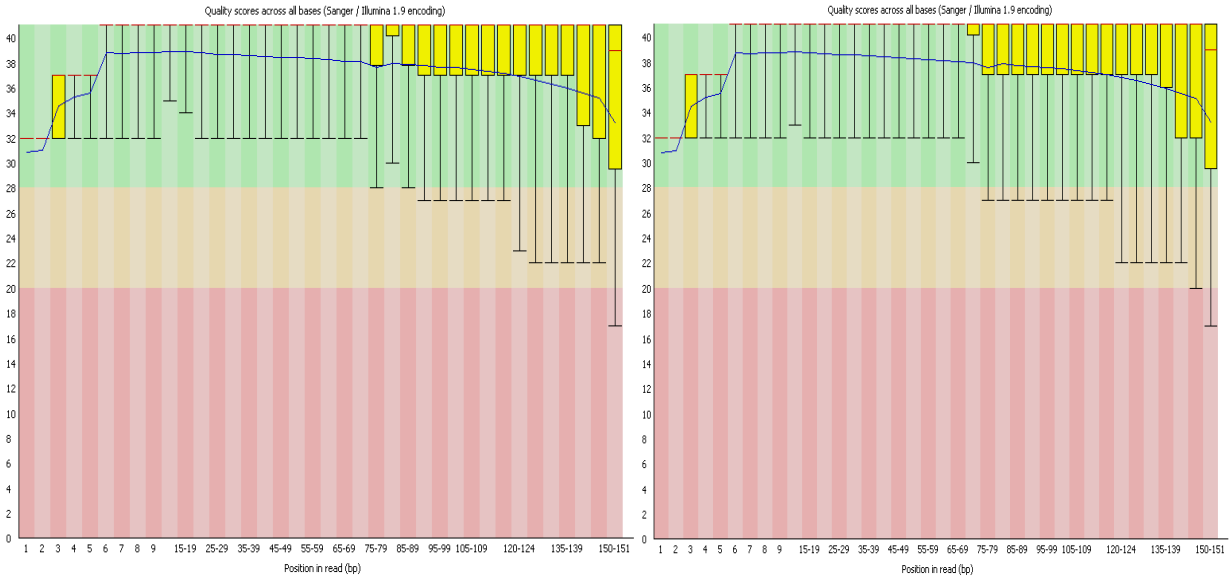

A. Raw data B. Adapter trimmed reads

Figure E2: FastQC per base quality images of adaptor trimmed forward and reverse sequenced reads. A (all images): Quality of forward and reverse RNA sequenced reads of each sample before adaptor trimming. **B (all images):** Quality of forward and reverse RNA sequenced reads of each sample after adaptor trimming.

Alignment and mapping of sequenced reads to the HG38 reference genome.

Each trimmed read (R1 and R2) of each replicate strain was aligned and mapped to the homo sapiens HG38 genome downloaded from the University of California Santa Cruz (UCSC) browser, using Tophat (v2.1.0). Mapping rates for all replicates of each strain were similar and greater than 94 %, with the highest rates observed for the mutant RNA reads (Table D2).

Table E2: Mapping rates of aligned sequenced reads to the HG38 reference genome.

Strains	Samples	Input reads	% mapped reads
Wildtype	WT1	35 279 795	94. 8 %
	WT2	31 502 310	95.1 %
Mutant	M1	32 624 109	95.4 %
	M2	31 275 318	95.0 %
Uninfected	UN1	25 393 145	94.5 %
	UN2	37 878 312	94.4 %

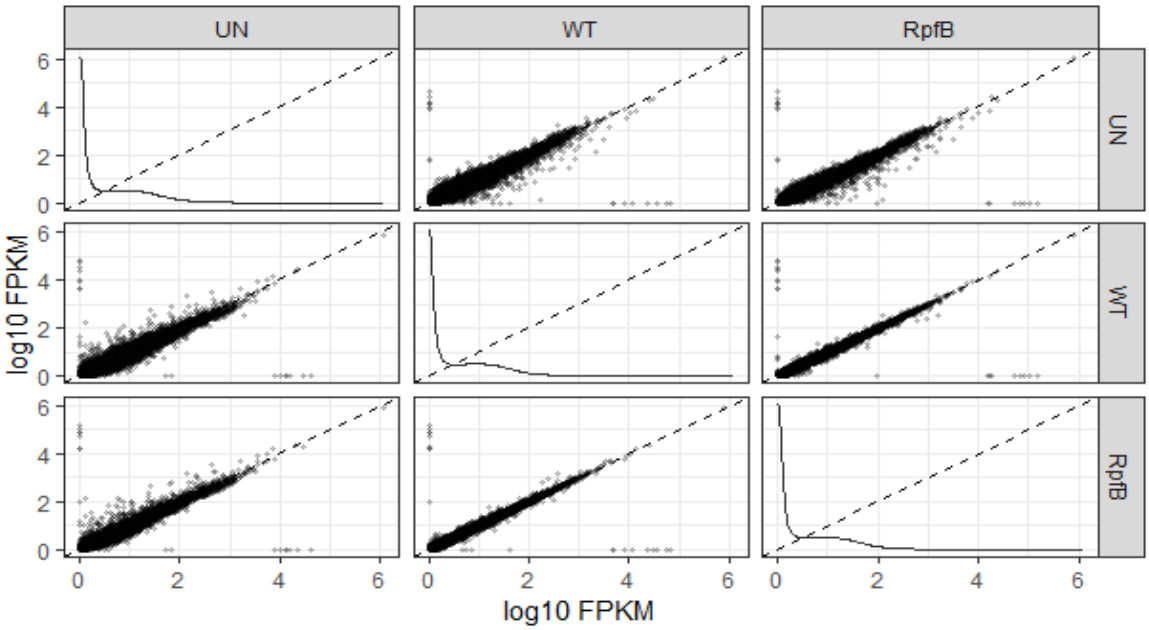

Figure E3: FPKM pairwise scatterplot comparison of global gene expression profiles of WT and Δ*rpfB* mutant infected macrophages at 72 hours P.I, relative to uninfected macrophages. The x and y-axis represent FPKM values of the genes in each assay. FPKM intensities are depicted at the left (near the y-axis) and bottom (near the x-axis). The black diagonal line represents the regression line. Genes with similar expression values can be seen on the regression line. Genes below the regression line represent greater expression in the infection model indicated to its right while genes above the regression line represent greater expression in the infection model above it. Comparison between infection models shows similar levels of expressions between WT and mutant infected macrophages, with very few genes showing greater expression in the WT and in the mutant. The plot was created using the CummeRbund package v. 2.20.0.

Appendix F: Significantly differentially and commonly expressed genes

Table F1: Fold changes of commonly induced SDEGs expressed in THP-1 macrophages infected with the WT and Δ*rpfB* mutant strains.

Gene	WT	RpfB
ABCG1	-3.96061	-1.61267
ABHD16B	1.74902	1.66664
ADAMTS15	-2.93795	-2.04062
ADAMTS7	-2.34933	-1.75399
ADAMTS7P1	-2.69765	-1.87331
ADAMTS8	-2.13335	-1.65843
ADGRB2	-2.89628	-1.65876
ANKRD1	2.7821	2.75476
ANKRD30BP3	2.90177	2.34812
ANLN	-2.58526	-2.01536
APOBEC3A	-2.59172	-1.85423
ASPM	-2.6137	-2.20829
ATP1A2	-3.23505	-2.42988
ATP2B2	-3.13819	-1.67826
AURKB	-2.64862	-2.52388
AXL	2.20679	2.49787
BATF2	2.04001	2.20371
BIRC5	-2.45776	-2.07077
BUB1	-1.86596	-1.57403
BUB1B,PAK6	-2.08713	-2.15079
C11orf96	1.80173	2.37954
C1orf101	2.01261	2.10333
C1QTNF1	1.84093	1.57574
C5AR1	2.35474	1.66061
C7orf57	-2.47212	-1.88386
CAMK2B	-2.74992	-2.12291
CCL20	1.86793	1.90754
CCL22	1.55309	1.90253
CCNA2	-2.10883	-1.92885
CCR7	5.22815	5.47248
CD1D	-2.83625	-2.95224
CD274	1.72081	1.6082
CD300LB	-3.04024	-1.80855
CD38	1.6479	1.78229
CDC25B	-2.14952	-1.83605
CDCA3	-2.02914	-1.61632

CDCA5	-1.92597	-1.70588
CDCA8	-1.61733	-1.50309
CDK1	-2.18427	-1.92468
CDKN3	-2.11933	-1.57312
CENPA	-1.79966	-1.80853
CENPF	-1.83068	-1.93629
CENPM	-2.02226	-1.62545
CEP55	-2.11341	-1.62794
CGREF1	-2.35647	-1.79401
CHST6	-2.04301	-1.64479
CLDN14	1.6428	1.9555
CMPK2	3.86755	4.59141
CRLF2	6.26571	5.5693
CTSW	-2.34036	-2.09837
CXCL1	3.88493	3.30778
CXCL10	2.45564	2.98928
CXCL11	2.53874	3.1614
CXCL14	-1.73537	-1.88191
CXCL2	4.58861	4.05917
CXCL3	3.64635	3.20104
CXCL5	2.91304	2.08746
CXCL6	3.47567	2.82639
CYP26B1	-2.62566	-1.88888
DDX58	2.43359	2.94289
DEPDC1	-2.78875	-1.98904
DEPDC1B	-1.86097	-1.98904
DIAPH3	-2.11697	-2.27827
DLGAP5	-2.43219	-2.38612
DNAJC5B	-1.9221	-1.95096
DPP4	1.92456	1.54472
DRAM1	1.88817	1.79202
DTL	-1.76594	-1.50261
DTX3L	1.90508	1.94056
E2F1,PXMP4	-1.57942	-1.58462
E2F8	-1.75508	-1.51399
EIF2AK2	2.33782	2.58813
EOMES	4.57654	3.98874
EPHB6	-1.64618	-1.57145
EPSTI1	3.32622	3.45761
ETV7	3.65364	3.72677
FAM57B	-1.64792	-1.73432
FAM83D	-1.82589	-1.90509
FAM86EP	-2.54526	-1.95253

FGF13	3.03743	2.52224
FOXM1	-1.93721	-1.61361
FUT11	1.64074	1.53074
GALNT12	-1.7748	-1.57768
GBP1	3.45392	3.35344
GBP5	3.48125	4.3528
GCH1	1.76673	1.59854
GRASP	1.90997	2.43327
GTSE1	-1.8851	-1.93243
GXYLT2	-1.86502	-1.52941
HCAR2,HCAR3	3.76109	3.53447
HERC5	2.64257	3.37252
HERC6	3.54425	3.58857
HEY1	-1.93728	-2.03879
HHATL	-3.17336	-1.95216
HIST1H2AD,HIST1H3D	2.74961	2.17108
HIVEP2	2.21257	1.95375
HJURP	-3.05797	-2.43858
HOMER2	-2.11587	-1.81896
HSH2D	2.40127	3.31356
IFI27	9.07864	8.71927
IFI35	2.11427	2.35741
IFI6	2.81024	2.90489
IFIH1	1.69862	1.92883
IFIT1	4.84061	5.50523
IFIT2	2.0146	2.7206
IFIT3	3.32386	3.89036
IFIT5	3.46558	3.81763
IFITM1	3.77753	4.86282
IFITM3	1.55516	2.23154
IL1R1	2.01823	1.57936
IL23A	1.75057	2.32095
IL24	4.05186	2.8731
IL33	1.85682	2.49009
IL36G	2.82746	2.82026
IL36RN	4.32336	3.2754
IL3RA	2.16341	1.59424
INHBA	4.13298	3.82549
IRG1	3.96478	3.96618
ISG15	2.75025	3.38058
ITGA11	-1.9897	-1.66356
ITGA2	2.40561	1.98089
ITGA3	-3.18655	-1.91869

ITIH3	-2.64636	-2.01461
JHDM1D-AS1	2.22192	1.55691
KCNIP3	-2.26175	-3.01523
KIAA0101	-1.60717	-1.65839
KIAA0922	2.84609	2.03503
KIF11	-1.68063	-1.65793
KIF18B	-2.47526	-2.20404
KIF2C	-2.61318	-2.1293
KIF4A	-2.14087	-1.64734
KIFC1	-2.17598	-1.62962
KRT78	-1.67517	-1.65798
LGALS3BP	2.7119	2.88241
LILRA1	-2.14404	-1.75767
LINC00462	1.62951	1.50911
LINC00877	-2.30592	-1.79094
LINC01050	1.99532	1.72742
LINC01127	-2.24063	-1.51408
LINC01271	1.82287	3.00017
LINC01572	3.54343	2.92748
LINC01605	-3.04688	-2.45794
LOC100419583	1.92019	1.89038
LOC101927045	1.67683	1.59127
LOC441155	2.4931	1.55368
LOXL2	-2.30974	-1.64758
LPAR5	-2.66932	-2.68851
LRRC25	-1.73916	-1.84732
LRRC32	1.59491	1.8399
LRRK2	2.80771	1.64047
LY6E	2.79772	3.05031
LZTS1	-2.03422	-2.0044
MAD2L1	-1.87173	-1.71151
MARCO	-2.13051	-2.39774
MELK	-1.82875	-1.6973
MET	3.29081	2.26273
MIR146A	1.83826	1.68137
MKI67	-2.5281	-2.12101
MLPH	-1.60961	-1.54748
MMP8	2.15723	1.90093
MND1	-1.75255	-2.1507
MOK	2.44868	1.53631
MYBL2	-1.74622	-1.54956
NAP1L3	-1.92229	-2.11884

NEK2	-2.5272	-2.96449
NFKBIZ,NXPE3	1.8866	1.51568
NPTXR	-1.91156	-1.56964
NR4A1	3.26178	3.61854
NR4A2	1.94529	2.02968
NR4A3	1.89609	2.05949
NRG1	2.41866	1.80785
NRGN	-1.7799	-1.69213
NRSN1	-2.85547	-2.12853
NTN1	4.00845	3.10088
NUF2	-2.65632	-1.89836
OAS1	2.87087	3.2787
OAS2	3.98281	4.54643
OAS3	2.8572	3.32987
OASL	2.49988	3.27146
OGFRL1	2.00564	1.59457
OSM	2.29932	2.58129
OSMR	3.00698	2.58129
OTOF	2.83668	3.31122
PADI2	-4.09768	-2.93351
PARP9	2.66422	3.00761
PCDH20	3.31129	2.28597
PCYOX1L	-1.8583	-1.55452
PDE4A	2.42026	1.8228
PF4,PPBP	2.7549	1.70566
PID1	3.89969	3.57217
PIK3IP1	-1.92713	-1.50699
PILRA	1.88593	1.65181
PLEKHA4	2.00348	2.55446
PLK1	-1.966	-1.50666
PLK2	2.91871	2.41618
PLK4	-1.52801	-1.6889
PLSCR1	2.45789	2.82662
PRC1	-2.47278	-1.52141
PRF1	-3.4341	-1.85137
PRR11	-1.84557	-1.56377
PSD2	-3.21867	-2.29052
PTGES	4.65469	4.52931
PTGFRN	-1.58284	-1.74988
PTGS2	2.91445	2.69211
PTPN14	-1.62692	-1.74753
PVRL1	-3.42621	-2.4172
RAD51AP1	-1.59776	-1.50992

RADIL	-2.30394	-2.10787
RASD2	-2.10582	-1.7177
RASL11B	-2.75943	-1.6074
RASSF9	-1.72825	-1.55234
RBM24	2.36112	2.14077
RBM44	-2.75948	-1.88002
RHOH	2.56735	1.84717
RMI2	-2.1823	-1.74119
RND3	2.08696	1.83119
RNF144B	3.32089	3.3046
RSAD2	5.9529	6.47611
RSPO3	3.204	3.14038
RTP4	1.81123	2.27064
RXFP2	-3.17686	-1.7993
S100A8	3.9785	2.80123
S100A9	2.99416	2.48562
SAMD9	2.43187	2.67531
SAMD9L	2.21749	2.45365
SCART1	-3.16561	-1.74179
SDS	2.62924	2.4924
SEMA6B	1.91541	1.78121
SERINC2	1.70922	1.5828
SERPINB2	2.28674	2.10759
SERPINB7	4.51118	3.47254
SGOL1	-2.06948	-2.29414
SHCBP1	-1.71656	-1.71075
SIAE	-1.91575	-1.71876
SIGLEC1	4.08719	4.39259
SIX4	-1.86809	-1.5402
SLAMF7	2.4711	2.06668
SLC16A10	3.47032	2.77532
SLC1A2	3.55183	2.90755
SLC43A2	3.55825	2.92942
SLC7A11	3.12608	1.74058
SMAD3	-1.88917	-1.86568
SOCS3	2.33878	2.18079
SOD2	2.45972	2.1308
SORL1	-3.68895	-3.04245
SORT1	-1.6508	-1.60296
SP110	1.99605	2.15751
SPARCL1	-3.439	-2.15414
SPC24	-3.31383	-1.71071
SPOCK1	-3.38395	-2.65516

SRGAP3	-2.27888	-1.57617
STAC2	-3.17109	-1.90856
STAT4	2.17381	2.13498
STMN1	-2.32474	-2.00875
SYTL1	-2.53352	-2.61008
TCF19	-1.57327	-1.71642
TDO2	3.46877	2.02307
TESC	-1.90833	-1.72484
TICRR	-2.57523	-1.79212
TMEM106C	-1.66488	-1.56044
TMEM8B	-1.93859	-1.93083
TNC	-2.54701	-1.51359
TNFAIP6	4.64509	3.79112
TNFRSF11A	2.90435	2.38894
TNFSF10	1.94018	2.25953
TNIP3	5.50277	4.8948
TOP2A	-2.47757	-2.22769
TRAF1	2.39041	2.26446
TRIB2	-1.56237	-1.82482
TRIM22	2.67501	3.78738
TRIM34	1.84161	2.63074
TRIM69	1.64442	1.79094
TRNP1	-1.8582	-1.83721
TSLP	1.66874	1.94452
TSPAN10	2.1234	1.98501
TSPAN13	-2.15131	-1.50603
TTK	-2.58781	-1.9641
TTTY14	-2.2028	-1.67331
TYMS	-2.19195	-2.39962
UCP3	2.04792	1.54394
UPP2	-2.55977	-1.70783
USP18	1.64636	2.29276
VIPR1	-2.55413	-2.45344
VSIG4	-2.25779	-1.92195
XAF1	2.30353	2.49436
ZCCHC2	1.90024	1.62699
ZNF235	2.09443	2.149
ZNF469	1.9759	1.74931

Table F2: Fold changes of SDEGs exclusively induced by WT infection.

Gene	Log1.5(fold_change)
ABCG2	1.75968
ABL2	1.69244
ABLIM2	-2.43003
ADCY6	-1.63072
ADGRA2	-1.53349
ADGRD1	-1.58057
ADRA2B	-1.51889
ADRA2C	-1.51381
AIFM2	1.85996
ALOX5	-2.01383
AMOTL1	-1.61202
ANGPTL4	2.30643
ANKRD66	2.63707
ANOS1	-1.78961
AOC1	-1.67462
APH1B	1.51924
ARHGEF9	-1.537
ARL4D	-1.53083
ARMC9	1.64868
AS3MT	1.78543
ATF5	1.86918
ATP10A	-1.77733
ATP2B1	1.75315
BAIAP2L2	-1.58146
BATF	1.86787
BEAN1	-1.91101
BNIP3	1.53722
BTNL8	4.03774
C1orf228	-1.8553
C20orf166-AS1	-1.55397
C21orf58	-1.75511
C21orf91	1.77474
C22orf42	2.05807
C3AR1	1.57272
C6orf165	2.00488
CACNA2D3	1.9792
CAPN11	-1.76511
CAPRIN2	-1.50577
CARD6	1.81365

CCDC74A	-1.52733
CCDC74B	-1.92067
CCDC85A	1.7431
CCNB1	-1.75798
CCND2	-2.8163
CD180	-1.99613
CD6	-2.06945
CD84	-1.60039
CD9	-1.66926
CDCA7L	-1.70052
CDCP1	1.85933
CDT1	-1.78496
CEBPE	1.53261
CEP162	1.59921
CEP170P1	-2.07049
CIART	-1.73261
CKAP4	-2.26072
CLU	-1.77198
COL13A1	-1.51095
COL23A1	-1.91372
COL6A3	-1.75319
CPE	-1.64999
CPED1	-1.55018
CREG1	1.5504
CREM	1.57079
CSF2RA	1.90213
CSPG4	-1.9087
CX3CL1	-1.57633
CXADR	-2.05619
CXorf57	-1.52736
CYB561	1.64306
DCANP1	-3.34367
DDO	-2.34238
DDX12P	-1.66216
DHCR7	-1.56394
DIRC3	-1.87091
DISC1FP1	1.51172
DLL4	2.74955
DMRT2	-1.72122
DNAJC3-AS1	2.14166
DNM1	-1.70476
DSCC1	-1.8465
DUSP16	1.68015

DYRK4	-1.56121
EDNRB	1.53677
ELOVL7	1.61783
EML6	-1.77091
EPHB3	-2.02405
ESCO2	-1.62306
EXO1	-1.51361
F2RL3	1.65615
FA2H	-1.70752
FAHD2A	-1.51611
FAHD2B	-1.56985
FAHD2CP	-1.7219
FAM13A	-2.26556
FAM179A	-1.75385
FAM19A3	-1.79246
FAM84B	-1.59984
FANCD2	-1.5324
FBP1	-2.26164
FCGR2B	-2.03275
FCRLA	-1.83315
FCRLB	-1.91561
FGD4	1.96019
FHL1	-1.58413
FIBCD1	-1.55144
FIGN	1.8525
FKBP7	-1.87346
FLJ42351	-2.67406
FSBP	-1.54809
FTX	1.71387
GALNT18	-1.75607
GDAP1	1.8761
GIMAP6	-1.54284
GINS3	1.84738
GLIPR1	1.71135
GNAT2	-2.163
GNLY	1.86087
GPAT3	2.19056
GPR160	1.54116
GPRC5C	-1.70315
GPT2	-1.56231
GS1-259H13.2	-2.48324
GSDMB	-2.21356
GSG2	-1.53854

HADH	-2.24751
HIST1H2BC	2.9072
HIST2H2BC	2.07018
HMOX1	1.51123
HOPX	-2.34205
HSPA12A	-1.50465
HSPG2	-1.95995
ICAM5	-1.57137
IFI44	3.82788
IFI44L	5.95072
IL10	2.90069
IL36B	2.33795
KALRN	-1.73926
KCNJ11	-1.80796
KIF15	-1.77198
KIR2DL4	1.79688
KLHDC8B	-2.15687
KLHL21	1.52075
KLHL29	1.79399
KNTC1	-1.52059
KRT4,KRT79	-1.81831
KRT7	-2.58494
KYNU	1.51011
LACC1	2.1991
LAMB2P1	-1.83618
LDHD	-1.98016
LGI4	-1.75014
LINC01094	1.5562
LINC01268	2.72198
LINGO1	-1.62522
LMNB1	-2.11214
LOC100129434	1.50426
LOC100130705	1.71631
LOC100507156	-1.72316
LOC101927740	1.77523
LOC101927755	2.59272
LOC101929260	5.09837
LPAR1	1.96341
LPCAT4	-1.81296
LRP11	-1.57904
LRRC20	-2.2746
LRRTM4	-2.4068
LYRM9	-1.71561

MACROD1	-1.85282
MCOLN1	1.75829
ME3	-1.93606
MEFV	1.72168
MEIS3P1	1.95906
MIR100HG	-3.18789
MIR600HG	-1.52028
MS4A14,MS4A7	2.13496
MSR1	1.63045
MYH14	-2.38629
MYLIP	-1.69396
MYO1D	-2.01905
MYOZ2	-1.68841
N4BP2	1.95897
NAMPT	1.89333
NCAM1	2.05183
NCAPH	-1.90956
NCOA5	1.74729
NDC80	-1.69928
NPAS2	-1.51706
NR1H3	-1.61804
NT5M	-2.63413
NTNG1	1.66134
NUSAP1	-1.99851
OAF	-1.67584
OR5B21	1.96482
ORC6	-1.55043
OSBPL7	-1.70351
OXCT1	-1.56831
PALD1	-1.68515
PAQR8	-1.6706
PARK2	-1.92131
PBK	-2.04341
PDCD2L	-1.60654
PDE3B	1.6643
PDE4B	1.54479
PDZD7	-1.98906
PLD4	-1.56048
PLIN2	1.86263
PLOD2	1.79198
PNOC	-1.88311
PRAM1	-1.63949
PRR32	-1.68462

PRSS23	-1.7292
PRSS30P	-1.82996
PTGER3	4.14775
PVRL3	1.65943
RAB17	-2.39684
RAB26	-2.41227
RAD51	-1.64046
RAMP1	-2.23638
RAP1GAP	-2.61615
RASL12	-1.81457
RASSF8	1.8332
REL	1.6718
RGS3	-2.06019
RXFP1	1.79793
S100A16	-1.9611
SAMSN1	1.97756
SAPCD2	-1.57036
SARDH	-1.71827
SCD	-1.65738
SEMA3C	1.69396
SERPINE1	-2.33824
SERPING1	6.64804
SGMS1	1.5637
SHF	1.72367
SIK3	1.64572
SKA1	-1.72077
SLAMF6	-2.45801
SLAMF9	-1.59744
SLC16A2	-1.53405
SLC22A4	1.807
SLC28A3	-2.68616
SLC29A2	-1.77541
SLC38A7	1.58446
SLC6A7	-1.8986
SLPI	1.79672
SMTNL2	-3.1961
SOAT1	1.51839
SP6	-1.73321
SP9	1.70802
SPARC	-1.72447
SPON2	-1.54166
SPTBN2	-1.83618
ST6GAL1	-1.71529

ST7L	1.51802
ST8SIA5	-1.69444
STAR	-1.59672
STK38L	1.59666
TARBP1	-1.70464
TBC1D29	-1.69053
TBX2	1.77307
TBX3	1.88557
TBX6	-1.71081
TCAF2	2.2951
THBS1	4.84306
TIFAB	-2.0239
TK1	-1.78246
TLE6	-1.86172
TLR10	-2.05204
TMC1	2.17185
TMCC2	-1.7501
TMEM163	-2.48689
TMEM178A	-2.54922
TMEM63C	-3.31374
TNFRSF10D	-1.53421
TPCN1	-1.52644
TPX2	-1.9934
TREML1	1.93731
TRIM16L	1.62438
UBE2T	-1.92313
UNC5B	-1.79604
VAT1L	-1.80849
VEPH1	-1.55544
VWF	-1.5151
WDR62	-1.52432
WDR78	1.51917
YPEL4	-2.44752
ZC3H12C	1.67639
ZNF281	1.62513

Table F3: Fold changes of SDEGs exclusively induced by Δ*rpfB* mutant infection.

Gene	Log1.5(fold_change)
ACKR3	1.6545
ADD2	-1.60504
AQP7	-3.06281
CCL4L1,CCL4L2	1.85389
CCNB2	-1.57175
CHIT1	1.59605
CRACR2B	-1.52048
CSF2	2.68025
DCANP1,TIFAB	-2.16814
DDX60	1.76222
DIRAS2	1.76952
DPEP1	-2.49168
GBP4,GBP7	1.8167
GCM1	1.52765
GPRC5A	1.50544
GRM8	-1.68166
HEATR6	-8.00344
HELZ2	1.64848
HMMR	-1.61857
IFI16	1.77701
IFI44,IFI44L	4.37481
IRF7	1.63004
ISG20	1.78493
KIF15	-1.66361
LIF	1.85103
LOC100506403	2.46157
LOC102467080	-1.86228
LONRF2	-2.09277
LRRC28	1.69376
MIR100HG,MIRLET7A2	-1.70044
MMP17	-1.69511
MRPL23-AS1	-3.82004
MX1	2.22117
MX2	2.06556
NCOA7	1.56718
NEIL3	-1.57465
OVCH1-AS1	1.55021
P2RX7	1.7413
PARP14	1.85205
PNPT1	1.86656

PODXL	-2.05638
RN7SL1	1.83974
RN7SL2	2.02486
SCO2,TYMP	1.57256
SMTNL1	1.68528
SSTR2	1.9572
STAT1	1.76419
TPRG1	1.68792
TRIM5	1.66959
TXNDC16	-1.51427
WIPF3	-3.54724
WNT5B	-1.65732

Appendix G: Ingenuity Pathway Analysis

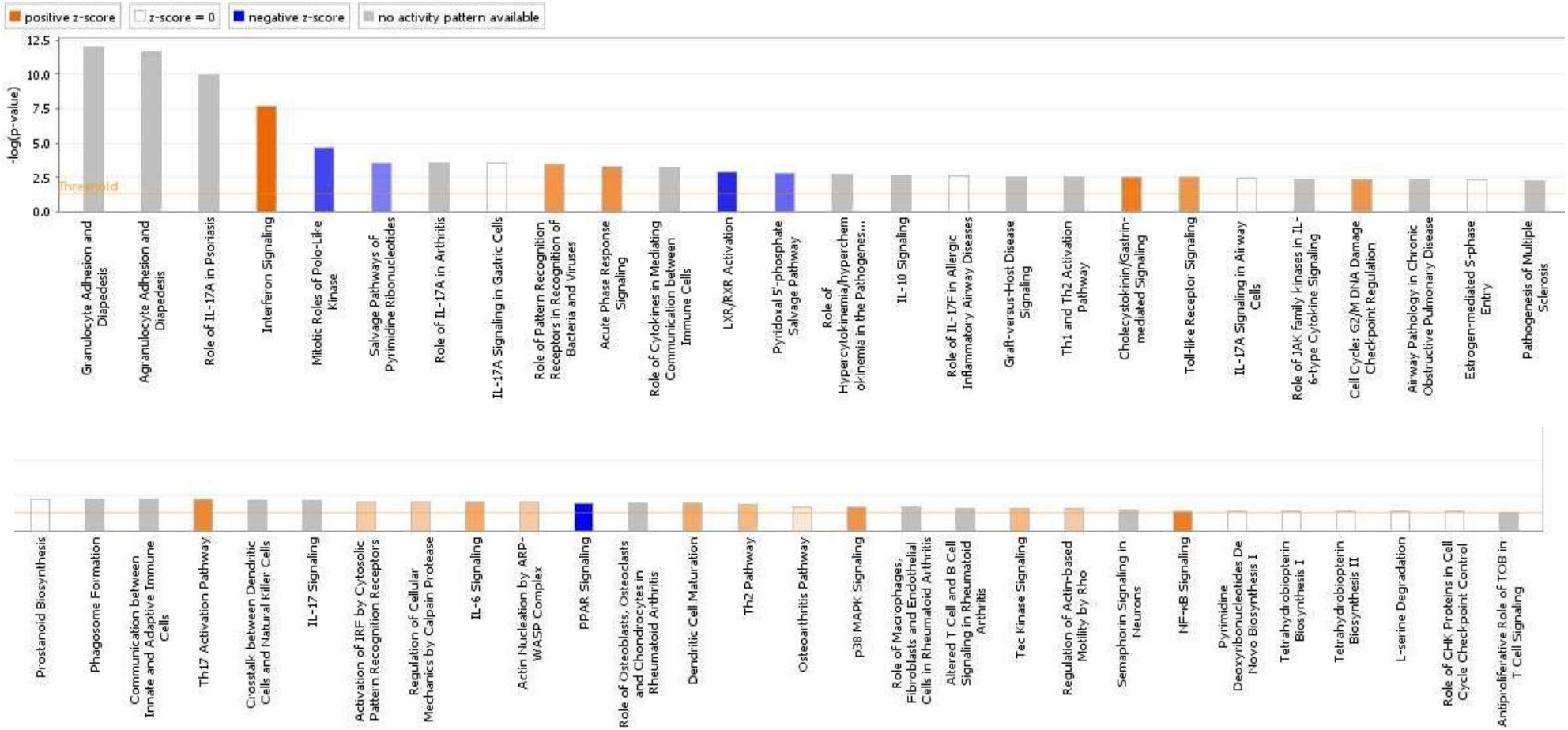

Figure G1: **Canonical pathways commonly enriched in WT and Δ*rpfB* mutant infected macrophages at 72 hours P.I.**

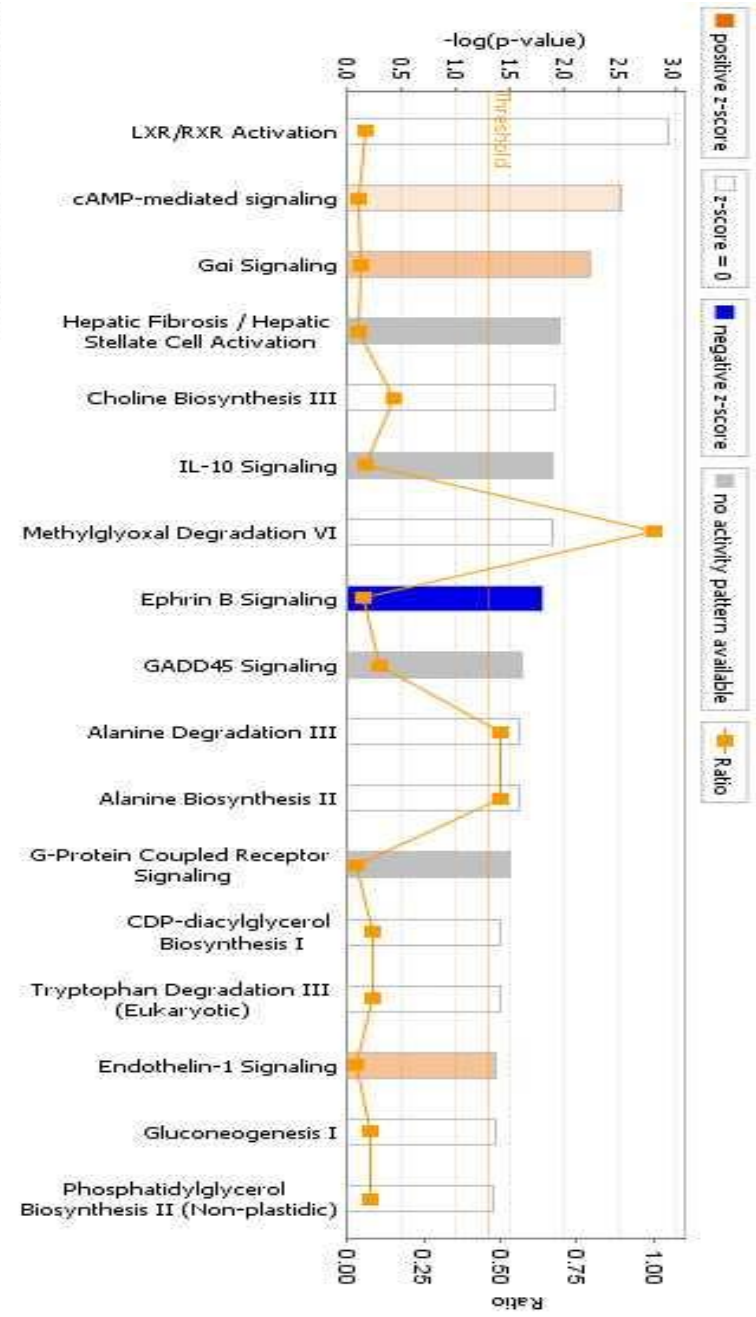

Figure G2: Canonical pathways enriched in WT infected macrophages, 72 hours P.I

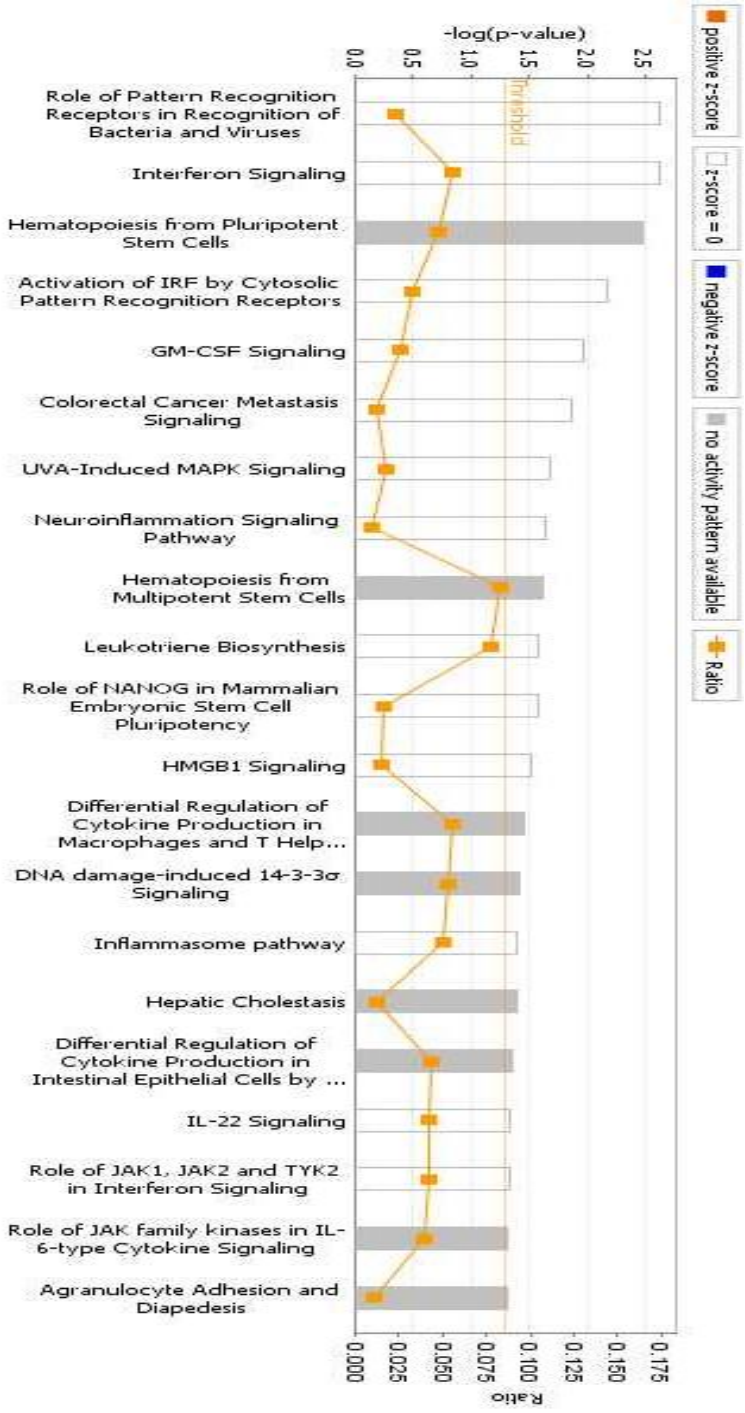

Figure G3: Canonical pathways enriched in Δ*rpfB* mutant infected macrophages, 72 hours P.I

Table G1: Top 5 canonical pathways induced by WT and Δ*rpfB* mutant infection in THP-1 macrophage cells at 72 hours p.i. The –log (p-value) refers to the level of enrichment.

Canonical pathways	-log (p-value)
WT	
LXR/RXR Activation	2.95
cAMP-mediated signalling	2.51
Gαi signalling	2.23
Hepatic Fibrosis/ Hepatic Stellate Cell Activation	1.96
Choline Biosynthesis	1.91
Δ*rpfB* mutant	
Role of Pattern Recognition Receptors in Recognition of Bacteria and Viruses	2.63
Interferon Signalling	2.62
Hematopoiesis from Pluripotent Stem Cells	2.49
Activation of IRF by Cytosolic Pattern Recognition Receptors	2.17
GM-CSF Signalling	1.96

Table G2: Top 5 diseases and disorders associated with WT and Δ*rpfB* mutant infected THP-1 macrophages.

Disease and disorders	p-value	Number of molecules
WT		
Cardiovascular Disease	1.32E-02 - 2.66E-06	58
Organismal Injury and Abnormalities	1.32E-02 - 2.66E-06	253
Endocrine System Disorders	1.32E-02 – 3.63E-06	73
Gastrointestinal Disease	1.32E-02 – 3.63E-06	238
Metabolic Disease	1.32E-02 – 3.63E-06	44
Δ*rpfB* mutant		
Antimicrobial Response	2.01E-03 – 5.49E-10	9
Inflammatory Response	2.98E-02 – 5.49E-10	14
Infectious Diseases	3.17E-02 – 2.64E-06	11
Dermatological Diseases and Conditions	2.78E-02 – 3.71E-05	31
Organismal Injury and Abnormalities	3.17E-02 – 3.71E-05	38

Table G3: Top 5 Networks elicited by WT and Δ*rpfB* mutant infected THP-1 macrophages.

WT	**Score**
1. Cellular Function and Maintenance, Cell-To-Cell Signaling and Interaction, Hematological System Development and Function	42
2. Connective Tissue Development and Function, Skeletal and Muscular System Development and Function, Tissue Development	42
3. Immunological Disease, Dermatological Diseases and Conditions, Organismal Injury and Abnormalities	24
4. Cellular Movement, Cancer, Organismal Injury and Abnormalities	20
5. Cell Death and Survival, Tissue Morphology, Cellular Development	10
***ΔrpfB* mutant**	
1. Tissue Morphology, Cellular Movement, Hematological System Development and Function	29
2. Inflammatory Response, Hematological System Development and Function, Tissue Morphology	5
3. Cancer, Cell Death and Survival, Cellular Development	2
4. Cell Death and Survival, Cellular Development, Cellular Growth and Proliferation	2
5. Cell-To-Cell Signaling and Interaction, Cancer, Gastrointestinal Disease	2

Appendix H: qRT-PCR

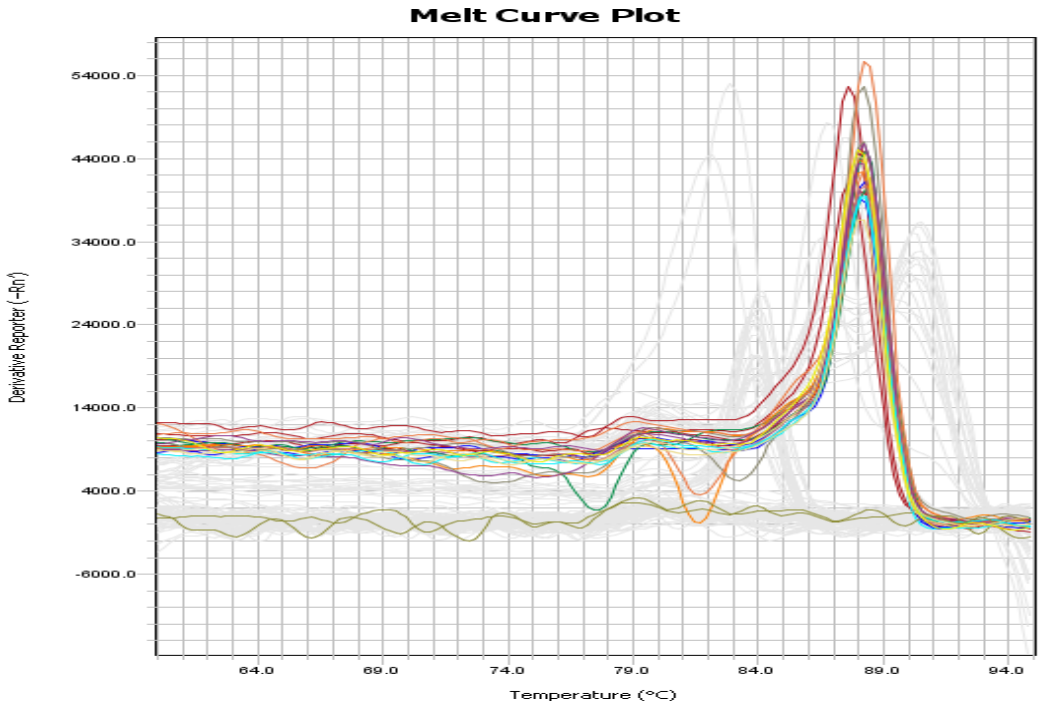

Figure H1: Melt curve plot of the *IL-1B* gene

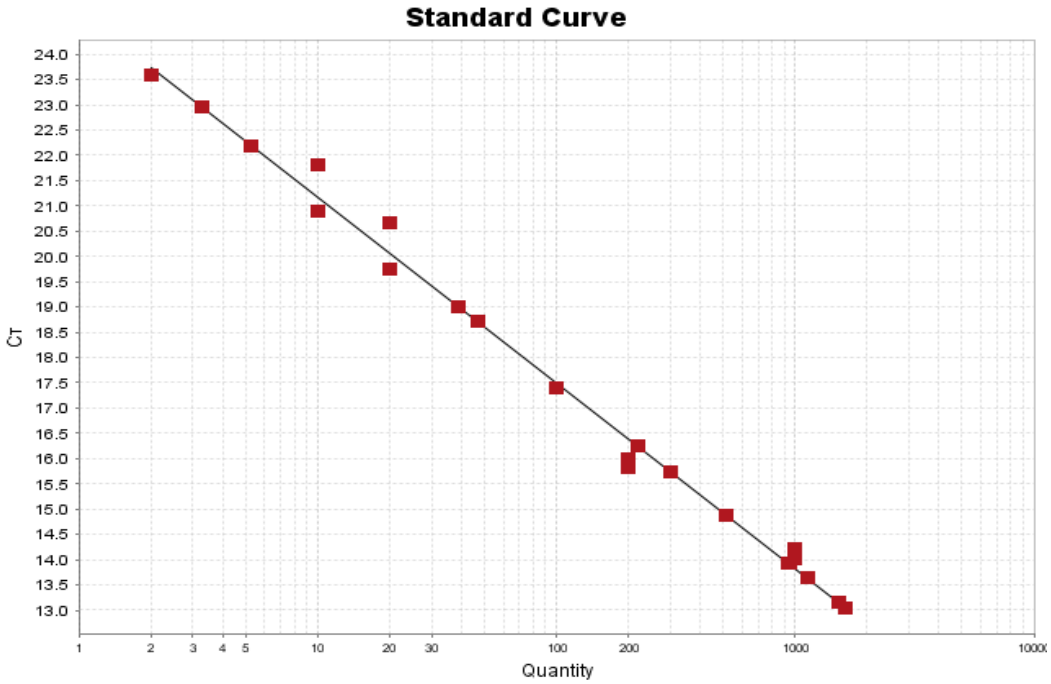

Figure H2: Standard curve of the *IL-1B*gene (PCR efficiency: 87.201%; Error: 0.166).

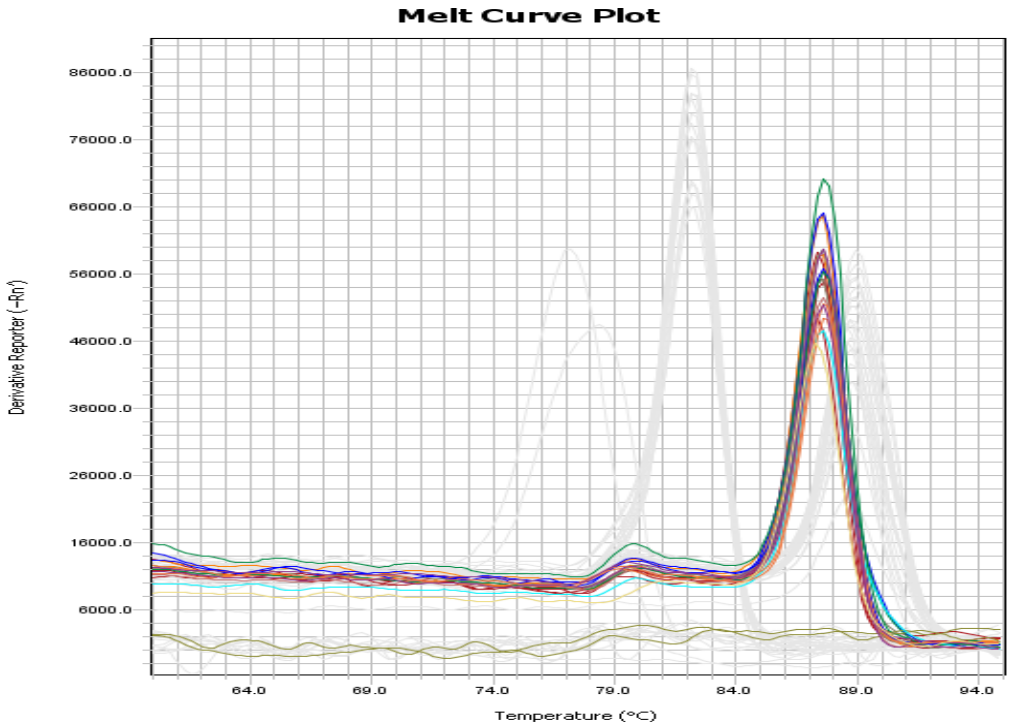

Figure H3: Melt curve plot of the *GM-CSF* gene

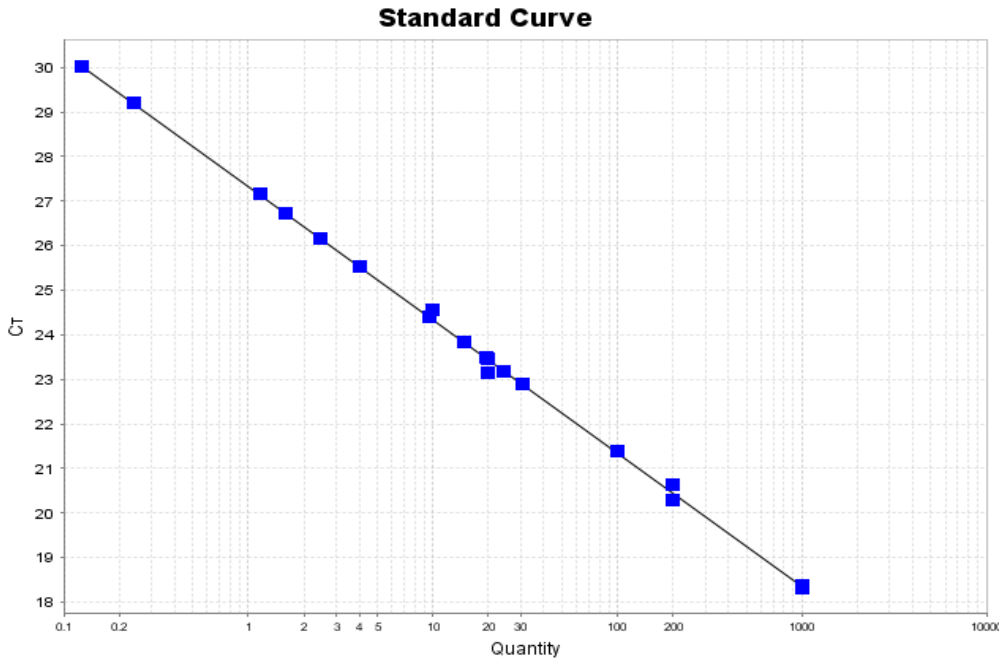

Figure H4: Standard curve of the *GM-CSF* gene (PCR efficiency: 115.714%; Error: 0.104).

Table H1: Showing the quality means of *GM-CSF* and *IL-1B* including the housekeeping gene, *GAPDH*.

Samples	GENES		
	GAPDH	***GM-CSF***	***IL-1B***
1-U	2.4275	1.864	46.982
2-U	2.037	2.989	38.942
3-W	5.007	134.346	513.572
4-W	2.782	144.288	943.021
5-M	39.003	282.165	1626.271
6-M	39.175	269.413	1517.164

NB: U = Uninfected, W = Wild type, M = *ΔrpfB* mutant, C = *rpfB*-complemented strain

Table H2: The quality means of the samples for each gene divided by *GAPDH*.

Samples	GENES	
	GM-CSF	***IL-1B***
1	0.768	19.354
2	1.467	19.117
3	26.831	102.570
4	51.864	338.974
5	7.234	41.696
6	6.877	38.727

Table H3: Averages of the quality means of the samples for each gene divided by *GAPDH*.

Samples	***GM-CSF***	***IL-1B***
U	1.118	19.236
W	39.348	220.772
M	7.056	40.212

Table H4: Fold changes of all strains for each gene for qRT-PCR.

Strains	Genes	
	GM-CSF	***IL-1B***
W	35.19	11.48
M	6.31	2.09

Table H5: Comparison of gene expression as measured by qRT-PCR and RNA Seq.

Gene	Strains	Fold change	
		RT-PCR	**RNA Seq**
GM-CSF	W	35.19	2.58
	M	6.31	2.68
IL-1B	W	11.48	0.913
	M	2.90	0.808

Fold change (unknown /known)

Eg. Average WT ratio divided by average control (uninfected strain)

Appendix I: Turnitin report

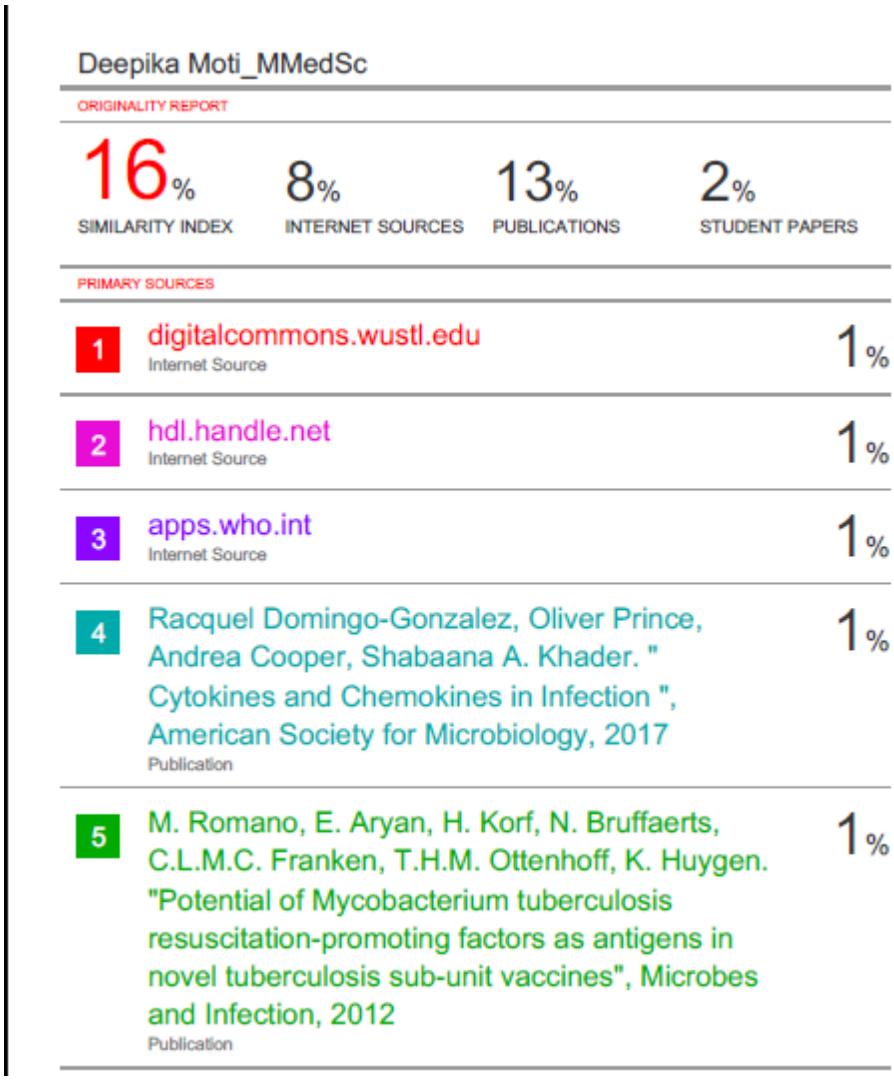

Deepika Moti_MMedSc

ORIGINALITY REPORT

16%	8%	13%	2%
SIMILARITY INDEX	INTERNET SOURCES	PUBLICATIONS	STUDENT PAPERS

PRIMARY SOURCES

1	digitalcommons.wustl.edu Internet Source	1%
2	hdl.handle.net Internet Source	1%
3	apps.who.int Internet Source	1%
4	Racquel Domingo-Gonzalez, Oliver Prince, Andrea Cooper, Shabaana A. Khader. " Cytokines and Chemokines in Infection ", American Society for Microbiology, 2017 Publication	1%
5	M. Romano, E. Aryan, H. Korf, N. Bruffaerts, C.L.M.C. Franken, T.H.M. Ottenhoff, K. Huygen. "Potential of Mycobacterium tuberculosis resuscitation-promoting factors as antigens in novel tuberculosis sub-unit vaccines", Microbes and Infection, 2012 Publication	1%